Universidad
Carlos III de Madrid
www.uc3m.es

DOCTORAL THESIS

Assessment of the Eutectic Trough and Properties of a Multiphase Alloy in the NiAl-Cr-W System

Author:

Arcadio Varona Caballero

Advisor:

Dr. Srdjan Milenkovic

Tutor:

Dr. Srdjan Milenkovic

DEPARTMENT OF MATERIALS SCIENCE AND ENGINEERING AND CHEMICAL ENGINEERING

Leganés, September 2016

Universidad
Carlos III de Madrid
www.uc3m.es

TESIS DOCTORAL

ASSESSMENT OF THE EUTECTIC TROUGH AND PROPERTIES OF A MULTIPHASE ALLOY IN THE NiAl-Cr-W SYSTEM

Autor: *Arcadio Varona Caballero*

Director: Dr. Srdjan Milenkovic

Firma del Tribunal Calificador:

Firma:

Presidente: Dr. Frank Stein

Vocal: Prof. Dr. Easo George

Secretario: Dr. Mónica Campos

Calificación:

Leganés, 23 de septiembre de 2016

A mis padres, Arcadio y Dulce

A mi hermana Esther

A Angelines, mi madrina

“*Nothing in life is to be feared, it is only to be understood. Now is the time to understand more, so that we may fear less.*”

Maria Skłodowska-Curie

Acknowledgements

Firstly, I would like to express my gratitude to my supervisor, Dr. Srdjan Milenkovic, for the confidence he has shown in me during these 4+ years in which I have been at IMDEA Materials, always showing his most human side in every situation, and with the door always open to me. Moreover, there are many great researchers in the institute, and most, if not all, have helped me to carry on with the work in one way or another. Among them, I would especially like to thank both Dr. Teresa Pérez Prado and Dr. Ilchat Sabirov, who have continued to guide me willingly since my Bachelor's thesis back in 2009. From the institute, there have also been excellent researchers who have guided me, and without whom I could not have completed this thesis. I would like to gratefully acknowledge Dr. Martin Palm for hosting and supervising me during my stay at the Max-Planck Institut für Eisenforschung (MPIE). Likewise, I sincerely thank Dr. Frank Stein for his advice, and the whole Intermetallics Group for their help. All of these people, and also those from Structure and Nano-/Micromechanics of Materials Department, made me feel part of the team while I was in Düsseldorf.

In this dissertation, there is a great deal of work which I cannot claim as my own. Therefore, it is only fair to acknowledge the hard work and endless time that Marcos Angulo Martín expended with me in the furnace. Thanks to him, the continuous failures were more bearable. Similarly, I very much appreciate the hard work of Álvaro Menduiña Fernández, without whom, an important part of this thesis would not be here, and whose attitude encouraged me to continue. In addition, I sincerely appreciate the extraordinary help of Mr. Gerhard Bialkowski with the mechanical behavior testing of the material in such a short space of time, without any kind of complaint and always willing to assist. Moreover, I sincerely acknowledge the help of 'soon to be' Dr. Jian Peng, from the Institute of Applied Materials (IAM) in the Karlsruhe Institute of Technology (KIT), for performing the Thermocalc calculations, and his supervisors, Dr. Peter Franke and Prof. Dr. Hans Jürgen Seifert, for the database used in the calculations.

Moving to another aspect and putting aside the formalities, I would like to thank above all, the people behind the names. During these 4+ years I got to know many people who have accompanied me during all or part of the journey. I

cannot mention each of them individually, but these people, You, are the ones I will keep with me. Some, I hope I will see again as friends, some unfortunately only in memory, but all of them represent the friendly side of this part of my life that has already passed. Thank you.

Finally, I will finish with the most important people, my dearest ones. They have supported me in my darkest moments, and are truly responsible for the completion of this thesis. Among them, my deepest appreciation goes to my closest family: My father, Arcadio Varona Madrid; my mother, Dulce Estrella Caballero López and my sister, Esther Varona Caballero; along with my godmother, María Ángeles Varona Madrid. Thank you very much for always being there.

Resumen

Los compuestos intermetálicos ordenados han ganado atención en la comunidad científica durante las últimas décadas, debido a la interesante combinación de propiedades que presentan, siendo candidatos perfectos como materiales estructurales para aplicaciones de alta temperatura. Especialmente prometedoras son las propiedades de los aluminuros metálicos, entre las que se cuentan: un alto punto de fusión, alta conductividad térmica, alto límite elástico, baja densidad, y una excelente resistencia a la oxidación, debido a la formación de alúmina en la superficie.

De entre ellos, el NiAl fue señalado como el candidato más prometedor para mayores temperaturas. Sin embargo, su baja ductilidad y tenacidad a fractura a temperatura ambiente, así como su baja resistencia y resistencia a fluencia a alta temperatura, hicieron que se redujese el interés por este material. A pesar de ello, se continuó investigando para superar estas desventajas, y los materiales compuestos *in situ* de eutécticos de NiAl, como son NiAl-Cr, NiAl-W, etc., han mostrado los mejores resultados. Aún así, las aleaciones eutécticas binarias tienen una limitación intrínseca, ya que la composición está fijada, y por ello también lo está la fracción volumétrica de la fase reforzante.

En este trabajo se exploró una manera de abordar esta limitación. A través de la introducción de un elemento específico, es posible obtener un material compuesto *in situ* eutéctico de NiAl, en el que la fracción volumétrica de la fase reforzante sea ajustable. Esto se debe a que los eutécticos binarios forman líneas eutécticas en el diagrama de fases ternario, en las que la composición y la fracción volumétrica de la fase reforzante es variable. Este planteamiento fue aplicado al sistema NiAl-Cr-W.

Debido a la gran diferecia entre los elementos de dicho sistema, el procesado de las aleaciones tuvo que ser perfeccionado. Se investigó la producción y uso de prealeaciones como ruta de procesado, lo cual derivó en resultados satisfactorios tanto en colada como en solidificación direccional.

Mediante la medida de la composición del microconstituyente eutéctico en las aleaciones, se evaluó de manera preliminar la línea eutéctica en el diagrama

de fases pseudo-ternario. Los resultados indicaron la existencia de una línea eutéctica discontinua, de la que se determinaron dos secciones en las regiones de alto y bajo contenido en Cr, y además se confirmó la existencia de un hueco entre ambas.

Dicha evaluación fue mejorada por medio de un análisis exhaustivo del recorrido de las aleaciones durante la solidificación, principalmente mediante una mejor caracterización de su microestructura y la composición de sus fases. Además se utilizaron cálculos asistidos por ordenador de forma complementaria. Este estudio demostró que la línea eutéctica discontinua se debe a la existencia de otra línea de reacción en el sistema pseudo-ternario, que no había sido detectada hasta el momento. Esta línea de reacción se forma a causa de la región de inmiscibilidad que presenta el diagrama de fases de Cr-W desde temperaturas muy altas, y se extiende a través del diagrama pseudo-ternario como una reacción peritéctica. La interacción de ambas secciones de la línea eutéctica con esta nueva línea de reacción, es la razón por la cual existe la discontinuidad, formando un punto de equilibrio de cuatro fases de clase II, también llamado reacción tipo U, en el sistema pseudo-ternario. Además, se estudió el efecto de la naturaleza cuaternaria del sistema, respecto al enfoque pseudo-ternario seguido en la investigación, confirmando la validez del método.

Adicionalmente se estudió el comportamiento mecánico a alta temperatura de la aleación multifásica NiAl-20Cr-4.5W (en porcentage atómico), y los resultados indicaron que la aleación presenta unas propiedades a alta temperatura menores, pero comparables, con aquellas de las aleaciones de NiAl más avanzadas desarrolladas hasta el momento. Estos resultados animan a continuar la investigación de éste y otros sistemas de una manera similar, ya que la aleación estudiada no posee una microestructura optimizada como la de las avanzadas.

Abstract

Ordered intermetallic compounds have gained attention over the past decades in the research community, due to their interesting combination of properties, which make them attractive candidates as potential structural materials for high temperature applications. Especially promising are the properties of metal-aluminides, which include high melting point, high thermal conductivity, high yield strength, low density, and excellent oxidation resistance due to the formation of alumina scales.

Among them, NiAl was initially identified as the most promising candidate for higher temperatures. However, its low ductility and fracture toughness at room temperature, as well as its low strength and creep resistance at high temperatures, reduced the interest in this material. In spite of this, further research has been carried out in order to improve the drawbacks, and *in situ* composites of NiAl-based eutectic alloys like NiAl-Cr, NiAl-W, and so on, have brought the best results. All the same, binary eutectic alloys present an inherent limitation, as the composition is fixed, and thus, the volume fraction of reinforcement phase is fixed as well.

In this work, an approach to overcome this limitation is explored. By the introduction of another specific element, it is possible to obtain a NiAl-based fully-eutectic *in situ* composite with a tuneable reinforcement volume fraction. This is because fixed-composition binary eutectics form eutectic troughs in the ternary phase diagram, in which the composition and volume fraction of the reinforcement phase is variable. This approach was studied in the NiAl-Cr-W system.

Due to the large differences between the elements in the system, the processing of the alloys had to be improved. A prealloy production route was investigated, which yielded satisfactory results in casting and directional solidification.

Through the measurement of the composition of the eutectic constituent present in the alloys, the eutectic trough in the pseudo-ternary phase diagram was initially assessed. The results showed a discontinuous eutectic trough, in which two sections in the Cr-rich and Cr-lean regions were assessed, and a gap between both was acknowledged.

The assessment was enhanced by thorough analysis of the path followed during solidification of the alloys, mainly by further characterization of their microstructure and phases composition. Complementary computer-aided calculations were also used. The study revealed that the discontinuous eutectic trough occurs due to the existence of a non-reported reaction line in the pseudo-ternary system. This line forms owing to the miscibility gap present in Cr-W phase diagram, which extends up to high temperatures in the pseudo-ternary diagram, and develops as a peritectic reaction. The interaction between the eutectic trough sections and this new reaction line is the cause of the discontinuity, forming a point of class II four-phase equilibria, or U-type reaction, in the pseudo-ternary system. Furthermore, the effect of the quaternary nature of the system in the pseudo-ternary approach used in the investigation was studied, and the method validity was confirmed.

Additionally, the high temperature behavior of multiphase NiAl-20Cr-4.5W (in at.%) alloy was studied, and the results revealed that the alloy exhibits high-temperature properties which are inferior, but comparable, to those of the most advanced NiAl-based alloys developed so far. These results are encouraging for further research in this and other systems with a similar approach, as the tested alloy does not possess an optimized microstructure like that of advanced alloys.

Contents

List of Abbreviations and Acronyms

at.	atomic
bal.	balance
BCC	Body Centered Cubic
BSD	Back Scatter Detector
BDTT	Brittle-Ductile Transition Temperature
CTE	Coefficient of Thermal Expansion
COP21	21st Conference of the Parties
DS	Directional Solidification
EDM	Electro-Discharge Machining
EDX	Energy-Dispersive X-ray Spectroscopy (also EDS or EDXS)
EPMA	Electron Probe Micro-Analysis
ESA	European Space Agency
EU	European Union
FAST	Field-Activated Sintering Techniques
FAHP	Field-Assisted Hot Pressing
FEM	Finite Element Model
GE	General Electric
HIP	Hot Isostatic Pressing
HV	*Vickers* Hardness
IAM	Institute for Applied Materials
KIT	Karlsruhe Institute of Technology
LMC	Liquid Metal Cooling
LOM	Light Optical Microscopy

LPT	Low-Pressure Turbine
MA	Mechanical Alloying
MPIE	Max-Planck Institut für Eisenforschung
NPU	Northwestern Polytechnical University
ODS	Oxide-Dispersion Stregthening
PM	Powder Metallurgy
ppm	parts per million
RT	Room Temperature
SE	Secondary Electrons
SEM	Scanning Electron Microscope
SPS	Spark Plasma Sintering
TBC	Thermal Barrier Coating
TIT	Turbine Inlet Temperature
ZMLMC	Zone-Melted Liquid Metal Cooling

List of Figures

List of Tables

List of Tables

Nomenclature

$^\circ$C	Degree Celsius
d	Grain size
E	Young modulus
K	Kelvin
n	Stress exponent
Q	Activation Energy
ρ	Density
T_m	Melting Temperature
T_O	Critical Ordering Temperature

1

Introduction and State of the Art

1.1 The recurrence of an old challenge

Currently, humankind stands at a critical point in its history. The socioeconomic juncture together with the new “green” politics, legislated in order to build a base for a sustainable prosperity, have created a new set of environmental conditions suitable for fostering further development. The evidence on global climate change was visible at the recent United Nations Climate Change Conference (COP21), and is supported by global agreements and expensive observation programs. One of them is the European Space Agency’s (ESA) Copernicus program, with a budget of several billion euros, to cover the operation of the sentinel satellite network that has already been deployed, and the construction of the remaining satellites. This, combined with the global economic crisis, increasing competitiveness, and globalization, constitute the main reasons for this course change.

In this context, it is understandable that in many sectors there is great interest in reducing costs, in order to maintain competitiveness, as well as trying to comply with the increasingly demanding international regulations which are particularly strict in the European Union (EU). This is especially relevant in the transport sector. The strict carbon emissions regulations in this field have led recently to rigged results by some leading automotive industries, in their desire to be able to benefit from tax exemptions.

In the case of the aircraft industry, due to sustained growth in the demand for air travel in recent decades, these emissions are accounting increasingly for a significant part of the total fossil fuel emissions, therefore becoming increasingly significant in tackling the problem. Moreover, there is concern relating to the reduction of aircraft operational costs, which largely depend on the consumption of this fuel [1]. This issue is connected to the development of more efficient jet engines.

The fuel consumption in an engine is directly related to the maximum temperature of the thermodynamic cycle, which in this case is the Turbine Inlet Temperature (TIT) [1–3] of the gas turbine. This increase can significantly enhance the performance of turbines, thus reducing fuel requirements. It is important to note that this fact applies equally to the power generation industry, being important in increasing efficiency, which will lead to a reduction in emissions in a sector which is the largest contributor to the total emissions [4]; it will also to the optimization of use of resources in new power plants [5]. However, this is not a simple task, as the TIT is ultimately limited by the maximum working temperature of the materials from which the components are made.

From the first gas turbines, the development of new materials with higher working temperatures, combined with cooling systems and thermal barrier coatings (TBC), to reduce the component working temperature, has been a keynote in order to increase their efficiency. Nickel-based superalloys have been the quintessential materials for this purpose for decades. However, despite new developments, these types of alloys are reaching their limits, in some cases already working at temperatures near to 90% of their melting point [6]. Moreover, there is an absolute limiting factor for the capability of Ni-based superalloys, which is the melting temperature of its base material, nickel [7]. Therefore, a significant research effort is being carried out to develop new materials which are able to work under the intended operating temperatures and at the same time, maintaining acceptable mechanical properties, as well as withstanding the extremely aggressive environment which they would be exposed to.

1.2 Intermetallics: The eternal promised land

The use of refractory materials in the hottest parts of gas turbines has been a recurring theme recent decades [8–15], as a possible solution to overcoming the temperature limitations of Ni-based superalloys. The research efforts have focused on Niobium and Molybdenum as bases for the novel alloys. However, these systems have shown two major deficiencies at high temperatures: inadequate mechanical behavior and catastrophic corrosion resistance.

Over the past decades, there has been rapid research growth in ordered intermetallic aluminides as potential materials [16, 17], as they exhibit an interesting combination of properties for high temperature applications [18], such as: high melting point, high thermal conductivity, high yield strength, low density and excellent oxidation resistance due to the formation of alumina scales, as can be seen in Table 1.1 [19–28].

Table 1.1: Properties of some metal-aluminide intermetallics [19–28].

Intermetallic	Crystal Structure	T_m/T_O(°C)	ρ(g cm^{-3})	E(GPa)	BDTT(°C)
Ni_3Al	fcc ($L1_2$, cP4)	1390/1390	7.5	179	Ductile at RT
NiAl	bcc (B2, cP2)	1674/1674	5.86	294	400
Fe_3Al	bcc ($D0_3$, cF16)	1540/540	6.72	141	Ductile at RT
FeAl	bcc (B2, cP2)	1250/1250	5.56	261	300-400
Ti_3Al	hcp ($D0_{19}$, hP8)	1600/1180	4.2	145	600
TiAl	Tetragonal ($L1_0$, tP4)	1460/1460	3.91	176	700-800
Nb_3Al	bcc (A15, cP8)	2060/2060	7.28	169	1200
Nb_2Al	Tetragonal (σ, tP30)	1940/1940	6.91	-	1200

T_m = Melting Temperature; T_O = Critical Ordering Temperature; ρ density; E = Young Modulus; BDTT = Brittle-to-Ductile Transition Temperature.

Intermetallic materials constitute a unique class of metallic materials which form long-range ordered crystalline structures (Fig. 1.1) below a critical temperature [30]. These alloys usually exist only within a narrow composition range, around simple stoichiometric ratios. The interest in intermetallics decayed in the 60s due to their high brittleness at temperatures lower than their brittle-to-ductile transition temperature (BDTT), which is usually relatively high, typically showing no ductility at room temperature (RT). One of the distinctive mechanical characteristics of these ordered compounds is that they have, in general, a very well-marked transition from brittle to ductile behavior happening at a certain temperature, which can range from below RT to several hundred degrees. Due to such high brittleness at RT, they could not even be manufactured, or when possible, the fracture toughness was so low that their use in components such as structural materials was not

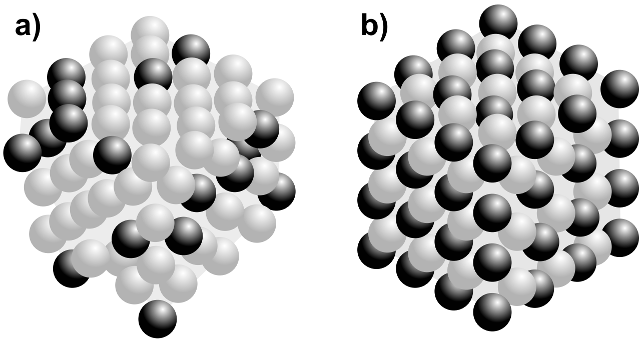

Figure 1.1: Atomic arrangement in a) a regular alloy with disordered structure and b) in an intermetallic compound with long-range ordered structure [29].

acceptable.

However, since the 1970s, new results have been published [31–33], reporting that the ductility and manufacturability of some intermetallics could be enhanced drastically through metallurgically-based principles. One example is the case of Ni_3Al, whose ductility was increased by adding small amounts of Boron [34]. Moreover, Ni_3Al is one of the main reasons why Ni-based superalloys show such outstanding properties.

Since then, an enormous effort has been carried out in order to improve the properties of intermetallic alloys for their application as structural materials. And it was not until recent years, when the improvements in terms of processing and mechanical behavior have been sufficient, bringing a whole new set of current and future applications, including gas engine and automotive high-temperature components, tools, dies, corrosion resistant materials for piping, coatings, and so on. [16, 28].

This is the case, for example, of Ni_3Al- and FeAl-based alloys for transfer rolls, trays and posts for heat treatment, rails, radiant-burner tubes, grate bars, die blocks, ceramic mixing paddles, nuts and bolts, automotive piston valves, corrosion resistant tool bits and porous gas-metal filters [35], in most cases substituting parts previously made of steel. This substitution is promoted in the industry, not only due to the better properties, but also because of the difference in price compared with advanced chromium steels used for high temperature applications.

On the other hand, titanium aluminides have gained attention for their application in the automotive and aerospace industries mainly due to their low density, strongly reducing the structural weight of components and therefore, increasing engine performance and fuel efficiency. The applications include: turbocharger wheels, piston valves and low-pressure turbine (LPT) blades [36]; the latter already implemented in some General Electric (GE) turbofan engines and flying in the latest airplane generations.

The research into intermetallics for ultra-high temperature applications, namely silicides of Mo or other transition metals such as Nb, is progressing as well for applications in gas turbines, molten-metal lances, protection sheaths, gas burners and glow plugs among others [28], with advances in their mechanical behavior at these ultra-high temperatures, and especially in their oxidation resistance [25].

However, in Table 1.1 it can be seen that there is still an intermetallic compound whose set of properties identify it as a great candidate for high temperature applications: The NiAl.

1.3 The great potential of NiAl intermetallic compound

Ordered B2-NiAl intermetallic compound has attracted a lot of attention as one of the most promising candidates for these high temperature applications. It has a B2 structure, which in turn is based on a body centered cubic (BCC) type structure, in which the Ni atoms are located at the corners, while aluminum is found in the center, as with FeAl intermetallic (Fig.1.2b). NiAl exhibits a high melting point (1674 °C [27]), relatively low density (5.86 g cm^{-3}), and high Young's modulus and yield strength ($>$1000 MPa) [21, 29, 37, 38]. In addition, it has high thermal conductivity (92 W m^{-1} K^{-1} [39]) and an excellent resistance to corrosion and oxidation due to the formation of alumina scales [40, 41], which can be enhanced with additions of other elements [42, 43]. The major drawbacks of NiAl are its low ductility and fracture toughness at room temperature, as well as limited strength and creep resistance at high temperatures. However, the ductility increases above 400 °C, and NiAl becomes very ductile above 600 °C [21, 28, 37, 38].

From the phase diagram (Fig.1.2a) it can be also seen that NiAl is stable in a wide range of compositions around the stoichiometry, and its properties vary depending on whether it is in the Ni-rich or Al-rich zone, due to the introduction of substitutional atoms or vacancies respectively [21, 28, 37, 38]. All these exceptional properties have led to its use as thermal barrier coatings (TBC) for some Ni-based superalloy components [44].

Thermal Barrier Coatings (TBC) refer to the coatings on the superalloy surface of components used in environments at high temperatures as in a gas turbine, which lower the actual working temperature of the component while at the same time, serving as protection from oxidation [48–52]. As shown in figure 1.3, the coating is actually composed of two layers: The top ceramic coat is responsible for temperature decrease, while an oxidation resistant metallic bond coat is responsible for bonding between component and ceramic. In the latter case, the outstanding properties of NiAl play a fundamental role.

All the same, there are some mechanisms which can lead to degradation and failure of

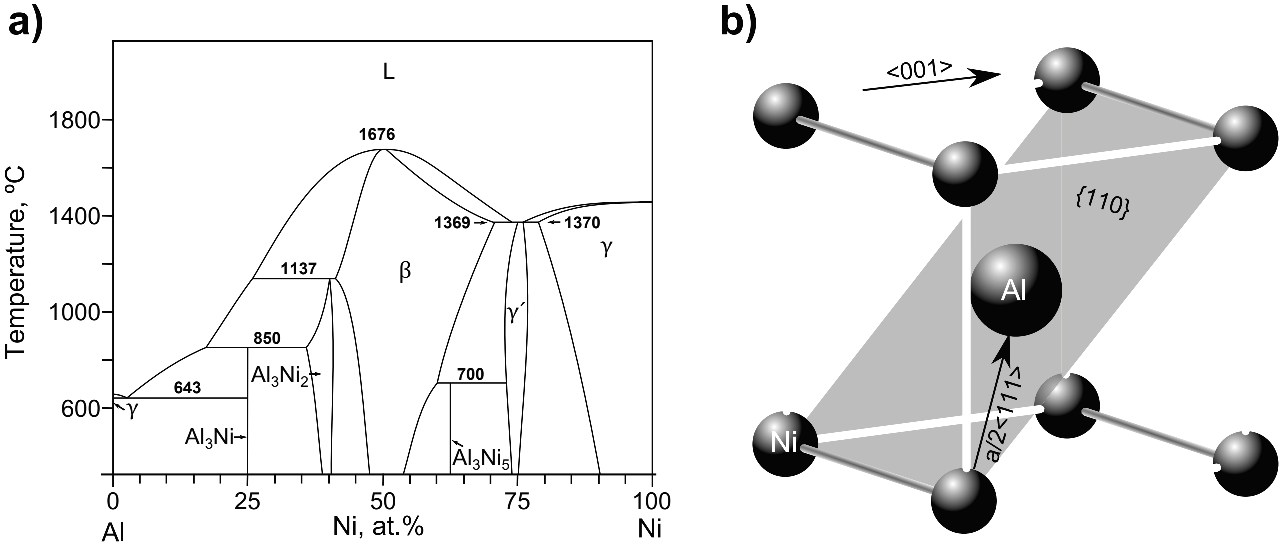

Figure 1.2: Binary phase diagram a) of the Al-Ni system [45, 46] including the NiAl region (β) around the 50 at.% and b) its cell unit with the main slip system [47].

NiAl bond coats, and thus reduce the life-time of the substrate. One of the most important degradation mechanism comes from the composition gradient between bond coat and substrate, which on exposure to very high temperatures for long periods of time, acts as a diffusion couple and activates interdiffusion. Due to the difference in composition, Al diffuses into the substrate, which can induce several changes in the system [49–51, 56–58] such as:

- Formation of new phases in the substrate which can be detrimental to its mechanical behavior.
- Transformation into Ni_3Al, which changes properties of the coating, including the thermal expansion coefficient (CTE), which is of paramount importance in this application and can induce troublesome stresses.
- Reduction of the oxidation resistance of the bond coat due to Al depletion.

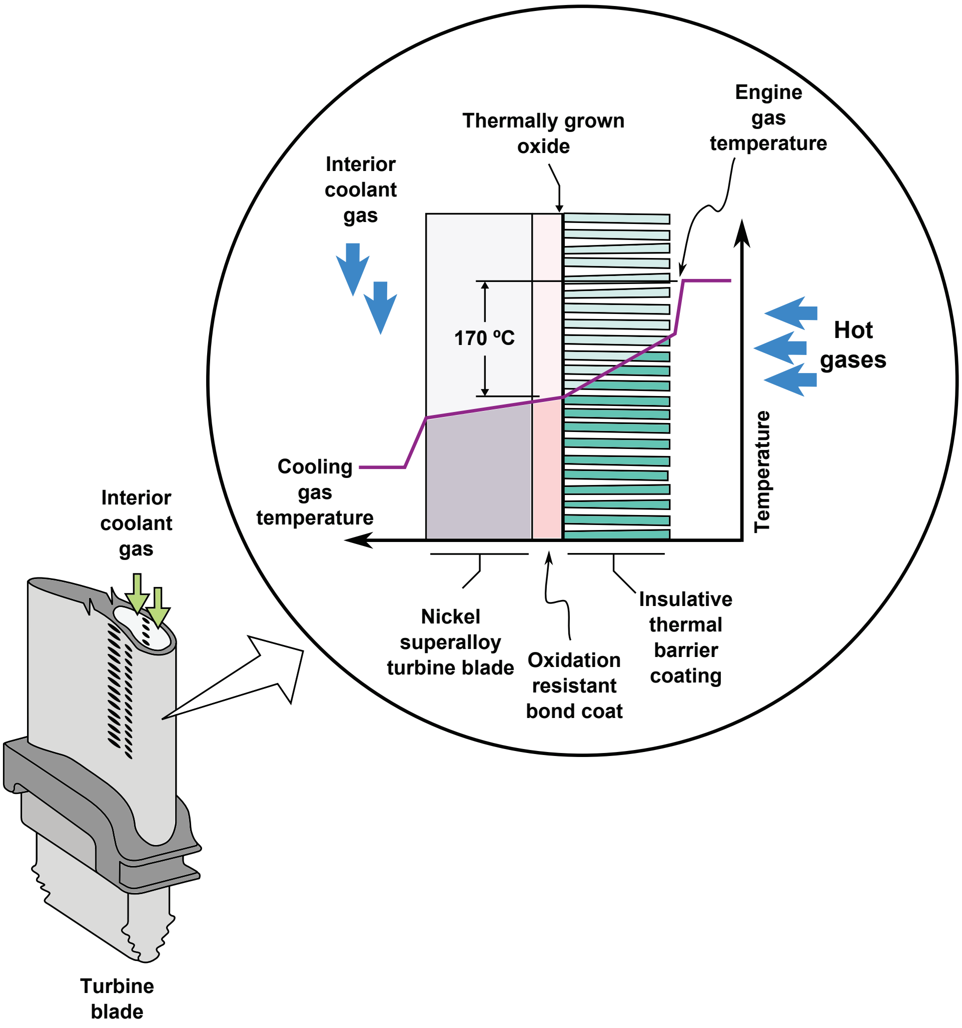

Figure 1.3: Model of the heat gradient in a turbine blade due to the effect of a TBC and cooling systems [53–55].

This phenomenon limits the life time of such a coating assembly. Therefore, research has been carried out [49, 50, 57, 58] in order to enhance the life time by additions of some elements like platinum (Pl), palladium (Pd) and Ruthenium (Ru). However, these elements are rather expensive and, due to the working conditions, this limitation will not be suppressed unless the composition gradient is avoided. For that reason, using NiAl intermetallic as a blade material seems to be a good approach to reducing compatibility issues. Moreover, the cooling systems associated with these kind of components would be much more efficient owing to the greater thermal conductivity of NiAl. This results in a decrease on the effective working temperature of the component, adding value to the use of this intermetallic compound.

Despite there having been progress following decades of research, and its application for implementation in gas turbines having been tested, NiAl has not yet been developed as a viable material for structural applications, and greater efforts should be made in order to overcome its drawbacks. However, NiAl compound is interesting enough to keep research [59]. Additionally, it is being studied as a shape memory alloy [60], which adds relevance to the research of the material, opening the door to multifunctional components.

1.4 The (re)search for the final enhancement

From all the drawbacks hindering the implementation of NiAl intermetallic, the most difficult challenge is probabloy increasing the ductility at RT at the same time as improving the mechanical behavior at high temperatures. Research is being carried out on approaches to overcome these problems, such as reduction of grain size, the introduction of a ductile phase as reinforcement, as well as the introduction of a hard phase.

1.4.1 Size matters: The grain size approach

NiAl BDTT has been studied as a function of grain size, where it was found that in samples prepared by powder metallurgy hot extrusion, a large increase in ductility (fig. 1.4) could be observed at 400 °C for grain sizes below 20 μm [61]. Moreover, nanocrystalline-grained intermetallics have shown an improvement in RT ductility [62, 63], as well as in other mechanical properties [64].

In that regard, it is interesting that powder metallurgy (PM) is being extensively used in superalloy production for highly alloyed components, and the alloys produced have demonstrated improvements in the properties through the control of grain morphology and by prevention of segregation [65]. For production, powders are usually produced by atomization under inert atmosphere, which are later consolidated by extrusion and/or hot isostatic pressing (HIP), with the latter being used to produce the final component or billets

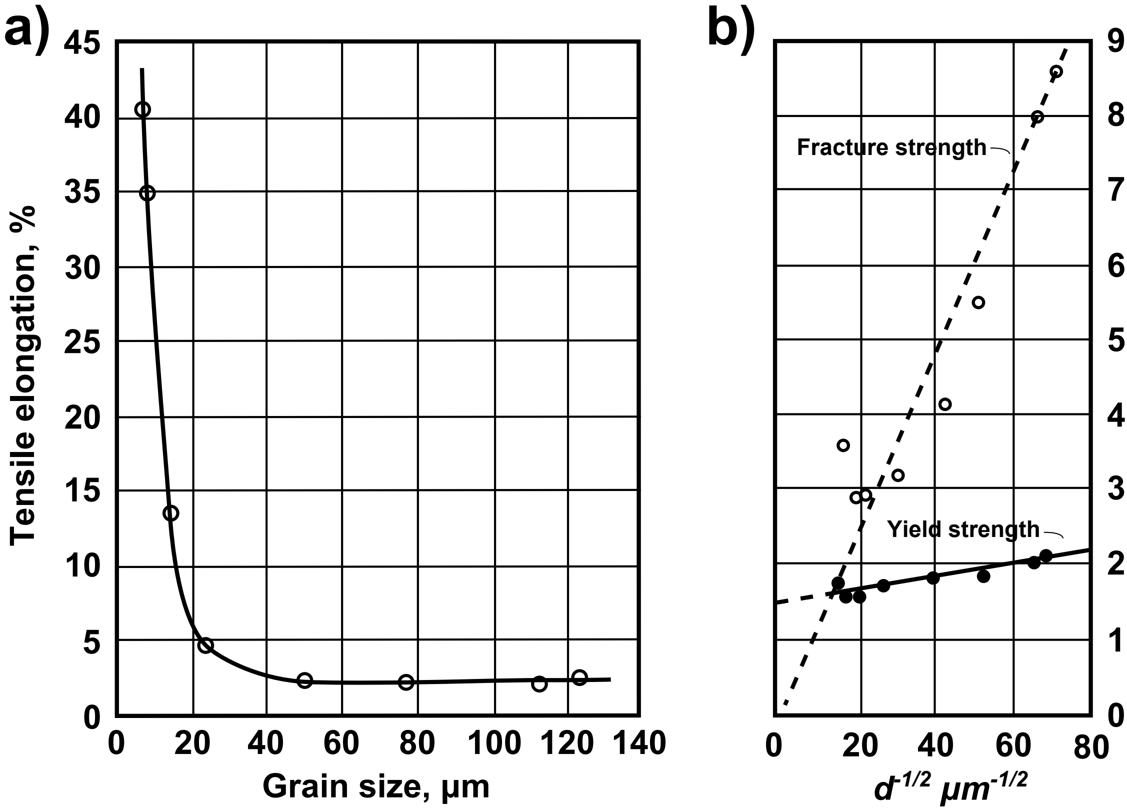

Figure 1.4: Effect of grain size (d) on the properties of NiAl at 400 °C: a) tensile elongation and b) yield and fracture strengths [61].

that are finally forged.

Mechanical alloying (MA) [66] is another method for powder synthesis and grain refinement which has been established as a simple solid-state technique to obtain equilibrium and non-equilibrium phases from the elemental powders with nanocrystalline-grained microstructure. The feasibility of obtaining solid solutions and intermetallic phases in different systems through MA [67–69], including nanocrystalline-grained NiAl compound has been reported [70–73]. Additionally, mechanical alloying is suitable for oxide dispersion strengthening (ODS) [74–76], as well as forming other composite materials of NiAl [77, 78]. Afterwards, the powder is consolidated.

In order to achieve a good control on the microstructure of the final components, activated sintering techniques are the best choice so as to obtain homogeneous, near-full dense materials, avoiding grain growth. This activated sintering refers to those techniques that lower the activation energy for sintering. The interaction of pressure and temperature shows advantages for sintering nanocrystalline-grained powders compared to conventional methods, mainly reducing the consolidation temperature. New plasticity-driven densification mechanisms such as local yielding as well as creep and stress-assisted diffusion are activated. Moreover, pressure can induce rearrangement of particles and collapse of pores, increasing the contacts between particles [79]. Several methods have been applied successfully for NiAl and other intermetallic alloys. In these studies, methods such as reactive sintering and hot isostatic pressing (HIP) were used, and the effect of ternary element additions on the process has been investigated [80–82].

Besides, the application of an electric current can also enhance the sintering kinetics of the process, resulting in higher densities at lower temperatures and shorter times. Various field-activated sintering techniques (FAST) have been developed [79], such as spark-plasma sintering (SPS), being successfully applied to NiAl [83] and other materials [84–86]. Recently, a novel method denominated field-assisted hot pressing (FAHP) has been established and successfully applied to TiAl and NiAl intermetallics [87, 88].

Therefore, obtaining nanocrystalline-grained NiAl bulk components reinforced by hard phases is possible through mechanical alloying of elemental powders, and posterior consolidation by activated sintering techniques. Moreover, these techniques are currently used to produce superalloy components for application, so the technology is available. For that reason, it is an encouraging approach to try to increase the intermetallic ductility at low temperatures, as well as improving its mechanical behavior at high temperatures.

1.4.2 Quantity or quality: The reinforcement phase approach

On the other hand, large parts of the research being carried out to overcome NiAl implementation issues have leaned towards the introduction of a ductile phase as reinforcement of the intermetallic matrix [89], in order to increase ductility and fracture toughness of components [90, 91]. This approach benefits from the eutectic reaction taking place in some pseudo-binary phase diagrams between NiAl and different refractory metals [47], including, among others, chromium, molybdenum, rhenium, tungsten and vanadium.

The formulation ”pseudo” to describe a phase diagram comes from the fact that any system containing NiAl plus another element will have in fact three elements (Ni, Al and the third element, whether it is Cr, Mo, etc.) and therefore be a ternary diagram. However, NiAl intermetallic compounds ideally have a fixed stoichiometric composition which remains constant, as well as a congruent melting point, being possible to treat it as one component. These pseudo-binary diagrams are indeed only a section of a ternary diagram, where the rules used to calculate phase compositions and volume fractions are no longer applicable, because of the actual compositions of the phases lying outside of the pseudo-binary. As a matter of fact, the different solid solubility of Ni and Al in the second phase has been detected in this investigation as well as in other studies [92]. Therefore, the Ni/Al ratio is not kept constant to one as it is for stoichiometric NiAl. Nevertheless, a ”pseudo” phase diagram can be used as an approximation.

A eutectic is a reaction present in some alloy systems, and is characterized by the simultaneous growth of two or more phases from the liquid. Eutectics have an excellent casting behavior, similar to that of a pure metal, plus the benefits of a composite in their properties [93]. In the case of NiAl, these eutectic alloys exhibit a composite structure consisting of a NiAl matrix reinforced by the refractory metal in the form of lamellae or fibers, depending on the volume fraction. The eutectic reaction enables the production of *in situ* composites from the liquid state. With high thermal gradients and low growth rates, a planar solid-liquid interface can be kept, growing steadily in the direction of the thermal gradient. This is the case with directional solidification (DS) technique, where well-aligned, fully eutectic microstructures can be formed.

These *in situ* composites, due to their processing, are inherently more stable up to their melting point. The eutectic structure may be subjected to coarsening like any other microstructure at high temperatures; however, no chemical reactions will take place between matrix and reinforcement, as could be the case of metal-matrix composites produced by other liquid-state techniques, and especially for solid-state techniques. Additionally, the existence of perfectly aligned, evenly spaced, continuous reinforcement can greatly improve the mechanical response of the alloy [94]. In order to improve the strength and fracture toughness in these multiphase intermetallics, there are some factors which have a decisive role [94]:

- The properties of the reinforcing phase such as Young's modulus, yield strength and ductility.
- The properties of the interface, its strength and the crystallographic orientation between both phases.
- The volume fraction, size and morphology of the reinforcing phase.

The plasticity mechanisms, which control the deformation and fracture in these alloys, result in an enhanced fracture resistance compared to that of the intermetallic. The toughening mechanisms responsible for this enhancement can be of an intrinsic or an extrinsic type. If the plasticity of the matrix is improved, then we are talking about intrinsic mechanisms. It occurs when the yield strength of the reinforcing phase is lower than that of the matrix, so it yields first. This leads to stress concentration at the interface due to dislocation pile-up, which is relieved by a slip transfer from the reinforcement to the matrix, thus increasing the composite global plasticity. Intrinsic mechanism is typical for face centered cubic (FCC) metal reinforcement [94, 95].

On the other hand, extrinsic mechanisms are the ones dependent on the interaction of NiAl cracks with the reinforcement. These mechanisms are basically crack bridging and crack trapping (Fig 1.5) [90, 94]. Extrinsic mechanisms are highly dependent on the properties of the interface, as well as on the volume fraction and morphology of the

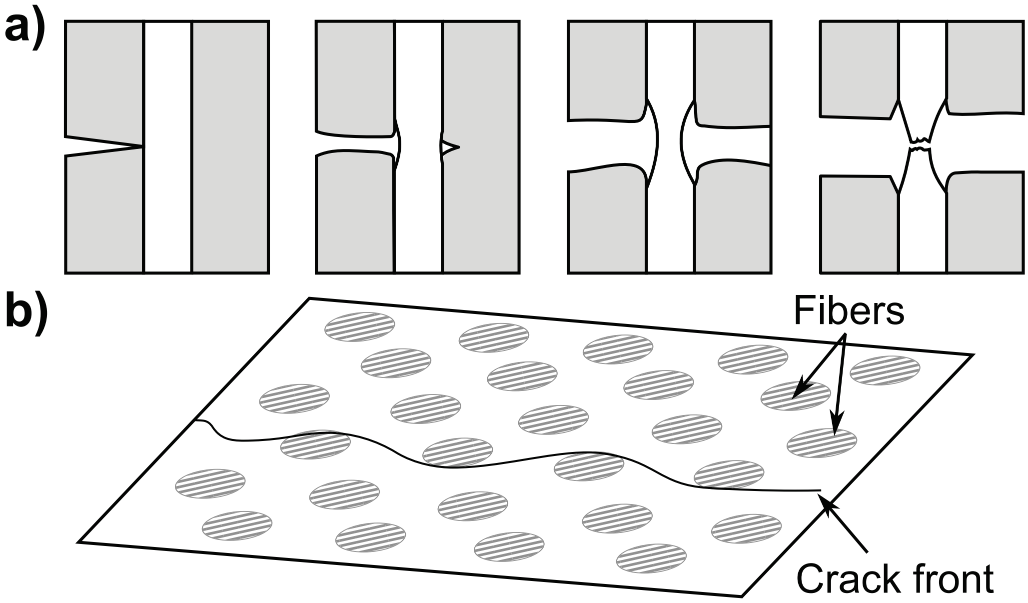

Figure 1.5: Extrinsic toughening mechanisms in eutectic *in situ* composites: a) crack bridging and b) crack trapping [90].

reinforcing phase [90]. Therefore, it is important to have strong interface cohesion to avoid debonding, together with a high volume fraction of the reinforcing phase. The total toughness enhancement will be the result of the contributions of both intrinsic and extrinsic mechanisms taking place. The occurrence of these mechanisms in NiAl in situ composites with bcc refractory metals has been reported, improving its fracture toughness [90, 94–98].

Regarding this matter, several alloy systems have been studied such as NiAl-Cr [47, 96, 99–101], NiAl-Mo [47, 102–104], NiAl-V [105–109], NiAl-Re [47] and NiAl-W eutectics [110]. Furthermore, the addition of other elements has been studied as well, such as Ta [80], Hf, Ho and other rare earth metals [111–114]. The purposes of adding new elements to the alloy were diverse: from rare earth elements to increase ductility, to elements forming hard phases, such as Heusler phases with Hf, in order to increase the high temperature strength and creep behavior of the alloys [115, 116]. *In situ* composites from NiAl plus Laves phases have been produced as well, exhibiting high creep strength close to that of a single crystal Ni-based superalloy, but with poor fracture toughness [117, 118].

One of the most promising alloys was the NiAl-Cr eutectic, with a reinforcement volume fraction of about 35% [47]. The microstructure of this eutectic is fibrous, with NiAl matrix and Cr fibers evenly distributed. This fact greatly enhanced the fracture toughness of the intermetallic. The Young's modulus (*E*) was also increased, being one of the highest among these alloys, which was reflected in very high flow stresses at RT [47]. However the mechanical properties drop rapidly when increasing the temperature, which is related to its relatively low melting temperature, of 1455 °C [119]. Similarly, NiAl-Mo eutectic with a reinforcement volume fraction of about 12% [99], also showed a fairly good mechanical behavior, and the drop at high temperature was less steep than for Cr. Its better thermal stability could be connected to its higher melting temperature, of 1600 °C [47]. Later on, more complex alloys were produced mainly by substitution of some Cr by Mo in the NiAl-Cr pseudo-binary eutectic. These NiAl-Cr(Mo) alloys showed a change in the microstructure from fibrous to lamellar, maintaining or even increasing fracture toughness at room temperature, together with a better high temperature behavior [96]. This change from fibrous to lamellar morphology depends mainly, although not only, on the volume fraction of the reinforcing phase [93, 108].

On the other hand, NiAl-W eutectic [110], and its very similar counterpart NiAl-Re eutectic [47], showed the most promising improvements of the mechanical behavior of NiAl intermetallic mainly at high temperatures. The high melting temperature of both eutectics, around 1665 °C [27, 110], could account for their better thermal stability, retaining the good mechanical properties up to very high temperatures. However, although the Young's modulus of Re and W are higher than those of Cr and Mo, the composite Young's modulus is not enhanced as it is in the Cr and Mo eutectics [47, 99]. Nevertheless, these two eutectics show a very low reinforcement volume fraction, with just 1.4% in the case of NiAl-W [110], hindering a full enhancement of the intermetallic behavior.

1.4.3 Quantity does matter

Although NiAl-based *in situ* composites exhibit encouraging enhancements in the mechanical behavior of NiAl intermetallic, especially in the pseudo-binary eutectic systems with refractory metals, the improvement in these alloys is still inadequate to substitute the current generation of Ni-based superalloys [7, 59]. Further development has to be carried out in order to greater improve the effect of toughening mechanisms. As previously explained in 1.4.2, these mechanisms depend highly on the volume fraction of the reinforcing phase. Therefore it would be interesting to follow this approach as an attempt to enhance the mechanical behavior of NiAl-based alloys and study the effect of volume fraction increase. However, there is an intrinsic limitation on this approach, as the volume fraction in a eutectic alloy is fixed.

In keeping with previous explanations, the eutectic reaction is an invariant where a liquid phase is in equilibrium with two or more solid phases at a certain temperature. The reaction takes place at a given composition on the phase diagram. This means that the highest volume fraction achievable in an alloy of a eutectic system happens in a fully eutectic alloy, where the amount of each phase is determined. In the case of binary or pseudo-binary eutectic systems, as is the case of NiAl with refractory metals, the eutectic constituent is composed of two phases, each having a set fraction of the volume. Although the morphology of a eutectic can change depending on the processing conditions, it is not possible to change both the size and spacing of the reinforcement in these *in situ* composites independently, because the volume fraction is constant. The spacing will change depending on the growth rate and undercooling of the process, the latter being ideally minimal for equilibrium conditions. As the growth rate increases, the interspacing of phases in the eutectic decreases, whilst the same happens with their size, decreasing with increasing growth rate, and the volume fraction remaining fixed [93, 120]. Therefore, pseudo-binary eutectic systems have a limited toughening capability.

However, it is known that out of near-equilibrium conditions, at compositions close to the eutectic and at a range of growth conditions, the eutectic phase can grow faster than the primary phases, outgrowing them. Therefore, coupled eutectic growth can happen in off-eutectic compositions, obtaining fully eutectic microstructures. These conditions can be reached for example in DS processing, with low growth rates and/or high temperature gradients [93, 121]. This off-eutectic compositions region where eutectic growth is possible, is called the coupled zone, and it has also been observed in some NiAl pseudo-binary eutectics [27, 90, 110]. The coupled zone can be symmetric or skewed (Fig.1.6), depending on the regularity of the eutectic, which is associated with the similarity of the undercooling of both phases. Regular eutectics have typically symmetric coupled zones, whilst irregular ones have skewed coupled zones. Due to these skewed couple zones, alloys which have eutectic compositions can show dendrites of a primary phase, and off-eutectic compositions can show full eutectic microstructure. This can lead to trouble in determining the eutectic composition, as was the case of NiAl-W and NiAl-Re systems, where different eutectic compositions were reported by different authors [27, 110, 122, 123]. In any case,

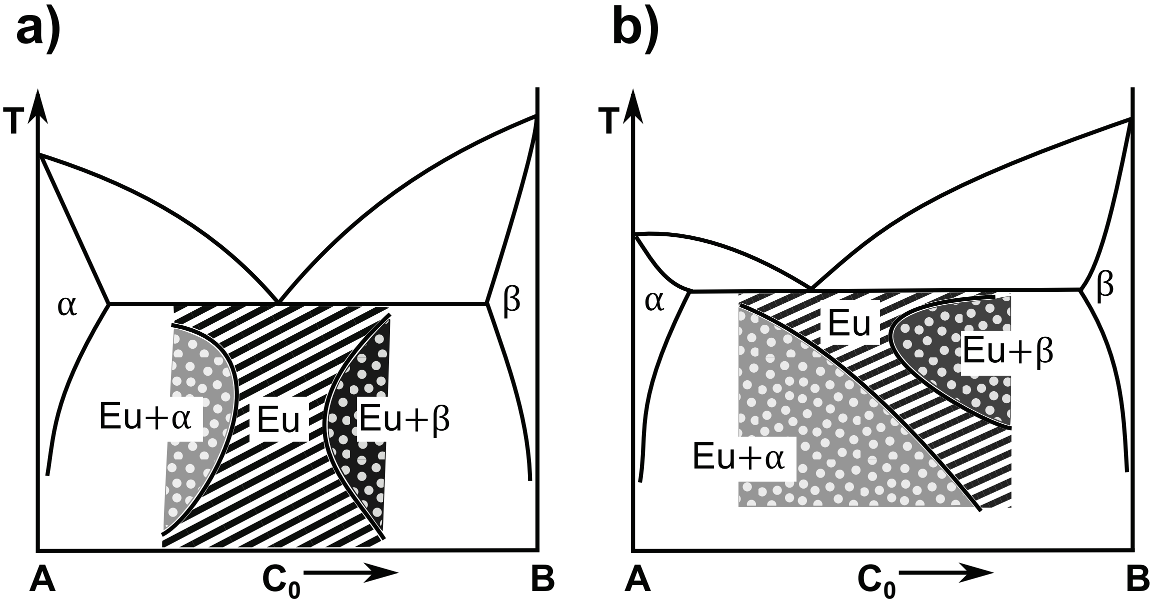

Figure 1.6: Phase diagrams of a eutectic system with a) symmetric coupled zone and b) skewed coupled zone [121].

symmetric and skewed coupled zones can lead to the production of alloys with fully eutectic microstructure from off-eutectic compositions, opening up the possibility of finally modifying the volume fraction of the reinforcement.

This approach was followed recently by Zhang *et al.* [90], where alloys of NiAl-Mo with different compositions (7.8, 9, 13 and 16 at.% Mo) were produced by directional solidification. It was reported that all the alloys presented a full eutectic microstructure, with uniform, well-aligned Mo fibrous structures. The increase on Mo content decreased the spacing between fibers and increased the size and the overall volume fraction of the fibers. The increase in volume fraction promoted the toughening extrinsic mechanisms of crack trapping and bridging, reflected in a higher RT fracture toughness, which increased from 13.5 to almost 19.5 MPa m$^{-1/2}$ when the Mo content was increased from 7.8 to 16 at.% [90]. These values are already close to those reported for NiAl-Cr eutectic, although still a bit lower than those of NiAl-Cr(Mo) [96].

A similar approach was followed even more recently by Shang *et al.* [98] on NiAl-Cr(Mo) alloys, where the content of the reinforcing phase was increased from 34 to 42 at.% Cr(Mo) by keeping the Mo content fixed to 6 at.% and increasing Cr content from 28 to 36 at.%. The alloys produced showed a fully eutectic lamellar microstructure. A RT fracture toughness of 25 MPa m$^{-1/2}$ was reported with the highest reinforcement volume fraction (59%), highlighting the positive effect of this method. However, the material response in these studies depended strongly on the final microstructure and also on the morphology of the solid/liquid interface during solidification, which ultimately defines the alignment of the reinforcement [124]. The best results were obtained when primary dendritic growth was suppressed and planar interfaces were achieved. For this to happen the solidification conditions were a high thermal gradient of about 250 K cm^{-1} and low growth rates of 6 μm s^{-1}, which were obtained by liquid metal cooling (LMC) DS. In order to increase the growth rate for faster production, keeping the planar interface, a thermal gradient of 600 K cm^{-1} was needed, and obtained through the zone-melted liquid metal cooling technique (ZMLMC) [98]. Although growth rate parameters are similar to those of other DS systems, the thermal gradients which can be achieved in industrial-scale furnaces are one order of magnitude lower [103], making it imposible to produce these alloys on a large scale.

1.5 Adding a new degree of freedom: The pseudo-ternary diagram

An alternative approach can be followed in order to try to avoid extreme solidification conditions, at the same time as adding a new degree of freedom to reach an increment on the volume fraction of the reinforcing phase. As already explained, the eutectic reaction is an invariant reaction happening at a fixed composition in the phase diagram. This is true for binary eutectics in binary phase diagrams and for ternary eutectics in ternary phase diagrams. As many as four different phases have been observed growing simultaneously in what would be a quaternary eutectic [93]. However, a new dimension is obtained by adding a new element to a binary eutectic system. In this ternary diagram, the binary eutectic diagram is nothing more than a boundary condition of the ternary, and the binary eutectic taking place at the boundary will continue into the ternary phase diagram. The result would be what is called a eutectic trough [125].

A eutectic trough is a monovariant line on the liquidus surface of a ternary phase diagram, with a temperature lower than the surroundings, forming a valley-like shape on the liquidus surface. On each point along this line, another binary eutectic reaction will take place forming different eutectics, each of them being formed by slightly different phases. This fact enables the possibility of modifying the reinforcement volume fraction in a binary or pseudo-binary eutectic by the addition of a new element. In the case of a ternary system in which the boundary conditions, namely the three binary phase diagrams between each two of the three elements, form two binary eutectic systems, and the third system presenting complete miscibility, a ternary phase diagram with a continuous eutectic trough joining both binary eutectics could be obtained [125]. In figure 1.7 a model of a system with these characteristics is presented in order to better understand the concept.

In the context of NiAl eutectics, by combining two pseudo-binary eutectic systems with two refractory metals which have complete miscibility between each other, it would be possible to develop new NiAl-based eutectic composites with tunable properties. Especially interesting would be to combine two systems, where one has a high enough volume fraction of reinforcement phase, as is the case of NiAl-Cr, to increase the toughening effect, and the other system showing higher thermal stability and being able to retain the good mechanical properties at high temperatures; this is the case of NiAl-Re and NiAl-W. Luckily, one of these two possibilities is feasible. The Cr-W system shows complete miscibility at high temperatures in the binary phase diagram, opening up the possibility of having a continuous eutectic trough in the pseudo-ternary diagram, upon which properties could be tuned. Along this hypothetical eutectic trough, both the volume fraction and composition of the reinforcing phase could be modified in order to design the alloy properties.

Along with the system proposed here, the Cr-Mo binary phase diagram also shows complete miscibility at high temperatures. This is the reason why a fully binary eutectic microstructure is obtained in the alloys studied of the pseudo-ternary NiAl-Cr(Mo) system [96]. In this pseudo-ternary system, the eutectic trough close to the NiAl-Cr binary eutectic seems to follow a straight line, in which the combined content of Cr and Mo is constant to 34 at.%, up to at least 28 at.% of Cr. This would be the only part of the eutectic trough that has been confirmed so far. However, the purpose of adding Mo in these alloys was not to assess

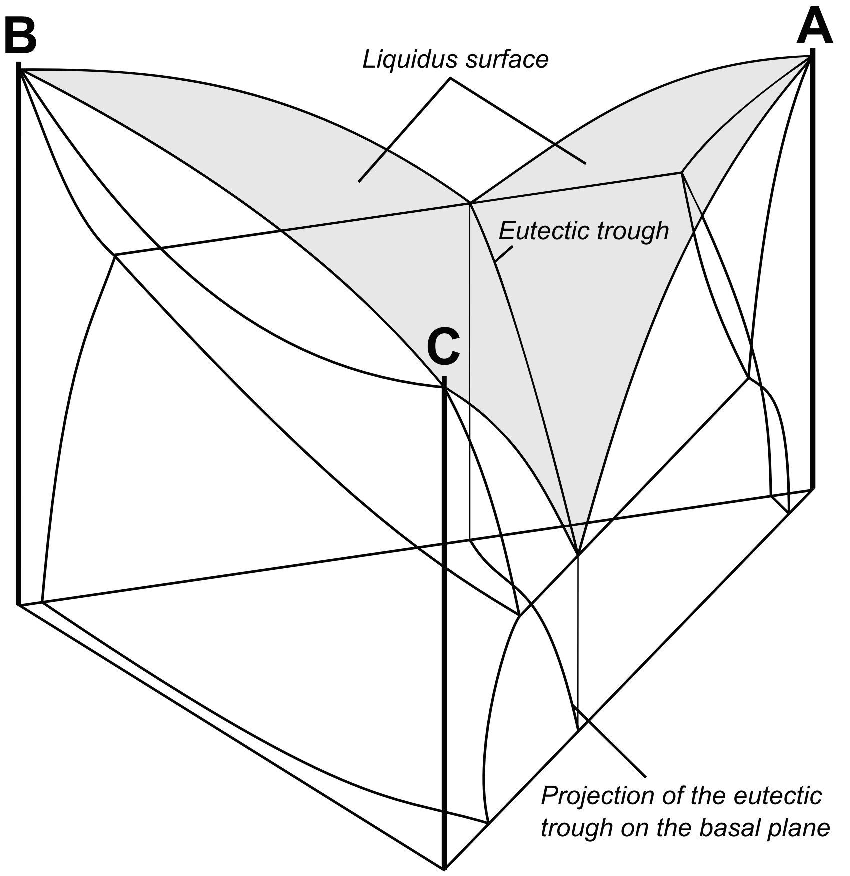

Figure 1.7: Model of a ternary system in which the elements A and B, and A and C form two binary eutectic systems, while B and C have complete miscibility, opening up the possibility of having a continuous eutectic trough in the ternary that joins both binary eutectics [54, 125].

the eutectic trough on the system, in order to tune the volume fraction of the reinforcement. The purpose was rather to change the eutectic morphology of NiAl-Cr from fibrous to lamellar [91, 92, 98, 113–115], as well as an approach to changing the reinforcement mechanical properties. This was also the case in NiAl-Mo(Re) alloys [97, 126]. Only now, a project on assessment of the NiAl-Cr(Mo) pseudo-ternary system is being carried out at the Insitute for Applied Materials (IAM) at the Karlsruhe Institute for Technology (KIT). Peng *et al.* are working on the thermodynamic assessment of the Al-Mo-Ni system and its quaternary extension with Cr, during which they have found indications of a continuous eutectic trough in the pseudo-ternary system. However, its actual path has not yet been reported [127].

These results were encouraging to follow up with the study on the proposed system, as NiAl-W pseudo-binary eutectic showed more potential than its NiAl-Mo counterpart [99, 110]; only being hindered by the low volume fraction of the reinforcing phase. If we go back to figure 1.7, in the case of NiAl-Cr-W, *“A”* would represent NiAl intermetallic, whereas *“B”* and *“C”* would correspond to Cr and W. If a continuous eutectic trough exists, both parts of the liquidus surface will form this valley, where the temperature is minimum. The projection of the liquidus surface will give us the alloy compositions for the eutectic trough, among which the properties could be changed, simultaneously keeping full eutectic microstructure after solidification. As a consequence, each alloy along the eutectic trough will exhibit a different melting point, volume fraction and composition of the reinforcing phase. By this approach, further optimization of properties, which could surpass those of the state-of-the-art NiAl-based pseudo-binary eutectic systems, could be hopefully obtained.

1.6 A new step towards implementation

Despite all the research carried out and efforts made during recent decades, which is explained throughout this chapter, the NiAl intermetallic compound has not yet made it into any structural application. Its low ductility and fracture toughness at RT make it a difficult material to process, and very sensitive to defects on its mechanical behavior. On the other hand, its low strength and creep resistance at high temperatures, make it too soft a material to be implemented in components under high working temperatures. Of course, significant progress has been achieved throughout the years, leading to key points in the improvement of some NiAl properties, such as an increase in the fracture toughness at RT and the high temperature strength of the material.

However, under current socio-economic circumstances, together with the present available materials, it is imperative to continue the research to the bounds of existing technology and towards new cutting-edge materials. Therefore, research on this topic is not only relevant for a material with promising properties and still pending of improvements for its implementation, as is the case of NiAl, it is also a step forward in the field of intermetallic alloys, as the new approach could open new possibilities for improvement in other systems. Moreover, the study of the NiAl-Cr-W eutectic trough will increase the knowledge of the system, and help to assess it. This will help to create better databases, which are playing an increasingly important role in materials design. Furthermore, the high melting temperatures of the elements and compounds, especially that of W, will become a huge challenge in order to produce the samples and process them, obtaining a know-how which will be invaluable for further production of alloys and processing of *in situ* composites.

All the above is relevant enough to carry out this research project, in order to increase the knowledge and the know-how, and to go a step further towards the implementation of NiAl as a viable material for structural applications in the future.

2

Motivation and Objectives

2.1 Motivation for the study of NiAl eutectic *in situ* composites

Although NiAl intermetallic compound possesses a set of properties which make it an attractive material from the point of view of high temperature applications, it has major drawbacks which make it unsuitable for structural purposes. Extensive research has been carried out on intermetallic materials including NiAl compound since the second half of the last century. However, while properties of other intermetallic materials have been improved sufficiently to reach the goals for implementation, and are, in fact, already being used as structural materials, NiAl has not yet been able to make it into any structural application. Nonetheless, important achievements have been made over the last few decades of development, in which the material properties have been improved significantly. The results obtained by the introduction of a ductile phase as a reinforcement have been particularly good.

The approach is based on the fact that NiAl reacts eutectically with some elements, giving the alloys a eutectic microstructure which resembles a composite material. These composite materials have a NiAl matrix reinforced by a second phase, ideally keeping the good properties of NiAl, while working towards eliminating the not-so-good drawbacks. The eutectic reaction also enables the possibility of processing the alloys by directional solidification (DS), in order to produce *in situ* composites with aligned reinforcement, greatly improving its mechanical behavior. Additionally, although subjected to possible coarsening at high temperatures like any other microstructure, due to their formation from a eutectic reaction, these alloys are inherently more stable up to their melting point and no chemical reactions will take place between matrix and reinforcement. However, the enhancement in this approach is highly influenced by the volume fraction of the reinforcing phase, which is fixed by the unique composition of the eutectic reaction.

Therefore, opening a new window to tackle the problem of fixed volume fraction by adding a new variable to the system, seems to be a key point in order to develop a new generation of NiAl-based eutectic composites, in which the properties and volume fraction of the reinforcing phase could be adjusted to the desired applications.

2.2 Aim of the present study

In accordance with the above, the main objective of this research project is to study the path of a hypothetical continuous eutectic trough in the NiAl-Cr-W pseudoternary system. This is done in order to obtain new NiAl eutectic *in situ* composites with variable properties and volume fraction of the reinforcing phase, for the purpose of obtaining alloys with tailored properties, which could surpass those of the state-of-the-art NiAl-based alloys. In that scope the following is expected:

- The first goal is to produce alloys successfully in this system. Taking into account the really high temperatures involved, it constitutes a particularly important challenge for DS processing.

- Once the alloys are produced, the objective is to measure the eutectic compositions, in order to determine the path of a hypothetical continuous eutectic trough between both NiAl-Cr and NiAl-W pseudobinary eutectics.

- In the light of the results obtained, the route to be followed is to study the microstructural features and the influence of processing parameters on them. This will help to better assess the eutectic trough and its particularities.

- The final aim is to evaluate the mechanical properties of the developed NiAl-Cr-W eutectic alloys.

2.3 Outline of the work

After a short introduction and review of the current knowledge of NiAl and state-of-the-art NiAl-based alloys, which is briefly summed up in the present chapter in order to outline the motivation of the work, the thesis continues with the material used, processing techniques applied and mechanical testing performed during the research. Then, the core of the dissertation is presented in 4 sections.

The first part focuses on the challenges faced during the processing of the alloys, together with preliminary results derived from them. In the second part, the results of the assessment of the eutectic trough, through measurements of the eutectic cells composition in the alloys is presented. Following on from the results obtained, part 3 focuses on the microstructural features of the alloys, in order to try to understand the solidification path, with the objectives of proving the validity of the approach used, and shedding light on the possible reactions taking place in the system. Finally, the results of the mechanical behavior of as-cast NiAl-20Cr-4.5W alloy are presented in part 4 in order to obtain a first impression of the mechanical properties that could be expected from NiAl-Cr-W eutectic alloys. To conclude, the most relevant findings of the research are presented together with some possible work lines to follow in forthcoming research.

3

Materials and Experimental Methods

3.1 Material and processing

The alloys used in the present study were produced through different techniques, from highly pure elements Al, Ni, Cr, and W, with different formats and shapes depending on each processing route.

3.1.1 Arc melting

The arc melting technique was used to produce part of the alloys for this investigation. This technique consists of applying a potential difference between a tungsten electrode and a water-cooled copper crucible, which forms an electric arc between both. This electric arc can reach temperatures over 3000 °C, being able to melt high-melting materials such as refractory metals. This includes W with a melting point of around 3400 °C, the highest of all metals. The advantage of this technique is that samples can be produced faster, as there is no need to use ceramic crucibles, which are sensitive to thermal shock due to high temperature gradients. Therefore, the speed of heating and cooling depends on the equipment. Furthermore, the water-cooled copper crucible enables the possibility of producing high purity alloys. Additionally, smaller samples can be produced, reducing the waste of material in characterization. Alloys for a preliminary study were produced by this technique at the Northwestern Polytechnical University (NPU) in China, at the Department of Material Science and Engineering, due to the absence of in house equipment. Later, most of the alloys were produced at IMDEA Materials Institute in an Arc 200 Mini Vacuum

Arc Melter from Arcast Inc. The furnace is able to melt, cast and rapidly solidify alloys in a copper cold crucible equipped with a casting module (fig. 3.1).

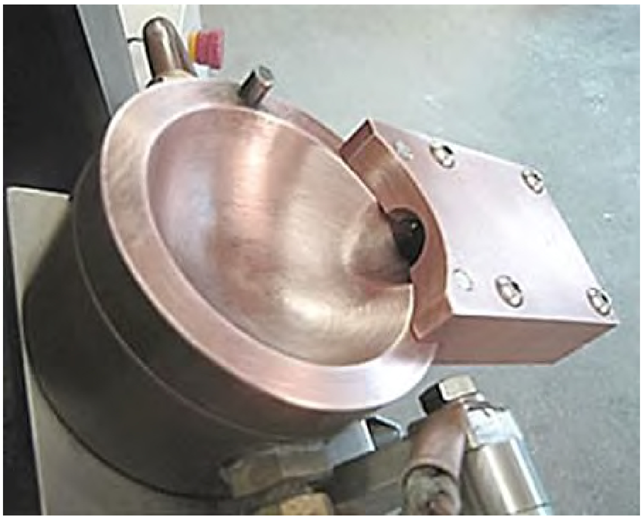

Figure 3.1: Copper casting module attached to the water-cooled copper crucible in the Arc 200 Mini Vacuum Arc Melter from Arcast Inc.

The furnace is also equipped with a magnetic stirrer device, which enhances the homogenization of the alloys produced. The process was performed in an Argon inert atmosphere after applying high-vacuum cycles to reduce oxidation.

The starting material used to produce the alloys through this technique was: 99.9 wt.% Al granules, 99.9 wt.% Ni pieces and 99 wt.% Cr pieces supplied by Alfa Aesar, and 99.95 wt.% W lumps supplied by Goodfellow.

3.1.2 Induction melting

Induction melting was another technique used to produce the alloys; this consists of heating the material through a magnetic field, which is generated by the electric current applied on a coil. This magnetic field, which is changing with high frequency (up to 10 KHz), induces eddy currents in the material which heat it up. This means that for the material to heat up, it has to be conductive. The temperatures reached can also be very high and depend basically on the power supply. The advantage of this technique is that the heat is generated inside the material, and no external source of heat is needed; this implies power savings as the material can be heated exactly as needed. For the same reason, no heat conduction or contact is needed for the heating. However, the molten material has to be contained, usually in a ceramic crucible. The material which the crucible is made from is the true limiting factor for the maximum temperature achievable in the furnace and the maximum heating and cooling rates, as ceramics are prone to thermal shock; it is, therefore, paramount to have a good control of the materials temperature. An extensive explanation on the processing challenges is given in 4.1.

Alloys were produced at IMDEA Materials Institute in a VSG 002 DS from PVA TePla AG. To contain the molten metal, a double crucible setup was used. In this setup, a slip cast alumina crucible with a smooth surface from Almath Crucibles Ltd. was placed inside a back-up crucible, in this case a uniaxially pressed zirconia crucible supplied by Zircoa Inc.. Zirconia powder was used as the backing material between both crucibles due to its lower thermal conductivity. It was thoroughly compressed for better insulation, and to fix the inner crucible tightly. Finally, the whole crucible setup was fixed into the coil by means of an alumina blanket and sheet, in order to prevent its movement during tilt casting. Good control of the material temperature was achieved by a two color pyrometer ISR6 Advanced-TV from LumaSense Technologies. With a temperature measuring range from 800 to 2500 °C, the pyrometer covered the temperatures of interest for our particular process.

The starting material used with this technique was similar to that with arc melting: 99.9 wt.% Al granules, 99.9 wt.% Ni pieces, 99 wt.% Cr pieces supplied by Alfa Aesar and 99.95 wt.% W lumps supplied by Goodfellow. The materials were melted under Argon atmosphere to avoid oxidation and reduce evaporation, after applying high-vacuum cycles. Moreover, an alloy with nominal composition Ni-37.75Al-20Cr-4.5W at.% was prepared by induction melting under inert atmosphere, and drop cast into a cylindrical copper mould. A rod, 200 mm long and 30 mm in diameter, was produced for testing at the facilities of the Max Planck Institute for Iron Research (MPIE) in Düsseldorf, Germany.

3.1.3 Directional solidification

The directional solidification technique was used to further process some of the alloys. The basis of this technique consists of the solidification of the molten material in a specified direction by the application of a thermal gradient. This directional thermal gradient causes the solidification front to be ideally planar and perpendicular to the solidification direction. Consequently, the microstructure obtained after the process consists of oriented columnar grains, or even single crystals, when a seed is used to select a single grain growth. For the investigation, this oriented growth implies that the eutectic fibers or lamellae will be aligned in the processed piece, affecting the mechanical behavior of the material.

There are several ways to perform directional solidification. For this study, the process was performed in the induction melting furnace VSG 002 DS from PVA TePla AG, which is equipped with a Bridgman type device. In directional solidification by the Bridgman method, the thermal gradient is generated by moving the material away from the heating source. In this case, the heating source is the induction coil. The system is equipped with a water cooled table to hold the hot crucible, this table rotates, and is slowly removed downwards in order to generate the necessary thermal gradient (fig. 3.2).

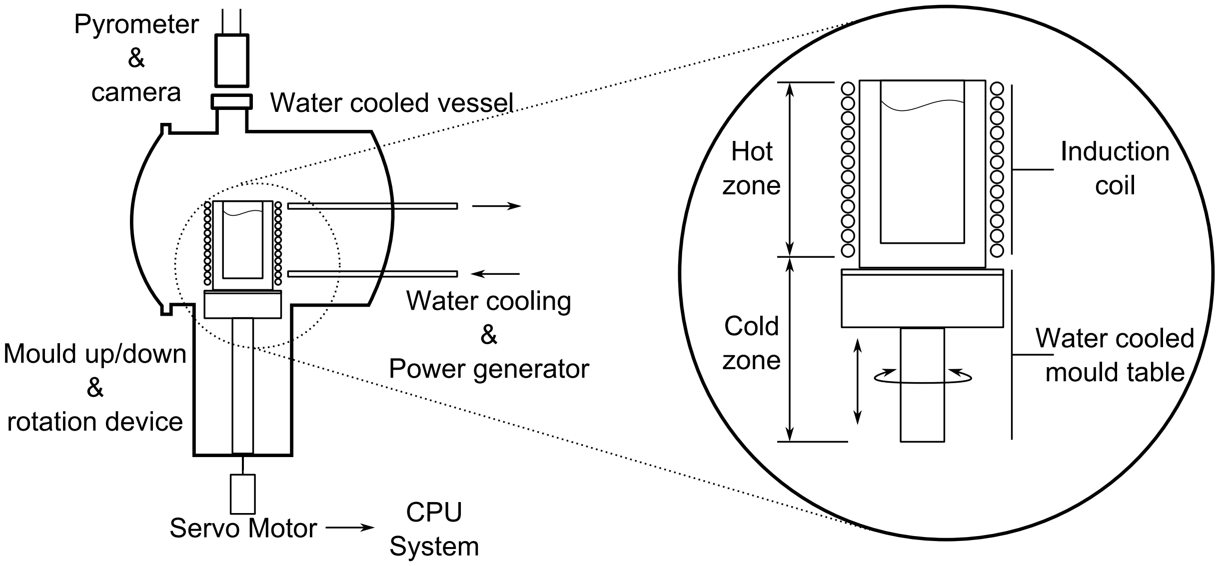

Figure 3.2: Diagram of the bridgman device in VSG 002 DS induction melting furnace from PVA TePla AG used in the present study.

The crucible setup used was similar to the one used for induction melting and tilt casting, except for the alumina paper and blanket; this was due to the need for free movement of the whole crucible/table set. Additionally, a new setup was designed, consisting of four point-bottomed slip cast crucibles from Almath Crucibles Ltd. with smaller diameter, instead of the single cylindrical crucible used previously. The four crucibles were placed inside and fixed tightly with backing material. This setup was tested and used to process more alloy compositions in a single experiment, thus saving processing time.

Although the process could start from the elemental materials, because melting is a necessary step, it was soon discarded due to undissolved Tungsten. Instead, pre-alloyed cast rods of 100 mm length, produced in house at IMDEA by induction and arc melting, were used for better homogeneity. The experiments were performed in an Argon atmosphere after applying high-vacuum cycles to reduce oxidation and evaporation, which can be important given the long processing time of over 5 hours. The surface temperature was controlled by the pyrometer, and kept constant above the melting point. All the experiments were conducted at a growth rate of 20 mm/h.

Additionally, a NiAl-W alloy from a previous study was tested for comparative purposes and its production is described in [110]. As a starting material, nickel (99.97 wt.%), electrolytic aluminum (99.9999 wt.%) and tungsten pellets (99.9 wt.%) were used to prepare the alloys with nominal composition Ni-49.25Al-1.5W at%. The composition was close to the nominal values for the major elements, with deviations less than 0.5 at% for Ni, 0.8 at% for Al, and 0.1 at% for W, indicating negligible losses during processing. The impurity content was 550 ppm Fe, 100 ppm O, $<$ 100 ppm Si, 65 ppm C, $<$ 10 ppm N and $<$ 2 ppm S on average. Pre-alloys were prepared by induction melting under inert atmosphere and were drop cast into a cylindrical copper mould. Subsequently, the ingots, as cast, were machined to fit into the alumina crucibles, and were directionally solidified in a Bridgman type crystal growing facility. The experiments were conducted at a temperature of 1700 °C, with a thermal gradient of approximately 40 K cm^{-1}, and growth rate of 30 mm h^{-1}.

3.2 Microstrucural characterization

The microstructural characterization of samples with different atomic composition and different processing methods was one of the key points of this study. It was used in order to identify the eutectic microconstituent and its composition, the phase volume fractions within the eutectic microstructure, and the compositions of the phases forming it. In addition, the characterization step was critical later on, in order to obtain local compositions, phases present, and to study possible solidification paths and reactions. The characterization included the use of light optical microscopy (LOM), scanning electron microscopy (SEM), energy-dispersive X-ray spectroscopy (EDX), and electron probe micro analysis (EPMA).

The preparation of samples was similar for all the characterization techniques used. First the samples were mechanically cut, either with a wheel or a wire cutting machine, in such a way that the largest possible amount of surface of the interesting zones could be observed. Afterwards, they were hot-mounted using a mounting press with a conductive bakelite resin, in order to make preparation easier, and to be able to use them in the previously mentioned equipment. Thereafter, the surfaces were ground with SiC abrasive paper to get rid of cutting defects and coarse scratches. Finally, the surfaces were polished using diamond paste with decreasing particle size up to 1 μm, and no etching was used. At this point the surface was already mirror-like and prepared for characterization.

3.2.1 Optical microscopy

Optical microscopy is capable of capturing low-magnification, high-quality images in a very fast way. Therefore, this technique was used in order to make an initial quick characterization of the sample, to check if the feature size was large enough and to check whether the processing was successful; The homogeneity of the sample was also checked and the technique was used to identify interesting zones that should be further studied.

This characterization was done at the facilities of IMDEA Materials with an Olympus BX51 optical microscope. The microscope is equipped with the image processing software AnalySIS auto, which was also used to perform calculations of the phase volume fraction in the eutectic microconstituent.

3.2.2 Scanning electron microscopy

In general, the microstructural features that were the aim of the study were too small to be studied only by means of optical microscopy. Therefore, scanning electron microscopy (SEM) was used to achieve higher magnifications. As the name already indicates, the technique consists of using electrons instead of light to create an image. This results in a better resolution than in optical microscopy, allowing a much higher magnification. In the case of SEM, the electron beam is generated by a source gun, and then is condensed and focused by a series of magnetic lenses. Controlled by different coils, the beam scans the selected surface. Finally, the image is generated from the signals obtained by the different detectors, which is one of the strengths of the technique. There are different detectors which monitor the phenomena occurring when the electron beam interacts with the sample, yielding different important information for each of them (fig. 3.3).

For this study, the basic detectors used were a secondary electron detector (SE) and a back-scattered electron detector (BSE). A SE detector yields high resolution images with topographic features, whilst a BSE detector yields composition-contrast images. The latter was especially interesting in this study for the discrimination of the different phases. An EVO MA15 scanning electron microscope from Zeiss located at IMDEA Materials Institute was the main equipment used in this study, although the facilities at Carlos III University and MPIE were also essential for the investigation. The conditions used were an acceleration

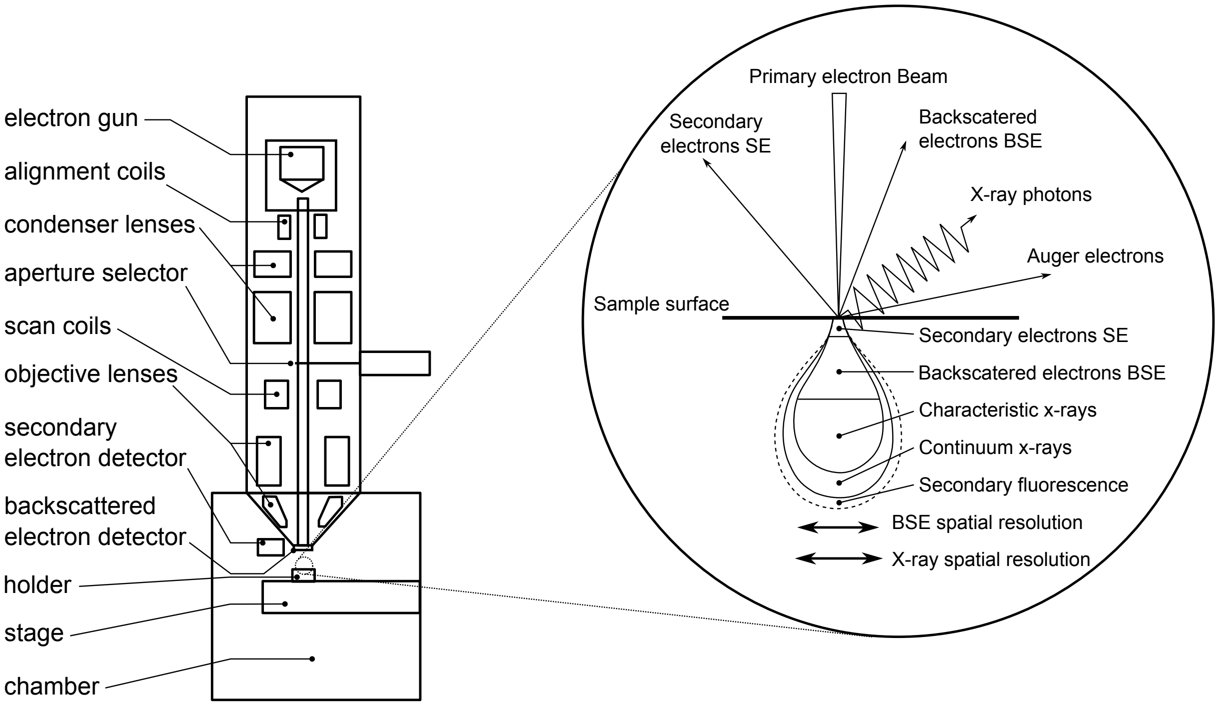

Figure 3.3: Schematic drawing of a scanning electron microscope and the electron beam interactions that can be detected in order to obtain fundamental information of the material.

voltage between 15 to 20 kV, a spot size between 400 to 500 and a working distance between 8 and 10 mm.

3.2.3 Energy dispersive X-ray spectroscopy

Additionally, an energy-dispersive X-ray spectroscopy (EDX, EDS or EDXS) was used in order to analyze the compositions of the samples and phases; this was fundamental for the study. The technique is based on the X-rays emitted by an atom when it is excited, as the energies of these X-rays are characteristic for each element. This can be achieved in a SEM when the electron beam interacts with the sample, exciting the atoms affected by the beam, which in turn release some of this energy as X-rays. By means of an energy-dispersive spectrometer, the energy and amount of the X-rays emitted by the sample can be detected and quantified, thus yielding a pattern. As each element has its characteristic pattern, the results can be analyzed in order to find out which elements are present in the affected zone, and therefore the composition of the zone.

For this study, the technique was performed with an Oxford INCA 330 microanalysis system installed at the scanning electron microscope described in 3.2.2; this was the main equipment used for this study. However, the facilities at MPIE were also essential for the investigation. The acceleration voltage used for the analyses was 20 kV. The typical spot size was 1 μm, although for area measurements the surface of the sample was scanned. At least three composition measurements were performed for each phase. The resolution in energies of the equipment is of 130 eV at 5.9 KV.

3.2.4 Electron probe micro analysis

Moreover, electron probe micro-analysis (EPMA) was used to obtain qualitative and quantitative elemental analysis of the composition of the different phases, which was one of the main parts of the study. The basis of the technique is similar to that of EDX, described previously in 3.2.3. The X-rays emitted by the different elemental species, excited by the electron beam have also characteristic wavelengths. The wavelength can be recorded by a wavelength dispersive spectrometer, which uses a number of monocrystals as monochromators in order to obtain the composition. The strength of wavelength dispersive spectroscopy (WDS) is that EPMA is a fully qualitative and quantitative method, providing much better results than standardless EDX systems. Therefore, it was used to compare and validate EDX measurements.

EPMA analyses were performed initially at the JEOL Superprobe JXA-8900 M, available at the ICTS National Electron Microscopy Centre at Complutense University for the preliminary studies. Later, the JEOL JXA-8100 at MPIE was essential for these measurements. The conditions used for the quantitative analyses were an acceleration voltage of 15 kV and a probe current of 20 nA. The typical spot size was 1 μm, although widened beams of 5 and 10 μm were used for small area measurements. At least three composition measurements were performed for each phase. An error of 1% is typical for measurements with this technique.

3.3 Mechanical testing

Besides the microstructural characterization of the samples used to study the eutectic trough and phase diagram, due to the future prospects of application for these alloys, the determination of their mechanical behavior was found to be of major importance. Therefore, a composition was selected to perform mechanical testing. The alloy with nominal composition Ni-37.75Al-20Cr-4.5W at.% produced by induction casting at the facilities of MPIE was selected. From all the alloys produced, this was the one produced in larger size, also having enough eutectic phase in the microstructure and its microstructure being homogenous within the cast rod.

The bulk of the mechanical testing was performed at the facilities of MPIE in Düsseldorf, Germany, due to the outstanding capabilities of the institute for very high temperature testing. Additionally, previously produced samples, that were tested at IMDEA Materials within the scope of the project, are hereby presented for purposes of comparison.

3.3.1 Microhardness testing

Hardness is one of the simplest methods to mechanically characterize a material, as it does not require special preparation of the sample, the equipment is relatively inexpensive, and the test can be carried out quickly. Moreover, a quantitative relationship between hardness and other mechanical properties has been reported [128, 129].

Micro-indentation hardness testing is performed using a micro-indenter, which is pressed on to the surface applying a known load. The hardness is then related to the dimensions of the indentation on the sample. The *Vickers* test utilizes a diamond, square-based pyramid-shaped indenter. Based on the indentation dimensions, a hardness value is calculated. This type of test has the advantage of using a single scale to measure hardness for all materials.

For this study, *Vickers* hardness (HV) measurements were performed at IMDEA Materials in a SHIMADZU HMV-2 micro-indenter applying a 2 kg load for 15 seconds, in agreement with the ASTM E384-11e1 standard. Several measurements were performed to verify the homogeneity within the samples.

3.3.2 Compression testing

Compression loading occurs in a wide variety of applications and material processes, thus being of major importance to understand the behavior under these conditions. Moreover, due to the intrinsic brittle behavior of intermetallic compounds at low temperatures, uniaxial compression testing is one of the most widely used methods to characterize the mechanical behavior of this kind of materials.

In a uniaxial compression test, a cylindrical or prismatic shaped sample is loaded uniaxially with a given strain-rate between flat plates. These are made of a hard metal or ceramic depending on the testing temperature, so that they do not deform during testing. The advantage of this technique is that the initial defects in the sample, such as internal pores or cracks, as well as surface scratches which could have a notch effect, do not play as important a role in the results as they would in a tensile test. In addition, the samples are simpler to fabricate and use less material, making them interesting, when good tensile sample fabrication is difficult or the material is scarce. This way, brittle materials can be tested up to the yield point and over [130]; as a material property, this should be the same as for tensile testing. However, some precautions must be taken to assure correct behavior during testing. Thus, aspect ratios of 2 or lower are used to avoid buckling or shearing.

For this study, rectangular prismatic samples of 5 x 5 x 10 mm^3 were electro-discharge machined (EDM) from the as-cast Ni-37.75Al-20Cr-4.5W at.% alloy rod, and tested at the facilities of MPIE. The tests were performed at a strain rate of 10^{-4} s^{-1} and at temperatures of 25 (RT), 400, 600, 800, 1000, 1100, 1200, 1300 and 1400 °C. The tests were conducted up to about 5% strain rate, so that the yield point could be measured. The high temperatures tested were selected due to the importance of the material behavior in this range.

Additionally, powder metallurgy NiAl and directionally solidified NiAl-W eutectic, which were previously tested at IMDEA Material Institute within the scopes of the project, are brought in here for comparison purposes. Due to the small amount of material, samples of 2 x 2 x 4 mm^3 were cut from the powder metallurgy NiAl consolidated by FAHP at 1200°C. The samples were tested in an INSTRON 3384 mechanical testing machine, equipped with a furnace for high temperature testing up to 600°C. The tests were conducted at a strain-rate of 10^{-4} s^{-1} at RT, 300 and 600°C. All tested samples were ground with SiC grinding paper up to 2000 in order to remove possible surface defects.

3.3.3 4-point bending test

One of the characteristic properties of intermetallic materials in general, and therefore also in B2-NiAl compounds, is that they present a very well-marked, sharp change in the mechanical behavior from brittle to ductile with the temperature. In order to obtain this brittle-to-ductile transition temperature (BDTT), it is common to use bending tests, from which it can be determined whether or not the material is ductile.

Bending tests, in contrast to other mechanical tests, are usually designed to give a more qualitative result than quantitative result. However, fracture toughness can be very accurately and quantitatively determined using 3-point bending. In the case of the 4-point bending test, a material beam is subjected to flexural deformation by a load, which is applied to two points of the sample. The beam lays on another two supporting points as shown in figure 3.4. Due to the applied force, the beam is deflected until it breaks or until the test finishes. This deflection is the parameter being measured and, depending on the value reached before cracking, the material is determined to behave in a ductile or a brittle manner at the tested temperature.

In this study, 4-point bending tests were performed at the facilities of MPIE on Ni-37.75Al-20Cr-4.5W at.% beam samples of 3 x 6 x 18 mm^3. The dimensions described in figure 3.4 are: l = 15 mm, e = 6 mm, b = 6 mm and h = 3 mm. The samples were ground with SiC grinding paper up to 2000 in order to remove possible surface defects. Special care was taken to finish the grinding on the longitudinal direction of the samples, to reduce any possible notch effect from scratches which could initiate cracking. The tests were conducted at different temperatures ranging from 500 to 800 °C at a strain-rate of 10^{-4} s^{-1}. When flexural strains of 3-4% were reached without breaking, the tests were stopped. After testing, the fracture surface was analyzed to study the fracture behavior, and to detect possible defects in the material prior to testing, which could have led to contradictory or misleading results.

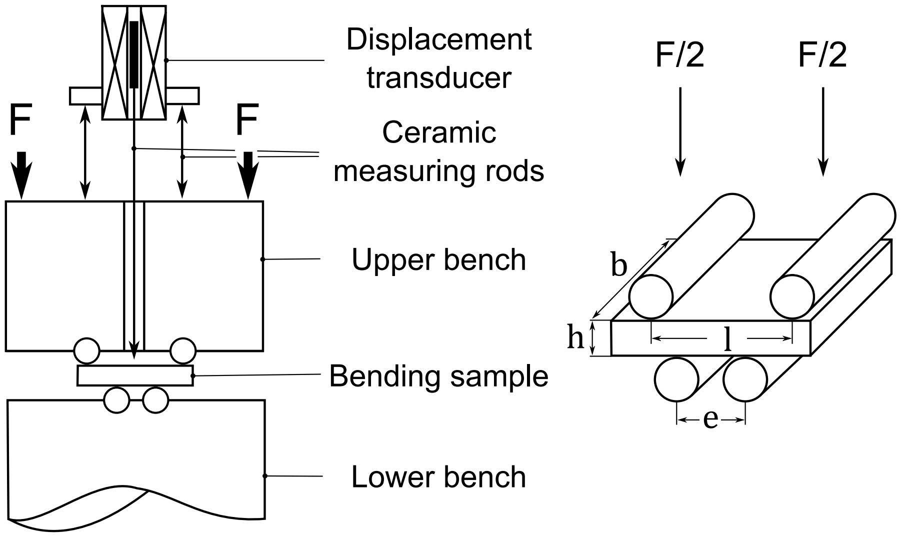

Figure 3.4: Schematic drawing of a 4-point bending test setup and relevant dimensions of the tested beams.

3.3.4 Tensile testing

Tensile testing is by far the most developed and used method to characterize the mechanical behavior of materials, in order to determine properties such as yield point, plastic deformation, and fracture, among others. However, the amount of deformation achieved is limited by necking [130]. Also, as previously explained in 3.3.2, the initial defects of the sample, such as internal pores or cracks, as well as surface scratches, can play an important role in the results, especially with brittle materials; this is the case with intermetallic compounds like NiAl. However, being the most widely used method, it is of major importance to perform the testing when possible. In this case, also in order to complement and validate the results of yield strength from compression testing, which in principle should be the same for both methods, as it is a material property.

For this study, uniaxial tensile tests were performed at the facilities of MPIE to dog-bone Ni-37.75Al-20Cr-4.5W at.% samples, with gauge dimensions of 2 x 3 x 13.5 mm. The tests were conducted at a strain-rate of 10^{-4} s^{-1} and temperatures of RT, 400, 600, 800 and 1000 °C.

3.3.5 Creep testing

In general, creep is described as the plastic deformation occurring in a material over time, when subjected to a constant stress, which is lower than the yield strength of the material. The idea that materials have only one, well-defined value for the yield strength and that it only undergoes plastic flow over the yield point, although convenient, is only true at absolute zero. As a kinetic process, the rate at which the material flows when constant stress is applied depends on the time and the temperature. This phenomenon is considered to be a high temperature mode of deformation. Its dependence on the temperature becomes much stronger when reaching roughly around 0.5 T_m for metals and ceramics, being therefore relatively high temperatures in respect to each given material.

For materials intended to be used in components working under high temperature conditions, as it is the case for many intermetallics and specifically concerning NiAl-based alloys, it is of paramount importance to understand its behavior under these extreme conditions. Creep testing can be performed applying a constant load or constant true stress to the material, either in compression or tension at relatively high temperatures. To this respect, the equipment needed for this kind of testing is similar to that used for compression or tensile testing, but made with more specific materials. The strain rates measured in a creep test can be as low as 10^{-9} s^{-1}, or even lower, so tests can run from hundreds to thousands of hours continuously. Therefore, special equipment, which can undergo these long tests at high temperature without being deformed, is needed. At the same time, these tests being performed at high temperatures for very long periods of time, it is important to be as sure as possible that the microstructure will be stable during the whole test. If the structure was not stable, the results could be misleading due to the effect of stabilization, hindering or even hiding the actual mechanisms taking place during deformation.

For this reason, a piece of the Ni-37.75Al-20Cr-4.5W at.% alloy rod was subjected to a heat treatment of 1000 h at 1000 °C in air, and cooled afterwards in the furnace. The temperature and time of the heat treatment were selected as a compromise between the available equipment and desired conditions for creep testing. After heat treatment, rectangular samples of 5 x 5 x 10 mm^3 were electro-discharge machined (EDM) from the piece, and were ground with SiC grinding paper up to 2000 in order to remove possible surface defects. Afterwards, constant-load creep tests were performed on the samples at temperatures of 800, 900, 1000 and 1100 °C. The load was increased stepwise after creep rate on each given load reached a steady state. The tests were conducted up to about 5% strain to maintain the setup close to initial conditions. The high temperatures tested were selected due to the importance of the material behavior in this range. Both heat treatment and creep tests were performed at the facilities of MPIE.

4

Initial Processing Challenges

4.1 Induction casting development

Prior to the analysis of the eutectic trough, the first challenge was to successfully produce good quality alloys at IMDEA Materials Institute thus allowing further research. The first step in this direction started with the acquisition, reception, and commissioning of the VSG 002 DS induction furnace from PVA TePla AG. Unfortunately, having a brand-new technologically high-developed piece of equipment with a relatively simple operation, does not necessarily imply an easy production of advanced alloys. As previously explained in 3.1.2, normally for induction melting and casting the melted material has to be contained, and this is done typically in a ceramic crucible. The crucible material is the truly limiting factor of not only the maximum temperature attainable in the furnace, but also the maximum heating and cooling rates, as ceramics are prone to thermal shock. This fact was especially critical in the present study, due to the very high melting temperatures of NiAl and the alloying elements Cr and W, important for a proper dissolution in order to obtain a homogeneous alloy. Additionally, the formation of NiAl intermetallic from the elements is a highly exothermic reaction, implying an uncontrolled rapid increase in the temperature of the melt, subjecting the container material to intense heating rates. For all the above mentioned reasons, the design of an effective setup, and the selection of appropriate materials for the crucible, became major concerns for successful research.

4.1.1 Crucible configuration

In induction melting, the crucible is placed inside the coil and has to be fixed to it. From the point of view of this crucible setup, the purpose of the equipment is a key factor for choosing one or another type of configuration. At an industrial level, where the material is similar in each production line, a crucible fixed to the coil with a refractory mortar bed is the best option to enhance the life and performance of the crucible. However this method is inadequate for a laboratory furnace, where different types and amounts of alloys are required. In this case, removable fixing materials such as alumina sheet and blanket are the best choice, which were the materials initially used. These materials are much more versatile for the purpose desired in the study, and for better utilization of the equipment, which can also be used in other projects carried out at the institution. Different crucibles could be easily changed; this greatly facilitated initial tests, done with better known alloys such as titanium alloys, steels, and Ni-based superalloys. Tests with these alloys were successful, and the crucibles could be tightly fixed in the coil; this enabled tilt casting to be carried out safely, and the coil to be insulated from the high temperatures reached in the crucibles, thus, protecting the system. However, while the setup worked successfully for these less demanding alloys, the special characteristics of NiAl alloys subjected the crucible to extreme conditions reaching their limit, and sometimes failing catastrophically (Figure 4.1).

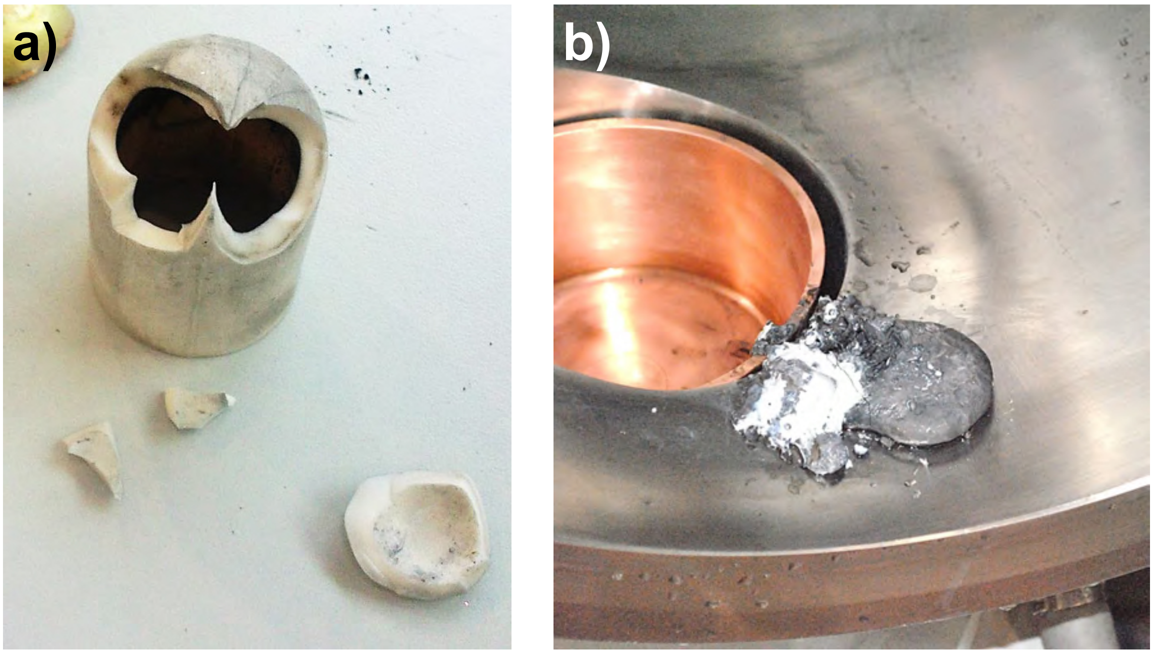

Figure 4.1: Images from some tests performed with alumina sheet and blanket configuration as fixing materials: a) a crucible breakage due to thermal stresses, and b) effect of a major molten NiAl leakage with perforation of the water cooled vessel.

Although alumina sheet and blanket are good thermal insulators, the insulation may not be sufficient to keep the temperature of the crucible as constant as possible within its wall thickness. A too high thermal gradient in the wall between the inner and outer part of the crucible generates thermal stresses which cannot be withstood without cracking. Also, these fibrous materials are highly porous, allowing a gas flow, due to convection, inside the chamber, increasing this pernicious thermal gradient. This is exactly what happened in figure 4.1. Once the crack was initiated, it rapidly propagated through the crucible. Despite being tightly fixed, the alumina sheet and blanket are not rigid, so cracks expanded and formed a crevice through which the molten material leaked. The flexible materials presented almost no resistance to the advance of the molten metal, and a leakage passed through. Although the entire process was carried out inside an isolated water cooled vessel, a leakage may constitute a danger, mainly for the equipment, especially when cracking is as catastrophic it was. In this case the crucible collapsed causing a major leakage, which was not withstood by the water-cooled coil and the water-cooled walls beneath the crucible, resulting in damage of the coil, vessel wall perforation and flooding of the system.

After these results with flexible materials, and the impossibility of permanently fixing the crucible to the coil, a compromise solution was developed. Initially, several setups were produced in-house with a sinterable wet refractory alumina mortar; this was in order to obtain a better crucible hold. The mortar was used either directly covering the crucible, or as a shell in order to use backing material between both, which was thoroughly compacted, and sealed with a drilled upper mortar layer. Although the results were already much better and the crucible could withstand cracking during the melting processes, the control on the perpendicularity, straightness, dimensions, and cracking due to manual production and sintering was too low for our needs. Also, it could hardly be reused (Figure 4.2). Finally, in order to maintain both, versatility in the usage of the furnace, and safety conditions for

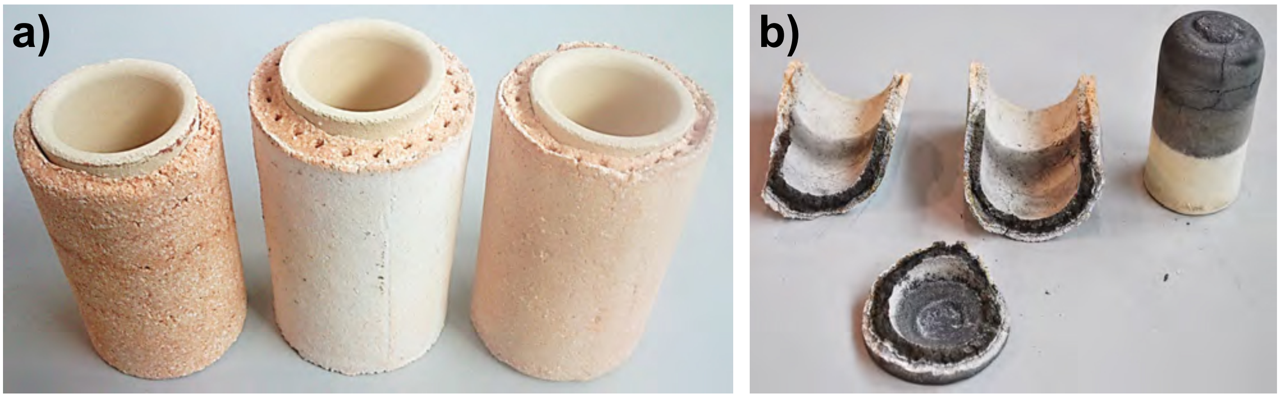

Figure 4.2: Different setups produced with mortar a): left with only mortar as back-up, right with mortar shell produced in two steps, and center, the last development, with mortar shell produced in one step. After usage of the latter b), the crucible held throughout the process although damaged.

the casting process, both concepts were combined in a so called double-crucible setup. In this configuration, the crucible which will contain the molten metal, is placed inside another crucible with a larger diameter. The inner crucible is fixed to the outer with a backing material, a ceramic powder between both, which is thoroughly compacted to make sure that it is tight. After filling the gap, it is sealed at the top with firmly pressed alumina blanket. This will prevent the powder being sucked by the vacuum system as well as spilling when tilt casting. The whole can then be fixed to the coil by means of alumina sheet and blanket (Figure 4.3).

With this double-crucible configuration, the versatility is kept to freely work with different alloys and amounts. The second crucible acts as a back-up of the primary crucible in case of a leakage. At the same time, a leakage is unlikely to happen, as the highly compacted ceramic powder is a better thermal insulator, keeping a lower thermal gradient through the wall thickness. In addition, due to the temperature increase, the powder expands and may slightly sinter, holding the primary crucible without deformation. So, also after cracking, the primary crucible can still contain the molten metal and continue the process normally. Due to this, the setup even allowed to repeat the process more than once with a cracked crucible. However, when the inner crucible was highly damaged, it could be easily removed together with the backing material, which could be partially reused. The back-up crucible, as subjected to significantly less demanding conditions, was reusable in all cases. On the

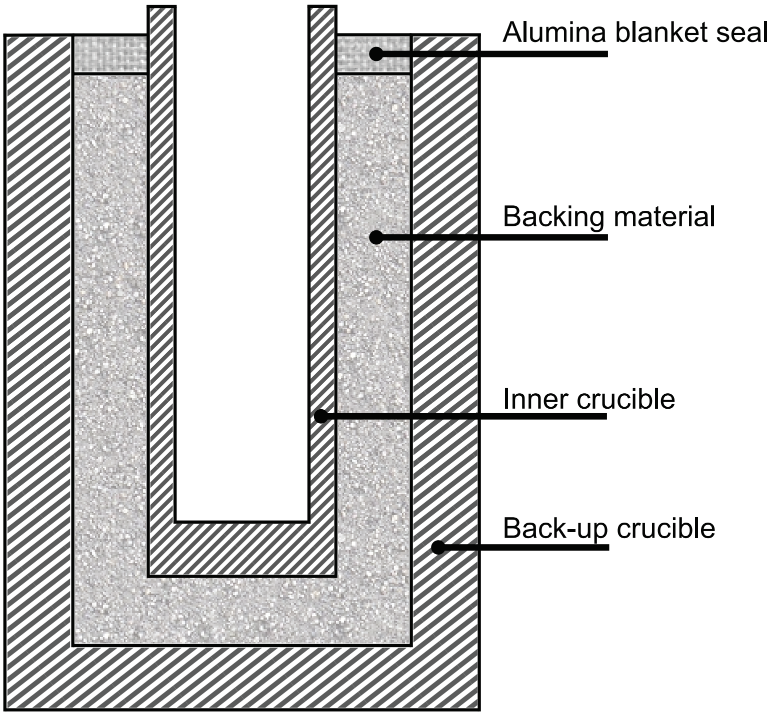

Figure 4.3: Diagram of a double-crucible setup. The inner crucible is fixed to the outer with a backing material, and sealed at the top with alumina blanket.

other hand, a double-crucible configuration limits the dimensions of the primary crucible, and therefore, the amount of material which may be processed. The back-up crucible has to fit in the coil, be thick enough to withstand the stresses due to the thermal expansion of the powder, as well as leave a gap wide enough so the backing material can be effectively compacted. Despite this, the double-crucible configuration showed excellent results on tilt casting and also for DS, which was not possible with any of the previous configurations. Moreover, as the outer crucible is responsible for the stability of the whole setup, as long as it is flat bottomed, the inner crucible can have different shapes, being for example point bottomed for better growth, or even contain more than one crucible to process more samples by DS at a time, resulting in important time savings. During the investigation up to 4 point bottomed crucibles were processed by DS in a single run, reducing to 25% the time used, which could be around 6 to 8 hours for each DS process.

4.1.2 Crucible selection

Another issue during alloy production was the selection of the crucible. Different parameters had to be taken into account in order to select the best option for liquid-state processing of NiAl alloys. During testing, the parameters which were found to be more important were: the material from which the crucible is made and the inner surface roughness.

From the point of view of the material, the maximum working temperature of the crucible was taken first as the key parameter for a proper selection. According to this, zirconia crucibles are the ones with higher maximum working temperature among the ones commonly used, with about 2400 °C, where alumina and magnesia have a maximum working temperature of around 1800 °C. Considering that the melting temperature of NiAl is 1674 °C, and the alloying materials even higher, the use of alumina and magnesia crucibles is possible and could be enough, though with a slightly narrow safety gap. For this reason, at first zirconia crucibles were chosen. However, as can be observed in figure 4.4, zirconia crucibles reacted with the molten alloy leading to crucible damage, alloy contamination and formation of different compounds.

Although molten metals at such high temperatures are already an aggressive media for crucibles, for the NiAl alloys processed in this study, Cr proved to be the most problematic element. The issue with Cr has been addressed before and at least one method for the production of high purity Cr with zirconia crucibles has been patented [131]. However, in the present study the inner surface roughness of the crucible was found to be critical for the reactivity with the melt. When decreasing the roughness, the damaging effects of the aggressive environment were reduced or omitted. The surface roughness depends on the manufacturing process used for the crucible production. Whilst isostatically pressed zirconia crucibles (fig. 4.4) exhibited poor resistance to the aggressive environment,

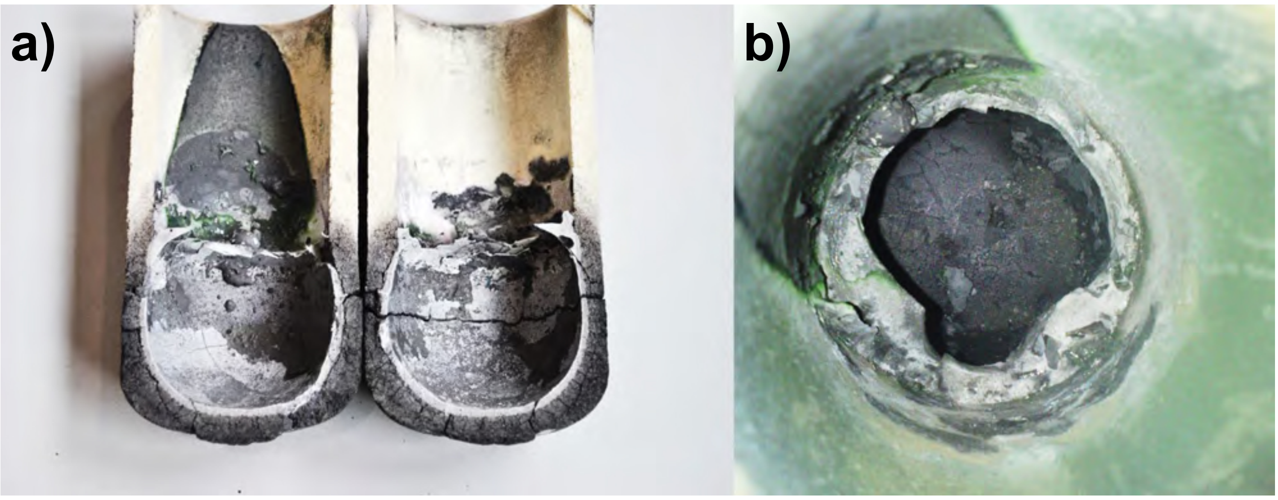

Figure 4.4: Image of a zirconia crucible a) which reacted with a NiAl-Cr-W molten alloy during tilt casting. The green color in b) is due to the reaction with Cr and subsequent formation of Cr oxide.

uniaxially pressed zirconia crucibles, which have an improved surface finishing, already showed great resistance enhancement. From this perspective, crucibles produced by slip casting showed the best surface finish, and therefore, an optimal performance against wear and chemical attack. However, slip casting crucibles are more sensitive to thermal gradients. Consequently, they are more prone to suffer thermal shock, to which zirconia is especially sensitive, breaking during the process, as was shown in figure 4.1a. On the other hand, crucibles pressed isostatically or uniaxially, showed higher strength and thermal shock resistance.

On the basis of the foregoing, the crucible configuration selected was optimal, as different crucible materials and manufacturing processes could be combined to get the best result. Therefore, slip casting was chosen for the inner crucible, in order to have a smooth surface in contact with the molten alloy, and reduce the reactivity during processing. The material selected for this purpose was alumina rather than zirconia, as it has better thermal shock resistance and lower reactivity. For the back-up crucible, a uniaxially pressed zirconia crucible was chosen in order to have: higher strength and thermal shock resistance to hold the setup; higher thermal insulation to reduce thermal gradients in the inner crucible; higher maximum working temperature in case of failure; still adequate outer surface for better positioning, which is especially important for the DS processing. The combination of properties obtained with these, resulted in the best available conditions for NiAl alloys processing in liquid-state.

4.1.3 Temperature measurement

The importance of controlling the temperature of the process has already been mentioned; this is important not only to know the conditions, but also to comply with the maximum temperature and heating/cooling rate of the ceramic crucible containing the melt, and to work under safe conditions. This is a major issue, as the main controllable parameter in the induction furnace is the applied power, which is not directly related to a heating rate. The heating rate is influenced by the material volume, the material shape, the material position respect to the coil, and what is more: the material temperature.

The VSG 002 DS induction furnace was initially equipped with a type S immersion thermocouple. These types of thermocouples are covered with a ceramic cup, which enables their use for measuring the temperature of the liquid when immersed. As a general rule, temperature measurements with thermocouple are very precise. However, some issues should be taken into account. The ceramic cup protecting the thermocouple from the melt, acts as a thermal insulator, so it has to be kept immersed for some time in order to obtain the correct measurement. On the other hand, the magnetic field generated with the coil will affect the thermocouple as it is conductive, leading to an inaccurate measurement. Therefore, it has to be immersed for a short time, but cannot be used continuously, being especially troublesome for DS processing. Additionally, the molten material wets the ceramic cup, covering the thermocouple when immersed and forming a layer on it. This layer would contaminate further melts if the composition was not the same, being difficult to remove without breaking the ceramic cup. At the same time, as the cup is made of a ceramic material, it is also prone to thermal shock and could break during immersion. All the above mentioned issues were experienced during the development of the process. If we add the fact that an S type thermocouple can only be used to measure temperatures up to approximately 1600 °C, when NiAl melting point is already close to 1700 °C, the use of the thermocouple and immersion method for temperature measurements was unsuitable for our purposes. Moreover, as the alloy studied has a high melting point, it was also of great importance to control its temperature in the solid state, because it crosses ranges which are critical for the crucible in terms of thermal stresses. This is not possible with an immersion thermocouple. Another issue with heating in an induction furnace, and especially when done in ceramic crucibles, is that the electrical properties of the materials can change significantly from solid to liquid state. This could mean a rapid increase in the temperature after melting without changes in the power input of the furnace. The issue worsens the conditions for the ceramic material, as the liquid is now in direct contact with the crucible, heating it faster than the part above the melt level. At this specific point, an abrupt thermal gradient is generated; this can be very harmful for the crucible performance due to thermal shock, if the temperature of the melt is not carefully controlled. On the other hand, because of the magnetic forces generated by the coil and the convection phenomena, the material as a melt has more homogeneous temperature than in solid state.

In order to surpass the previously mentioned issues and have good control of the temperature, a two-colour pyrometer ISR6 Advanced-TV from LumaSense Technologies was acquired. A pyrometer is a device which can measure an object's temperature remotely from the radiation emitted by it. Without needing direct contact, a continuous measurement of the temperature of the material is possible, both in solid and liquid state. Together with a fast response and high repeatability, a better control of the processes was achieved. Moreover, two-color measurement is more accurate and does not depend as heavily on the emissivity of the material as a monochromatic measurement. Additionally, measurement in two colors is preferable for liquid state, as fumes from the melt and other issues can reduce the intensity of the signal. With a temperature measuring range of between 800 and 2500 °C, the selected pyrometer covered the temperatures of interest for NiAl alloys tilt casting and DS. This allowed better control of the temperature, and thus, reduced the harmful effects. However, there is still an issue inherent to induction melting tilt casting with ceramic crucibles. As the heat is generated in the material only, after pouring there is no material to be heated up. Therefore, the cooling rate of the crucible cannot be controlled, increasing the chances of cracking. As a consequence, the crucibles tended to crack at the end of the process, relegating them usually to either a single melting, or a few more when cracks were not critical for the two crucible setup to hold. It becomes clear how important the selection of materials and control of parameters is in this technique, its use and setup not being straightforward, especially when referring to advanced alloys and particularly high temperatures.

4.2 Preliminary study

In view of the complexity of the induction furnace preparation for the production of NiAl alloys, during the time needed for the setup of the technique, a preliminary study was conducted on samples produced by arc melting at the Department of Materials Science and Engineering of the Northwestern Polytechnical University (NPU) in China. It was carried out in order to have an initial understanding of the NiAl-Cr-W system, the microstructural features and the path of the hypothetical eutectic trough. For this purpose, 8 samples with different compositions were produced. First of all, both NiAl-Cr and NiAl-W pseudo-binary eutectics were produced, which would be the endpoints of the eutectic trough. The composition of the pseudo-binary eutectic with W is 1.5 at.% W and NiAl bal. [110], and this was the one produced. The composition produced for the pseudo-binary eutectic with Cr was 33 at.% Cr and NiAl bal.. Although there has been disagreement about the true composition of NiAl-Cr pseudo-binary eutectic [120], currently NiAl-34 at.% Cr is generally accepted. The other six samples had compositions in between both endpoints. Three samples had a constant amount of 10 at.% Cr, with W amount being 1.0 at.%, 1.4 at.% and 1.8 at.%. The other three samples had a constant amount of 20 at.% Cr, with W amount being 0.2 at.%, 0.5 at.% and 0.8 at.%.

Even knowing the endpoints of the sought eutectic trough, its path is commonly not a straight line. As can be seen in figure 4.5, the samples composition laid between both endpoints, but spread from the straight line in order to cover a wider area, and be able to detect a possible curvature of the eutectic trough. The compositions are plotted in a 2-axis diagram even though it is a pseudo-ternary system. This is done for the sake of clarity and simplicity on the representation of data, but one should always bear in mind the ternary nature of the system.

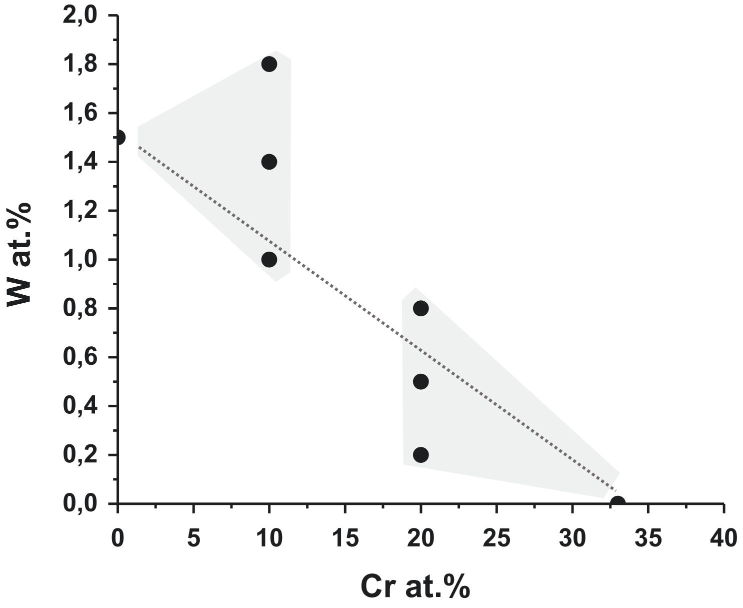

Figure 4.5: Nominal composition of the samples produced by arc melting for the preliminary study of the system. The area covered by the samples for possible paths is colored in gray.

4.2.1 Microstructural characterization

First of all, the most significant feature was that in almost all samples, the presence of undissolved W particles was observed. The presence of particles due to incomplete melting of an element affects the local composition of the samples, resulting in element-poor alloys. This was confirmed by EDX measurements on the overall composition of the samples and it is shown in table 4.1. In the samples with constant nominal composition of 10 at.% Cr, which were the ones with higher nominal content of W, only 0.69 at.% W was measured in the overall composition. This implied a higher amount of undissolved W, as it was also confirmed by LOM and SEM observations, and a larger deviation than expected with respect to the desired compositions. Sample 2 overall composition was not measured because its microstructure was essentially the same. In the same way, the sample with the nominal composition of the pseudo-binary NiAl-W presented just 0.75 at.% W, half of what was expected. On the other hand, in the samples with constant nominal composition of 20 at.% Cr, the overall composition was in line with the nominal, reaching up to 0.95 at.% W. The same was observed in the sample with the nominal composition of the pseudo-binary NiAl-Cr. The fact that W did not dissolve properly in spite of 5-fold melting, and thus deviated from the nominal values, was understandable due to the much higher melting point of it compared to the other elements. However, the higher at.% W reached in samples with higher at.% Cr indicated that Cr promotes a better W dissolution.

Table 4.1: Deviation of the composition of the samples due to undissolved W.

Sample	Nominal Composition (at.%)		Overall composition (at.%)	
	Cr	W	Cr	W
1	10	1.0	9.73	0.68
2	10	1.4	-	-
3	10	1.8	9.73	0.69
4	20	0.2	20.72	0.23
5	20	0.5	19.40	0.58
6	20	0.8	19.30	0.95
7	-	1.5	-	0.75
8	33	-	33.74	-

Regarding the pseudo-binary eutectic samples, the NiAl-W sample did not reach the eutectic composition due to undissolved W. It exhibited almost no eutectic cells but rather, W phase in a NiAl matrix; which was possible to induce due to the undercooling in arc melting and the strongly skewed coupled zone in NiAl-W phase diagram [110]. On the other hand, the NiAl-Cr sample exhibited almost fully eutectic microstructure with traces of NiAl dendrites, which indicate that the currently accepted value of NiAl-34Cr is indeed the correct eutectic composition.

In all ternary samples, NiAl was the primary phase indicating hypoeutectic composition, as can be seen in figure 4.6. The interdendritic Cr(W) phase was observed in the samples

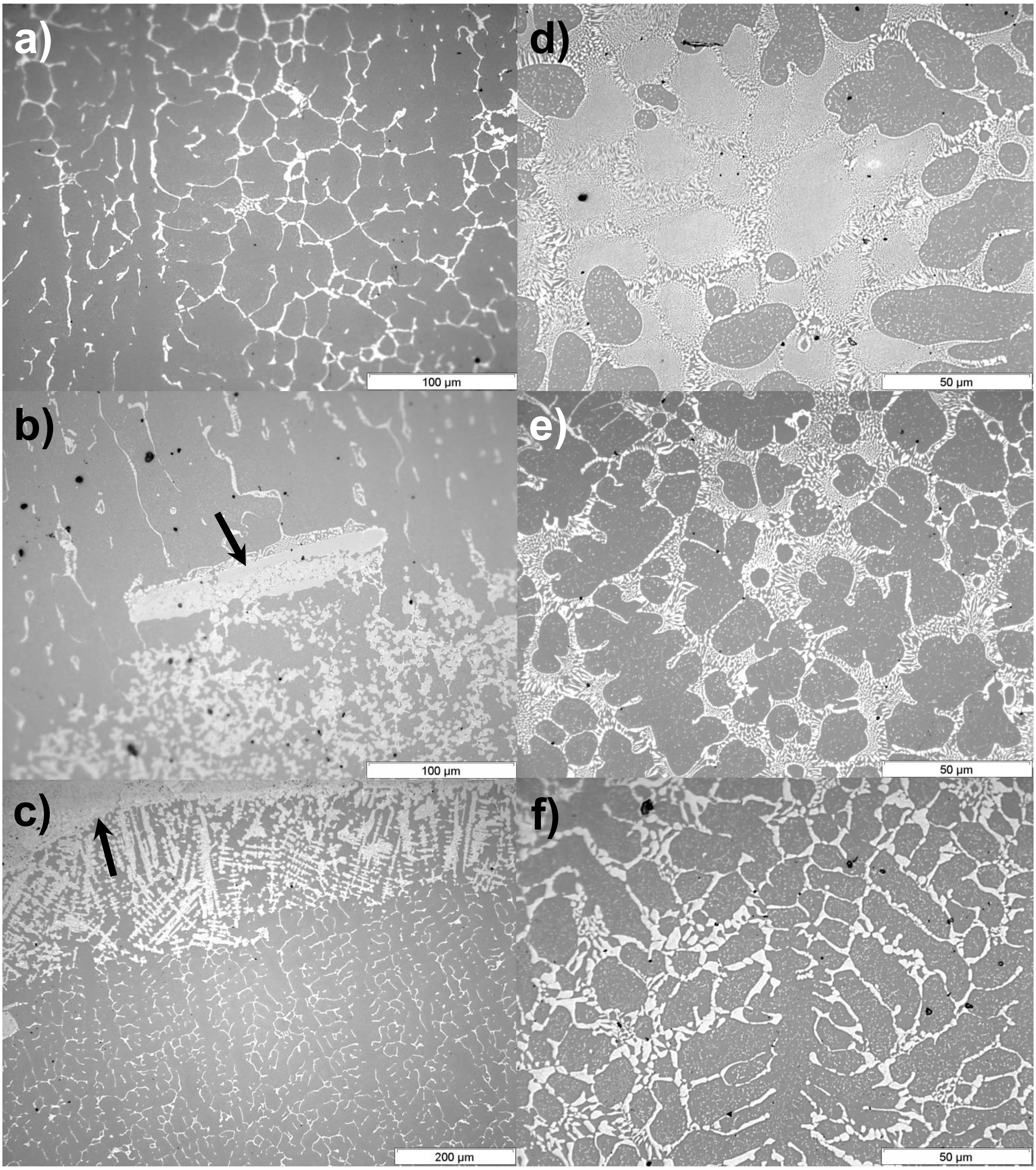

Figure 4.6: Different magnification optical micrographs of the six NiAl-Cr-W samples: a) NiAl-10Cr-1.0W, b) NiAl-10Cr-1.4W, c) NiAl-10Cr-1.8W, d) NiAl-20Cr-0.2W, e) NiAl-20Cr-0.5W and d) NiAl-20Cr-0.8W. Primary NiAl dendrites (dark phase) are observed in all samples, with interdendritic Cr(W) (bright phase) and some eutectic cells. Some undissolved W particles are shown in order to illustrate its effect on the surrounding microstructure.

with 10 at.% Cr, whereas hardly any eutectic constituent (fig. 4.6a) was observed, due to the low amount of W dissolved. Undissolved W particles, although present in all samples, were larger and more frequent in the samples with 10 at.% Cr. The particles severely influenced the surrounding microstructure, where sometimes W(Cr) dendrites were observed (fig. 4.6 b and c), due to partial dissolution. These particles served as nucleation sites for NiAl dendrites, which then grew into the remaining liquid exhibiting a columnar growth. On the other hand, samples with 20 at.% Cr consisted of NiAl dendrites and mainly interdendritic eutectic constituent, which was formed by NiAl and Cr(W) phases. The size of NiAl dendrites and eutectic cells decreased with increased W content, the eutectic constituent becoming the thicker and more irregular . The volume fraction of eutectic was higher in the NiAl-20Cr-0.2W sample, indicating that the eutectic trough is closer to that composition than it is to NiAl-20Cr-0.8W.

Among the ternary samples, differences could be observed in the eutectic constituent, not only in its volume fraction, but also in the morphology of the eutectic cells (fig. 4.7). The formation of eutectic cells is caused by the development of instabilities in the solid-liquid interface. For instance, impurities can destabilize the morphology of the eutectic, owing to the formation of a long-range diffusion boundary ahead of the solid-liquid interface [93]. Additionally, the solidification conditions such as undercooling and growth rate affect the morphology of the eutectic constituent. In figure 4.7, the hypoeutectic microstructure can be observed at higher magnification. NiAl dendrites presented extensive precipitation due to a decrease of solubility when cooling. In the same way, precipitation was observed in the Cr(W) phase, which was already observed and reported for NiAl-Cr(Mo) alloys [95, 97]. In that case, more Al than Ni partitioned towards the refractory phase. EPMA analyses performed in this study confirmed the observation for NiAl-Cr(W) as well.

As can be observed in figure 4.7, NiAl dendrites are surrounded by a Cr(W) phase layer, which is almost continuous, resembling a halo. The formation of a halo of one phase around a primary dendrite of another phase is a common feature in the solidification of off-eutectic alloys or sufficiently undercooled eutectic alloys [110, 132–135]. Theoretically, in an off-eutectic alloy, the nucleation of primary dendrites starts at the liquidus temperature, and they grow until the eutectic temperature is reached. Then, the eutectic constituent would nucleate on the primary dendrites [93]. However, some eutectic alloys exhibit non-reciprocal nucleating characteristics, which means that one primary phase is an effective heterogeneous nucleation site for the other, but not vice versa [110, 132, 135]. In this case, the primary dendrites keep growing in a metastable liquid which is supersaturated in the other phase, till eventually the nucleation of the other phase is forced, and coupled eutectic growth can finally take place. Therefore, in the studied samples, NiAl is a poor nucleating phase, although the feature cannot always be observed in the microstructure.

4.2.2 Eutectic composition

As the aim was to preliminary assess the eutectic trough, measurements of the composition of the eutectic cells were performed in the samples of 20 at.% Cr, where the eutectic constituent was present. Due to the size of the eutectic cells and phases inside the constituent, EPMA technique was used in order to cover the smallest features and support EDX measurements, which resulted in a good agreement. The analyses indicated an increase of W content in Cr(W) phase as the amount of W increased in the sample. Segregation of the W content within the Cr(W) phase was measured, as could also be noted from the different brightness of the phase in the BSE micrograph of figure 4.7. NiAl dendrites exhibited a similar trend, though the content of W was negligible. Although the precipitates were too small for analysis, the 7-8 at.% Cr content in the NiAl dendrites indicated that the precipitates are Cr rich. Likewise, the content of W in the eutectic constituent increased with increasing amount of W in the sample.

In figure 4.8, the composition of the eutectic cells is plotted, together with the overall composition of the samples and the average NiAl dendrites composition. The eutectic trough is defined by the composition of the different eutectic cells, whose values should lie around a line. However, there was significant scatter between cells, which could be due to the W segregation already mentioned. As can be seen, the amount of W in the eutectic increased as the Cr content decreased, keeping the combined at.% of Cr and W close to 34, which is the composition of the NiAl-Cr eutectic. This fact is not uncommon, as was already

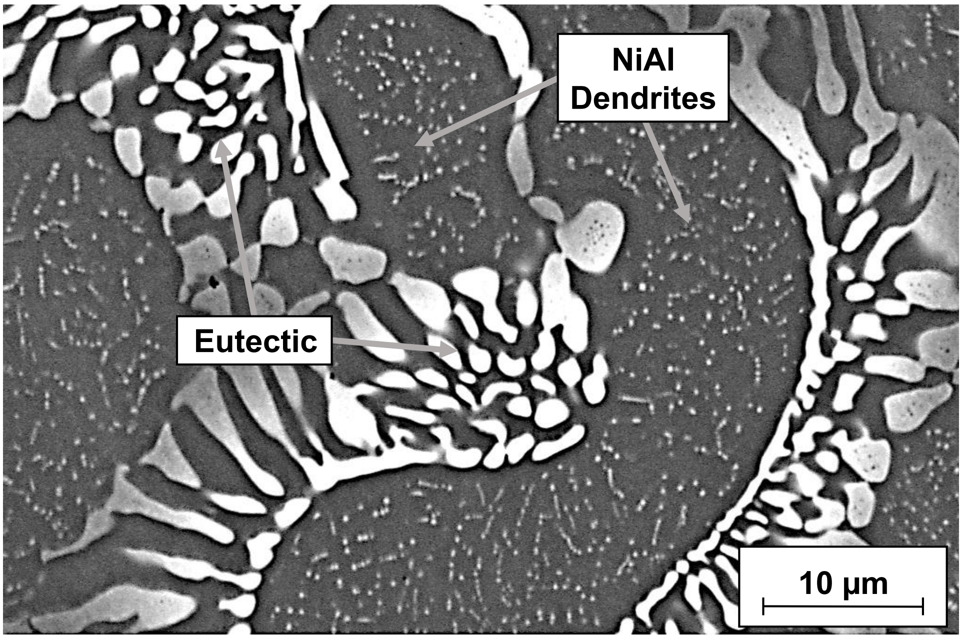

Figure 4.7: SEM BSD high magnification micrograph of the NiAl-20Cr-0.8W sample showing the principal features: NiAl dendrites, interdendritic eutectic constiuent, precipitation in both phases, precipitation-free zones, and halo formation.

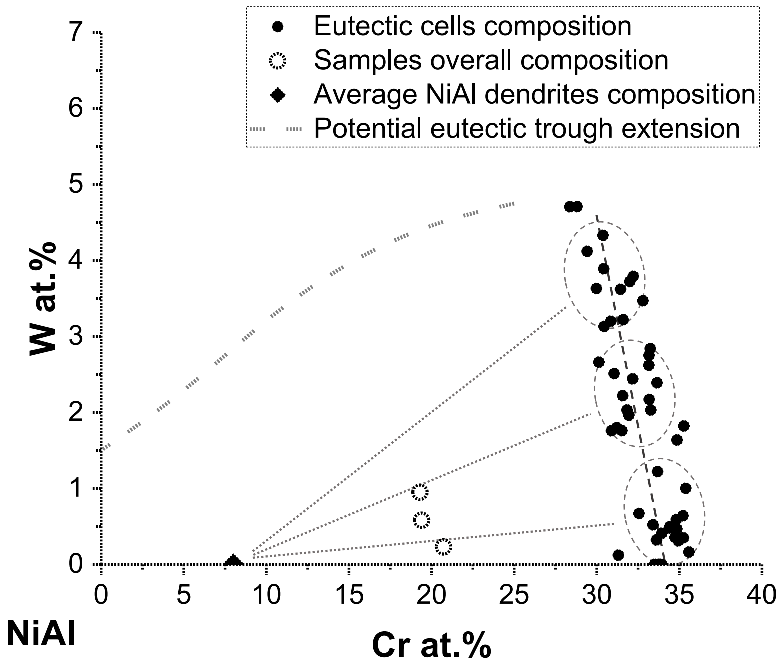

Figure 4.8: Composition of the eutectic cells within the studied samples, which partially define the eutectic trough. The overall composition of the samples and the average NiAl dendrite composition are also plotted, as well as a potential extension of the eutectic trough.

reported for NiAl-Cr(Mo) alloys [96]. However, the high increase in W, reaching almost 5 at.% at around 28 at.% Cr, was unexpected. Especially when considering the composition of NiAl-W eutectic, which has a W content of only 1.5 at.% [110]. Due to this unexpected behavior of the eutectic trough, together with the presence of undissolved W, obtaining a complete preliminary assessment was not possible with the produced samples. On the other hand, the section obtained on the Cr rich side was useful to propose a potential path of a hypothetical continuous eutectic trough for further study. Moreover, the section assessed was consistent with NiAl being the primary phase. This was also consistent with the observations of the higher volume fraction of eutectic constituent in the sample with the lowest amount of W, compared to the one with the highest W content, as the distance to the eutectic trough is different. It is important to keep in mind that local compositions do not correspond to overall compositions, as the samples were not homogeneous.

4.3 Alternative processing routes

Although the data gathered in the preliminary study provided the basis for further research, the issues related to the sample production and correct dissolution of elements were a key factor that needed to be overcome. Despite the use of techniques such as the Exomelt process to exploit the heat produced by the exothermic reaction between Ni and Al when forming NiAl, the production of the alloys directly from the raw elements was shown to be inadequate, probably due to the high melting point of W and its low solubility in NiAl. Therefore, an alternative production route was developed as an attempt to avoid the problem, or at least to reduce it. The development was carried out first with the induction furnace and later with the arc melting furnace.

4.3.1 The Ni-Cr-W approach

The first approach to the development of a successful processing route was the preparation of a prealloy which could enable a good dissolution and homogeneity of the sample. Due to the broad phase field of Ni solid solution in the ternary diagram with Cr and W (fig. 4.9), a Ni-Cr-W mixture was initially prepared with the required amount of each of the three elements and melted in the induction furnace. Once the elements melted, the molten alloy was kept for 20 minutes to ensure dissolution. Afterwards, Al pellets were added to the melt. During the addition of Al to the melt, the formation of NiAl, which is an exothermic reaction, led to an increase in the temperature of the melt. Therefore, the Al pellets were added gradually while the power input of the induction furnace was lowered, in order to minimize temperature increase and thus protecting the crucible from cracking. After the required

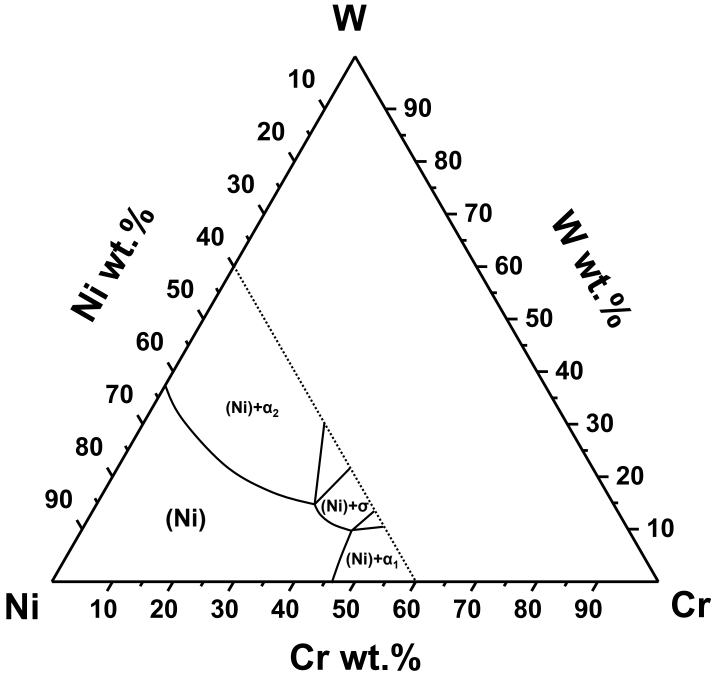

Figure 4.9: Section of the Ni-Cr-W phase diagram isotherm at 1250 °C, showing the Ni solid solubility phase field [136].

Al amount was added, the melt was kept for another 10 minutes in order to improve the homogeneity of the alloy. Finally, the melt was slowly cooled down and solidified in the crucible. The slow furnace cooling was done in order to keep the rod dimension for further DS processing. However, due to the large difference in densities between the elements, there was segregation in the rod, what was noted when extracting the rod from the crucible. Both the weight and external appearance of the rod were considerably different in each of the edges. Therefore, the ingot was placed upside down in the crucible to compensate the effect in the next step, where the ingot was remelted and processed by DS.

The first alloy composition to be prepared was NiAl-20Cr-4.5W (at.%). The composition was chosen from the results of the preliminary study, and laid around the proposed path extension. Although the eutectic path was not completely assessed, in order to obtain a fully eutectic microstructure, DS was performed so as to test the crucible configuration and check whether the conditions of thermal gradient and growth rate were sufficient for a successful DS processing. Moreover, due to the special conditions associated with DS, the obtained microstructures would be coarser and closer to the equilibrium. Therefore, even in an off-eutectic composition, the eutectic constituent present in the microstructure could provide more accurate and valuable data of the eutectic trough than that of arc melted samples. Results in that regard will be presented in Chapter 5.

Regarding the processing route, although the Ni-Cr-W mixture was kept molten for 20 minutes before the next step, the extensive presence of W particles (fig. 4.10) was observed mainly at the bottom of the DS rod. The shape and size of the particles, which included rounded particles with diameters of about 20 μm, suggested that there was only a partial dissolution of the W pellets, and that the dissolution could have been complete with longer times. On the other hand, the particles were surrounded by a Cr rich phase, which also contained W and, in a lesser proportion, Al and Ni. The layer exhibited significant precipitation, which was confirmed by EDX to be NiAl-based, with more Al than Ni partitioning to it. Hence, the layer was a Cr(W) phase similar to the one observed in the preliminary samples.

Furthermore, no interdiffusion zone between W particles and the Cr(W) layer was observed, but a clear boundary, indicating that both phases are different. Indeed, there was a sudden change between the composition of both phases. Whereas the Cr(W) phase contained up to 10 at.% W, the particles had around 87 at.% W, with the balance being mainly Cr, probably due to diffusion. Based on these results, an accumulation of Cr around the W particles suggested that the process took place in the melt. The formation of this layer stopped the contact of W with the melt, preventing it from dissolving and blocking its diffusion towards the melt. Due to the high melting point of W, Cr and their alloys, particles with layers remained solid in the melt.

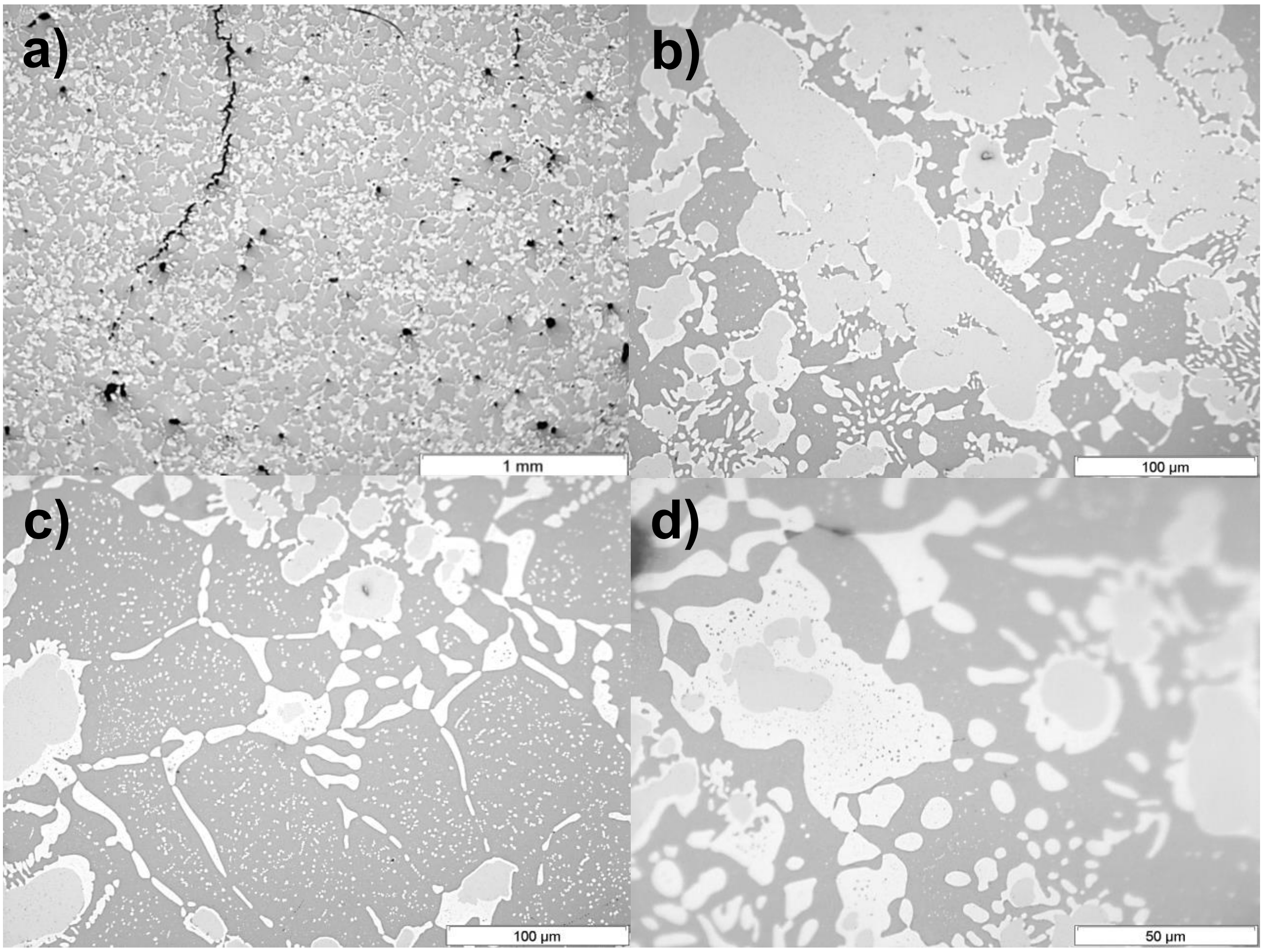

Figure 4.10: Optical micrographs of the DS NiAl-20Cr-4.5W sample processed by the Ni-Cr-W route showing: a) a general overview of the bottom, b) undissolved W particles (gray phase) surrounded by a Cr(W) layer (bright phase), c) NiAl dendrites with precipitates, and d) a thick Cr(W) layer with visible precipitation.

4.3.2 The Ni-W approach

Despite some positive results yielded by the previous approach, production of particle-free samples was not successful. These particles influenced the local composition, causing the microstructure to be heterogeneous. In view of previous results, the formation of a Cr(W) layer around the partially dissolved W impeded the total dissolution of the particles, which remained solid in the melt due to the high melting point of both phases. In order to tackle this problem, a new route was developed, by adding one step to the previous Ni-Cr-W route.

In the Ni-W approach, the production of Ni-Cr-W prealloy was split in two. First, a Ni-W solid solution was produced, preventing any formation of Cr layer, and the melt was kept for 1 hour to ensure W dissolution. From Ni-W phase diagram presented in figure 4.11, production of a Ni-W solid solution is possible in a wide range of compositions, with the advantage of relatively low melting temperature, which facilitates the processing. Once

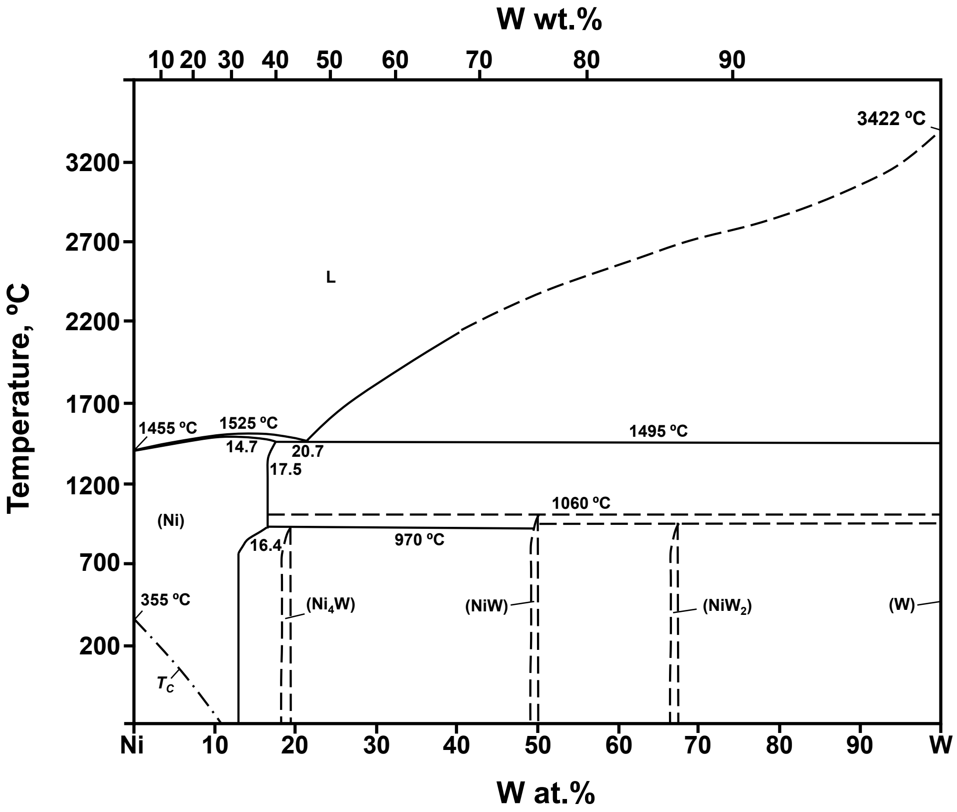

Figure 4.11: Ni-W phase diagram [137].

Ni-W prealloy was ready, Cr was added to the melt. However, to ensure total dissolution of W, the Ni-W prealloy was cast in the first test before adding Cr to study the microstructure. After, the route continued as in 4.3.1.

During testing, the cast rod of Ni-W prealloy was cut, and two samples from the top and the bottom were analyzed in order to verify the degree of W dissolution. The samples were observed by means of LOM and SEM, where no signs of W particles could be seen. In figure 4.12, the microstructure of the alloy is shown, which consisted of single phase columnar grains at the edge of the sample, and equiaxed grains at the center with an average size of 20 μm. This microstructure is typical of conventional casting in copper mold. EDX analyses were carried out in the samples which revealed the average composition to be in line with the nominal one. Moreover, there was negligible difference in composition between the edge and center, either in grains or in the whole samples, which indicated no segregation.

In view of the success of dissolving W, Ni-W prealloy was used for further steps in the production of another DS NiAl-20Cr-4.5W alloy. In this case, the alloy was also cast prior to DS processing, in order to avoid segregation due to different densities observed in 4.3.1. Afterwards, the alloy was remelted and DS processed with the same conditions.

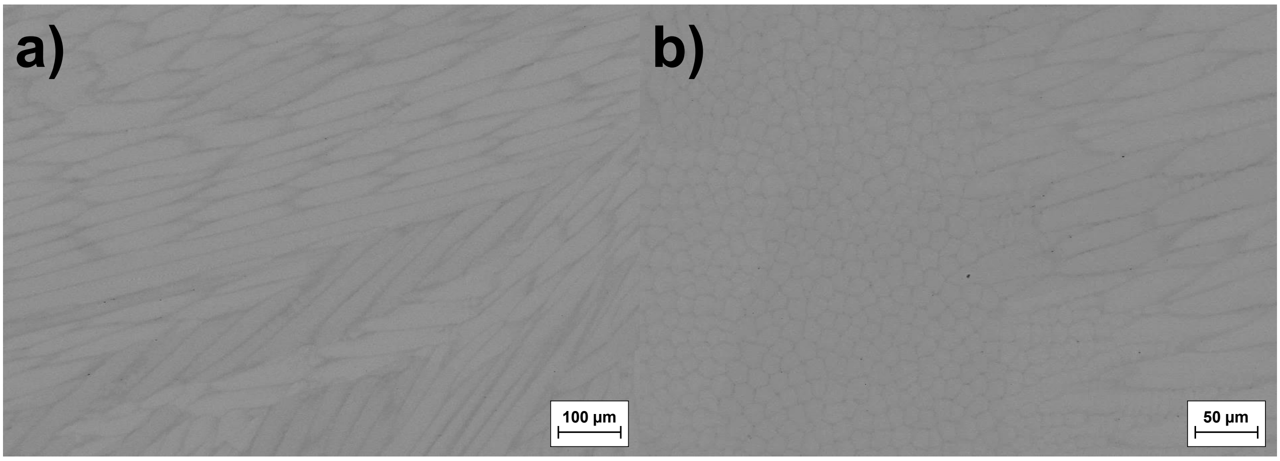

Figure 4.12: SEM micrographs of the single-phase microstructure of Ni-W prealloy a) at the edges and b) at the center of the sample.

After the DS process, the produced rod was analyzed. Characterization with LOM revealed the presence of W particles mainly at the bottom of the sample (fig. 4.13). The particles were similar to those observed in the sample processed by the Ni-Cr-W route in 4.3.1, with a rounded shape. However, some improvements were observed with the Ni-W route, as the particle size was smaller in general. The Cr(W) layer was also present around the particles as well, but with the particularity of not being continuous, thus, not completely surrounding them.

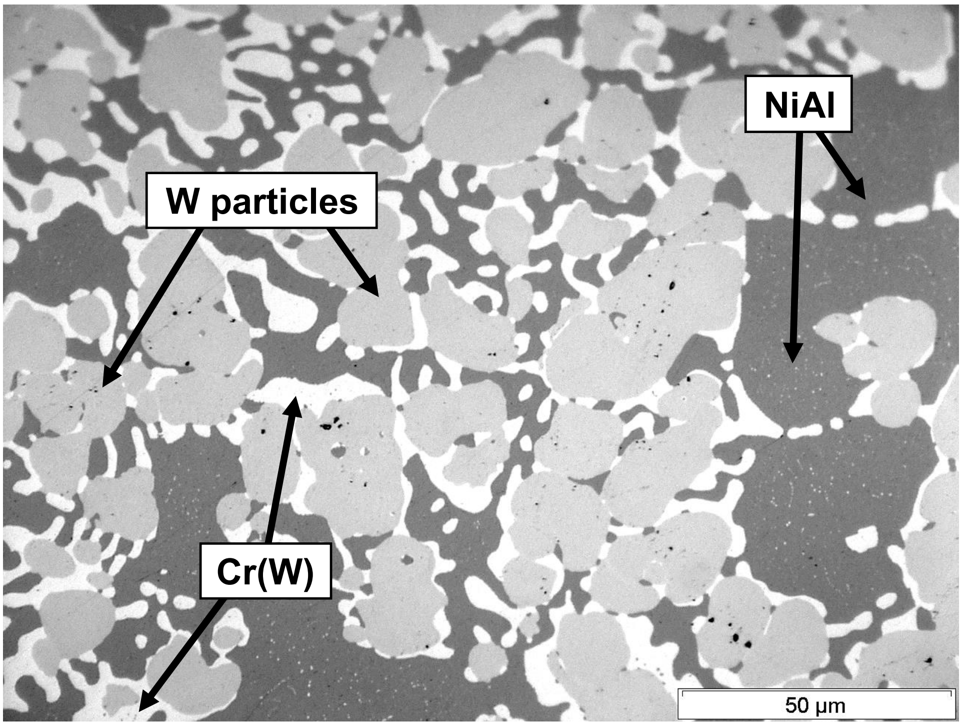

Figure 4.13: Optical micrograph at the bottom of the DS NiAl-20Cr-4.5W alloy processed by the Ni-W route showing the presence of W particles.

On the basis that a homogeneous alloy with fully dissolved W was used as prealloy for the production, the presence of these particles was an unexpected result. Their size was around 20 μm, which is larger than the grains observed in the Ni-W prealloy (fig. 4.12), and indicated that their formation happened in the subsequent steps of the processing. The addition of Cr to the prealloy, or the formation of NiAl when adding Al, could have triggered the generation of the particles and the Cr(W) layer surrounding them. Therefore, a thorough study of the microstructure was performed after each step of the process in order to identify the possible problem. The samples were produced by the Ni-W route in the arc melting furnace, in order to take advantage of its acquisition.

Chromium addition

To check whether the W particles formed during Cr addition, the Ni-W prealloy produced previously was arc melted together with the corresponding amount of Cr. The microstucture and composition of the resulting Ni-Cr-W alloy was analyzed. Figure 4.14 shows the microstructure obtained, which consisted of Ni solid solution dendrites as expected, with no signs of undissolved W or formation of particles. The overall composition was measured by EDX and was consistent with the nominal values. However, there was a slight difference of about 2 at.% between dendrites and interdendritic areas. While dendrites were richer in W, interdendritic had higher Cr content, indicating segregation. This fact is not uncommon during the solidification of solid solutions. In any case, a single phase microstructure was observed in the whole sample.

Ni-Cr-W solid solution prealloy had been successfully obtained by arc melting, and presumably the same happened in induction melting after Cr was added. Thus, Cr addition was not the critical step for the formation of W particles during the production.

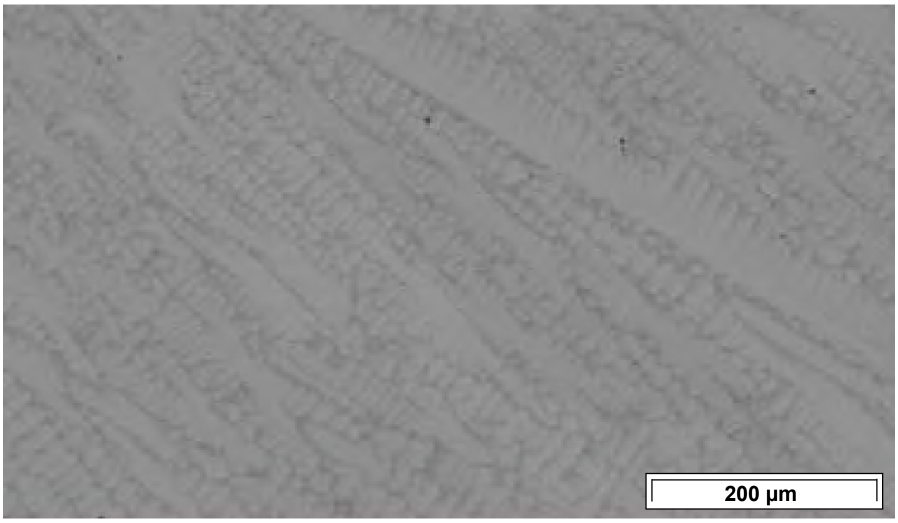

Figure 4.14: SEM BSD image of the arc melted Ni-Cr-W alloy microstructure.

Aluminum addition

Once the Cr addition step had been discarded as the cause of the particles issue, the study continued with the next step. The Ni-Cr-W solid solution was then arc melted with the necessary amount of Al, and the sample was prepared for characterization. Once more the microstructure contained W particles, although this time, the size was smaller than 20 μm. In view of the similar results obtained, the bottom section of the DS NiAl-20Cr-4.5W alloy processed by the Ni-W route was remelted by arc melting. This was done as an attempt to dissolve the particles after all steps, when NiAl intermetallic has already formed. With a more versatile technique such as arc melting, which can reach temperatures not limited by a ceramic crucible, and with a system equipped with a magnetic stirring device, the melting and dissolution should be more easily achieved.

In figure 4.15, the microstructure of the remelted sample is shown. In this case W phase was also present, but in the form of dendrites, indicating its formation from the liquid. On the other hand, NiAl phase also resembled a dendrite growth, with a lobed shape. The W phase size was sensitively smaller than it was before remelting (fig. 4.13), which was mainly surrounded by a Cr(W) layer, and eutectic constituent was present between dendrites.

The results indicate that the W particles present in the DS NiAl-20Cr-4.5W alloy produced by the Ni-W route, were completely dissolved in arc melting, and formed from the melt during solidification. By the same token, it is probable that in the Ni-Cr-W route, W was fully dissolved in all steps of the process, only forming during the solidification of the alloy. The fact that particles are located mainly at the bottom in DS samples could be explained by the different densities. As DS process runs for a long time, particles that form from the melt can grow and sink, piling up at the bottom.

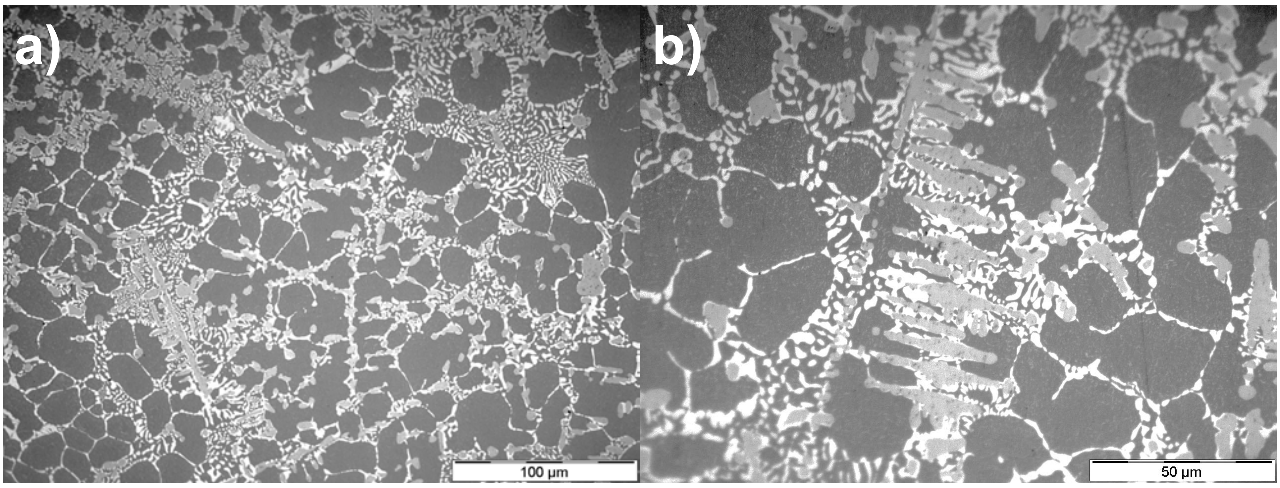

Figure 4.15: LOM micrographs of the bottom section of DS NiAl-20Cr-4.5W, remelted in the arc melting furnace. The W phase has in this case a dendritic structure, which is better appreciable at higher magnification.

The reason why the NiAl phase resembled a dendrite growth remained unclear. However, the Ni-W processing route exhibited fully W dissolution, and refined microstructure compared to preliminary samples, or even the Ni-Cr-W route processed alloy. Moreover, the arc melting technique was proven to be more efficient for producing the alloys for further DS processing. Therefore, the Ni-W route and arc melting technique, were both selected for the production of the following alloys.

5
Eutectic Trough

After obtaining the first results of the eutectic trough through the composition of eutectic cells in preliminary samples, the work continued with the production of new alloy compositions that imply different microstructures, and furthermore, in which a eutectic constituent with a different composition could be present to improve the assessment of the eutectic trough.

5.1 DS NiAl-20Cr-4.5W

The DS alloys from the tests performed to improve NiAl-Cr-W alloy production, were also used for the assessment of the eutectic trough, and their microstructure was characterized beyond shown in 4.3. When DS rods were cut, samples from the top and middle (relative to the growth direction) were taken in addition to the bottom already observed.

5.1.1 Alloys produced by the Ni-Cr-W route

Apart from the bottom section, where most W particles were observed (fig. 4.10), the microstructure of the middle section consisted of primary NiAl dendrites with interdendritic eutectic cells. However, almost fully eutectic microstructure could be found at the edges of the sample, as well as some W particles. On the other hand, the top section also contained NiAl dendrites but in lower amounts, as the volume fraction of the eutectic constituent was higher than in the middle section. Significant deviation from the nominal composition was observed, which was in agreement with these substantial differences observed.

Middle section

In figure 5.1, an overview of the microstructure and main features present in the middle section is given. Primary NiAl dendrites presented precipitates, which after EDX

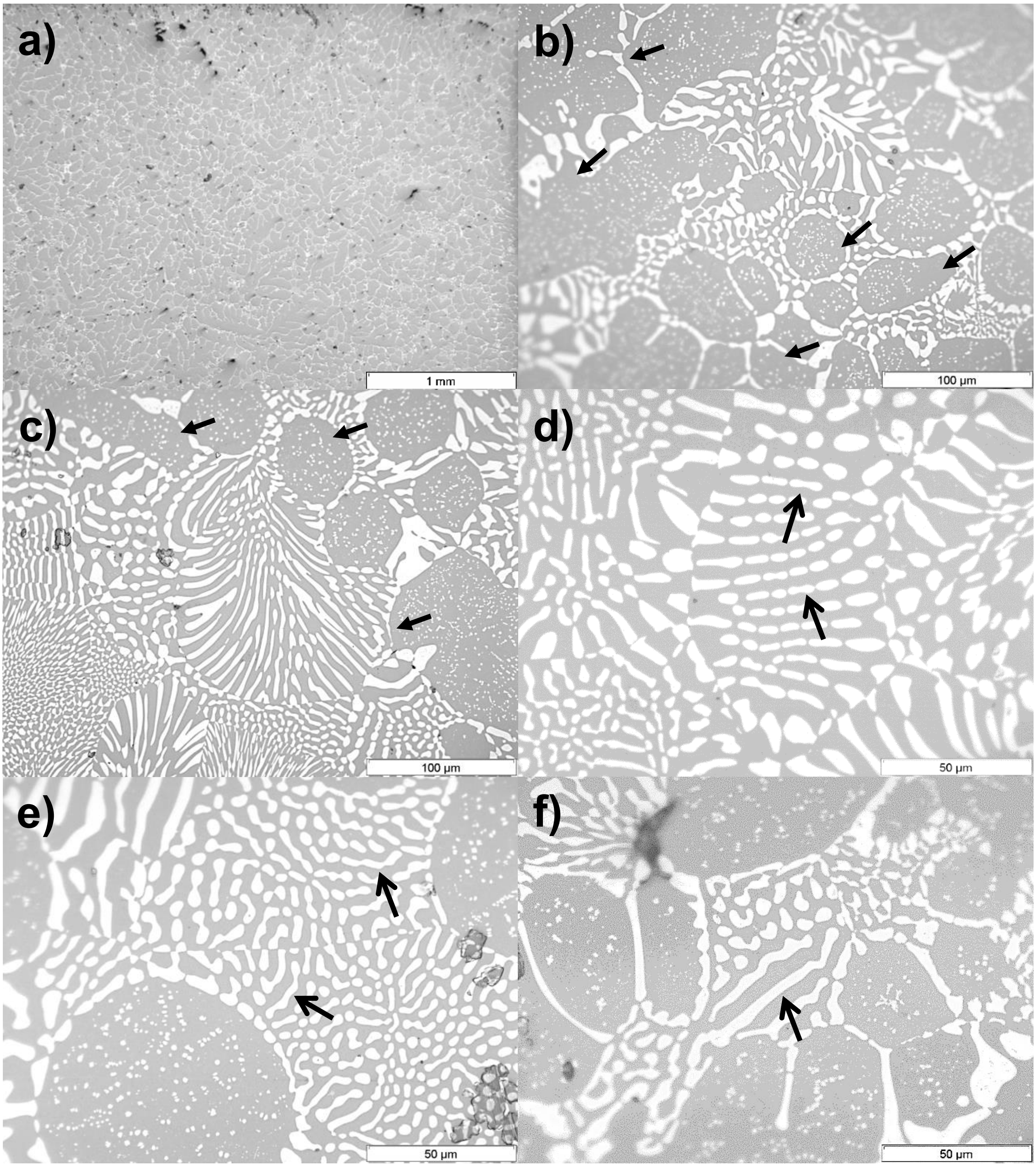

Figure 5.1: Different magnification optical micrographs of the middle section of DS NiAl-20Cr-4.5W produced by the Ni-Cr-W route. a) NiAl primary dendrites can be observed in low magnification. In b) and c) PFZ are indicated by the black arrows. Cell boundaries in colonies can be observed in c) and d). Special black arrows in d), e) and f) indicate the rod-lamellar transition.

measurements, and due to the negligible solubility of W in NiAl, were concluded to be Cr-based. Additionally, precipitate-free zones (PFZ) could be observed at the boundaries of NiAl dendrites (fig. 5.1b and c). Due to decreasing solubility during solidification, the excess of Cr formed precipitates within dendrites, with the exception at the borders of the dendrites, where the Cr in excess could diffuse towards the melt, leaving a PFZ. The Cr content in PFZ was about 3 at.%, compared to the 7 at.% Cr measured in the middle of the dendrites. Likewise, in the case where the Cr(W) phase was large enough, NiAl-based precipitates could also be observed inside it with PFZ at the borders, similar to figure 4.10d. The eutectic constituent had a cellular morphology, with well-defined cell boundaries (fig. 5.1c, d and e), owing to the different growth direction and interspacing between cells. The morphology of the eutectic constituent varied significantly along the sample. Different solidification conditions could lead to different morphologies. However, substantial differences were observed even between neighboring cells. In figure 5.1d and e, an emerging transition from a lamellar to a rod eutectic can be observed. During solidification, instabilities are formed in the lamellae. These instabilities grow until the lamellae are decomposed to form rods, completing the transition inside one cell (fig. 5.1f). The transition from one morphology to the other depends on the volume fraction and composition of the reinforcing phase.

Top section

The top section of the DS rod presented the highest volume fraction of eutectic constituent. Within it, a special microstructure could be sometimes noticed (fig. 5.2). The Cr(W) phase grew as a needle, with its length exceeding 100 μm, and it was surrounded by NiAl phase, from which the eutectic constituent nucleated and grew. An irregular Cr(W) phase was

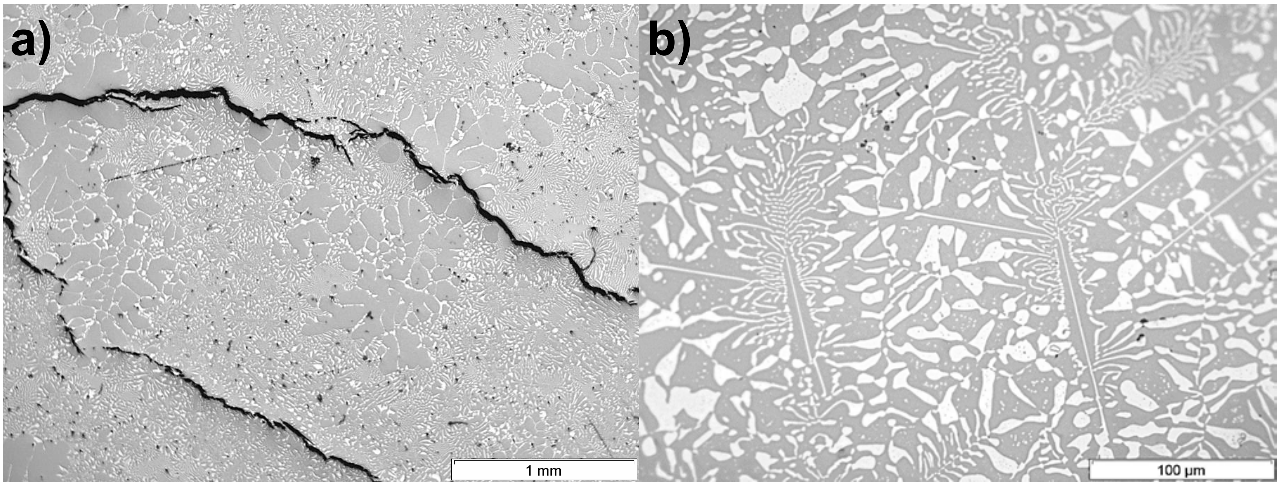

Figure 5.2: Optical micrographs of the top section of DS NiAl-20Cr-4.5W produced by Ni-Cr-W route. At low magnification a), NiAl primary dendrites and eutectic cell colonies can be observed. Special needle microstructure b) can be observed in some zones of the sample.

observed in the surroundings. Although this has already been reported for NiAl-Cr(Mo) alloys as well [138], the cause of the formation of needles is unknown. This type of structure is typical of faceted phases whilst Cr(W) should have an isotropic growth due to the low entropy of fusion of these phases.

Eutectic morphology and composition

The composition of the eutectic constituent was analyzed by EDX in several eutectic cells, which were selected individually, bearing in mind that they have an appropriate size and are regular enough to perform a reliable measurement. It was noted that the location and morphology of the eutectic cells was directly related to their compositions.

Eutectic cells with a rod morphology located next to or between W particles (fig. 5.3a and b), had a composition around 25 at.% Cr and 5 at.% W. The Cr(W) rods were about 5 μm in diameter. These eutectic cells (I) were found mainly at the bottom section, where most W particles were present. Some features indicated how the nucleation and growth of the eutectic happened. The Cr(W) layer around the particles exhibited a non-planar morphology, indicating a cellular instability that increased, growing into the melt to form the eutectic. On the other hand, signs of halo formation around NiAl were also present.

Isolated from W particles, eutectic cells with a similar rod size and morphology to the previous ones were observed (fig. 5.3c and d). These cells (II) had a slightly higher Cr content, with about 26 at.%, but a much lower W content, around 2.5 at.%. Without W particles, the eutectic nucleated in this case solely from NiAl dendrites. Moreover, growth of cells was observed to take place in colonies, rather than alone; furthermore, their average size was observed to be larger than the previous cells. Regular growth in the middle of the cell evolved into a coarse Cr(W) phase at the boundaries, where precipitation in both phases was visible.

Finally, eutectic cells with irregular morphology were observed. These cells (III) were found in the middle and top sections, like the previous ones, and even sometimes next to each other as part of the same colony. The Cr(W) phase had, in this case, an irregular morphology, not resembling any specific shape (fig. 5.3e and f). The composition of these cells was about 32 at.% Cr and less than 1 at.% W. Since the neighboring cells should have similar solidification conditions, the morphology transition from irregular to regular was influenced by the composition.

In figure 5.4, the results of the composition of the different eutectic cells measured by EDX are plotted. A wide scattering of data, even wider than observed in the preliminary samples in 4.2.2, made it difficult to state a trend for the eutectic trough; for example in the Cr variation between (I) and (II). However, a large number of eutectic cells were analyzed, supporting the idea of local composition variations in the sample, presumably due to

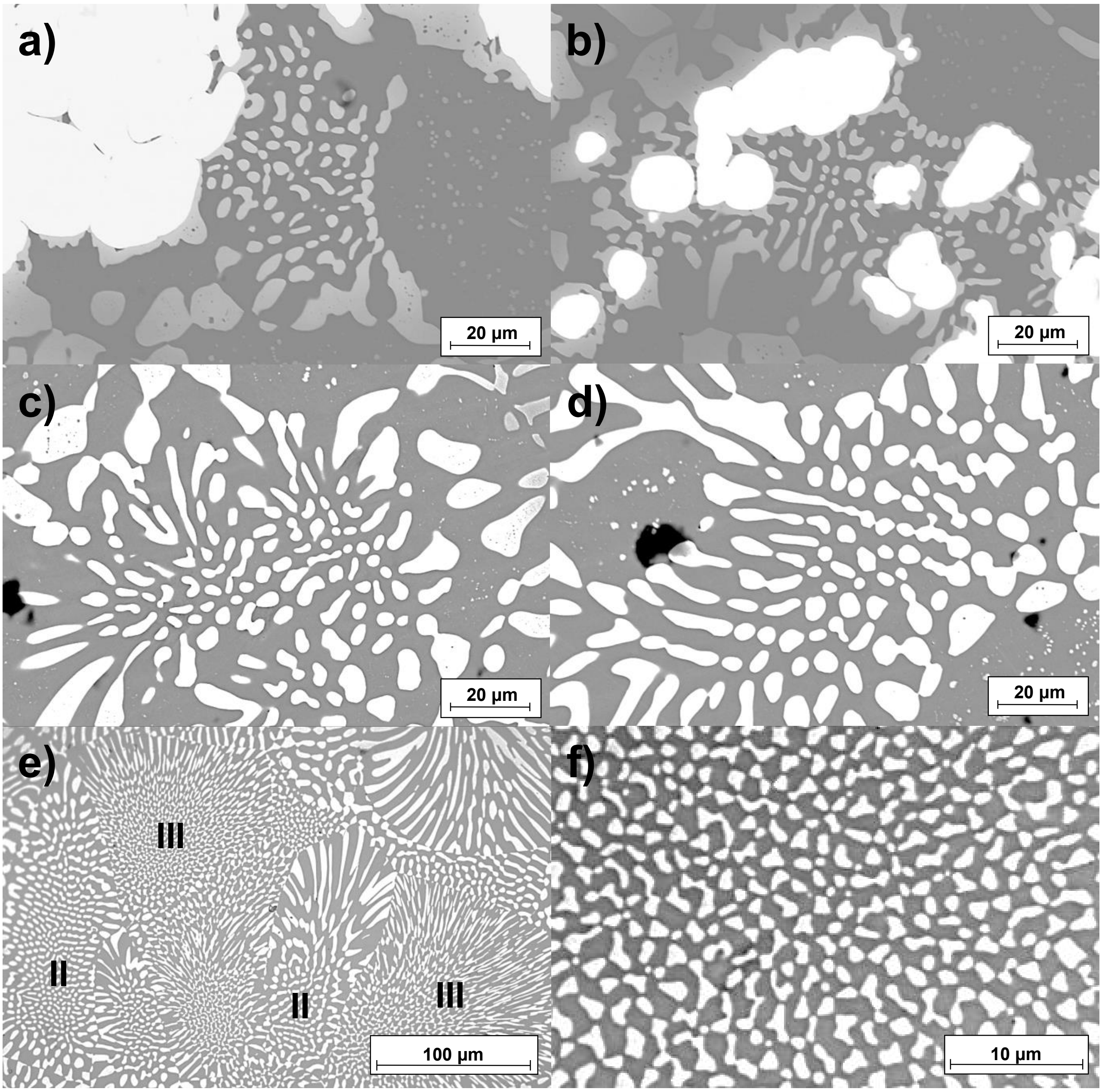

Figure 5.3: SEM BSD images of the different eutectic cells observed in the DS NiAl-20Cr-4.5W alloy produced by Ni-Cr-W route: a) and b) eutectic cells (I) observed next to particles; c) and d) eutectic cells (II) observed in e) cellular colonies, sometimes also next to f) eutectic cells (III).

segregation. In figure 5.4b the mean values are plotted together with the preliminary results, in order to emphasize the variation between both, which must be related to the different solidification parameters in arc melting and DS. Therefore, results from both techniques must be treated separately and only be compared with caution. Nevertheless, all results fit with a rapid increase of W content in the eutectic trough up to at least 6 at.%.

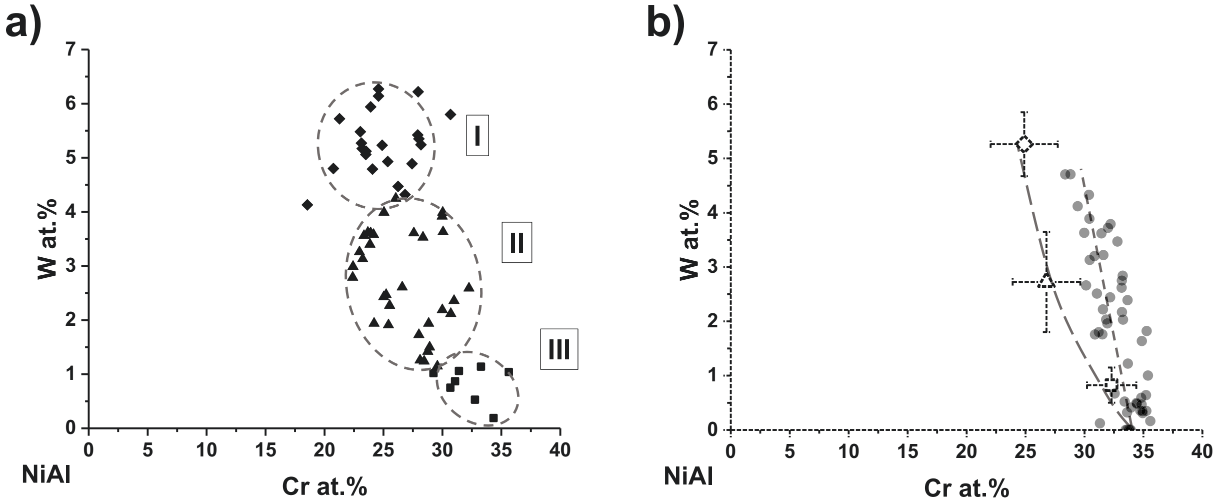

Figure 5.4: Composition of the different eutectic cells a) measured by EDX, and b) the mean values compared to the data obtained in the preliminary results.

5.1.2 Alloys produced by the Ni-W route

The microstructure of the alloy produced by the Ni-W route was similar to that of the one produced by the Ni-Cr-W route. Apart from the bottom section, where once again, W particles were observed (fig. 4.13), the microstructure of the middle section consisted of primary NiAl dendrites, eutectic colonies as well as some W particles; in this case (fig. 5.5), these eutectic colonies were composed mainly of regular rod cells. In the top section, a microstructure consisting of lamellar eutectic cells along with coarse Cr(W) and NiAl phases was observed.

Additional EDX measurements of eutectic cells were performed, and are plotted in figure

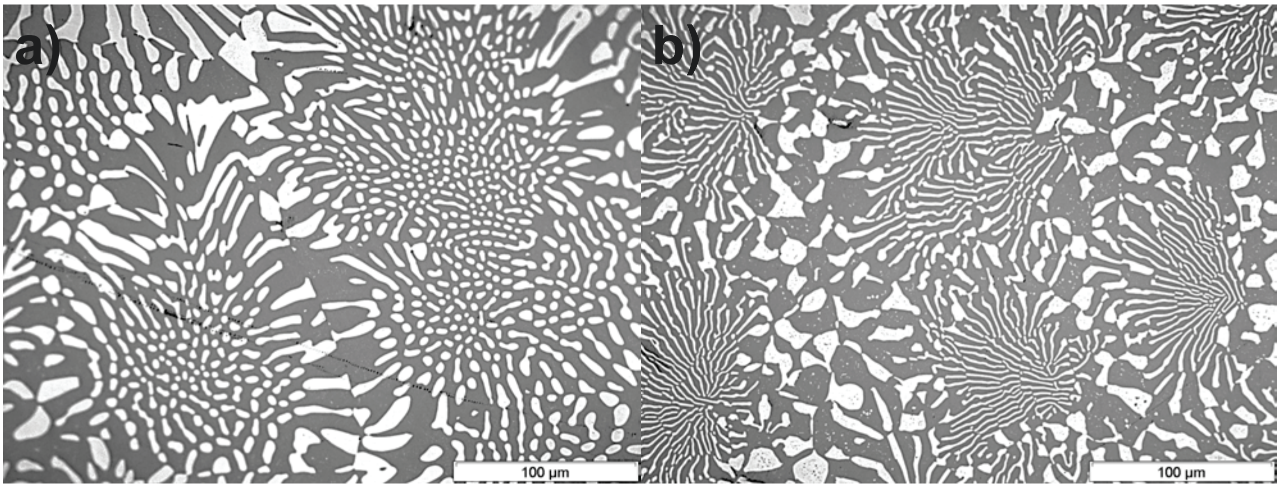

Figure 5.5: Optical micrographs of the microstructure of DS NiAl-20Cr-4.5W produced by Ni-W route: a) in the middle section and b) in the top section of the sample.

5.6, together with the data of the previous DS sample in figure 5.4a. As can be seen, the results match those of the eutectic cells (II).

Therefore, a fully-aligned microstructure with planar growth, as would be expected in the case of classical DS processing, could not be obtained. An insufficient thermal gradient or a too high growth rate could be the reasons behind this. Unfortunately, the thermal gradient achieved with the set-up is still unknown. However, growth rates of 20 mm/h or higher have been reported to be sufficient for NiAl-Cr(Mo) alloys. Another possible explanation could be that the presence of W particles or other phases in the melt, can act as heterogeneous nucleation points and as such, have an impact on the final microstructure, being essential in order to process a fully eutectic composition.

The results of eutectic compositions obtained with DS samples are similar to those obtained in the preliminary work, and are located on the Cr-rich side of the sought eutectic trough, close to the NiAl-Cr pseudo-binary eutectic. Therefore, further alloys were produced with compositions closer to the Cr-lean side, in order to obtain data from this area of the phase diagram that had not been assessed.

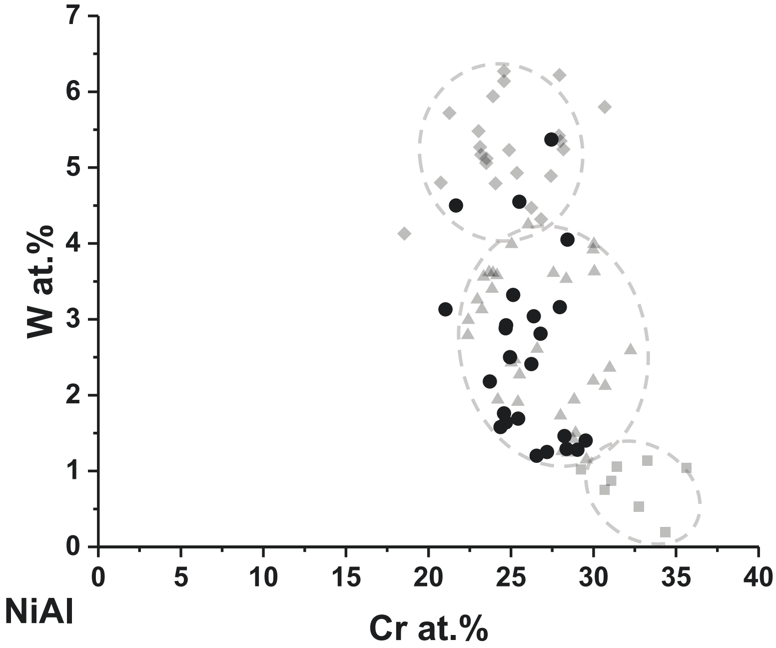

Figure 5.6: Compositions of the measured eutectic cells in the DS NiAl-20Cr-4.5W alloy produced by the Ni-W route (black dots), and overlapped with the data from DS NiAl-20Cr-4.5W alloy produced by the Ni-Cr-W route (in gray).

5.2 Arc melted alloys

In view of the results obtained with DS and the recent acquisition of an arc melting furnace by IMDEA Materials, further alloys for the assessment of the eutectic trough were produced by arc melting. The Ni-W route was used to produce them as it proved to be the most effective for W dissolution. The versatility of the arc melting furnace allowed the melting of the alloys several times between steps and mixing them with the magnetic stirrer system, ensuring better sample homogeneity.

5.2.1 Eutectic trough extension: NiAl-20Cr-4.5W and NiAl-10Cr-3.5W

During the optimization of the processing route and DS testing, two samples were processed by arc melting. In order to check whether the undissolved W already present could be dissolved by remelting, using the new equipment, the bottom and middle sections of the DS NiAl-20Cr-4.5W processed by the Ni-W route were arc-remelted. The microstructure of the samples has already been presented in figure 4.15 and characterized. However, EDX measurements of the eutectic constituent were also performed and are presented in figure 5.7. The composition of the eutectic exhibited the same trend as previous samples, but closer to the preliminary results, as the processing technique was also arc melting. Only few measurements deviated, getting closer to the DS values. Again, there was a wide dispersion between the results.

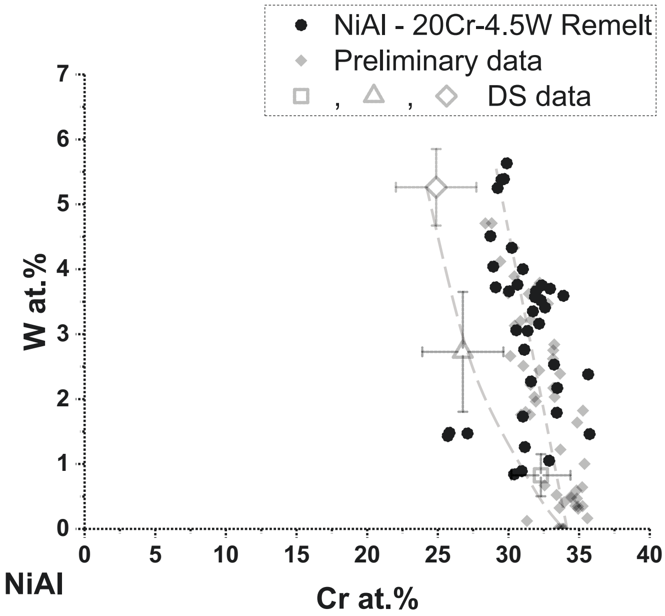

Figure 5.7: Composition of the measured eutectic cells in the arc remelted bottom and middle sections of the DS NiAl-20Cr-4.5W alloy produced by the Ni-W route (black dots). Overlapped can be seen the composition of preliminary data and DS mean values for comparison.

The other composition that was processed by arc melting during DS tests was the NiAl-10Cr-3.5W. The composition was chosen in accordance with the potential eutectic trough extension proposed in figure 4.8, and used to determine the W dissolution and microstructure after the Cr and Al addition steps. The former was already discussed in 4.3.2 and the latter is hereafter presented.

The microstructure mainly consisted of NiAl dendrites, with interdendritic Cr(W) phase and low amount of eutectic constituent in the form of cells, which were sometimes grouped in colonies. NiAl dendrites seemed to be the primary phase, indicating that the compositions are hypoeutectic. However, W particles with average sizes of less than 10 μm were also present. Some of them resembled a dendrite, but it was difficult to interpret whether they formed from the melt or not. Also, they were surrounded by a Cr(W) layer. A special feature was found in this sample and it is shown in figure 5.8. Small W-rich particles with an irregular shape formed around W particles, but also separated from them, and they were mostly surrounded by a Cr(W) layer, though not completely. The reason for this phenomenon is not clear and might be related to a not reported reaction. However, EDX measurements indicated an overall composition close to the nominal, and no signs of impurities, reducing it to amounts non-detectable by the technique. On the other hand, even though the overall composition was in agreement, the sample - and in general all arc melting samples - was very heterogeneous, implying significantly different local compositions. Eutectic cells were measured as well, and the results are plotted in figure 5.8b. As can be seen, the compositions follow the trend of previous samples, although the scatter is even wider, with some closer to the DS values.

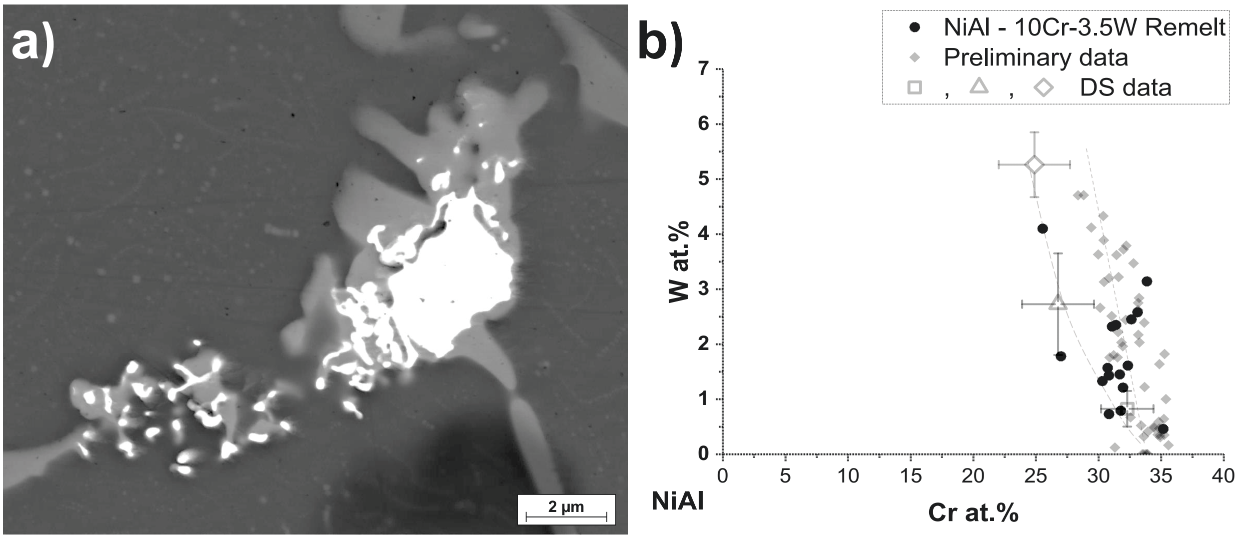

Figure 5.8: NiAl-10Cr-3.5W arc melted sample: Microstructural feature of a) W-rich particles with irregular shapes around and next to the W particles, which are semi-surrounded by the Cr(W) phase; b) composition of the measured eutectic cells in the sample (black dots). Overlapped can be seen the composition of preliminary data and DS mean values for comparison.

5.2.2 Cr-lean region

In view of the results obtained until this point, where all compositions gathered from the eutectic trough laid on the Cr-rich side, close to the NiAl-Cr pseudo-binary eutectic, new alloys with more specific compositions were produced.

Firstly, to seek for the other edge of the eutectic trough, compositions close to the NiAl-W pseudo-binary eutectic were produced. This region, with less than 10 at.% Cr, was designated as the Cr-lean region. For the full assessment of the eutectic trough there, three new alloys were produced: a NiAl-2Cr-3W alloy, a NiAl-3Cr-4W alloy and a NiAl-5Cr-2W alloy. Additionally, the NiAl-10Cr-1.8W alloy from the preliminary samples was remelted in order to fully dissolve the W particles and obtain data from the boundary of the region.

The microstructure of all the alloys was similar: a NiAl matrix in which some round W particles with micrometer size were present (fig. 5.9c). The particles were partially

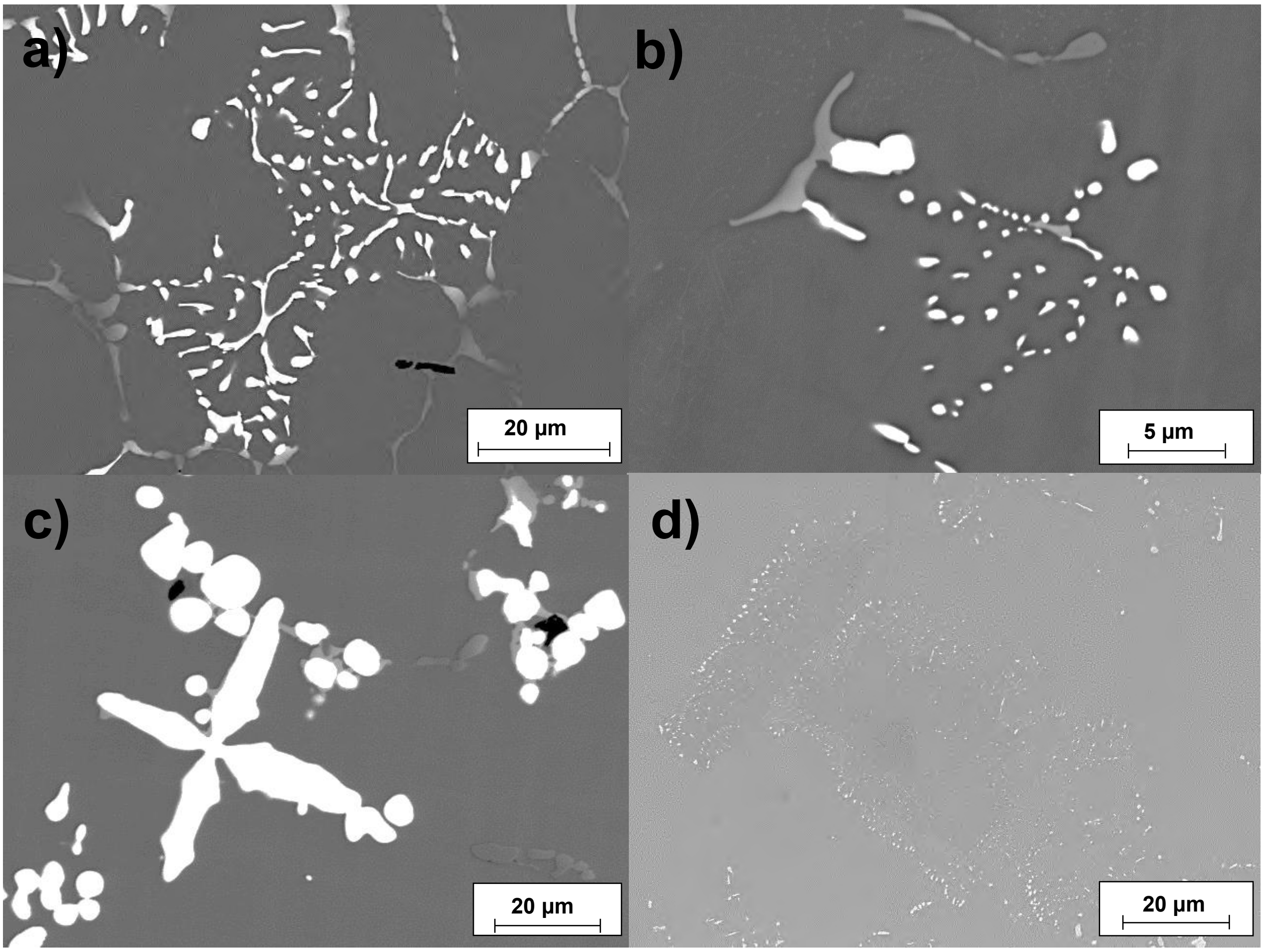

Figure 5.9: SEM BSD micrographs of the microstructure of Cr-lean samples: a) irregular eutectic constituent in NiAl-10Cr-1.8W sample, b) a eutectic cell in NiAl-5Cr-2W sample, c) rounded W particles partially surrounded by a Cr(W) phase next to a W dendrite, and d) regular eutectic cell in NiAl-2Cr-3W.

surrounded by a Cr(W) phase. Although it is not likely to have a Cr(W) phase, due to the position of the composition in the phase diagram, the formation of this phase could be due to these zones being the last to solidify, or because of local composition changes.The NiAl phase exhibited precipitates, but contained a lower amount of Cr than observed in previous samples. Some eutectic constituent was found, but the amount of eutectic cells was scarce. In case of the NiAl-10Cr-1.8W alloy, due to the higher Cr amount, NiAl formed dendrites which exhibited more precipitation, while Cr(W) phase formed at interdendritic spaces, similar to the observations before remelting. However, in this case eutectic constituent was also present. Its eutectic cells exhibited a very irregular morphology as shown in figure 5.9a. In the other samples, the eutectic cell morphology was rod-like and became increasingly regular from the NiAl-5Cr-2W alloy (fig. 5.9b) to the NiAl-2Cr-3W (fig. 5.9d), whose eutectic morphology was very similar to that reported for the NiAl-W pseudo-binary eutectic [110], with a fiber size of less than 500 nm. Nevertheless, the eutectic constituent was very scarce in the samples, the cells being too small to perform accurate composition measurements many times; this reduced the number of results.

In figure 5.10 all the measurements are plotted. As can be seen, a similar trend as observed in the other edge of rapid increase in the W content took place. However, the results were completely unexpected due to the really high amount of W reached in the eutectic composition, up to 12 at.%, several times higher than the NiAl-W pseudo-binary eutectic, and even higher than the potential eutectic trough extension proposed in the preliminary work. It was therefore understandable, that no data from this side of the eutectic trough was obtained from the preliminary samples, where most of the W in the samples

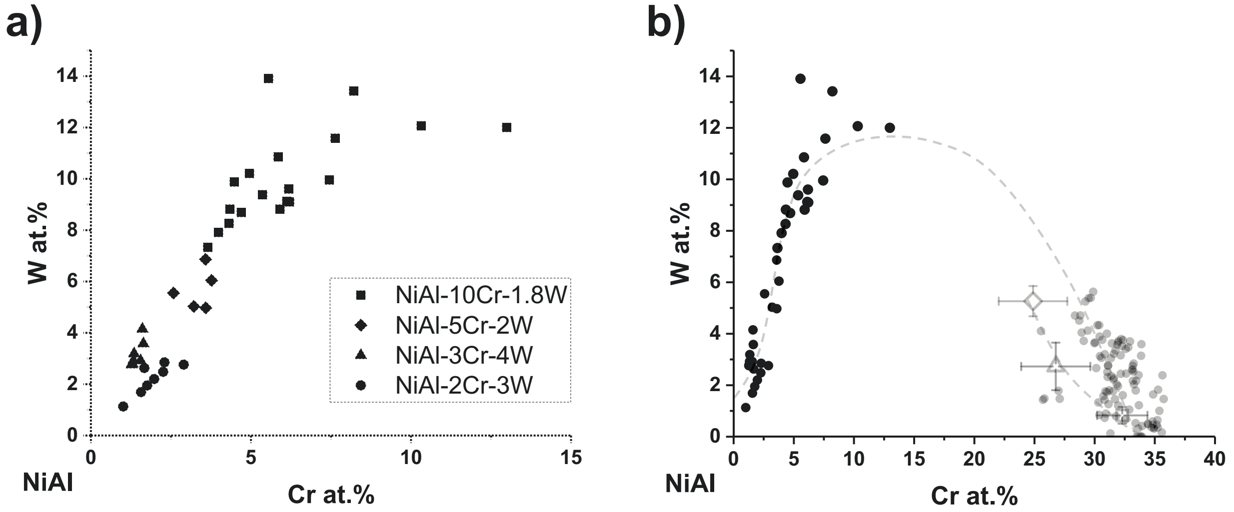

Figure 5.10: Composition of the measured eutectic cells a) of each of the Cr-lean samples, and b) of all Cr-lean samples (black dots), together with arc melting data obtained until now and DS mean values for comparison. A revised eutectic trough extension is proposed.

with lower Cr content remained undissolved. Moreover, after finally assessing the eutectic trough section in the Cr-lean region, both trends indicated that the extension proposed, underestimated the amount of W, and that a hypothetical continuous eutectic trough would imply higher W content. However, the scarcity of eutectic in the current samples, the irregularity and the scatter of compositions, made it difficult to state whether fully eutectic microstructures will be achievable.

5.2.3 Middle region

The assessment of the eutectic trough in the Cr-lean region of the phase diagram greatly exceeded the eutectic trough extension proposed in figure 4.8. The Cr-rich section exhibited a rapid increase of the W content too, reaching values of about 6 at.%, which is already significantly higher than the NiAl-W pseudo binary eutectic, and was not expected. However, the Cr-lean region reached values almost 10 times higher than the pseudo-binary, surpassing all expectations. In view of this, a hypothetical continuous eutectic trough should continue with this trend of high W content in the middle region. Therefore, in order to assess the path of the eutectic trough in the middle region, samples with very high amounts of W were produced in the region between 10 - 25 at.% Cr. The compositions selected for this purpose were: NiAl-25Cr-11W, NiAl-15Cr-15W, and NiAl-7Cr-11W.

The alloys produced, although processed by the Ni-W route, which included several steps to ensure W dissolution and to homogenize the sample, were not successful. The microstructure of the three samples presented undissolved W (fig. 5.11a), with W pellets which remained almost untouched, indicating that the amount of W in the alloys was too large to process them. The W that remained during the process, affected the composition of the samples, which presented significant differences in local composition, not reaching the objective. Furthermore, W rounded particles were present in the microstructure (fig. 5.11b), which could have formed during solidification, although this is difficult to judge. However, NiAl-15Cr-15W, due to its higher W content, exhibited the largest amount of W particles and, as can be seen in figure 5.11c, included what looked like a W pellet at an advanced stage of dissolution. As the pellet dissolved, rounded shapes formed on the surface, which at some point would detach from the pellet and be released into the melt. These released W particles would then mix with the melt and continue dissolving until the end of the process (fig. 5.11d). If the process ends before the W is completely molten and dissolved, the particles, which sometimes resemble dendrites, would affect the local composition and serve as nucleation sites for phases during solidification. This would be a possible explanation for the melting and solidification processes in NiAl-Cr-W alloys, and the formation of a Cr(W) layer surrounding the particles. However, there are also clear signs of dendritic growth of W phase (fig. 5.11e), making it very difficult to carry out a correct evaluation of the microstructure.

No significant differences were observed between the three microstructures, though

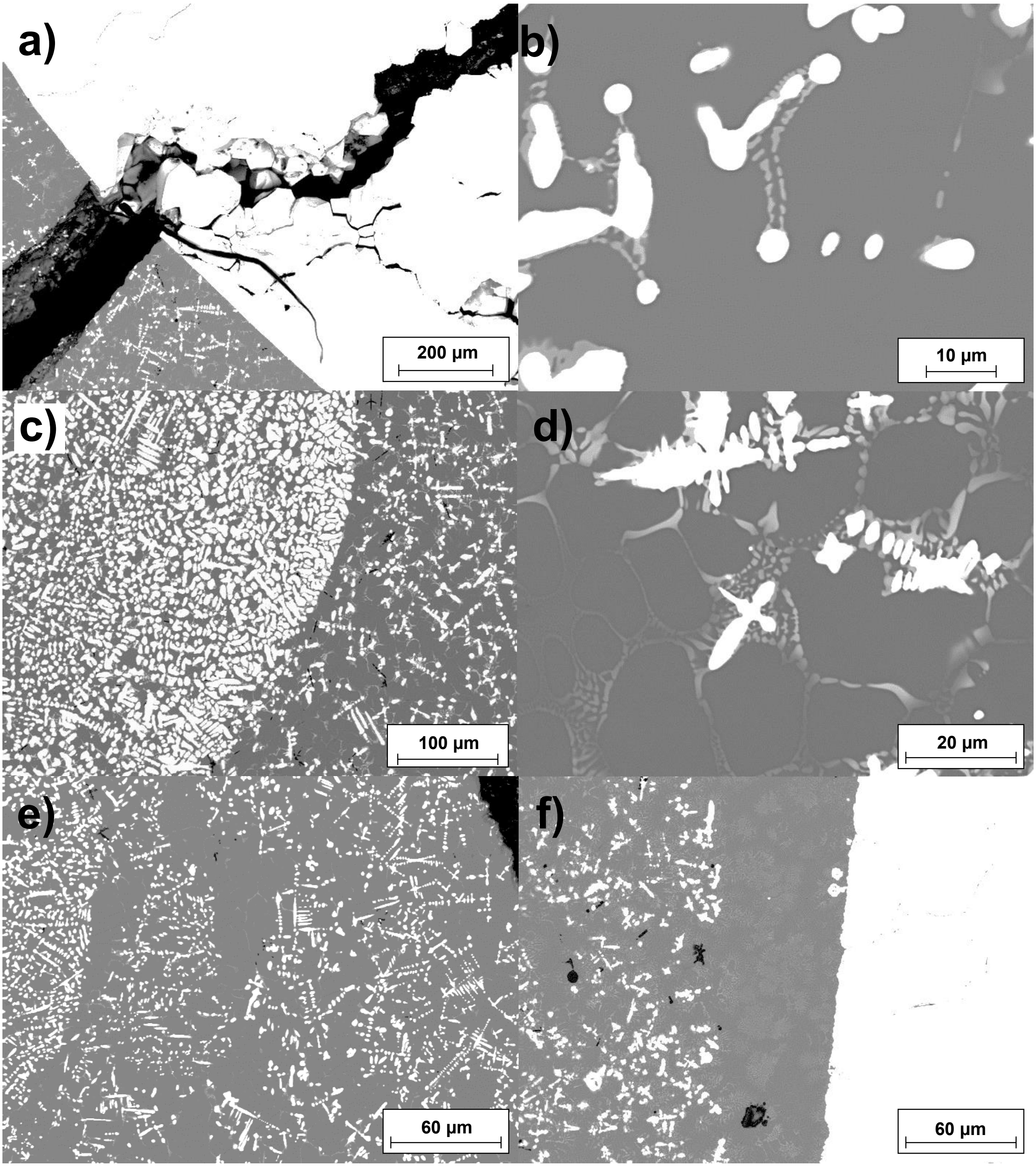

Figure 5.11: SEM BSD micrographs of features in the microstructure of middle region samples: a) undissolved W pellet where grains can be seen in NiAl-15Cr-15W, b) rounded W particles partially surrounded by Cr(W) phase in NiAl-7Cr-11W, c) partially dissolved W pellet, d) W phase dendrites in NiAl-15Cr-15W microstructure, e) apparently detached W particles (left) with allegedly W dendrites (right), and f) a large area of eutectic constituent in NiAl-25Cr-11W.

in NiAl-25Cr-11W, because of the higher Cr content, a higher amount of Cr(W) phase and eutectic constituent were present (fig. 5.11f). Although the areas with W dendrites were perfectly valid, owing to the large amount of undissolved W, the performed EDX measurements of the eutectic laid again in the Cr-rich side. This was because the local composition in these areas was in the Cr-rich region too, not giving any new information. Therefore, the data won't be presented here.

The findings observed in these samples, clarified the difficulties experienced previously in obtaining any data of the eutectic trough far from the Cr-rich side, especially in this middle region. They also support the fact that producing these kinds of NiAl-based alloys with a high W content is an enormous challenge, and that the constrains to be overcome for producing fully eutectic microstructures are still large.

5.2.4 Improved assessment of the Cr-rich section

Based on the results and observations from the work up to this point, the issues involved in obtaining data, and even producing samples in the middle region, or producing fully eutectic microstructures in the Cr-lean region, became evident. On the other hand, the assessment of the Cr-rich region had been successful, and more than enough data was gathered to obtain the path of the eutectic trough in that section, at least roughly. However, the wide scatter observed in the measurements, demanded a refinement of the study in the region. For that purpose, alloys with composition along the data obtained were produced. As the production technique was still arc melting by the Ni-W route, the data from DS was put aside for the moment, and two compositions were selected for the alloy production: NiAl-32Cr-3W and NiAl-29Cr-6W. They were chosen from the middle and the edge of the assessed section and the amount of Cr + W was constant at 35 at.% because of the slope observed. The compositions are very similar to those of the NiAl-Cr-Mo alloys being studied recently; this would allow a better comparison of the properties in the future.

NiAl-32Cr-3W

The microstructure revealed that the composition was not fully eutectic. Indeed, W particles were present in the sample, mostly in the form of dendrites, with no signs of any NiAl dendrites, indicating that the composition was hypereutectic. The microstructure was not homogeneous along the sample (fig. 5.12a), as is usually the case in all arc melted samples produced. Therefore, local composition deviations were expected, but the overall composition was in good agreement with the nominal one. EDX measurements revealed that the composition of the W phase was richer in Cr than in previous samples, with contents of 20 at.% or more. In consequence, the W(Cr) was the primary phase forming from the melt, which was then surrounded by Cr(W) as reported in previous samples. However, in this case, the W(Cr) phase sometimes exhibited a sort of torn granular structure (fig. 5.12b), whose formation was unclear, and the Cr(W) phase surrounding was thicker and

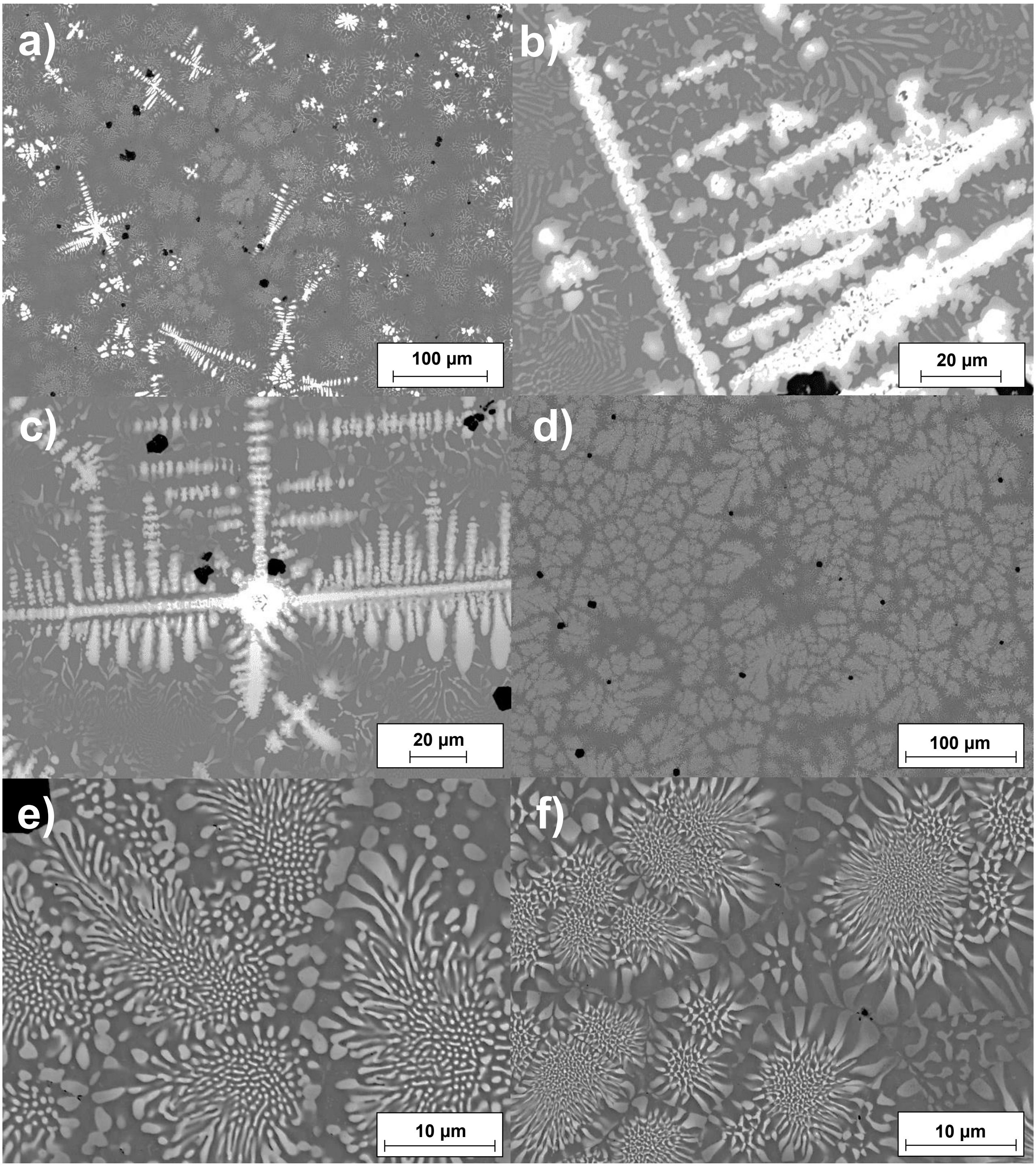

Figure 5.12: SEM BSD micrographs of features in the microstructure of NiAl-32Cr-3W sample: a) overview of the inhomogeneous microstructure, b) W phase resembling dendrite growth but with a sort of granular structure, c) a dendrite exhibiting phase change and segregation, d) large area with fully eutectic microstructure, e) cells with regular morphology in a eutectic colony, and f) cells with irregular morphology in other eutectic colony.

more irregular than observed before.

In figure 5.12c, a dendrite from the microstructure can be seen. The core of the dendrite was W(Cr) phase, and the dendrite seemed to have grown from it. Additionally, both primary and secondary arms of the dendrite exhibited a brighter core, which had higher W content, with a darker layer around. It is possible that the W(Cr) core acted as a nucleation site for the dendrite, however, the different brightness in the BSD images indicates a decrease in the W content - confirmed by EDX - which seemed to be a case of severe dendritic segregation. This is a typical feature of alloys that have a wide solidification range, where each zone of the dendrite solidifies at a different temperature and with different composition. Nevertheless, there were also signs of sudden change in the brightness and therefore in the composition, so the problem should be approached with caution. Strong precipitation was observed in the darker zones, which were richer in Cr. EDX measurements confirmed higher partitioning of Al than Ni into the phase. Despite not presenting precipitates, the brighter areas also contained Ni and Al, although the ratio was closer to stoichiometry or even reversed, with higher Ni partitioning where the content in W was higher.

The eutectic constituent volume fraction of the samples was very high, and even wide areas with fully eutectic microstructure could be found (fig. 5.12d). The eutectic constituent had a cellular shape, growing in colonies. The colonies were formed by eutectic cells with regular or irregular morphology (fig. 5.12 e and f), and both were sometimes nearby. This was already observed in 5.1, where the different cells were found even next to each other in the same colony. However, in this case, the composition was very similar, exhibiting the irregular one slightly higher contents of Cr and W, although the difference was negligible.

NiAl-29Cr-6W

The microstructure of this sample was similar to that of NiAl-32Cr-3W. Cr(W) dendrites, some with W(Cr) core, were present together with eutectic constituent. No signs of NiAl dendrites were observed, indicating that the composition is hypereutectic as well. Few particles were detected which could be identified as undissolved W. The dendrites exhibited a similar structure, with severe segregation, and precipitation in the outer Cr(W) phase. EDX measurements showed the similarities also in the composition of the eutectic cells. The results gathered from the samples are plotted in figure 5.13.

Surprisingly, although the nominal composition of the samples was chosen based on the results of eutectic composition obtained previously, and the overall composition of the samples matched with the nominal one, the eutectic constituent in the alloys had a very different composition. The values laid far from the data obtained in previous arc melting samples and closer to the data obtained in DS tests. Moreover, the data did not follow the same trend of rapid increase in W content with decreasing Cr, but rather it looked like the

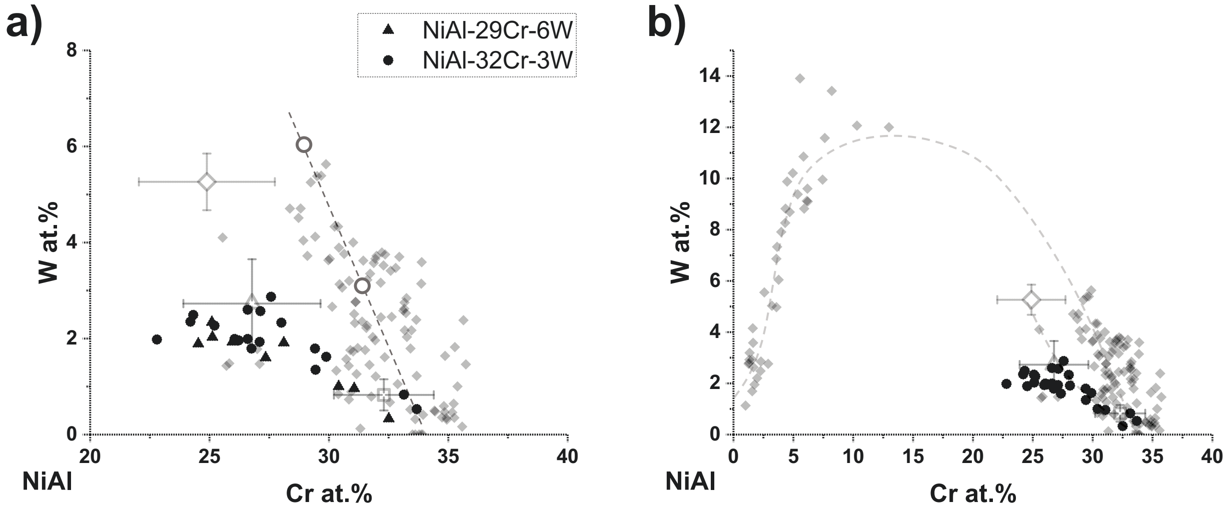

Figure 5.13: Composition of the measured eutectic cells: a) close view of results from NiAl-32Cr-3W and NiAl-29Cr-6W samples compared to the nominal composition (large rings) and previous results nearby, and b) same data together with all the arc melting data obtained until now and DS mean values for comparison.

limit in W would have been almost reached. These unexpected results, have widened the scatter of data, and opened up a huge question about the actual path of the eutectic trough sought.

In view of the results, due to the particles found in the microstructure which could be identified as undissolved W, and in addition to the sort of torn granular structure of some dendrites, both samples were remelted and studied again. Furthermore, a new alloy was produced with NiAl-27Cr-2W composition.

NiAl-27Cr-2W and remelted NiAl-29Cr-6W and NiAl-32Cr-3W

The remelted samples did not exhibit any significant change in the microstructure. On the other hand, NiAl-27Cr-2W sample provided a completely new microstructure. Particles of the W(Cr) phase were present in the whole sample, together with NiAl, which was in the surroundings of the particles as can be seen in figure 5.14a, but also as dendrites (fig. 5.14b, bottom left), indicating at first sight that it is a hypoeutectic alloy. In some cases, the similar microstructure in the surroundings suggested that a W(Cr) particle had been there before (fig. 5.14c), though is difficult to say. However, the particles and these ”particle traces” were both surrounded by NiAl phase lobes separated by Cr(W) phase and resembling a flower-like structure. It is not yet clear how this structure formed, although it looked like NiAl nucleated from the particle and then grew forming the lobes and sometimes formed dendrites. Finally, the eutectic phase nucleated and grew after a halo formation around the NiAl phase. On the other hand, the core of a W(Cr) particle is shown in

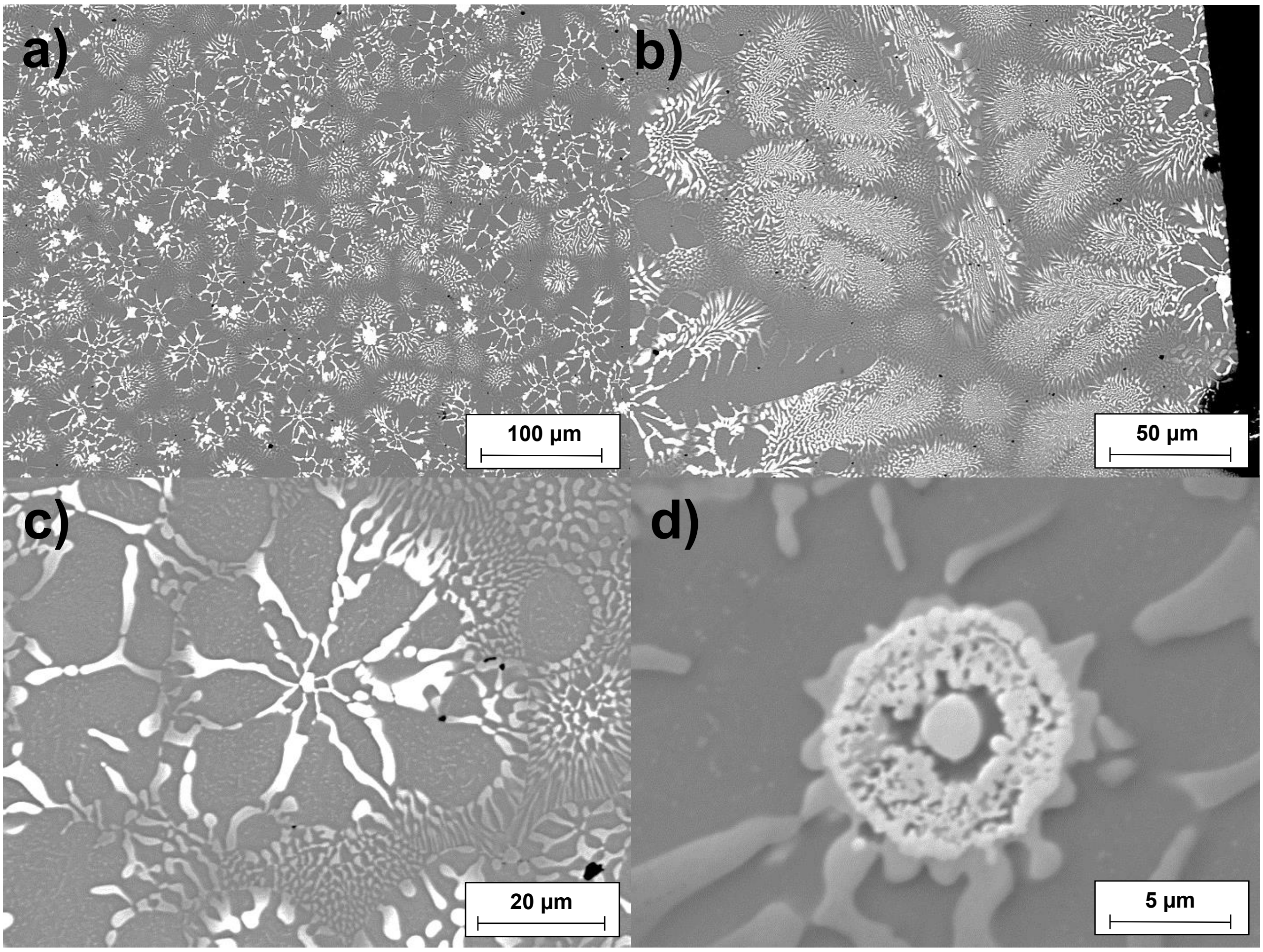

Figure 5.14: SEM BSD micrographs of features in the microstructure of NiAl-27Cr-2W sample: a) an overview of the microstructure of the sample, b) eutectic cell colonies and NiAl dendrites, c) ”particle traces” with a flower-like structure, and d) microstrucure of the core of a W(Cr) particle.

figure 5.14c. As can be seen, the phase exhibited this sort of torn granular structure, even divided in layers with different phases, which were too small to perform EDX measurements. Nevertheless, the particle was surrounded by a Cr(W) layer as usual.

The eutectic constituent was very similar to that observed in NiAl-32Cr-3W and NiAl-29Cr-6W both before and after remelting. The eutectic growth was cellular and it formed colonies. In figure 5.14b, eutectic colonies with regular and irregular morphology can be observed, as well as a few cells with distorted laminar morphology. EDX composition measurements were taken from several cells, and the data gathered is plotted together with data from the remelted samples in figure 5.15. As can be seen, the eutectic composition of cells in NiAl-32Cr-3W and NiAl-29Cr-6W remelted samples was this time closer to the nominal composition of each alloy, which means they presented higher content in W. However, they deviated from most of the previously reported data in arc melting samples, and matched to the DS data. On the other hand, NiAl-27Cr-2W alloy, whose composition was taken from the large fully eutectic areas observed in the other 2 samples, showed

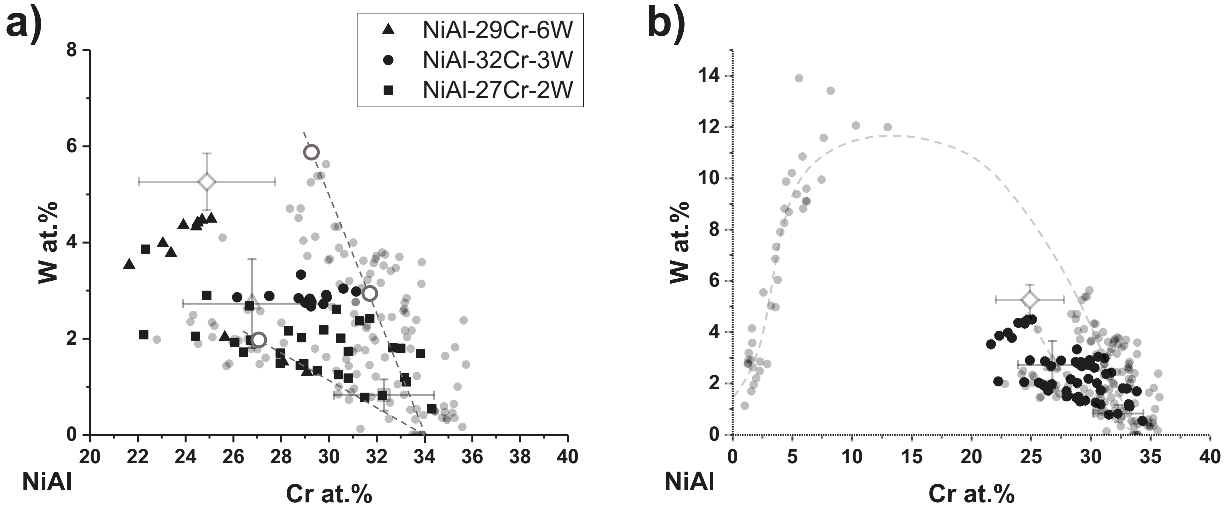

Figure 5.15: Composition of the measured eutectic cells: a) close view of results from NiAl-32Cr-3W and NiAl-29Cr-6W remelted samples and NiAl-27Cr-6W, compared to their nominal composition (large rings) and previous results nearby, and b) same data together with all arc melting data obtained until now and DS mean values for comparison.

a wide scatter in cell composition. The compositions were spread, with some data in agreement with the previous results and some in accordance with the latest ones, which was a very disconcerting outcome.

Arc melting samples exhibited in general an inhomogeneous microstructure and the solidification did not happen in equilibrium. Both factors could account for the conflicting results. Nevertheless, an estimation of the path of the eutectic trough in both the Cr-rich and Cr-lean sections could be obtained. Therefore, in order to verify the findings and to get further more reliable data, new alloys were produced. The compositions were chosen in accordance with all the observed data until this point, and they were processed by DS in a similar way to the tests performed in 5.1.

5.3 New DS alloys

The alloy compositions chosen for DS were: NiAl-3Cr-4W, NiAl-25Cr-5W and NiAl-30Cr-2W. As can be seen, the Cr-rich alloys selected had a slightly higher W amount than the last observed tendency. This was done in order to counteract the effect of the different element densities, noticed in the pile up of W at the bottom of DS rods, and to avoid W depletion in the rest of the sample. Firstly, the alloys were cast in the arc melting furnace. Then, they were directionally solidified with a set up similar to the double crucible. However, in this case the process was performed for all the samples at the same time, together with a NiAl-34Cr alloy, which was used to investigate the growth. A picture of the setup is shown in figure 5.16 during the DS process. As can be observed, four crucibles were placed inside

Figure 5.16: 4-crucible set up during DS of the NiAl-Cr-W alloys.

the back-up crucible, which was then retracted from the induction coil. The microstructure of the alloys was similar to that of others previously reported, and therefore no images will be presented here.

First of all, the DS NiAl-Cr eutectic alloy presented a cellular, fully eutectic microstructure. The cells exhibited good directionality, and the rods within the cells were reasonably well-aligned, parallel to the growth direction, which indicated that the undercooling and growth rate achieved in the process was sufficient for this alloy. However, DS NiAl-Cr-W alloys did not show this level of directionality, and only a few indications of it could be observed in a few eutectic cells.

All DS NiAl-Cr-W alloys exhibited W phase at the bottom of the rod, as previously observed in the DS tests. However, in the case of DS NiAl-30Cr-2W, this phase was dendritic, indicating that the composition was hypereutectic at the bottom. The microstructure of this sample then turned into fully eutectic in the middle region, whereas at the top of the rod NiAl dendrites were present, indicating a hypoeutectic composition. The dendrites presented some coarse precipitates that resembled tiny dendrites, which was also observed in DS tests. The eutectic constituent went through a change in morphology, from lamellar to rod/irregular.

The W phase in the other 2 samples resembled undissolved particles, similar to those observed before. DS NiAl-25Cr-5W presented NiAl dendrites in the rest of the sample, indicating it had a hypoeutectic composition. The eutectic constituent grew in cells which formed colonies. The eutectic morphology was mainly rod-like. However, indications of the transition and some lamellar cells could also be observed.

Finally, DS NiAl-3Cr-4W presented a very marked division between the bottom, which was full of rounded W particles, and the rest of the sample. Above this level, the microstructure consisted of a NiAl matrix with a mixture of fine and slightly coarser precipitation, few dispersed eutectic cells, and some smaller size W phase particles. The eutectic constituent presented a rod morphology, similar to those observed in the samples of 5.2.2 with close or similar composition.

The data obtained from the EDX measurements of eutectic cells in the samples is plotted in figure 5.17. As can be seen, data obtained from the DS NiAl-3Cr-4W matched with data previously obtained in 5.2.2, and followed the same trend of rapid increase in W content. On the other hand, DS NiAl-30Cr-2W cells exhibited lower W content, in line with the latest results from arc melting sample or even lower, reaching a maximum of about 2 at.% W. Eutectic cells with compositions in all the Cr-rich region were found, and the composition was usually relative to the position of the cell in the sample, with higher W contents in the bottom, and closer to the NiAl-Cr pseudo-binary eutectic in the top of the DS rod. The scatter observed was relatively lower than other data gathered, and similar to that observed in figure 5.13. However, DS NiAl-25Cr-2W sample again presented wide scatter. The composition of the cells was related to their position in the sample as well, showing a wider scatter in the bottom, where eutectic cells contain less Cr and more W. The data gathered from this sample agreed more with that of the DS tests. This was not totally unexpected, as the composition used for DS tests, the NiAl-20Cr-4.5W, was very similar to NiAl-25Cr-5W used at this point.

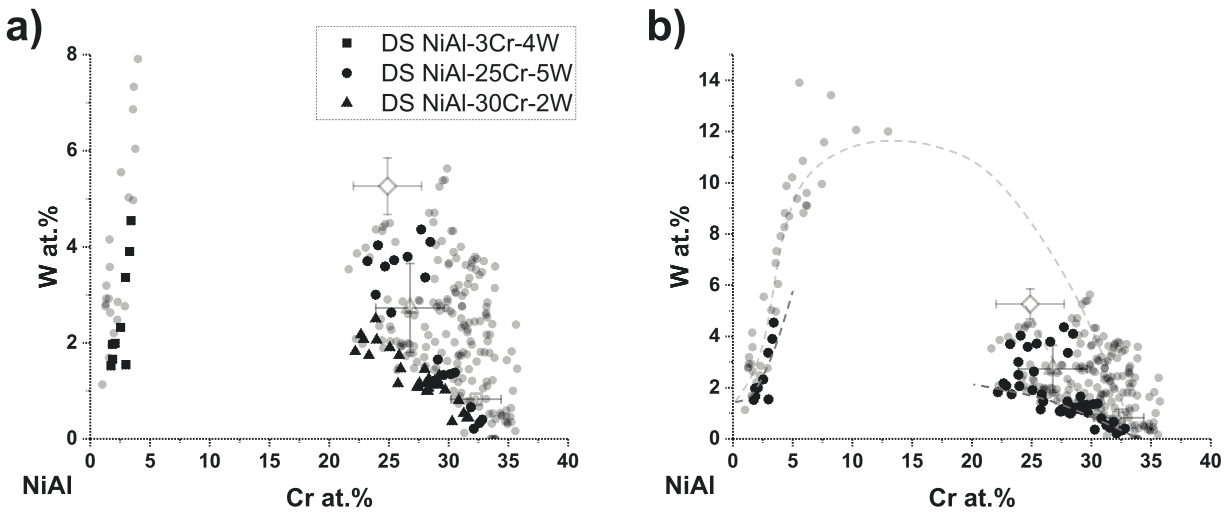

Figure 5.17: Composition of the measured eutectic cells: a) close view of results from DS NiAl-3Cr-4W, DS NiAl-25Cr-56W and DS NiAl-30Cr-2W, compared to previous results nearby, and b) the same data together with all arc melting data obtained until now, DS tests mean values, and the proposed extensions for comparison.

5.4 Discussion

After the study of the composition of the eutectic constituent present in all the samples produced, which was done in order to assess the eutectic trough in the NiAl-Cr-W pseudo-ternary system, it was not possible to determine whether a continuous eutectic trough exists or not. No eutectic constituent with a composition lying in the middle region could be found, leaving a gap in our assessment. Nevertheless, enough data was gathered from the Cr-lean and Cr-rich regions, especially in the latter.

The results were fitted and are presented in figure 5.18. Owing to the larger amount of data from arc-melted samples, all fittings were calculated from the results on arc-melted samples. In addition, DS and arc-melted alloy results matched in the Cr-lean region, or were in between in the case of the Cr-rich region. The fittings were done from average values of the eutectic constituent composition and, due to the wide scatter observed mainly in the Cr-rich region, two limiting approximations were proposed.

Although the plots of data were presented in 2-axis diagrams throughout the document, for the sake of simplicity in the plotting and in the distinction of data, the ternary nature of the system was not, and should not, be forgotten. Therefore, the fittings in a ternary diagram are presented in figure 5.18b. Note that the representation is done in a section of the ternary diagram, at the NiAl corner, and with proportional scale. By means of this plot, the real curvature of the sections assessed can be better observed. The slope is still considerably high. However, it is less abrupt than what could be thought from previous diagrams, and is more acceptable. Nevertheless, these results opened up new questions,

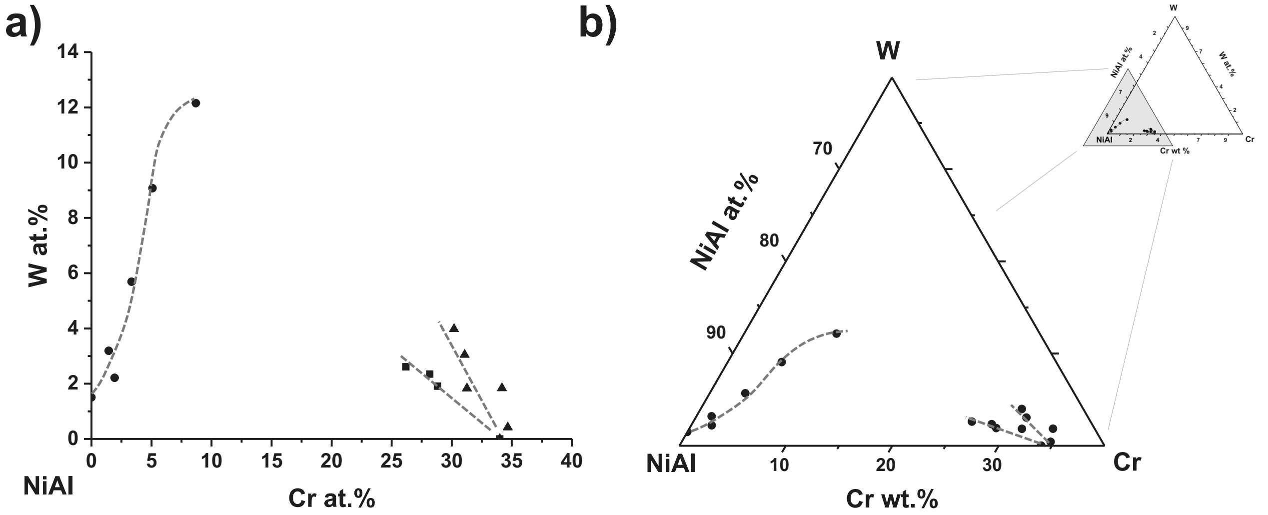

Figure 5.18: Fitting of the eutectic trough from all data gathered a) plotted similarly to previous results in a 2-axis diagram, and b) magnification of the NiAl corner section of the ternary diagram with the same fitting.

which will be discussed here.

5.4.1 Data scatter: The coupled zone

One of the main observations during the assessment of the eutectic trough was the strong scatter of the measured compositions of the eutectic constituent. This level of scatter hindered the determination of the actual path of the eutectic trough, which was the main objective of the investigation until now. Moreover, alloys produced with supposed eutectic compositions led to drifted data, which at the same time led, after new alloy production, to results in the opposite direction; these were closer to previous data, clearly indicating that it was non-equilibrium data.

As already mentioned in 1.4.3, compositions close to the eutectic may lead to eutectic microstructures depending on the growth conditions. The validity of a phase diagram is based on equilibrium conditions, where a fully eutectic microstructure is only achievable at a fixed composition. However, at non-equilibrium conditions, the eutectic constituent may grow faster than the dendrites if its growth temperature is higher, and, therefore, may become the leading phase. This is what happens in the coupled zone as seen in fig. 1.6. The example was given for a binary system, but it can be extrapolated to a pseudo-ternary system, in a section or isopleth of the NiAl-Cr-W (fig. 5.19). Additionally, the coupled zone may be symmetric or skewed. Due to the observations in the NiAl-W system, where the coupled zone was skewed towards the W side [110], and because of the proximity to the NiAl corner of the area concerned, it is most likely that in the NiAl-Cr-W system, the coupled zone is skewed towards the Cr(W) phase.

In arc melting, large undercoolings are reached, which are different in each zone of

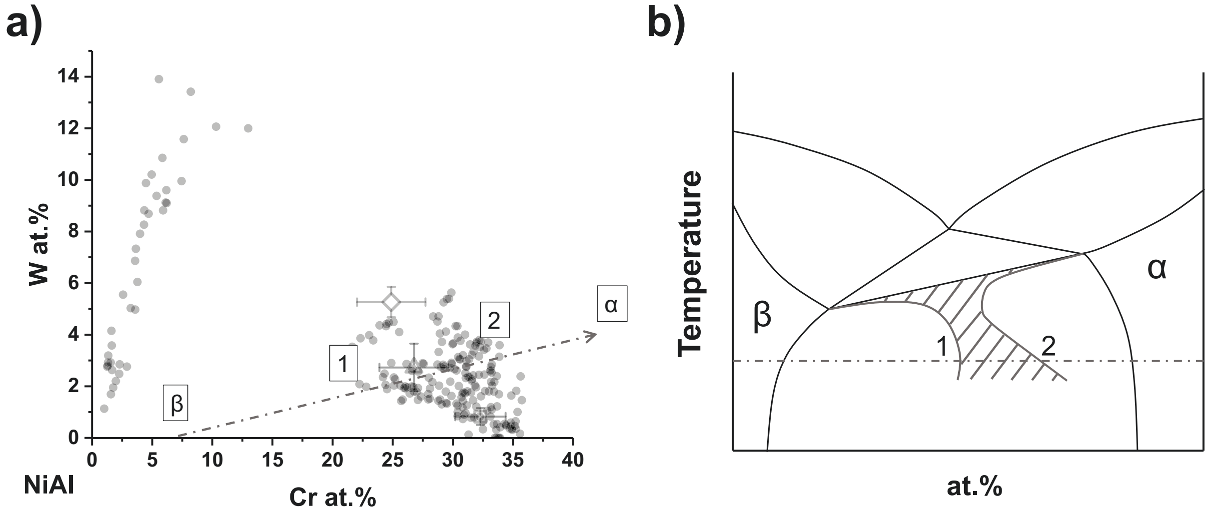

Figure 5.19: Composition of the measured eutectic cells from previous results: a) the line represents the isopleth section and b) skewed coupled zone in the isopleth.

the sample, whether it is in the contact zone with the water-cooled copper crucible or in the center of the sample. Therefore, it is possible that during solidification, compositions in the coupled zone grow, forming metastable eutectics. This would imply a significant increase in data scatter, only avoided through solidification in equilibrium. However, the scatter observed in the Cr-rich region is unreasonable even considering the coupled zone. Moreover, DS tests presented scatter as well. In reality, an undercooling is also present in DS, but the slow growth rate used would lead to more consistent microstructures. However, the DS processing was not successful, since the microstructures exhibited no directionality, and heterogeneous nucleation took place due to the W particles found.

5.4.2 The gap in the eutectic trough

On the other hand, a continuous eutectic trough could not be assessed, and a gap with no data was found between 10 to 20 at.% Cr. Since the preliminary results, this fact has been related to the presence of undissolved W particles in the microstructure of the samples. For this reason, new processing routes were developed which yielded better results. However, particles were still present in the microstructure.

Thorough analyses of the processing route steps revealed that W dissolved during the process and W(Cr) phase formed during solidification, being then characteristic of each alloy composition. Of course, there were some exceptions like NiAl-7Cr-11W, NiAl-15Cr-15W and NiAl-25Cr-11W; where poor dissolution of W was evident. Moreover, particles present in other alloy compositions also resembled undissolved particles, and to determine their origin was a difficult task. Nevertheless, W has the highest melting point of all metal elements ($>$3400 °C), almost double that of NiAl and Cr, not to mention elemental Al. This fact implies a steep slope in the liquidus surface around the eutectic trough. Furthermore, a liquid containing elements with such different properties will be prone to segregation, and small deviations in the local composition of the melt may trigger the formation of a solid nucleus. Once the solid nuclei have formed, density differences can increase the segregation and lead to local composition changes, as was seen in DS processing. In the case of arc melting, due to the fast heat extraction from the water-cooled copper crucible, and the high thermal conductivity of the melt, a solid nucleus may not receive enough heat to increase its temperature to remelt, even growing instead. An issue related to this was observed in the sample processing.

During alloy production, the ease or complexity of processing for each composition was experienced, especially in arc melting. While prealloys were usually easy to process, final NiAl-Cr-W alloys presented more difficulties. Some alloys presented high viscosity, did not melt completely and remained in a semisolid state. It is known that off-eutectic alloys present worse castability. However, due to the fast heat extraction in arc melting, these alloys could not easily be kept fully molten, and sometimes only the part of the sample directly affected by the arc was molten, while the rest remained in this semisolid state. Therefore, the heat input was insufficient, and could have promoted solid nuclei growth. If segregation does occur, and the growth of the nuclei continues, the composition of the remaining liquid would have a lower amount of W, inducing the formation of eutectic constituent in the Cr-rich region.

There is still another feature concerning the microstructure, which is the Cr(W) layer observed surrounding the particles. Similar to the halo formation observed around NiAl due to its poor ability to serve as nucleating phase for the eutectic constituent, the particles may not promote NiAl nucleation. The liquid around would then become supersaturated in Cr, eventually causing the formation of the layer. After this, NiAl dendrites and eutectic constituent form during solidification, resulting in the observed microstructures and no data of the eutectic trough in the 10 to 20 at.% Cr region. Only compositions in the Cr-lean region would yield valuable data. However, the W-rich dendrites observed in the microstructure of the alloys, together with the initial difficulty in determining whether or not the origin of these particles was an undissolved phase, made it difficult to justify this assumption.

Another possible explanation for this phenomenon could be the partially inaccurate premise on which the research was carried out. As explained in 1.5, a continuous eutectic trough could exist in a ternary phase diagram where the boundary conditions are two binary eutectic systems, and the third system presenting complete miscibility. However, Cr-W phase diagram (fig. 5.20) [139] presents complete miscibility only at high temperatures,

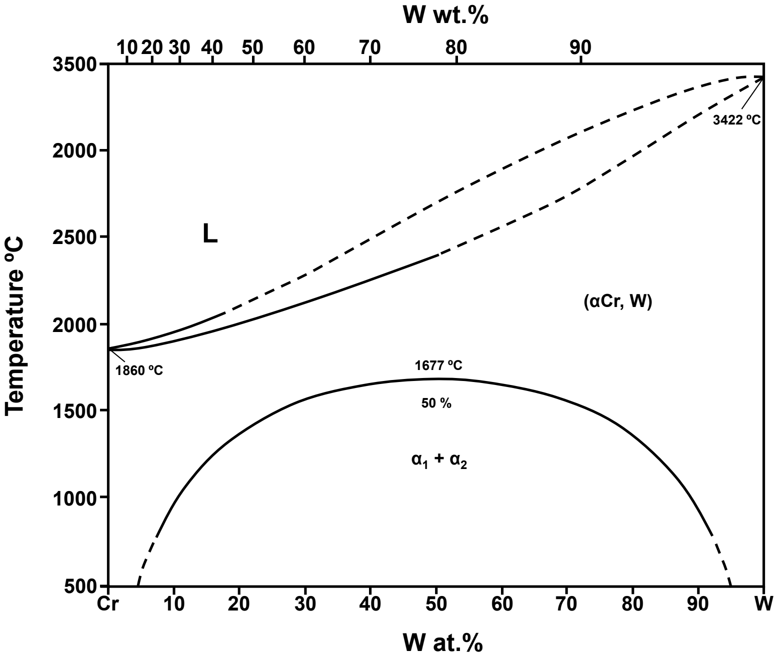

Figure 5.20: Cr-W phase diagram [139].

whereas a solid-state miscibility gap exists up to relatively high temperature.

As a consequence, the conditions for the existence of a continuous eutectic trough are conditioned by the influence of the miscibility gap in the pseudo-ternary phase diagram. Depending on the evolution of this region towards NiAl corner, the miscibility gap volume may affect some of the surfaces of the ternary phase diagram (solvus surface, solidus surface, and liquidus surface), changing the phase diagram from the model proposed in figure 1.7. Nevertheless, the model was only a schematic of the system, so a new model based on the binary diagrams (fig. 5.20 and 5.21) and the results obtained in the study, was made and is presented in figure 5.22, where the orientation of the system was changed, shifting Cr and NiAl for better visibility of the liquidus surface and miscibility gap. In the NiAl-Cr-W pseudo-ternary phase diagram, the eutectic trough is very close to the NiAl corner, which means in the opposite zone from the miscibility gap. Consequently, at first any possible effect was dismissed. However, we have ignored how the miscibility gap has evolved into the ternary. If the surfaces are severely affected, significant changes may take place in the phase diagram, including unreported reactions.

Moreover, the NiAl-Cr-W pseudo-ternary system, is just a section of the Al-Cr-Ni-W quaternary system. This fact will have an effect, for example, as observed from the different partitioning of Ni and Al into the other phases. Although NiAl intermetallic forms in a wide range of compositions, if the Ni/Al ratio is not constant, it is debatable whether it can be treated as a component. Indeed, this different partitioning of Ni and Al, and the deviation from stoichiometry observed in NiAl dendrites, which in general exhibited higher Ni content, indicates that we are no longer in the NiAl-Cr-W pseudoternary diagram, as we always considered stoichiometric NiAl, but rather in the quaternary Al-Cr-Ni-W phase diagram. This implies a 4-dimensional problem, where the eutectic trough which is trying

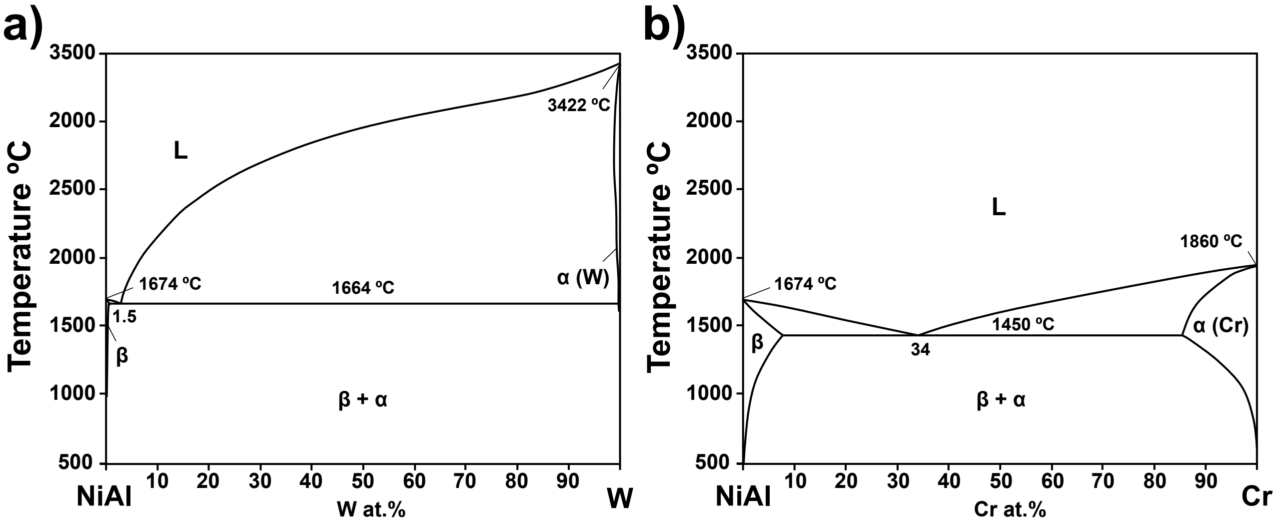

Figure 5.21: Pseudo-binary phase diagrams of a) NiAl-W and b) NiAl-Cr used for calculations.

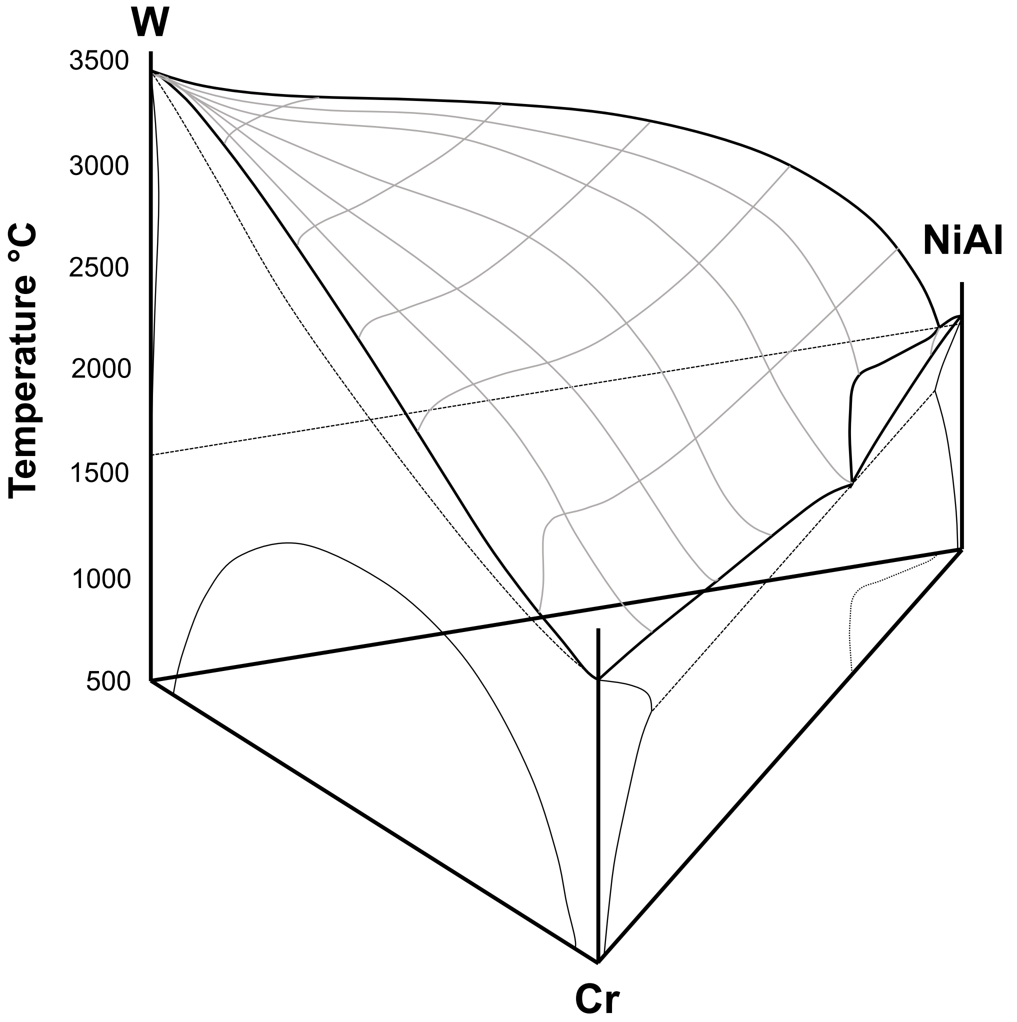

Figure 5.22: Model of the NiAl-Cr-W pseudo-ternary system based on the binary diagrams and the results obtained in the study up to now.

to be assessed, is just the intersection of a quaternary eutectic plane with the NiAl-Cr-W section. If data from the eutectic plane out of the section is plotted in this same section, under the assumption that NiAl is always stoichiometric, part of the scatter observed may be due to the projection of this plane. Therefore, an exhaustive investigation taking this quaternary effect into account was carried out, in order to obtain further insight into this problem.

6

Solidification Path: Pseudoternary Phase Diagram

In view of the results obtained from the composition of the eutectic constituent, and due to the questions that arose from them, the focus of the research shifted towards the pseudo-ternary diagram, with the study of the solidification path in the different alloys. As a first approach, and due to the lack of information about the system, computer aided calculations were performed with the available data.

6.1 Phase diagram calculations

The calculation of the phase diagram was performed with the CALPHAD method, which is an abbreviation for the original designation "Calculations of Phase Diagrams". Today the full name of the method is "Computer Coupling of Phase Diagrams and Thermochemistry". The calculations were performed in collaboration with the Institute of Applied Materials (IAM) in the Karlsruhe Institute of Technology (KIT). The Ni-based superalloys database used for the calculations was obtained from the Scientific Group Thermodata Europe (SGTE).

First calculations performed on the NiAl-Cr-W pseudo-ternary diagram are presented in figure 6.1. Initially, the main aim of the study was to determine the eutectic trough. Therefore, the most interesting calculation was the liquidus projection of the pseudo-ternary diagram, as that is where the eutectic trough is observed. In figure 6.1a, the result of this calculation is presented. It can be seen that the calculations show a continuous eutectic trough, in which the W content increases rapidly from the NiAl-Cr pseudo-binary eutectic,

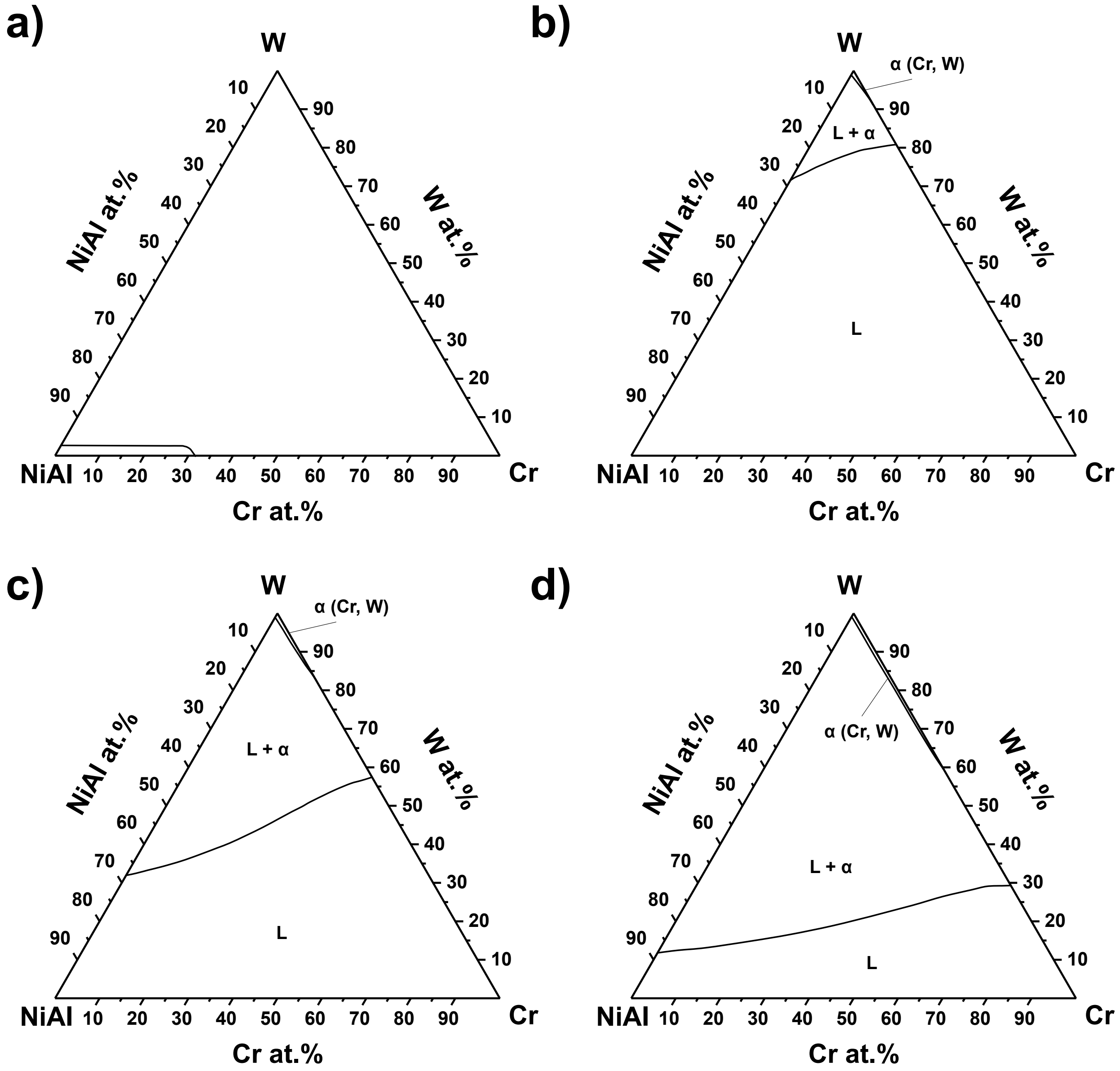

Figure 6.1: NiAl-Cr-W pseudo-ternary system phase diagram calculations: a) liquidus projection, isotherms b) at 3400 K, c) at 3000 K, and d) at 2500 K.

when decreasing the Cr content. However, in this case a limit value was quickly reached with about 1.5 at.% W, which remained constant while reducing the Cr content until the NiAl-W pseudo-binary eutectic was reached.

According to our previously presented results, there is evidence that a eutectic trough like the one calculated is incorrect. This was not surprising, since the database used was not created for this purpose. The Calphad method, and particularly calculations done with Thermocalc software, can be very accurate, as has been proven in materials with very large quantity of experimental data. With a large amount of data, very precise databases can be set up for the calculations, which is the case for steels for example. However, the

Al-Cr-Ni-W database used for these calculations was developed in order to focus on the Ni-rich corner, for the relationship of γ and γ' in Ni-based superalloys. The calculated results from NiAl-Cr-W pseudo-ternary are an extrapolation of the Al-Ni-Cr and Al-Ni-W systems, so it is comprehensible that the calculations deviate from the experimental data.

Nevertheless, calculations were useful for obtaining a better idea of another critical feature: the shape of the liquidus surface and understanding it (fig. 6.1b-d). Of course, calculated results deviated from the real liquidus surface, but steepness and curvature were taken as bases for the study. Moreover, the calculations were used to create the model presented in figure 5.22. However, it should be taken into consideration that features not taken into account in the database, due to incompleteness, probably will not yield any result. This could be the case in non-assessed reactions in the diagram.

On the other hand, calculations were performed at lower temperatures (fig. 6.2) in order

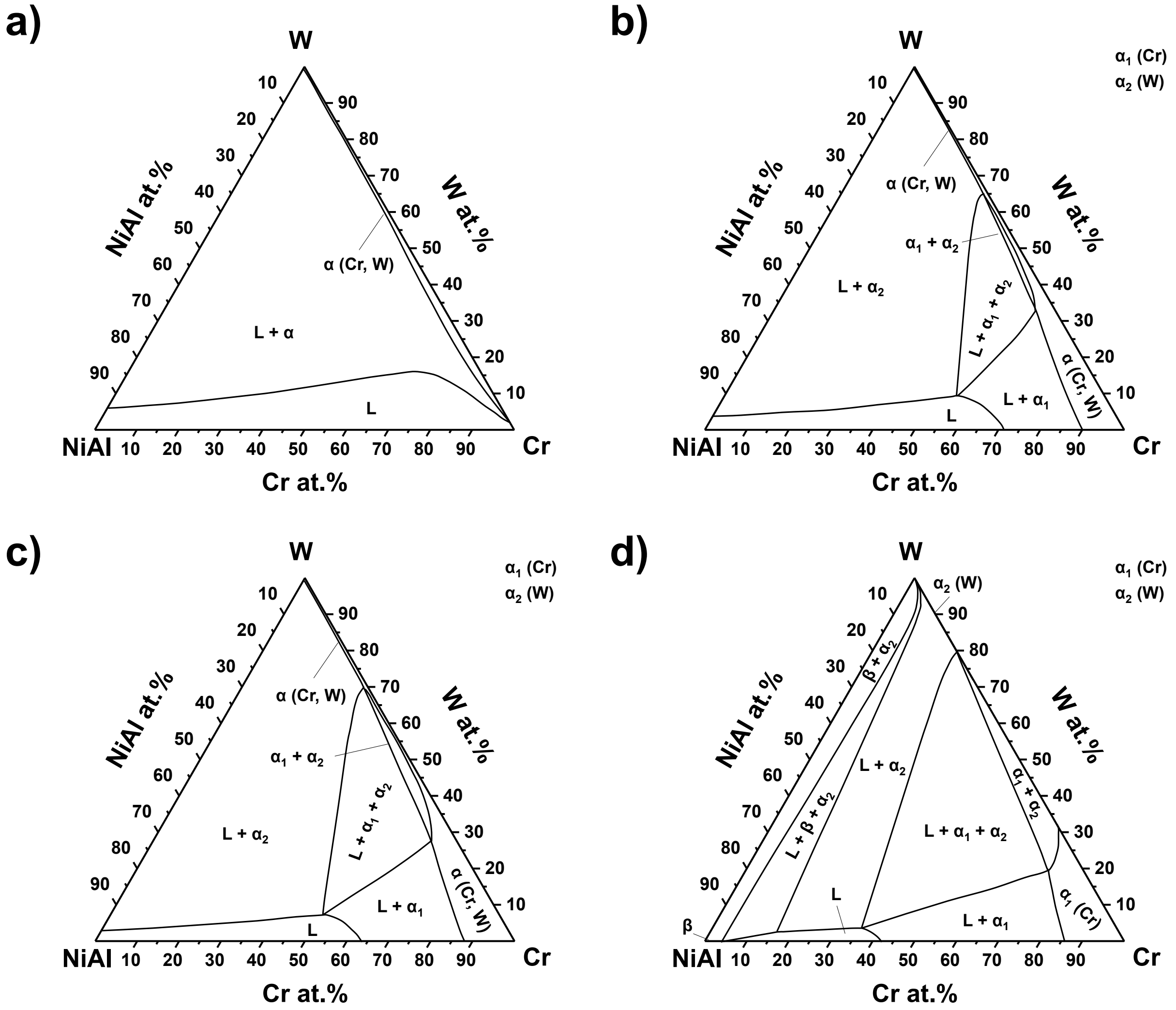

Figure 6.2: NiAl-Cr-W pseudo-ternary system phase diagram calculations: isotherms a) at 2200 K, b) at 2000 K, c) at 1950 K, and d) at 1800 K.

to study the Cr-W miscibility gap, and its development into the pseudo-ternary diagram. The miscibility gap in the binary diagram starts at a temperature of 1677 °C (1950 K). However, in the calculated pseudo-ternary diagram, the miscibility gap phase field at that temperature is considerably wide (fig. 6.2c). Even 50 degrees above (fig. 6.2b), when the gap was present. At 2200 K, there was no sign of it, so its maximum temperature increases between 50 and 250 degrees when entering the pseudo-ternary diagram. This increase is not negligible, considering the slope of the solidus surface, which was cut by the miscibility gap. Moreover, the gap expanded in the Cr-rich corner, entering relatively deeply into the pseudo-ternary diagram; therefore, the formation of a monovariant reaction at the corner of the 3-phase field triangle, induced by the miscibility gap in the calculated isotherms (fig. 6.2b, c and d), is understandable. This confirmed that the miscibility gap affects the surfaces in the pseudo-ternary diagram, which could influence the eutectic trough, despite the fact that the miscibility gap is located on the opposite side of the diagram. The fact that the 3-phase field triangles exhibit curved lines is because they are isothermal sections of a quaternary system. In this system, some of the phase equilibria tie lines are not in these isothermal sections, thus looking curved when projected.

In line with this, another aspect studied from the calculations was the effect of non-stoichiometric NiAl on the eutectic trough. Due to the different partitioning of Ni and Al towards the Cr(W) and W(Cr) phases, whose ratio was even opposed, the question arose of the effect of the quaternary nature of the system on the eutectic trough. In figure 6.3, calculations of the liquidus projection of different NiAl-Cr-W pseudo-ternary systems are presented, in which the NiAl composition was different from the stoichiometric, but within the limits of NiAl phase field in the binary phase diagram. As in the case of the miscibility gap, the NiAl phase field of the binary system will be modified when entering the quaternary system. However, as a first approach, this was not taken into account, and the compositions selected for NiAl were: 40Ni-60Al (fig. 6.3a), 45Ni-55Al (fig. 6.3b), and 70Ni-30Al (fig. 6.3a). In figure 6.3d, a comparison of the different eutectic troughs with the one from stoichiometric NiAl is shown.

As can be seen, the calculations led to quite different results depending on the NiAl composition. The difference between each case can be better appreciated on the Cr side, but it is similar at both ends and along the eutectic trough. The further from stoichiometry, the closer the eutectic trough is to the NiAl corner. This is consistent with the lower melting point of non-stoichiometric NiAl. Moreover, 70Ni-30Al, which has the lowest melting point in the NiAl phase field (fig. 1.2a), exhibits the most deviated eutectic trough in the pseudo-ternary. On the opposite side, 45Ni-55Al and 40Ni-60Al exhibit a gradual deviation. It is worth highlighting that the larger deviations were observed at the ends of the trough, and were almost negligible in the middle section.

Each Ni(x)Al(y)-Cr-W pseudo-ternary phase diagram is nothing but a section of the

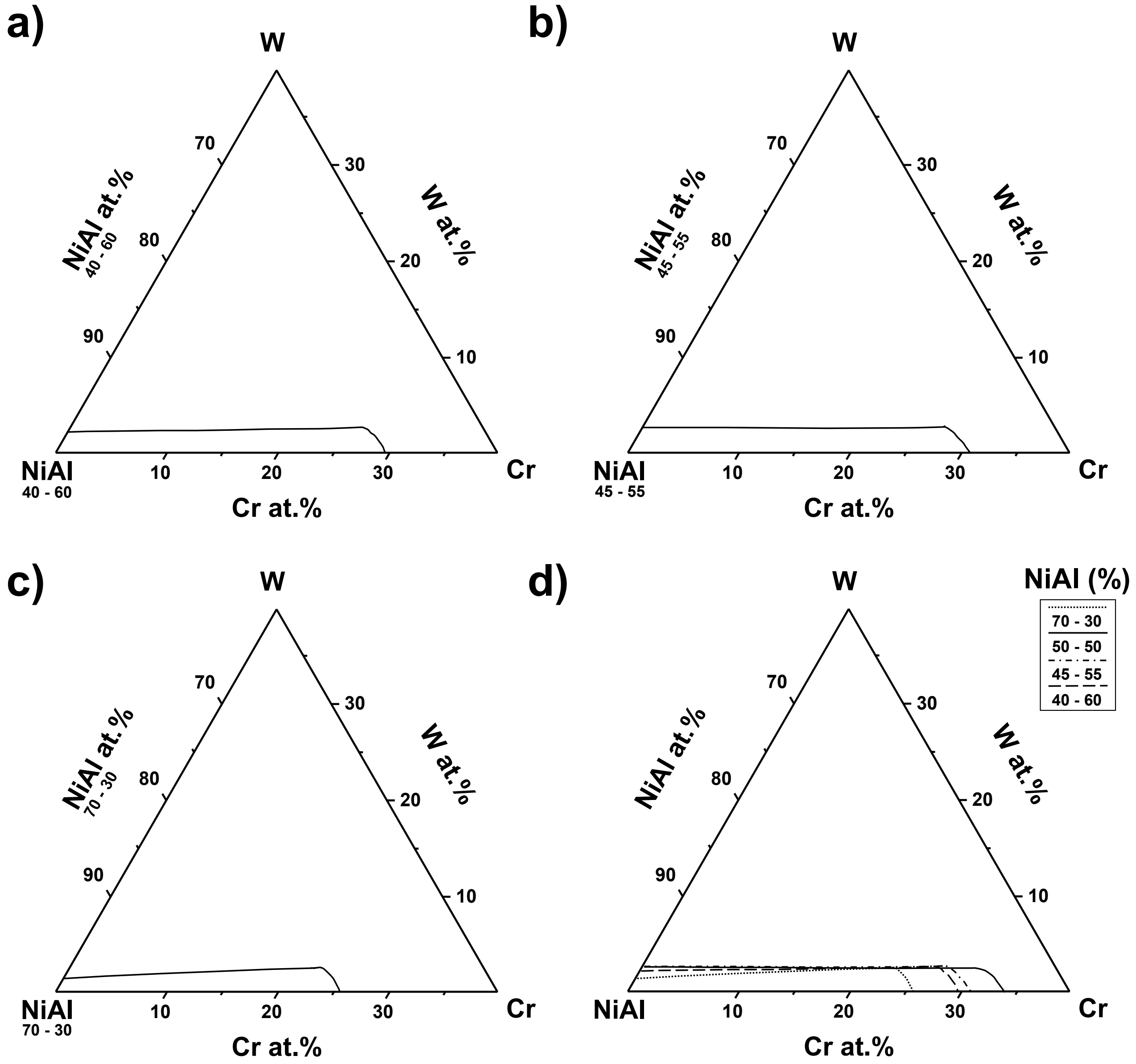

Figure 6.3: Calculation of the liquidus projection in the NiAl corner of 3 different Ni(x)Al(y)-Cr-W pseudo-ternary system phase diagrams: with a NiAl atomic composition of a) 40 - 60, b) 45 - 55, c) 70 - 30; and d) a comparison of them with stoichiometric NiAl.

quaternary Al-Cr-Ni-W phase diagram. The liquidus projection of a quaternary system is three-dimensional, and the eutectic troughs calculated are sections of the quaternary eutectic plane. In view of the results, this eutectic plane is concave towards NiAl. Therefore, as the NiAl phase in the alloys produced was not exactly stoichiometric, and indeed its composition varied between each sample, plotting all data in a single NiAl-Cr-W section implies introducing scatter. Results from chapter 5 evinced that the path of the eutectic trough calculated is erroneous, however, the findings obtained from calculations can explain part of the scatter observed during the assessment.

Having thoroughly studied the calculations, and extracted valuable information for understanding the NiAl-Cr-W and Al-Cr-Ni-W phase diagrams, a more detailed analysis was carried out in the produced samples, in order to supplement them with experimental data and obtain a more complete picture of the phase diagram.

6.2 Solidification path

In chapter 5, the characterization was focused on the eutectic constituent composition, shifting away from the rest of the microstructural features. However, due to the issues encountered, the focus was switched again, this time in order to try to understand the phase diagram through the solidification path. This means systematical study of local compositions, phases present and their evolution, as well as whether the phase forms from the liquid. All of this was carried out locally, with the objective of addressing unresolved features. The procedure was performed in several locations of most of the samples produced by arc melting. However, as the general microstructure of the alloys has already been discussed, only a few case studies will be described here.

For instance, the regions with eutectic cells in the NiAl-10Cr-1.8W arc melted sample were studied, as depicted in figure 6.4. As can be appreciated in the SEM BSD image of the location at the top of the figure, large volume fraction of NiAl was present, which was identified to be the primary phase due to the dendritic shape of the phase. The composition was constant along the dendrite, containing around 5 at.% Cr and negligible amount of W. Furthermore, the interdendritic Cr(W) phase was found between some dendrites, whose composition varied quite markedly depending on the point measured, especially in W content, as can be appreciated also from the different brightness. The eutectic constituent was located between NiAl dendrites too; here, the composition of the W(Cr) phase was measured and found to be rather steady, and the composition of NiAl was similar to that of the dendrites. The eutectic composition was very high in W, with around 12.5 at.%, and 8 at.% Cr. Moreover, this composition was consistent with the phases forming the eutectic, as their tie line is perfectly aligned in the pseudo-ternary diagram. The change in composition between both interdendritic features was found to be very sharp, as can also be appreciated in the image. In addition, the Cr(W) phase also resembled the formation of another constituent at some locations, though it could be that these locations were the last to solidify. Unfortunately, these were not appropriate for doing any correct measurement due to their irregularity and size. Nevertheless, the local composition - different to the nominal, and approximately NiAl-8.5Cr-0.75W - fell inside the triangle formed by the different phases, being therefore consistent with the results.

Another interesting case was the one presented in figure 6.5. This time, the study focused on a location of the NiAl-10Cr-3.5W arc melted sample, where W(Cr) phase was identified as the primary phase due to the clear dendritic shape of the phase in a large

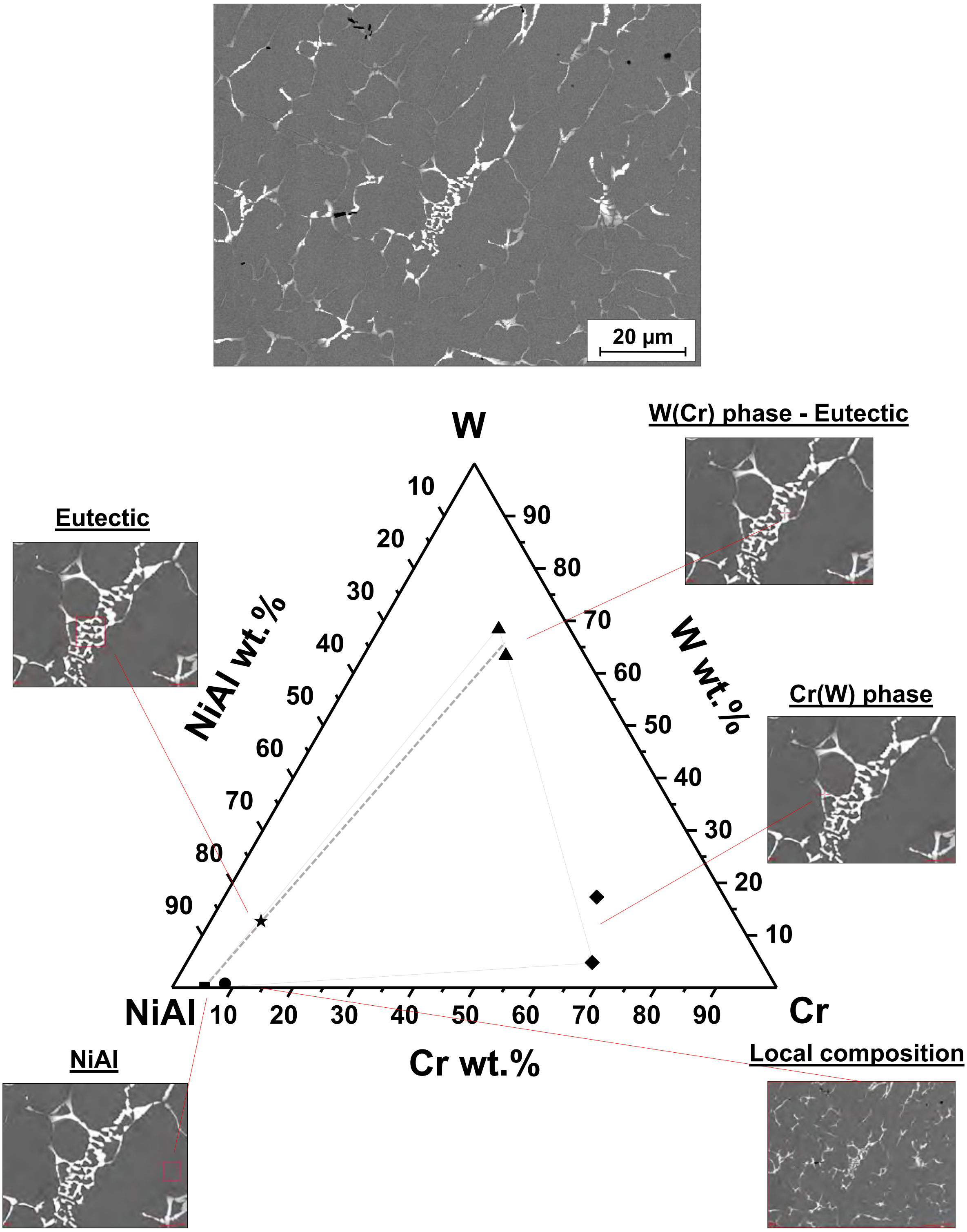

Figure 6.4: Schematic drawing of the study of the solidification path in NiAl-10Cr-1.8W arc remelted sample: SEM BSD image from EDX (top) and the composition of each phase (down).

region, as can be seen at the bottom right of the figure. In this case, the evolution of composition of the primary W(Cr) phase was studied by the measurement of different points. Due to a large solidification range, the composition of the dendrite varied from

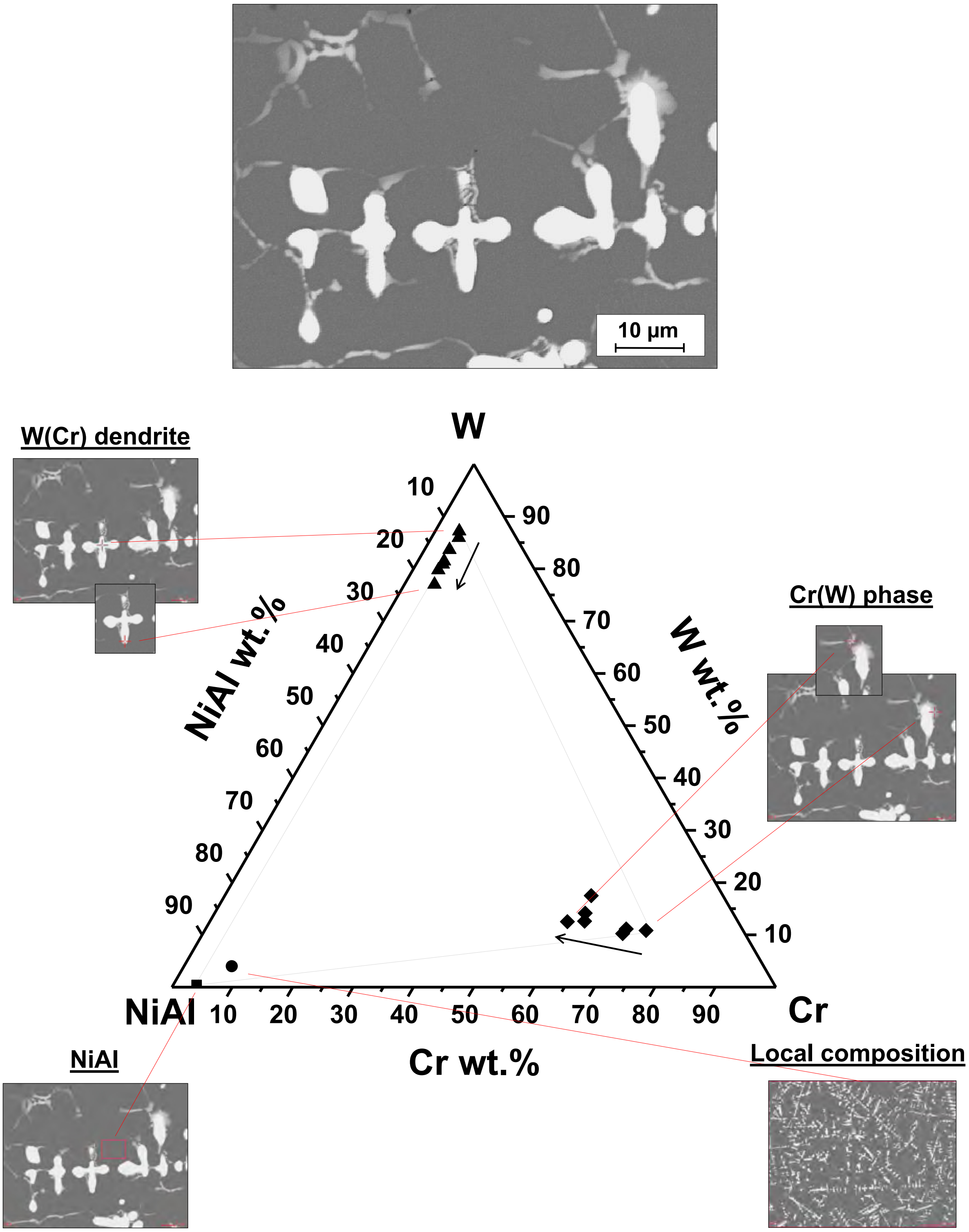

Figure 6.5: Schematic drawing of the study of the solidification path in NiAl-10Cr-3.5W arc melted sample: SEM BSD image from EDX (top) and the composition of each phase (down).

the core to the primary or secondary arms. While Cr content remained constant at about 4 at.%, W content decreased from 87 to 77 at.% and NiAl content increased from 9 to 18 at.%. However, as previously observed, the Ni content was higher and, while Al remained constant around 2 at.%, Ni content increased from about 4 up to 16 at.%, indicating the importance of this non-stoichiometry. Next, the Cr(W) phase that formed around the particles was analyzed. It grew into the melt, in some zones resembling a eutectic formation around the particles as it alternated with the NiAl phase. Its composition varied as well, decreasing the Cr content from 73 to 59 at.%, increasing the NiAl content from 16 to 28 at.%, and slightly the W content from 11 to 13 at.%. The content of Ni and Al was also different: Ni increased from 6 to 10 at.% and Al increased from 11 to 18 at.%, keeping a ratio close to 2. However, the phase could also be found in between the NiAl phase, which also resembled dendritic growth. A dendritic growth of two different phases was puzzling. Moreover, the Cr(W) interdendritic phase resembled the formation of another constituent at some locations, though these were not appropriate for doing any correct measurement. NiAl average composition was plotted and again, the study was consistent due to the position of the local composition - approximately NiAl-8Cr-4W -, which fell inside the phases triangle.

Similarly, an interesting location in the arc-remelted DS NiAl-20Cr-4.5W bottom sample was studied and is presented in figure 6.6. W(Cr) phase was identified as the primary phase due to its dendritic shape, as in the previous case. The evolution of its composition along the dendrite was studied as well, and the behavior was slightly different this time, where Cr did not remain constant but increased with the decrease in W. The size of the phase in the last measured point was, in principle, wide enough to perform a point measurement (1μm); however, due to the high content in Cr, it was probably influenced by the surroundings. The behavior of Ni and Al in the phase was similar, with more Ni content, although in this case the element varying the most was Cr, from 8 to 12 at.%. The Cr(W) phase formed around the W(Cr) dendrites, and again, in some locations the phase grew from the dendrites resembling a eutectic structure, alternating with NiAl phase. The evolution of the composition was different in this case, the W content was reduced from 14 to 6 at.%, as well as the NiAl content, slightly, from 22 to 17 at.%, while Cr increased from 66 to 72 at.%. Once again, Cr(W) phase was present between NiAl dendrites, which again resembled a dendritic growth. The interdendritic Cr(W) phase this time formed a eutectic constituent with an appropriate size and morphology to be measured, and whose composition was similar to the eutectic-resembling zones close to the dendrites. The NiAl phase evolution was studied as well this time, and the Cr content increased, reaching the maximum when it was part of the eutectic constituent, with about 11 at.%. The eutectic composition was consistent as it was fairly well-aligned with the 2 phases forming it. The local composition was approximately NiAl-17.5Cr-4.5W, close to the nominal, and consistent with the phase triangle.

As can be seen, the locations presented until now, which have been the most interesting, have been from the middle region, where no eutectic data of the trough were found. Finally, a zone in the NiAl-29Cr-6W arc melted sample is presented in figure 6.7. The phase

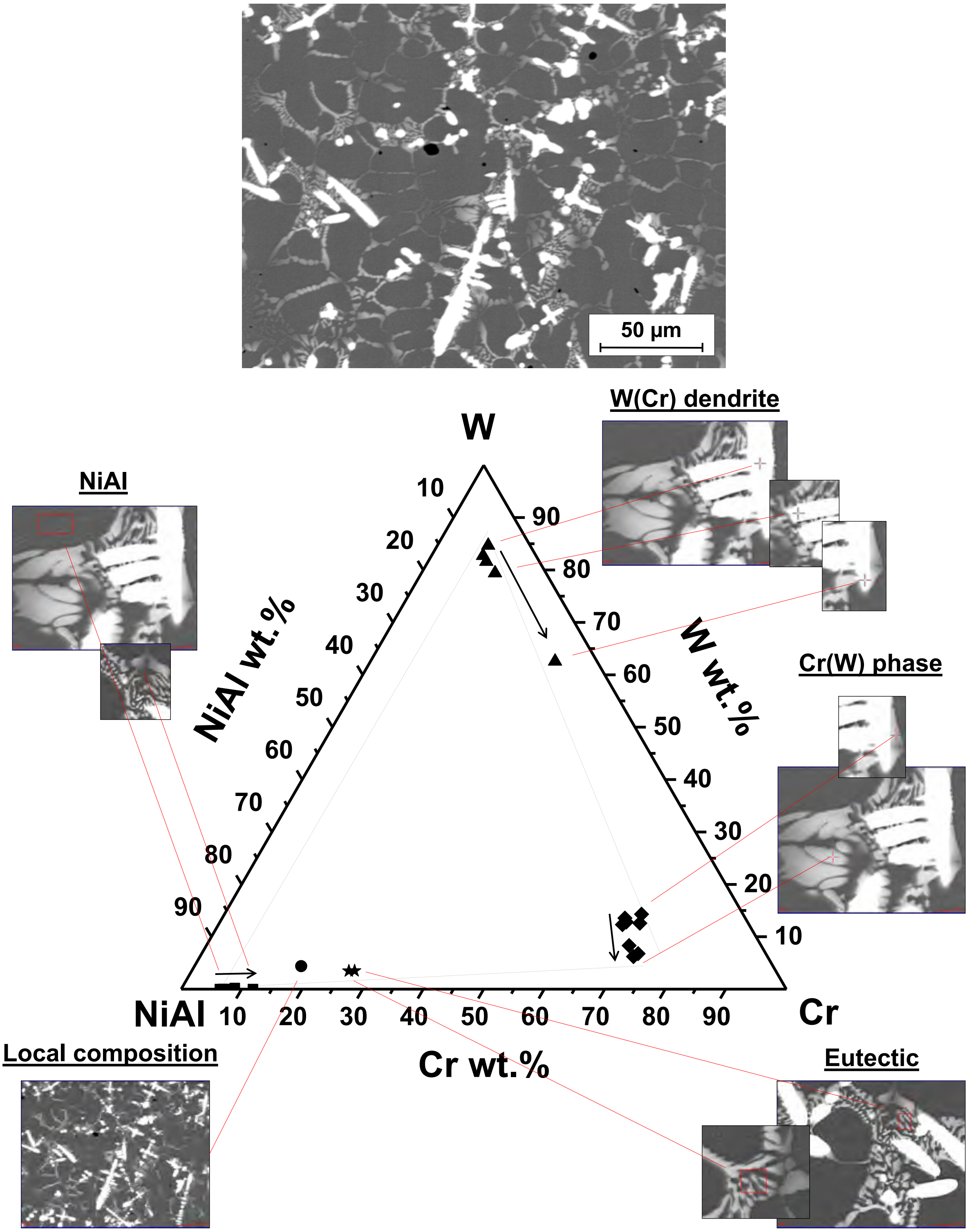

Figure 6.6: Schematic drawing of the study of the solidification path in NiAl-20Cr-4.5W arc remelted sample: SEM BSD image from EDX (top) and the composition of each phase (down).

forming the dendrites in this case was Cr(W), however, the core of some of them was W(Cr), indicating that the true primary phase would be W(Cr). A W-rich core was also observed in the NiAl-32Cr-3W arc melted alloy dendrites (fig. 5.12), and also in the NiAl-27Cr-2W

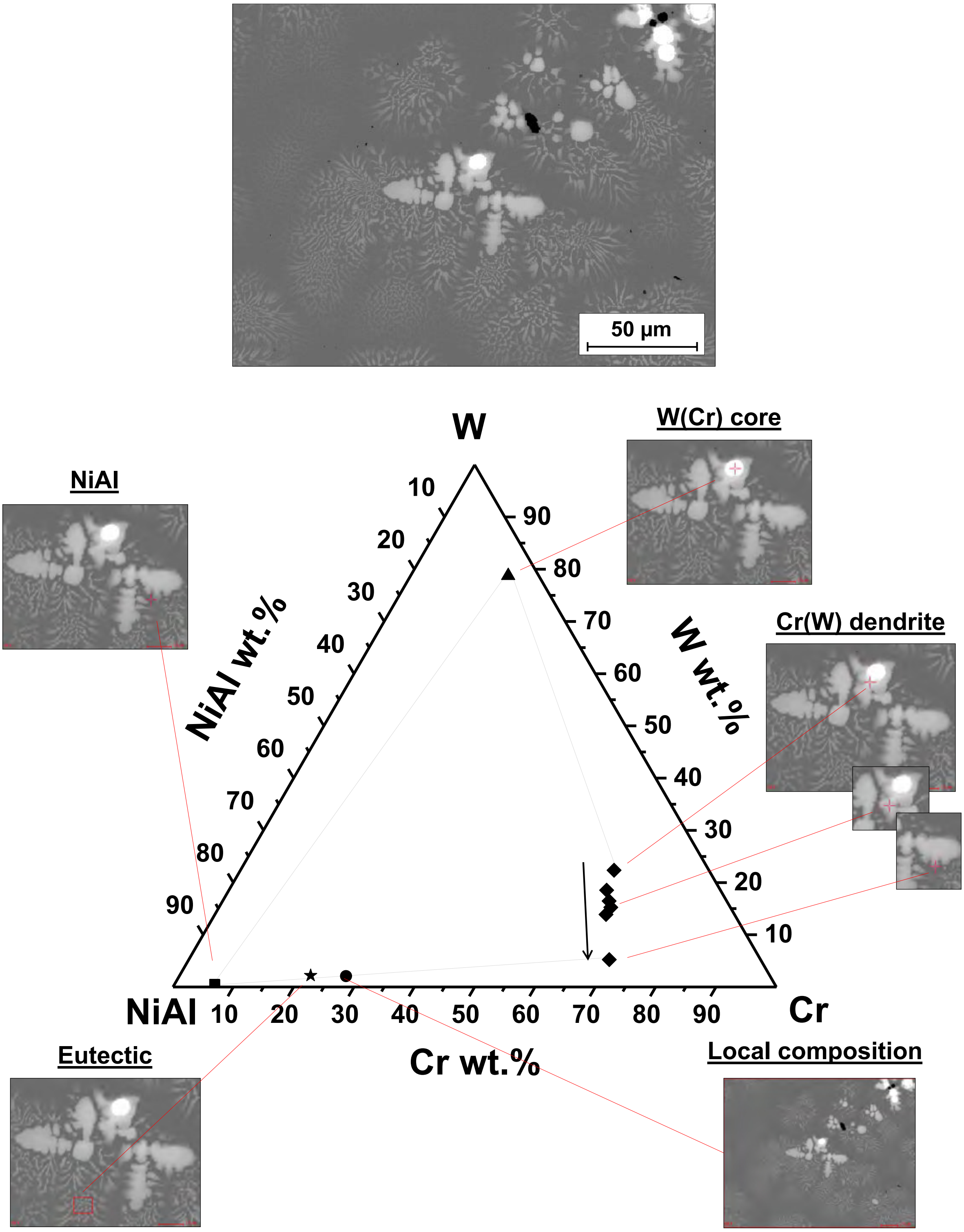

Figure 6.7: Schematic drawing of the study of the solidification path in NiAl-29Cr-6W arc melted sample: SEM BSD image from EDX (top) and the composition of each phase (down).

sample, with a torn granular structure (fig. 5.14), so it is representative. The W(Cr) core in the sample in the figure was W-rich with around 78 at.%. However, in other dendrites, measurements of the composition of the core gave values of around 50 at.% W, which would be in the miscibility gap range. The Ni content in the core was usually higher than the Al content, as in previous W(Cr) phases. Then, around the core, the Cr(W) formed and grew into the melt as a dendrite. The Cr content in the phase increased with increasing distance from the core, reaching about 70 at.% at the edges. On the contrary, the W content decreased sharply from about 22 to 5 at.%, while both Ni and Al content increased from 15 to 25 at.%. Once again, the content of each element was different with a higher amount of Al than Ni, whose content was about one-third of that of Al. Finally, the eutectic constituent nucleated and grew, completing the microstructure. The NiAl phase was only found as part of the eutectic constituent, and was thicker around the dendrites, as a sort of halo formation. The eutectic constituent was also, this time, consistent, and was aligned with the NiAl and Cr(W) phases forming it. The local composition was very different from the nominal, approximately NiAl-27.5Cr-2W, and fell inside the triangle formed by the different phases, being, therefore, consistent with the results.

6.3 NiAl composition: The quaternary system

The effect of NiAl stoichiometry on the eutectic trough, obtained from phase diagram calculations, together with the results from composition measurements of NiAl, Cr(W) and W(Cr) phases, which showed very different content of Ni and Al, raised a fundamental question: is considering the system pseudo-ternary an accurate approximation to approach this problem?

At the beginning, despite the wide composition range of NiAl intermetallic, it was considered a correct approach. However, as the composition range is wide, each composition change would mean a different section in the Al-Cr-Ni-W quaternary system, which was represented as a projection in the 50Ni-50Al-Cr-W system. The NiAl phase composition in the alloys produced was close to stoichiometry, but with some deviations, and was different in each sample. This could be because of the different partitioning of Ni and Al towards the other phases. Moreover, the partitioning observed was opposed in W(Cr) and Cr(W) phases, therefore, the NiAl ratio being different in each phase of the microstructure. This behavior was studied by means of the Al atomic fraction of the theoretical NiAl compound in each phase, eutectic constituent, and local compositions of each alloy.

The Al fraction was plotted in a 3D extended ternary diagram, and the results from the zones studied in 6.2 are presented here and divided into two figures, 6.8 and 6.9, for better

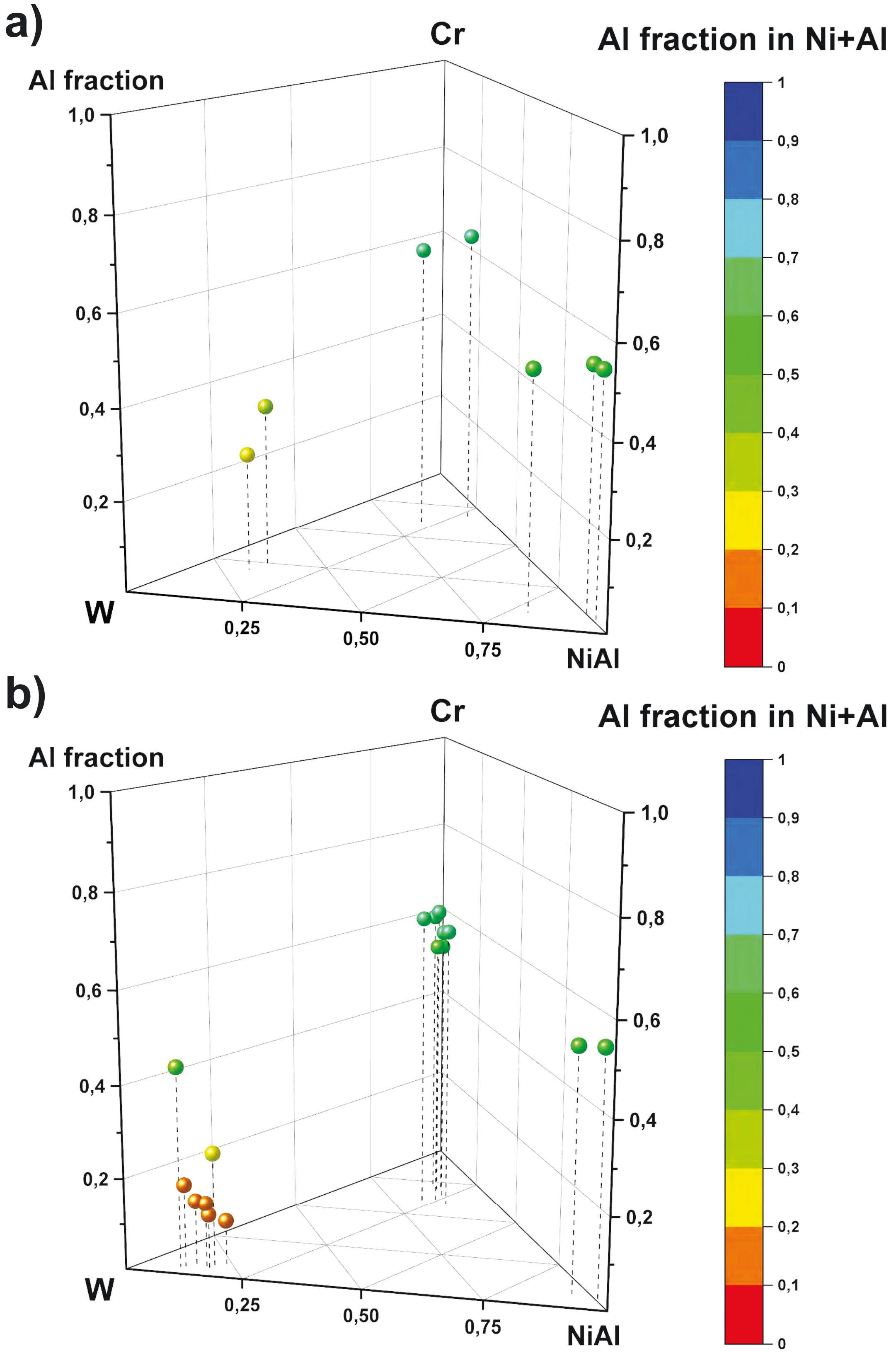

Figure 6.8: 3D representation of the Al fraction in relation to the Ni+Al amount in each phase of the microstructure in the locations studied of a) NiAl-10Cr-1.8W and b) NiAl-10Cr-3.5W alloys.

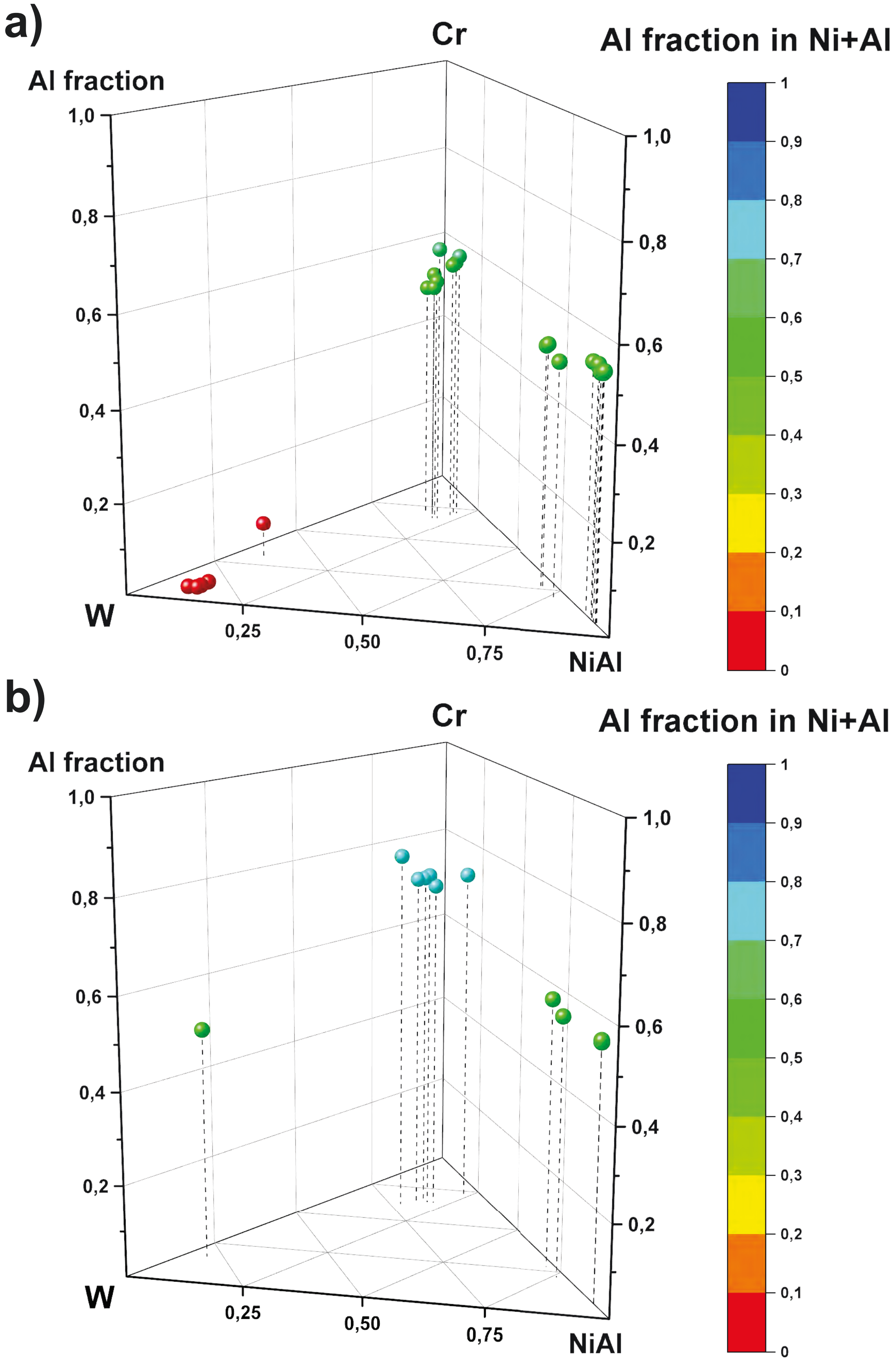

Figure 6.9: 3D representation of the Al fraction in relation to the Ni+Al amount in each phase of the microstructure in the locations studied of a) NiAl-20Cr-4.5W and b) NiAl-29Cr-6W alloys.

visibility. As a general trend, NiAl phase was close to stoichiometry, but slightly high on Al. On the other hand, Al fraction in W(Cr) phase was around 0.3, while for Cr(W) phase the Al fraction was around 0.7. However, there were also some uncommon values, such as the Al fraction in W(Cr) phase of NiAl-20Cr-4.5W zone (fig 6.9a), where EDX measurements detected no Al. This result was attributed to an error in the measurement, because all other measurements pointed towards some Al content in the phase. In contrast, W(Cr) phase in the zone of NiAl-29Cr-6W (fig 6.9b) exhibited an Al fraction of 0.5, which means stoichiometric NiAl. However, the content of both Ni and Al in the phase was rather low, about 2 at.%, and the stoichiometry detected was attributed to the higher Al content in this sample, compared to the others.

In any case, it became evident that the compositions are actually out of the pseudo-ternary section being represented and that each phase was located in a different section of the quaternary system. However, with this plotting it was not easy to get an idea of the situation, as the location of the data points is not representative. Therefore, further data processing was done to determine the effect of the inaccuracy on the results. In order to do this, the compositions were 3D represented in the quaternary Al-Cr-Ni-W system tetrahedron. This kind of representation is equivalent to that of the composition triangle for a ternary phase diagram, and the distances are truly representative, so the accuracy of the pseudo-ternary representation could be judged.

The plot of data from NiAl-10Cr-1.8W and NiAl-10Cr-3.5W in the quaternary tetrahedron is shown in figure 6.10. The NiAl-Cr-W section was also plotted as reference and projected as a comparison with representations used in 6.2. On the right, the tetrahedron can be seen parallel to the section, in order to appreciate the distance of data points from it. As can be seen, the composition of phases is close to the NiAl-Cr-W section, also for Cr(W) and W(Cr). In figure 6.11, it can be seen that even the composition of W(Cr) phase in NiAl-20Cr-4.5W (fig. 6.11a), and the composition of Cr(W) phase in NiAl-29Cr-6W (fig. 6.11b), are relatively close to the pseudo-ternary plane. This is due to the proximity of the composition to W and Cr corners respectively. Therefore, such a different Al fraction of each phase is compensated.

In view of these results, it could be stated that the NiAl-Cr-W pseudo-ternary approach used for plotting the data was a good approximation, and previous analyses of results can be used, even though some deviation is expected and should be kept in mind.

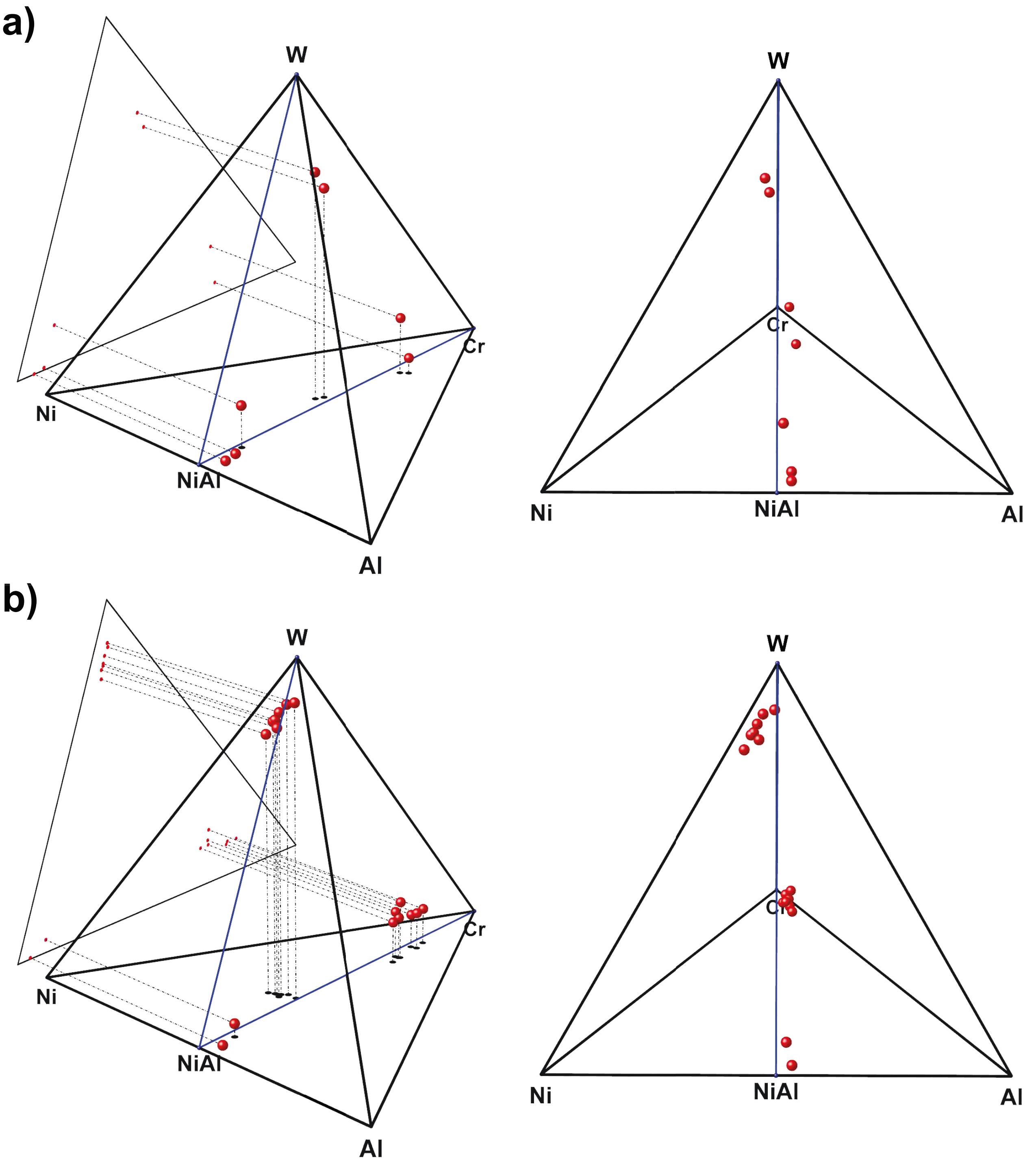

Figure 6.10: Phase compositions in the locations studied of a) NiAl-10Cr-1.8W and b) NiAl-10Cr-3.5W alloys, plotted in the quaternary phase diagram and compared to the NiAl-Cr-W section previously used.

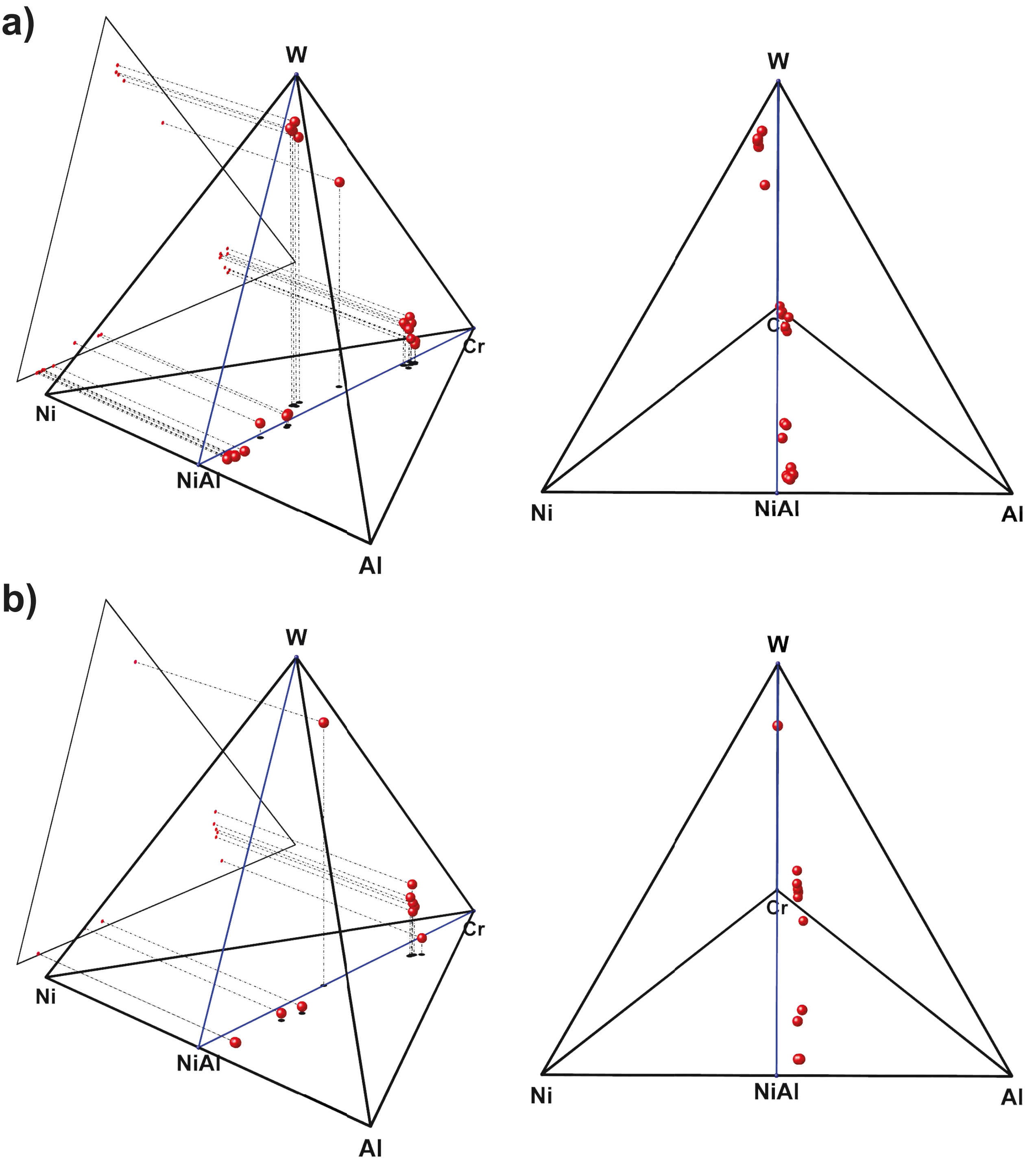

Figure 6.11: Phase compositions in the locations studied of a) NiAl-20Cr-4.5W and b) NiAl-29Cr-6W alloys, plotted in the quaternary phase diagram and compared to the NiAl-Cr-W section previously used.

6.4 Discussion

After all analyses of microstructure, composition, the path of the eutectic trough, phase diagram calculations and verification of the validity of the approaches used during this work, all data were put together and discussed, in order to understand the formation of the gap observed in the eutectic trough.

First of all, from the solidification path investigation presented in 6.2, the primary phase forming from the melt in each zone was assessed. In the region between the assessed eutectic trough sections, and lower W contents, NiAl was the phase found to be forming from the melt, with dendritic shape, as was the case of preliminary samples. Right from the Cr-rich section of the eutectic trough and above it, Cr(W) was the primary phase and formed dendrites, as could be seen in NiAl-32Cr-3W and in some zones of NiAl-29Cr-6W. However, in the latter some of these dendrites had a W(Cr) core. In these cored dendrites, and in the samples close to the Cr lean section of the eutectic trough, W(Cr) phase was the primary phase forming from the melt. Nevertheless, regions with a different primary phase should be, in principle, separated by some kind of reaction line, as is represented in figure 6.12.

However, in some of the samples it was not straightforward to determine the primary phase. This is the case, for example, for the zone studied in the NiAl-10Cr-3.5W alloy, the

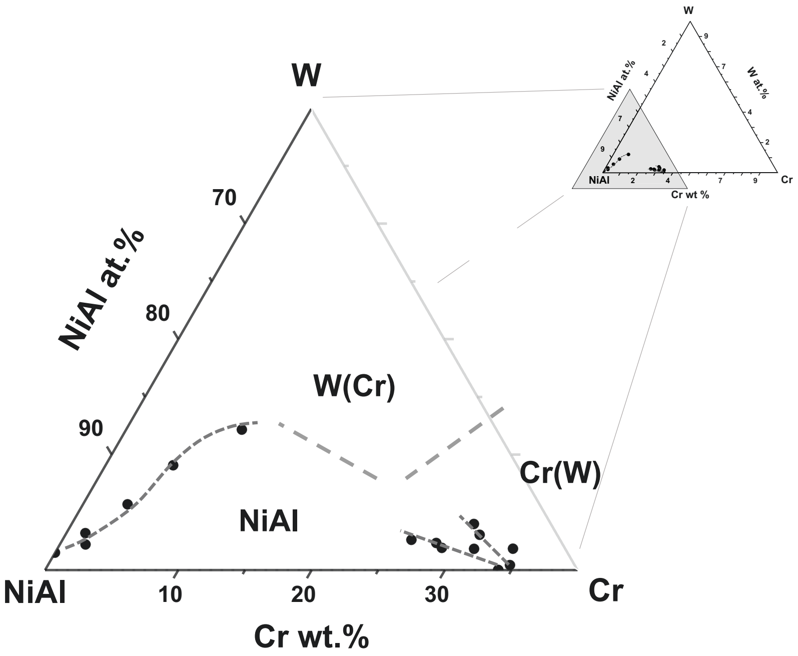

Figure 6.12: Magnification of the NiAl corner section of the ternary diagram showing the fitting of the eutectic trough from all data gathered, and the primary phase present in each zone. Regions with different primary phases are separated by a doted gray line.

local composition of which was approximately NiAl-8Cr-4W. As was shown in figure 6.5, dendrites of W(Cr) indicated this to be the primary phase. However, NiAl phase in the zone did also resemble a dendrite growth, and it was found at the edge of the sample dendritic growth of both phases; this can be observed in figure 6.13, where a W(Cr) dendrite seemed to have been expelled from the microstructure (fig. 6.13b). The black zones in the figure are remains of the mounting material. Moreover, from the results of Cr-lean samples (fig. 5.10), some of the eutectic cells showed compositions with a much higher amount of W than the local composition, pointing to a hypoeutectic composition and NiAl as the primary phase. On the other hand, these cells were scarce in the samples and their morphology was rather too irregular to ensure correct measurements. Therefore, determining the exact path of the eutectic trough in the Cr-lean region was not possible with the available data, though it definitely separates the different primary phase fields.

On the other hand, as observed in most of the samples, Cr(W) phase was found mostly around W(Cr) phase. Once the possible undissolved particles were discarded as main points of nucleation of the phase, and Cr(W) phase was also observed around primary W(Cr) dendrites, a so far unaccounted reaction was proposed. The nucleation of Cr(W) phase as a peritectic, would explain its formation as a sort of layer around W(Cr) phase.

In a peritectic reaction, the primary phase dendrite reacts with the remaining liquid to form a second phase, which would be, in this case, Cr(W). In this kind of reaction, the second phase forms around the primary dendrite, where it is in contact with the liquid and the reaction may take place; it then grows until the primary phase is isolated from the liquid and the reaction is inhibited, blocking the complete dissolution of the primary phase. As a result, the remaining liquid, which has a composition different from that of the local composition, would continue its solidification without the influence of the isolated

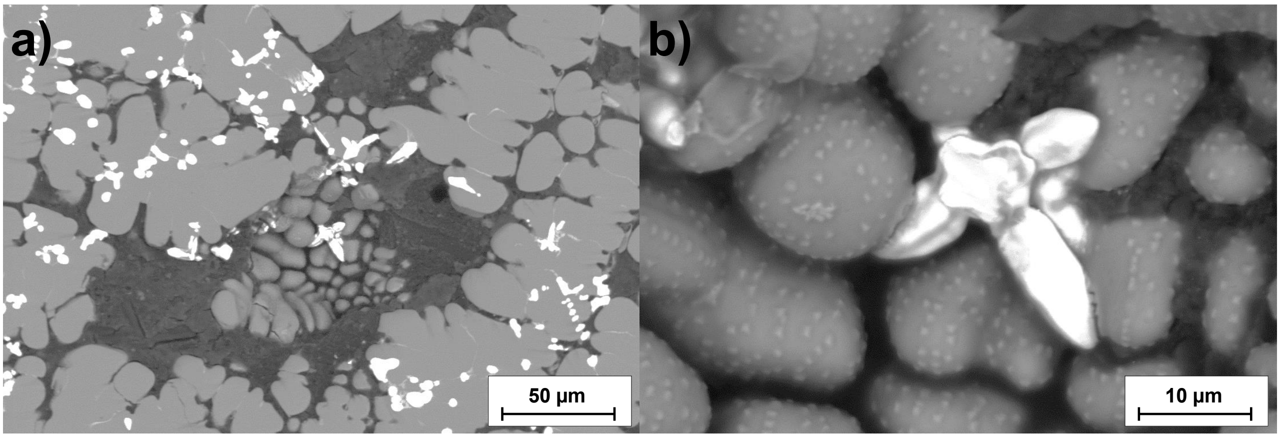

Figure 6.13: SEM BSD micrographs of the last solidified zone of arc melted NiAl-10Cr-3.5W a) with NiAl dendrite growth together with W(Cr) dendrites, and b) magnification of a W(Cr) dendrite between NiAl dendrite lobes.

primary phase. This would explain the microstructures observed and the contradicting microstructural features. Moreover, the peritectic is a reaction of the liquid with the primary phase, dissolving it to form the new phase. Clear signs of this W(Cr) phase dissolution, and other features which could be related, have already been observed in the microstructure of some alloys. It was the case for the arc-melted NiAl-10Cr-3.5W (fig. 5.8), NiAl-32Cr-3W (fig. 5.12) and NiAl-27Cr-2W (fig. 5.14) alloys described in 5.2, as well as NiAl-29Cr-6W alloy described in 6.2 (fig. 6.7). Further examples of dissolution signs are given in figure 6.14. Especially interesting were the cases where the primary dendrites had been dissolved, apparently inside out, leaving only a W(Cr) shell (fig. 6.14c). The process taking place for an apparent inside dissolution could be that during the Cr(W) formation by the peritectic reaction, the W(Cr) particle becomes porous. Therefore, the reaction continues taking place inside the particle, penetrating deeper into it, finally leaving a shell.

The existence of the peritectic also explains the different W(Cr) and Cr(W) primary phase fields in the phase diagram, being the reaction line that divides both regions. This

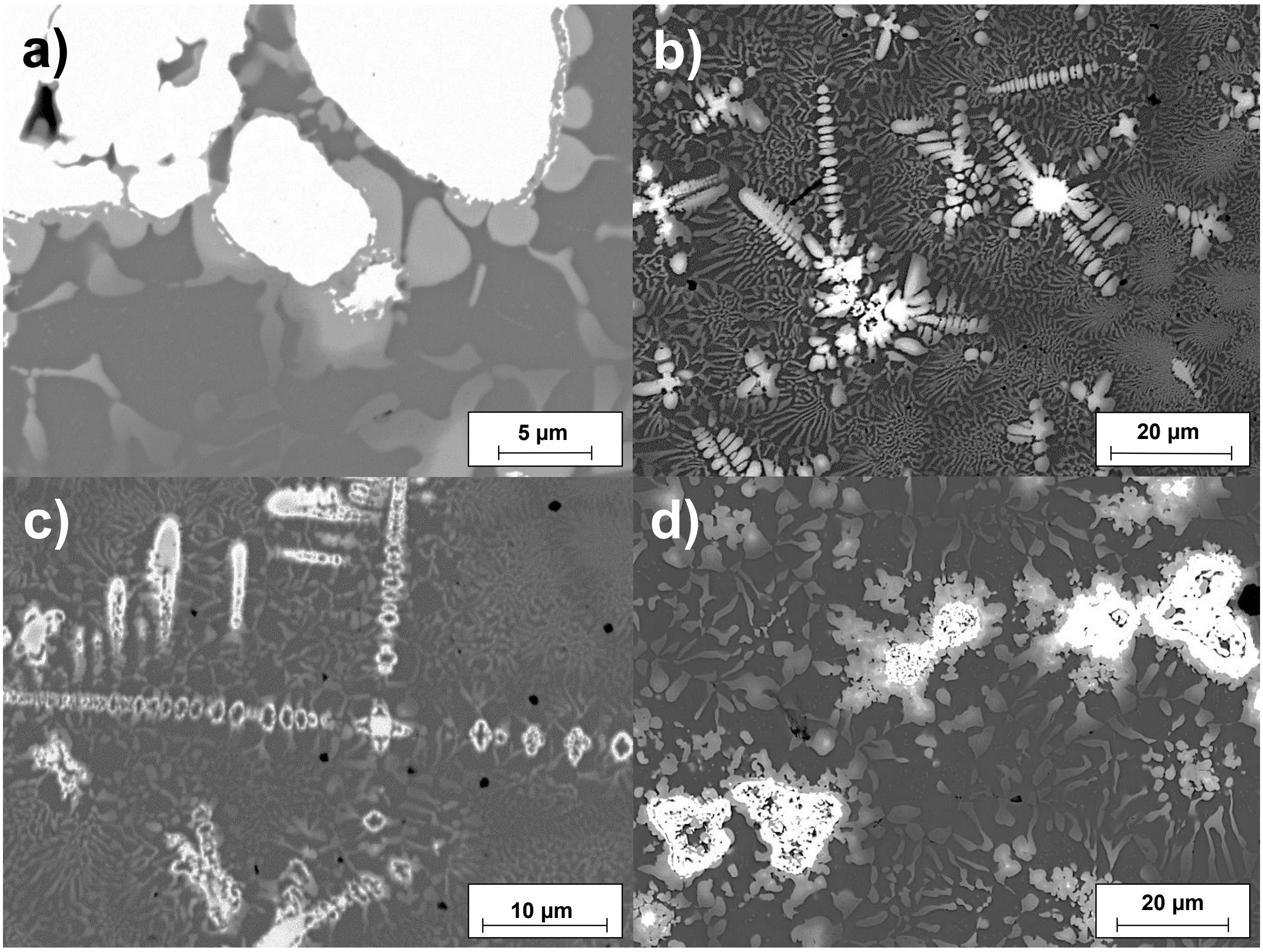

Figure 6.14: SEM BSD micrographs showing further sings of W(Cr) phase dissolution in the microstructure of a) NiAl-25Cr-11W, b) and c) NiAl-29Cr-6W, and d) NiAl-32Cr-3W samples.

peritectic reaction line did not reach the Cr-W boundary of the system, and its formation inside the pseudo-ternary is very probably caused by the expansion of the Cr-W miscibility gap, increasing its maximum temperature and the composition range, especially in the Cr corner, where in addition, melting temperatures are lower. As could be seen from the phase diagram calculations, the liquidus surface (fig. 6.2) exhibited the onset of a monovariant reaction induced by the miscibility gap. From the microstructures observed, a peritectic reaction must exist, ending in the eutectic trough.

On the other hand, the formation of Cr(W) phase on the W(Cr) phase was not observed in all samples, as some are not subjected to the reaction. However, in the samples where the reaction takes place and the Cr(W) layer forms, some W(Cr) particles were not completely surrounded, as should be the case for a peritectic reaction because of the direct contact of the liquid with the primary phase surface. Nevertheless, the thickness of the Cr(W) phase was not homogeneous, so it is possible that the layer in some zones is too thin to be observed with the techniques and magnification used. Also, as it was already exposed in 6.2, in some parts of the primary phase surface, a eutectic-like structure formed. This was observed in NiAl-10Cr-3.5W (fig. 6.5), but it was especially significant in NiAl-20Cr-4.5W (fig. 6.6); here, most of the primary phase exhibited this eutectic-like microstructure around the surface. The formation of this kind of structure could be explained through a class II four-phase equilibria, or U-type reaction. This is an invariant reaction of ternary diagrams similar to a peritectic in a binary, but in which the liquid and the primary phase react to form two, instead of one, solid phases growing simultaneously. The reaction would explain the eutectic-like microstructure observed on the surface of the W(Cr) primary phase, and matches with a potential interaction of the two eutectic sections assessed and the just reported peritectic reaction. A representation of this scenario is depicted in figure 6.15.

The exact composition of the U-type reaction is unknown, so the representation is just a mere approximation. However, the existence of a peritectic reaction line in the surroundings of a eutectic trough, strongly influences its path, which explains the unexpected behavior of rapid increase in W content, reaching several times the content in the NiAl-W pseudo-binary eutectic which can be observed. Moreover, the proximity of both reaction lines propitiates the intersection between them, giving rise to a ternary invariant reaction. These two features of the phase diagram account for the difficulties observed in the assessment of the initially sought eutectic trough.

With these in mind, a new model of the NiAl-Cr-W pseudo-ternary diagram was developed. The starting point of the reaction line between W(Cr) and Cr(W) phases was placed close to the Cr corner of the diagram, supported by the phase diagram calculations, and considering the liquidus corner of the three phase field caused by the miscibility gap. It should be taken into account that reaction lines may begin as one kind of reaction and then develop along the line into another reaction, depending on its curvature. It is possible

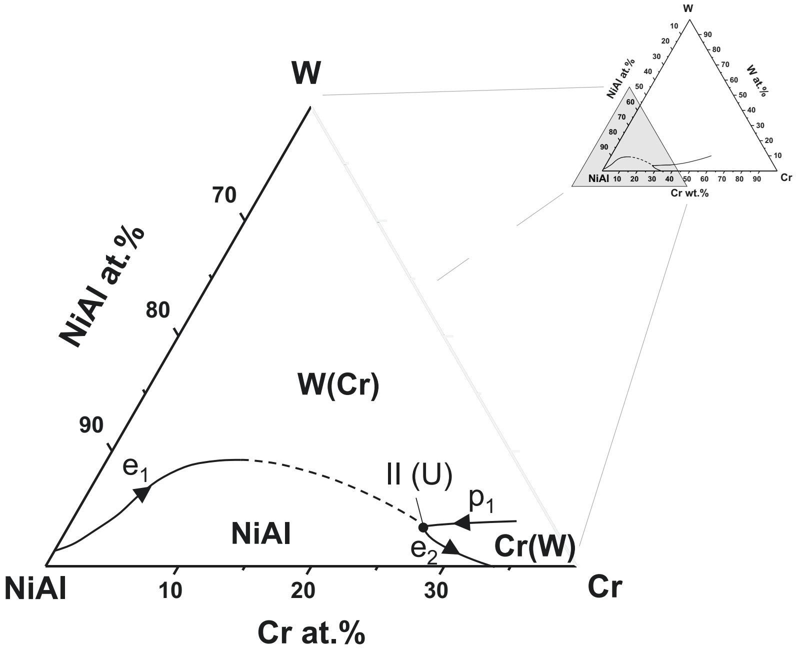

Figure 6.15: Magnification of the NiAl corner section of the ternary diagram, showing a representation of the reaction lines interaction to form a class II (U-type) four-phase equilibria reaction.

that the starting reaction was eutectic, however, the data gathered in the study correspond only to the NiAl corner of the system, where the microstructure indicated that a peritectic reaction was taking place.

The same behavior could take place in the sought eutectic trough, owing to the influence of the miscibility gap, and therefore, not being a continuous eutectic reaction. This fact would imply sections with no eutectic constituent, as this was also observed. Nevertheless, further research should be carried out to determine its existence in the studied system.

Furthermore, the U-type invariant reaction taking place due to the intersection of both reaction lines, influenced the data on eutectic compositions obtained in 5.2. In view of the significant amount of U-type structure observed in the zone of NiAl-20Cr-4.5W alloy (fig. 6.6), whose local composition was NiAl-17.5Cr-4.5W, and to a lesser extent in NiAl-10Cr-3.5W alloy zone (fig. 6.5), the invariant reaction was placed in the surroundings. The final model can be seen in figure 6.16, where the orientation of the system was changed again, shifting Cr and NiAl for better visibility of the liquidus surface and miscibility gap.

Ultimately, both peritectic and U-type reactions, are influencing the sought eutectic trough, and lead to complex microstructures, which are not easy to characterize. In order to accurately assess the corresponding reaction lines in the NiAl-Cr-W pseudo-ternary, further thorough research should be carried out, characterizing more alloy compositions, also using additional techniques to complement the results. Nevertheless, valuable data was obtained

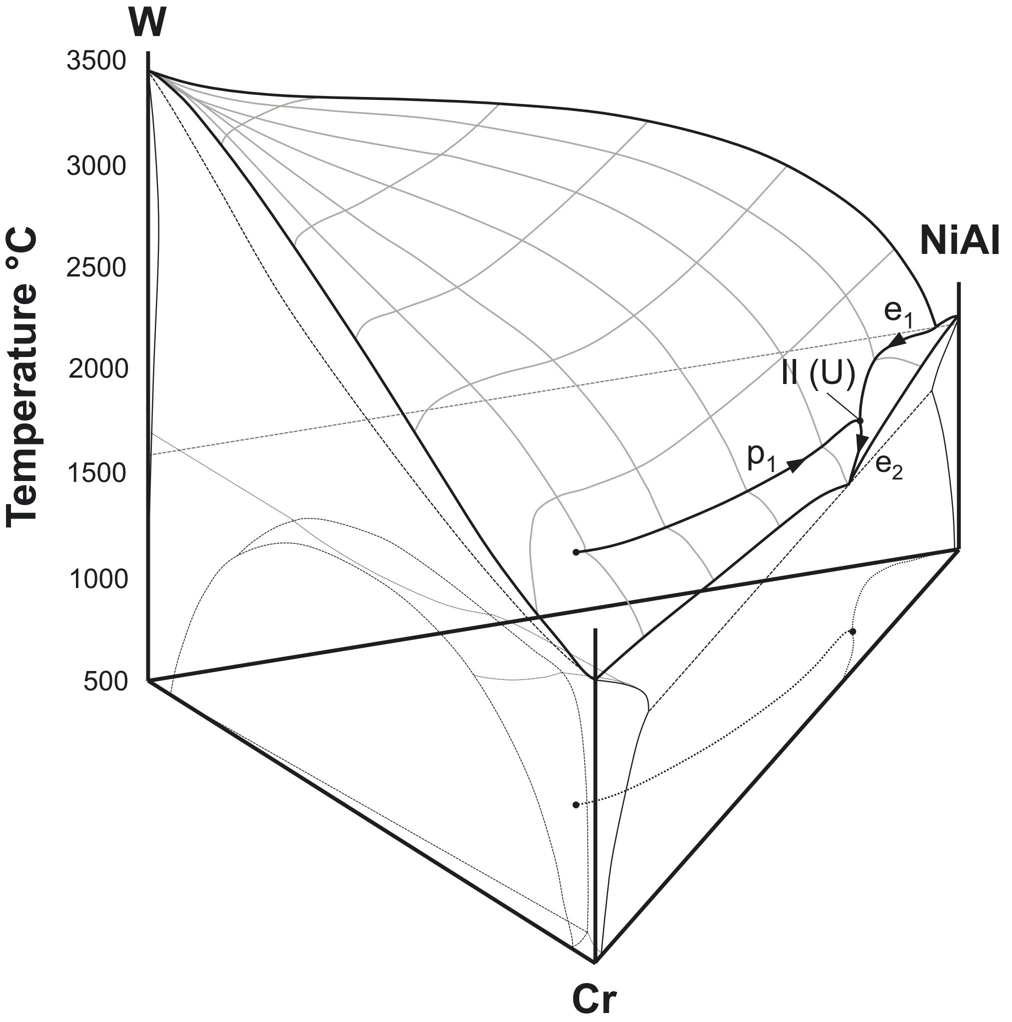

Figure 6.16: Model of the NiAl-Cr-W pseudo-ternary system based on the binary diagrams, Calphad calculations, the results obtained in the study and the reactions identified.

during the research and some light has been shed on the NiAl corner of the NiAl-Cr-W pseudo-ternary system.

7

Mechanical Behavior of NiAl-20Cr-4.5W Alloy

While studying the solidification path to improve the eutectic trough assessment and other features of the NiAl-Cr-W pseudo-ternary diagram, mechanical testing was carried out in an alloy, in order to get a first impression of the mechanical properties expected for these pseudo-ternary alloys.

The composition was selected based on several criteria, such as hardness (table 7.1), higher eutectic constituent volume fraction, and the homogeneity achieved in the sample. Samples in the Cr-lean region exhibited the lowest hardness, which indicates, in principle, better ductility. However, the volume fraction of eutectic constituent in these samples was very low. On the other hand, samples close to the NiAl-Cr pseudo-binary eutectic contained the highest eutectic constituent volume fraction, but their hardness was rather high. Moreover, their composition was low in W. The lower hardness was noticeable in DS samples, even with similar composition due to the different solidification conditions. Finally, a compromise solution was taken, and NiAl-20Cr-4.5W alloy was chosen to perform the mechanical testing.

The amount of material needed to perform the mechanical testing was too high to produce it in house with the arc melting furnace. Therefore, a new alloy rod was produced in an induction furnace at the facilities of MPIE, with dimensions of 200 mm length and 30 mm diameter. Wet chemical analyses were performed at the top and bottom of the rod, which indicated variations in the composition, especially in W content, probably due to density segregation. However, the top part of the rod exhibited a deep hollow core due to

Table 7.1: Hardness of the different NiAl-Cr-W samples produced by arc melting and DS, and NiAl-Cr pseudo-binary eutectic for comparison

Sample	Hardness	Sample	Hardness
NiAl-2Cr-3W	384 ± 21	NiAl-29Cr-6W	519 ± 12
NiAl-3Cr-4W	420 ± 27	NiAl-32Cr-3W	520 ± 11
NiAl-5Cr-2W	420 ± 20	NiAl-34Cr	496 ± 17
NiAl-10Cr-1.8W	445 ± 17	DS NiAl-3Cr-4W	350 ± 27
NiAl-10Cr-3.5W	440 ± 9	DS NiAl-25Cr-5W	375 ± 16
NiAl-20Cr-4.5W	449 ± 8	DS NiAl-30Cr-2W	374 ± 15
NiAl-27Cr-2W	497 ± 14	DS NiAl-34Cr	383 ± 7

shrinkage, as well as a higher level of cavities. Therefore, samples were cut by EDM from the bottom part, and EDX measurements showed the overall composition to be close to the nominal, with a W content of about 4 at.%.

7.1 Microstructure

Although the composition was the same as that of the previously produced and reported alloy, the different production technique led to different microstructures. As can be seen in figure 7.1, W(Cr) phase was rounded, and agglomerated together. Cr(W) phase with precipitation formed peritectically around the W(Cr) phase, as well as the eutectic-like structure from the U-type reaction. NiAl phase resembled dendritic growth and exhibited

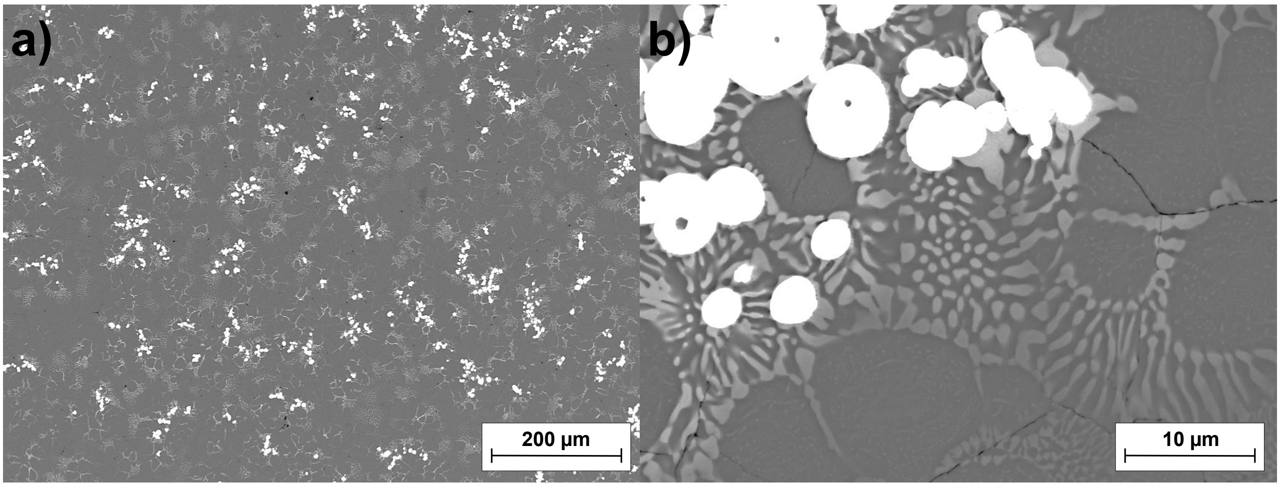

Figure 7.1: SEM BSD micrographs of the NiAl-20Cr-4.5W alloy produced by induction casting: a) a general overview of the microstrucure, and b) close view of the microstructural features.

precipitation too. The interdendritic Cr(W) phase and eutectic constituent completed the microstructure. The cracks observed in figure 7.1b, had developed during cutting and surface preparation, and were not present in tested samples.

EDX measurements in the as-cast microstructure revealed composition gradients within the phases, as was also observed in other alloys during the research. This is due to the non-equilibrium microstructure in this condition. Owing to this, a piece of the alloy was subjected to heat treatment, in order to prevent any effect of non-equilibrium microstructure in the creep behavior, where tests can take hundreds of hours and the influence can be significant. Therefore, the ingot was subjected to 1000 °C for 1000 hours in air and was furnace cooled.

After heat treatment, the sample exhibited a similar microstructure, though some coarsening of the eutectic constituent and the precipitates in NiAl could be clearly observed (fig. 7.2). Moreover, a new feature was present: the Cr(W) phase surrounding the W(Cr) exhibited bright precipitates (fig. 7.2b). The brightness indicated a high W content phase, however, the precipitates were too small to allow an individual composition measurement. Nonetheless, the W content in these regions was higher. Prior to heat treatment, Cr(W) phase close to the W(Cr) phase, exhibited a higher W content than the one furthest from it. These non-equilibrium zones were W supersaturated, and the high-temperature heat treatment triggered the precipitation. This segregation occurred due to the miscibility gap between both phases. Further EDX measurements indicated still some other composition gradients for example between the core and the surface of W(Cr) phase, which is understandable due to the low diffusivity of W. Nevertheless, the microstructure, after such a long heat treatment, was considered to be sufficiently equilibrated to perform reliable creep testing.

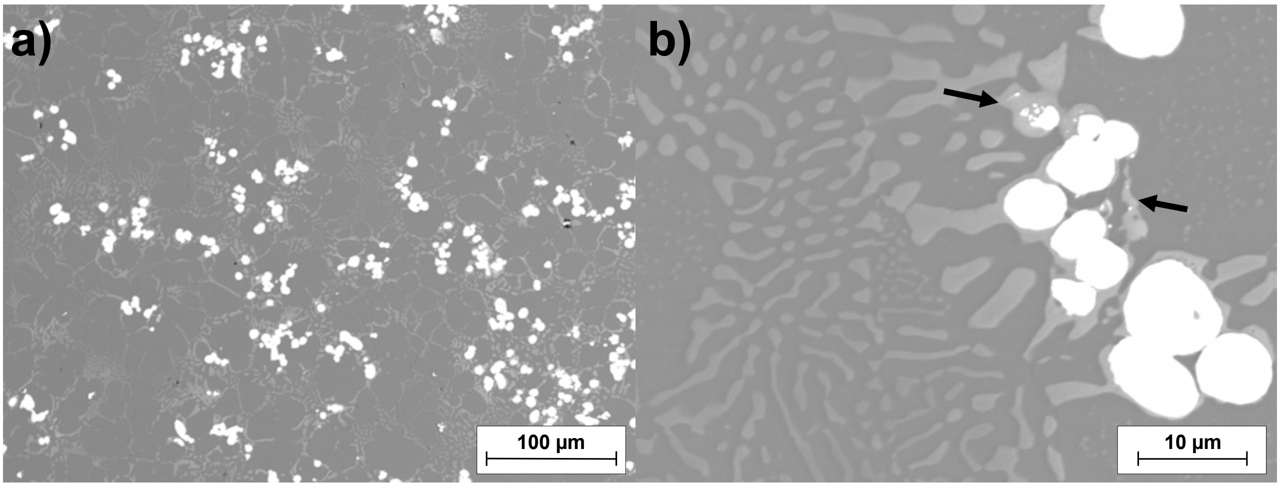

Figure 7.2: SEM BSD micrographs of the NiAl-20Cr-4.5W alloy after heat treatment at 1000 °C for 1000 h: a) a general overview, and b) close view of the microstructural features.

For the rest of the mechanical tests (compression, tensile, and 4-point bending testing), although they were also performed at high temperatures, the as-cast alloy microstructure was considered to be reliable enough, due to the short time required for testing.

7.2 Compression behavior

The first experiments performed to characterize the mechanical behavior of the alloy at high temperatures were compression tests. As was already explained in 3.3.2, tests were performed at a strain rate of 10^{-4} s^{-1} and at temperatures of 25 (room temperature or RT), 400, 600, 800, 1000, 1100, 1200, 1300 and 1400 $^{\circ}$C. In figure 7.3, the values of yield strength extracted from the compression curves at 0.2% strain are plotted.

There was a continuous drop in yield strength, with the strongest decrease taking place at 600 $^{\circ}$C. Above this temperature, the yield strength of NiAl alloys continues decreasing, but less than could be observed around 600 $^{\circ}$C. This behavior is typical of NiAl alloys due to the transition from brittle to ductile behavior, which is located in this range of temperatures. In some NiAl alloys this drop is more pronounced, and prior to it, an athermal regime can observed at RT, which can span more than 300 $^{\circ}$C. In the case of NiAl-20Cr-4.5W alloy, the value of yield stress obtained at 400 $^{\circ}$C does not indicate any athermal regime. However, it could take place below this temperature.

In addition, a comparison between the current alloy, polycrystalline NiAl, nanocrystalline NiAl (FAHP), and relevant NiAl-based alloys is presented [47, 88, 91, 96]. First of all, it should be noted that most alloys used for comparison are from DS, while NiAl-20Cr-4.5W alloy was tested in the as-cast state. Nonetheless, NiAl-Cr-W eutectic alloys were developed as *in situ* composites as well. The present alloy has a higher yield strength than polycrystalline NiAl, but also higher than DS NiAl-W, and its counterpart DS NiAl-Re eutectic alloys. This is true at all temperatures, but especially significant below 800 $^{\circ}$C.

On the other hand, [100]-oriented DS NiAl-Cr eutectic alloy, exhibits higher yield strength at all temperatures. This is due to the orientation in the hard direction, the intrinsic higher reinforcement volume fraction of the NiAl-Cr eutectic, and its fully eutectic microstructure. Likewise, DS NiAl-Mo exhibits higher yield strength. However, in this case the values are more similar, especially at temperatures below 800 $^{\circ}$C; above that temperature, the yield stress of DS NiAl-Mo is about 50 MPa higher. The behavior of DS NiAl-31Cr-3Mo is similar above 800 $^{\circ}$C, although RT values indicate a lower yield strength at lower temperatures.

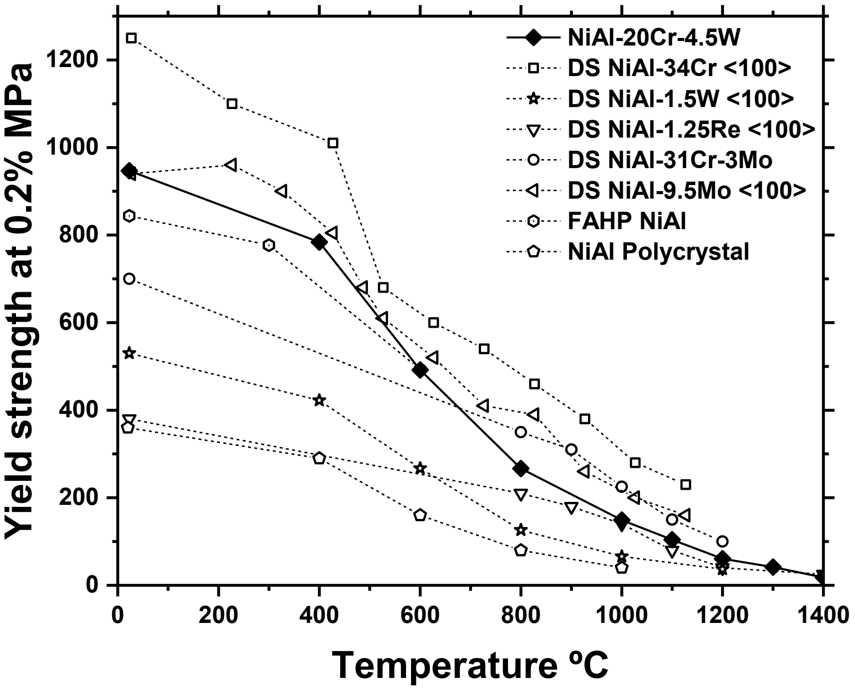

Figure 7.3: Yield strength of NiAl-20Cr-4.5W alloy obtained from compression tests compared to the yield strength of polycrystalline NiAl [47], field-assisted hot pressed (FAHP) nanocrystalline NiAl [88] and several NiAl alloys [47, 91, 96].

7.3 Tensile behavior

After compression testing, the tensile behavior of the alloy was tested under the same conditions of strain rate, in order to obtain information about any difference between tensile and compression behavior. As can be seen in figure 7.4, no values of yield strength could be measured for lower temperatures. The brittleness of the material at this temperature resulted in a sudden break of the specimen while starting to load. Due to defects in the microstructure, some samples did not even withstand mounting. However, at 600 °C, a 2% strain was already achieved, close to the yield point of the material. At higher temperatures, yield was reached without problems, and the material exhibited ductile behavior. Moreover, yield strength values from tensile tests match perfectly with that of compression, as expected. These results validated the data obtained for other temperatures in compression, where initial defects do not play such an important role.

In figure 7.5, the tensile yield strength of the material is compared to the values obtained by Bei and George [140] in a DS NiAl-9Mo eutectic alloy. As can be seen, the yield strength of DS NiAl-9Mo is higher than that of NiAl-20Cr-4.5W. However, tensile tests performed in DS NiAl-9Mo samples were done at a slightly higher strain rate of 4.2 10^{-3} s^{-1}. On

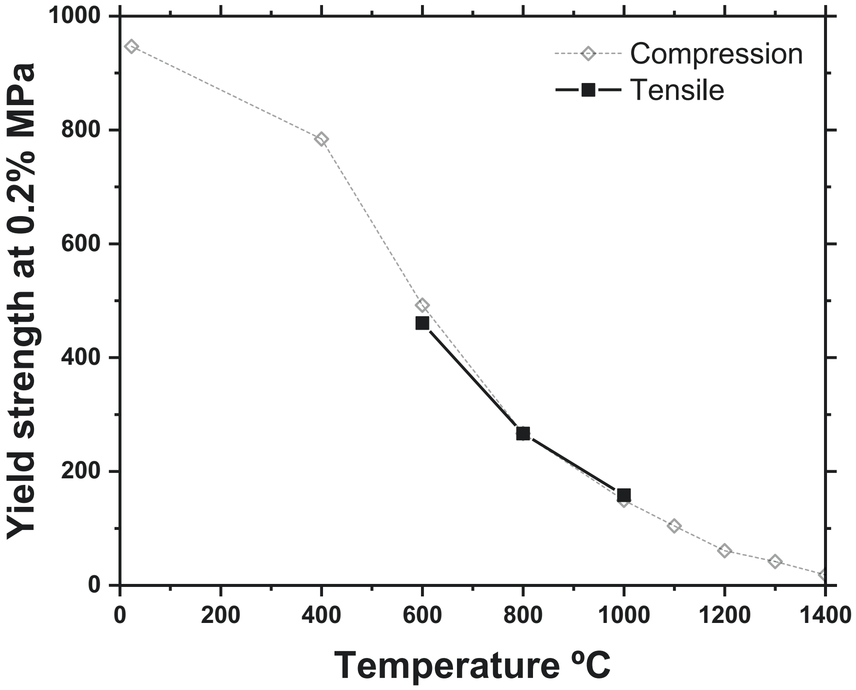

Figure 7.4: Yield strength of NiAl-20Cr-4.5W alloy obtained from tensile tests and compared to the values from compression testing (gray).

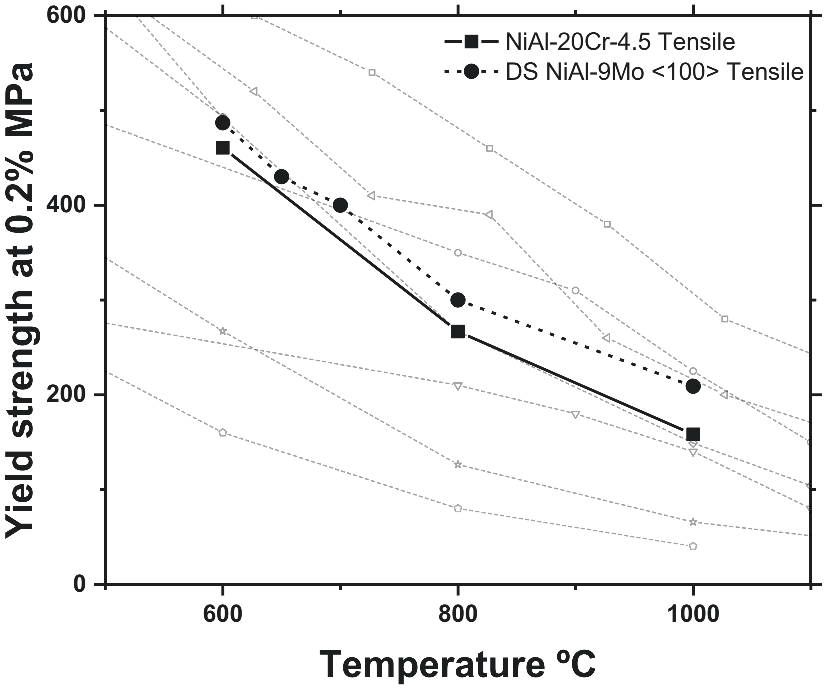

Figure 7.5: Yield strength of NiAl-20Cr-4.5W alloy obtained from tensile tests compared to the yield strength of tensile-tested DS NiAl-9Mo [140], as well as compression data from figure 7.3 (gray).

the other hand, the yield strength of alloys presented in figure 7.3 is also shown here in grey. The values of both DS NiAl-Mo alloys are very similar. DS NiAl-9Mo in tension has slightly lower yield strength than DS NiA-9.5Mo in compression. This is probably due to the higher reinforcement volume fraction of the latter. At the moment the accepted value of the NiAl-Mo eutectic is at 9 at.% Mo, however, as was explained in 1.4.3, fully eutectic microstructures can be obtained out of the eutectic composition if specific solidification conditions are met [90]. Either way, NiAl-20Cr-4.5W yield strength behavior is comparable to that of DS NiAl-Mo alloy.

7.4 Brittle-to-Ductile Transition Temperature

As could be observed from compression tests, NiAl-20Cr-4.5 alloy exhibited the strongest decrease of the yield strength around 600 °C. In tensile tests, a change in the mechanical behavior from brittle to ductile could be observed between samples tested below and above 600 °C. It is thus evident that the Brittle-to-Ductile Transition Temperature (BDTT) is located around this value. 4-point bending tests were carried out to determine more accurately the transition temperature.

In figure 7.6, the first set of results from bending tests at 500 to 800 °C is plotted. As

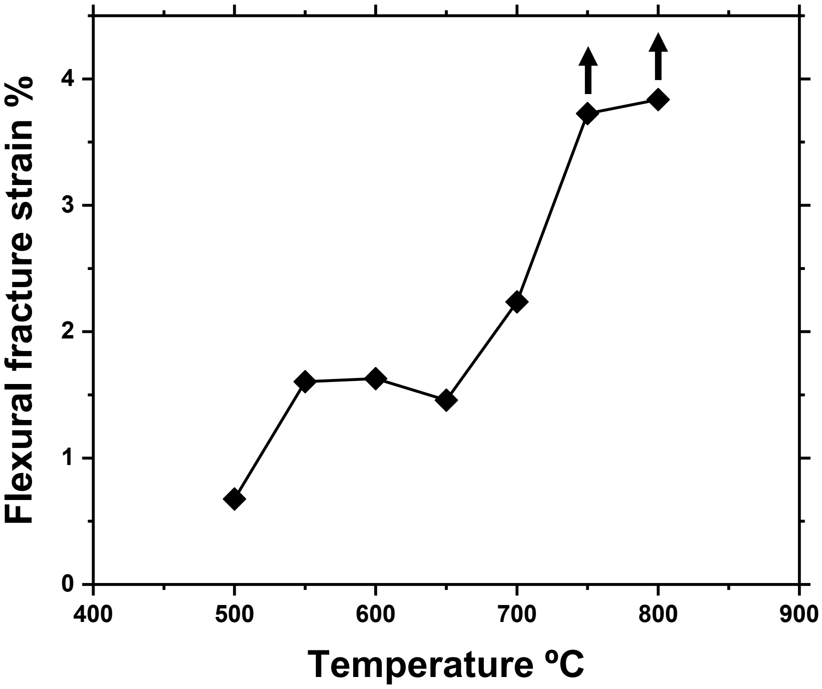

Figure 7.6: Data form the ductile-brittle behavior of NiAl-20Cr-4.5W alloy obtained from the first set of 4-point bending tests.

can be seen, the alloy exhibited abnormal behavior for an intermetallic compound. An intermediate regime can be noted between 550 and 700 °C, where the behavior is not completely brittle, becoming completely ductile at 750 °C. However, thorough analysis of the fracture surfaces indicated the existence of critical voids, which affected the result of tests. One of these voids is presented in figure 7.7. The presence of this void in the microstructure modified the mechanical behavior of the sample. As can be seen more clearly in the magnified micrograph (fig. 7.7b), the orientation of cleavage planes around indicates that fracture initiation occurred on the void surface. Then, the crack propagated around the void, and the sample failed catastrophically.

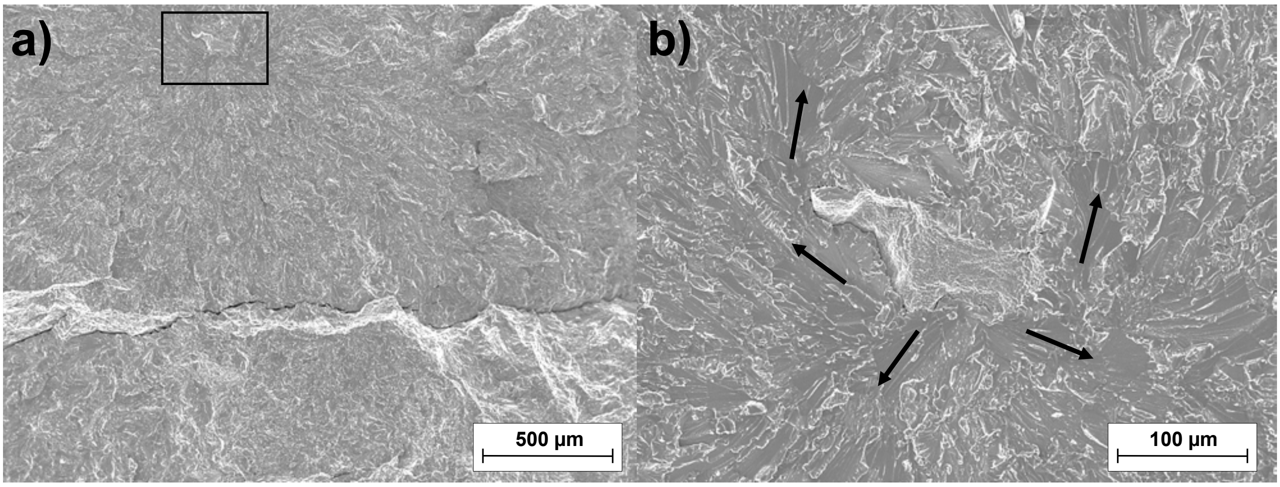

Figure 7.7: SEM SE micrographs of the fracture surface of NiAl-20Cr-4.5W alloy in the first bending test at 550 °C : a) a general overview of the surface, and b) close view of the void.

Consequently, further bending tests were carried out to exclude any effect of voids on the mechanical behavior of the samples. Results of the second set of tests are plotted in figure 7.8, along with the first set of values. As can be seen, the behavior in the second set of tests is more characteristic of that of intermetallic compounds. A sudden change in the mechanical behavior from brittle to ductile is observed between 600 and 650 °C, which is consistent with the results obtained from tensile and compression tests. Moreover, at 600 °C a fracture strain slightly higher than 0.5 % could be observed; this is in agreement with the limited 2% strain observed in tensile tests at the same temperature.

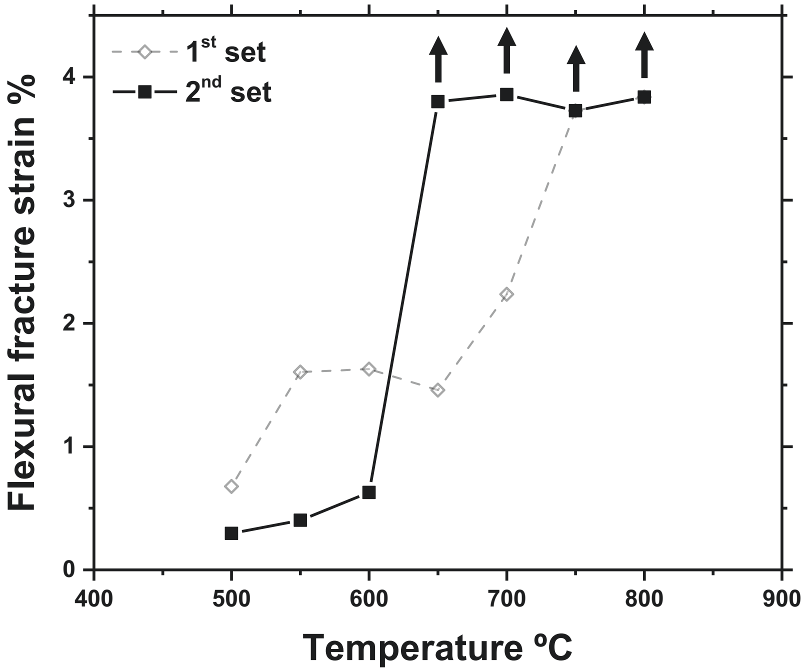

Figure 7.8: Data form the ductile-brittle behavior of NiAl-20Cr-4.5W alloy obtained from the second set of 4-point bending tests and compared to the values from the first set in figure 7.6 (gray).

The BDTT of NiAl intermetallic, as other mechanical properties, depends on the stoichiometry of the compound and the microstructural features. The range of this transition temperature varies from about 300 to 600 °C [21], but also a temperature as low as 200 °C has been reported [37]. In the case of NiAl alloys, the BDTT is usually higher, reaching 1000 °C or more for precipitate-strengthened alloys [141, 142]. In the case of NiAl-20Cr-4.5W, a value of approximately 625 °C is reasonably low. A BDTT between 650 and 700 °C was reported for DS NiAl-9Mo alloy [140], which is slightly higher but comparable to the results obtained here.

The fracture surface of the samples that exhibited brittle behavior and which broke during bend testing, was analyzed. Some examples are presented in figure 7.9. Cracks initiated typically in an internal defect and propagated by cleavage through the matrix (fig. 7.9a). In figure 7.9b, a crack front is deflected, forming several cleavage steps. Crack bridging is observed at the crack tip, where the ductile phase is deformed or broken in a ductile manner. At eutectic cell boundaries that were parallel to the fracture, the phases seem to have debonded, as can be seen in figure 7.9c and d. On the other hand, in figure 7.9e it can be seen how cracks were arrested or deflected by both Cr(W) and W(Cr) phases. Figure 7.9f is a close view of the ductile fracture of the Cr(W) phase in the eutectic constituent, and cleavage in NiAl phase. Pull out of the ductile phase was not observed on the surfaces analyzed.

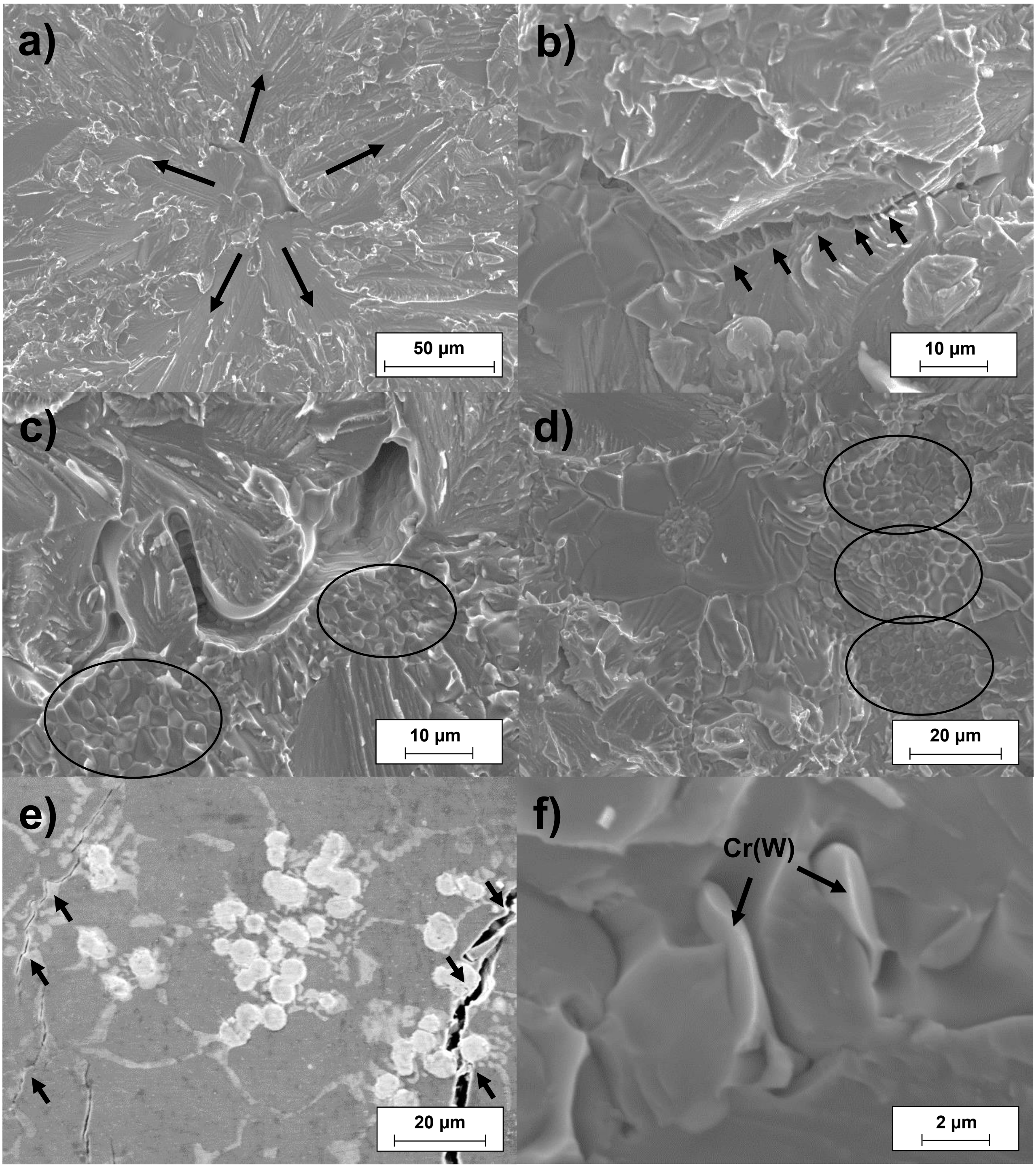

Figure 7.9: SEM SE micrographs of the fracture surface features in NiAl-20Cr-4.5W alloy subjected to bending tests.

7.5 Creep behavior

Finally, to complete the characterization of the mechanical behavior of NiAl-20Cr-4.5W alloy at high temperature, creep tests were carried out after the heat treatment at 1000

°C for 1000 h. The creep test results from testing at 800 to 1100 °C are plotted in figure 7.10. Although more data were obtained from the tests, the plotted points correspond to the steps where the minimum creep rates were clearly reached. As is shown, the stress exponent *n* varied from 9 at 800 °C to 4.5 at 1100 °C. Moreover, the difference was more pronounced between the lowest two and the highest two temperatures, while between these two sets the difference was not so significant. This behavior could be due to a change in the creep-controlling mechanism at about 950 °C. A stress exponent of 7 or higher is characteristic of precipitate-controlled creep, which could be the main controlling mechanism at 800 and 900 °C. The increase in temperature decreases the barrier effect of particles to the dislocation movement. Consequently, the stress exponent *n* was reduced to about 5 at 1000 and 1100 °C, typical of climb-controlled creep [143, 144]. Nonetheless, this increment in the stress exponent could be due to the larger stresses reached at temperatures below 1000 °C. Under these conditions, the creep behavior does not follow a power-law anymore but it rather becomes exponential, and the stress exponent starts to increase rapidly. Therefore, this increase would just indicate the onset of what is called power-law breakdown, where the power-law is no longer applicable. A similar increase of the stress exponent with increasing stresses was found by Seemüller *et al.* in DS NiAl-10Mo alloy [124].

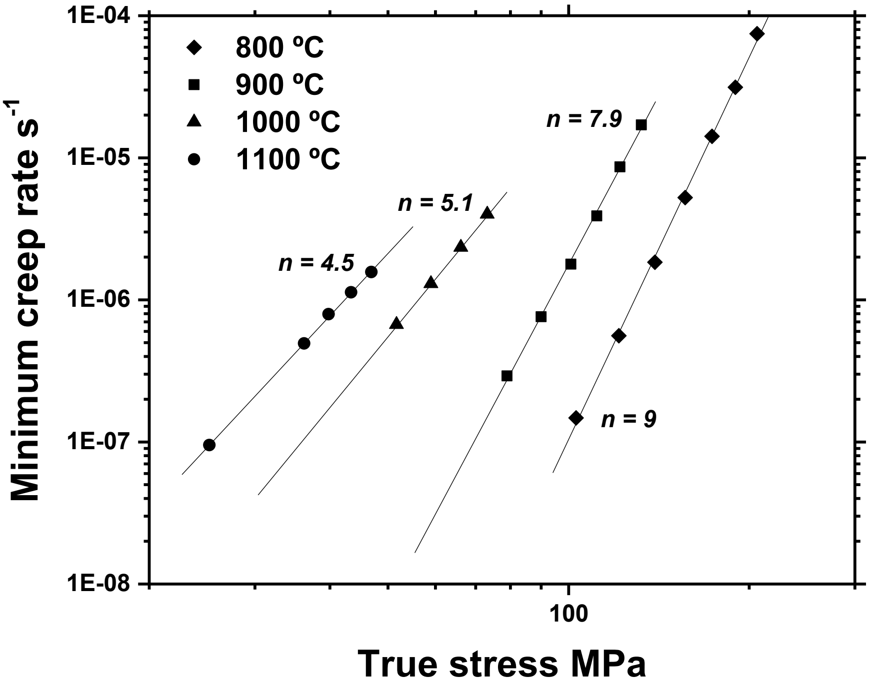

Figure 7.10: Creep behavior of NiAl-20Cr-4.5W alloy obtained from constant load compression tests at different temperatures.

The activation energy obtained from the creep tests was Q = 207 KJ/mol. This value is slightly lower than that reported for NiAl intermetallic, which is close to 291 KJ/mol, the activation energy for bulk diffusion of Ni in NiAl [144]. This fact is often taken as evidence of creep in NiAl being controlled by climb, which is a diffusion-controlled deformation mechanism [143–145]. The reason for the much lower activation energy observed in this study could be the onset of the power-law breakdown, which is usually coupled with a decrease in the activation energy.

In figures 7.11, 7.12 and 7.13 [96], the creep behavior of heat-treated induction-cast NiAl-20Cr-4.5W alloy is compared to that of other alloys at 800, 900 and 1000 °C respectively. As can be seen, the creep rates of the studied alloy lie between those of DS NiAl-W and NiAl-Re eutectic alloys. The values exceed those of DS NiAl-W alloy for most stresses in the temperature range studied. However, the different slope of the two alloys - that is their different stress exponent - make them cross below a stress level, where DS NiAl-W possesses a better creep behavior. On the other hand, DS NiAl-Re eutectic alloy has a better creep behavior than NiAl-20Cr-4.5W alloy for all tested temperatures and stresses. Nevertheless, the data exhibit a different slope as well, which is closer to that of DS NiAl-W. This is consistent, as the eutectic microstructure of both DS alloys is similar, while heat-treated NiAl-20Cr-4.5W presents a multiphase microstructure.

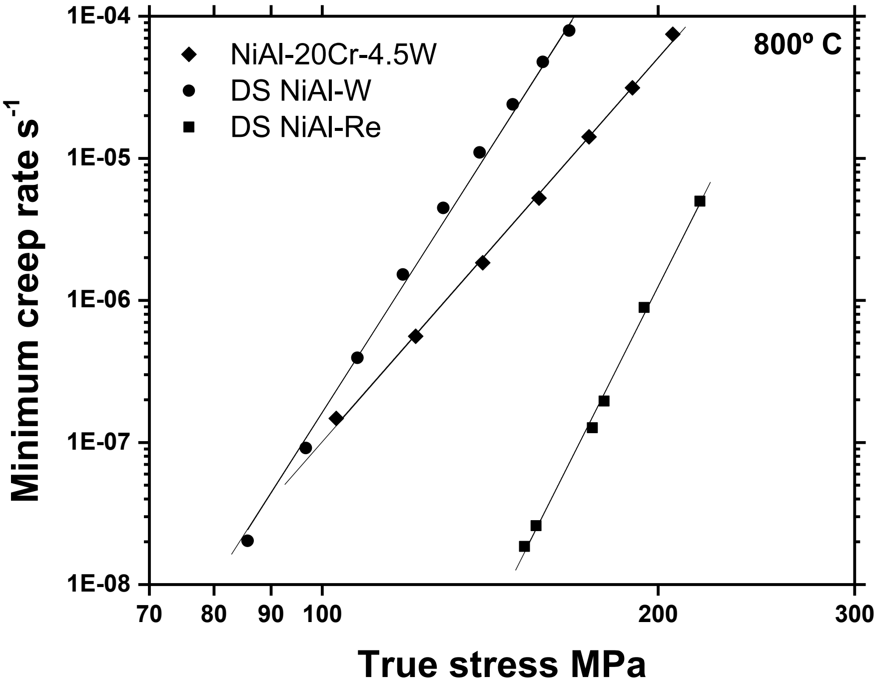

Figure 7.11: Creep behavior of NiAl-20Cr-4.5W alloy obtained from constant load compression tests at 800 °C in comparison with other NiAl-based alloys.

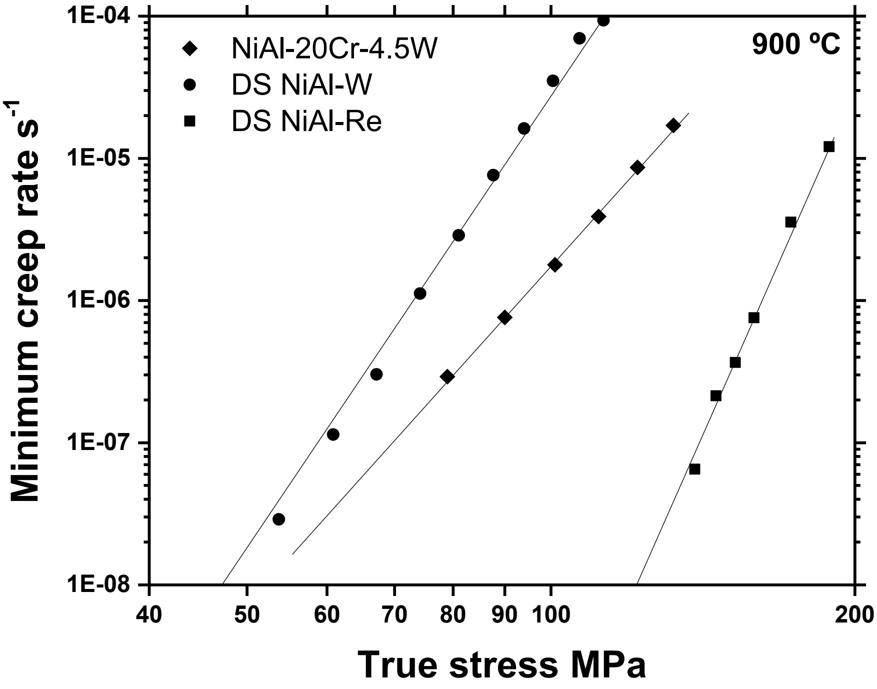

Figure 7.12: Creep behavior of NiAl-20Cr-4.5W alloy obtained from constant load compression tests at 900 °C in comparison with other NiAl-based alloys.

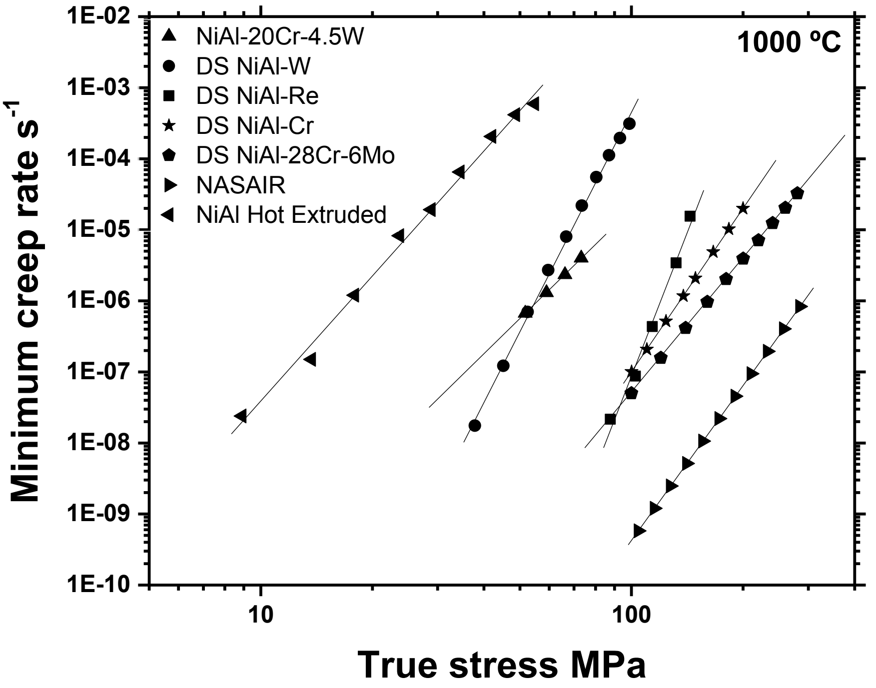

Figure 7.13: Creep behavior of NiAl-20Cr-4.5W alloy obtained from constant load compression tests at 1000 °C compared to extruded NiAl, NiAl-based alloys, and a first generation superalloy [96].

At 1000 °C, the behavior is also compared with an extruded NiAl alloy and first generation superalloy NASAIR. Heat-treated NiAl-20Cr-4.5W alloy presents a better creep behavior compared to NiAl, with several orders of magnitude difference in minimum creep rate for the same stress level. At the same time, the alloy creep behavior is still far from that of a first generation superalloy. However, the slope of both alloys is more similar than that of DS NiAl eutectic alloys with W and Re.

Crept microstructure

Although the alloy was heat-treated prior to creep testing, EDX measurements still revealed some composition gradients in the phases. Therefore, the microstructure after creep testing was analyzed in order to verify its stability after hundreds of hours under stress and high temperatures.

In figure 7.14, the microstructure of the samples after creep testing is presented. No phase coarsening could be observed in any of the samples, compared to the as-heat-treated microstructure (fig. 7.14a-d). The size of W(Cr), NiAl, and phases in the eutectic constituent remained constant, though the morphology of each eutectic cell in the microstructure was different within the same sample. W-rich precipitates in the Cr(W) phase were also common, mostly when surrounding the W(Cr) phase (fig. 7.14e and f). EDX measurements were performed, and composition gradients remained in the phases, which were more pronounced in W(Cr) phase. No significant changes in the eutectic constituent composition or in other phases could be detected, indicating excellent phase stability

An investigation of the oxidation behavior of the alloy was not an aim of the present study. However, as creep tests were carried out in air at high temperatures, and for long times, the samples were subjected to oxidation, and its effect was observed in the microstructural characterization of the samples (fig. 7.15). The composition of the oxides forming could not be analyzed and will need further experiments. However, EDX measurements indicated an important presence of oxygen in the dark phase, close to the sample's surface. The measurement of oxygen by EDX is more qualitative than quantitative due to the lightness of the element. Nevertheless, the presence of oxides in the dark phase could be confirmed by the results. In samples tested at 800 and 900 °C, the oxidation was minor and only close to the surface. At 1000 °C, the effect became more visible and oxygen started to penetrate into the microstucture. As can be seen in figure 7.15c, the oxidation progressed mainly along the boundaries of Cr(W) phase with the formation of oxides (dark phase), and continued reacting with it until the whole phase was eaten away, leaving W(Cr) phase alone (fig. 7.15a and b). The local structure was thus weakened, and started to fall apart, worsening the situation. At 1100 °C, the oxidation was severe, and the penetration reached up to 500 μm into the sample at the deepest location (fig. 7.15d).

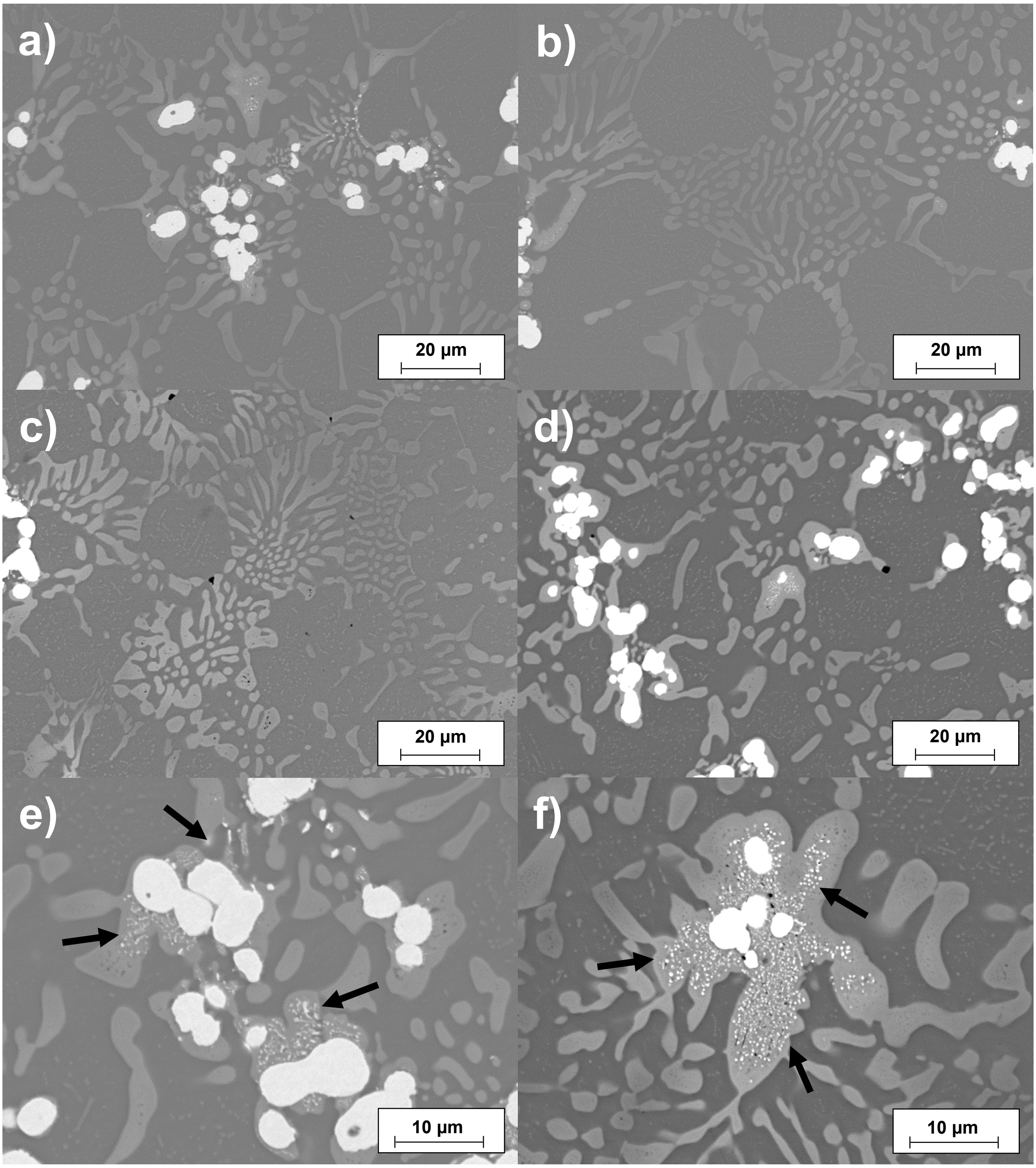

Figure 7.14: SEM BSE micrographs of NiAl-20Cr-4.5W alloy samples after creep testing at: a) 800 °C, b) 900 °C, c) 1000 °C, and d) 1100 °C. In e) and f) magnification of Cr(W) phase with high W rich precipitation.

Based on the observations, it became clear that the phase prone to oxidation in NiAl-20Cr-4.5W alloy is Cr(W), due to the advance and formation of oxides at its boundaries, being critical at temperatures above 1000 °C. This fact should be taken into account for further development of NiAl-Cr-W alloys.

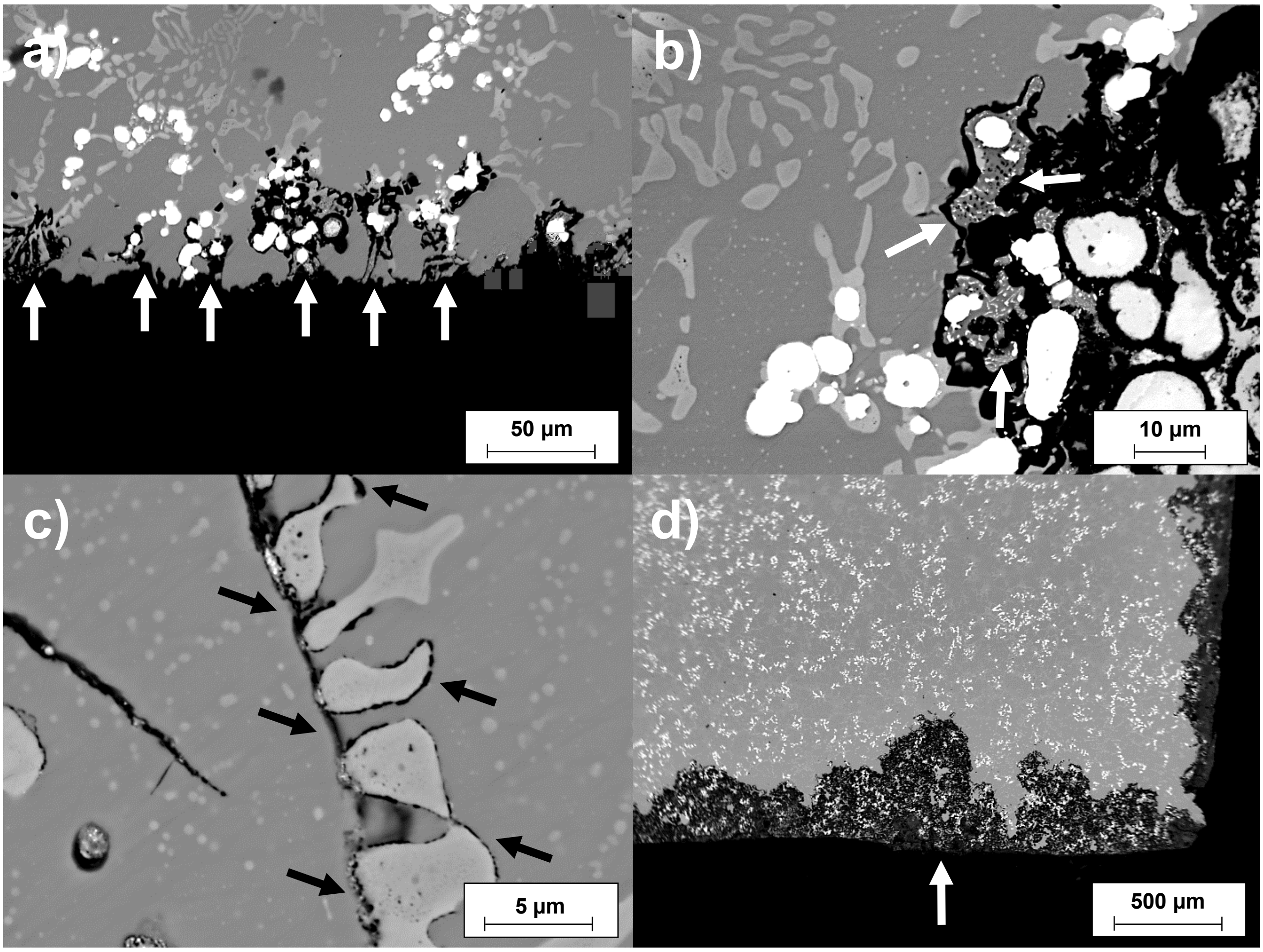

Figure 7.15: SEM BSE micrographs of the oxidation in NiAl-20Cr-4.5W alloy samples after creep testing at: a) and b) 1000 °C, c) 800 °C, and d) 1100 °C.

8

Conclusions and Future Work

8.1 Conclusions

The research work carried out and presented here includes the study of the processing, phase equilibria, and properties of novel multiphase eutectic alloys in the NiAl-Cr-W system. Each of the parts in which the research was divided led to important findings. These are summarized and disclosed here.

Alloy processing

During the production and processing of alloys through induction and arc melting, as well as directional solidification, the critical importance of the crucible selection and set up, together with the control of the temperature was shown, especially in highly demanding materials, as is the case for NiAl-Cr-W alloys.

Due to the large differences between the elements in the system, alternative processing routes were proposed. Specifically, the Ni-W processing route led to significant improvements in the element dissolution and homogeneity of the resulting microstructure. However, further efforts must be made in this regard in order to obtain fully homogeneous microstructures.

Eutectic trough

The eutectic trough assessment through eutectic cell composition measurements led to the conclusion that no continuous eutectic trough exists in the NiAl-rich corner of the NiAl-Cr-W pseudo-ternary system. Nevertheless, sections in the Cr-rich and Cr-lean regions have been preliminarily assessed, indicating a rapid increase of W content in the eutectic constituent on both sides, reaching values of several times the value of NiAl-W eutectic and far from the Calphad calculations.

On the other hand, wide scatter was observed in the composition of the eutectic cells. The scatter was partially attributed to the non-equilibrium conditions during solidification and a skewed coupled zone in the system, which led to a faster growth of eutectic constituent in out-of-eutectic compositions.

Pseudo-ternary phase diagram

After the study of the phase diagram through the solidification path, and supported by computer-aided calculations, a main conclusion was drawn: A continuous eutectic trough does not exist in the system.

The extension of the high-temperature miscibility gap into the pseudo-ternary system induces the formation of a new reaction line, which has not been previously reported. This monovariant reaction extends up to the eutectic trough sections assessed where it ends, forming a class II four-phase equilibrium or U-type reaction.

On the other hand, the validity of the NiAl-Cr-W pseudo-ternary approximation to approach the research was confirmed. However, the true quaternary nature of the system should be taken into account, as it implies a deviation which contributes to the observed scatter.

Mechanical behavior

The high temperature stability and mechanical behavior of NiAl-20Cr-4.5W alloy was studied by means of compression, tensile, 4-point bending, and creep tests. From the results obtained, it can be concluded that NiAl-20Cr-4.5W alloy exhibits a high-temperature mechanical behavior comparable to that of the most advanced NiAl-based alloys developed so far; in fact, even exceeding some of them, including its predecessor, the NiAl-W eutectic alloy.

Moreover, the results are encouraging, because NiAl-20Cr-4.5W alloy microstructure is not optimized. Other advanced eutectic alloys had fully eutectic microstructure and were directionally solidified in order to obtain a microstructure with aligned reinforcement.

However, the alloy tested here possessed a multiphase microstructure with no alignment. Therefore, there is scope for improvement in further NiAl-Cr-W alloys.

8.2 Future Work

Following the research work carried out, and in view of the conclusions reached, possible future work derived from the same is proposed here.

First of all, further research has to be undertaken in order to improve the alloy production and processing. By means of more refined routes that improve the element dissolution, and processing techniques that also prevent element segregation, alloy compositions with high W content could be produced successfully.

Once more alloy compositions can be produced successfully, then a precise assessment of the eutectic trough sections and other discovered reaction lines could be carried out through thorough microstructural and compositional analyses. Additionally, thermal analyses would be beneficial for the assessment.

Based on a precise assessment, the limits of the eutectic trough sections would be interesting starting points for fully eutectic alloy production. The rapid increase in W content observed in the current assessment, compared to the Calphad calculations and NiAl-W eutectic, indicate the possibility of obtaining higher W content and higher reinforcement volume fraction eutectic alloys, especially at those limit points. Presumably, the high-temperature mechanical behavior of these alloys would be the most promising, due to a higher reinforcement volume fraction and a higher melting temperature of a W-rich phase.

On the other hand, similar research work could be extended to the homologous NiAl-Cr-Re system. Although the Cr-Re system does not exhibit complete miscibility - not even at high temperatures - both elements present wide solid solution phase fields. These phase fields are larger than those of Cr-W below the miscibility gap temperature, so the discontinuous eutectic trough sections could reach higher Re content and higher reinforcement volume fraction in the eutectic alloys. Some NiAl-Cr-Re alloys have been produced and a preliminary assessment of the eutectic trough was carried out, which exhibited similar behavior to W, with rapid increase in Re content up to several times the NiAl-Re eutectic. What is more, the alloys were easier to produce, and eutectic cells in the samples were more regular and abundant in the microstructure.

Additionally, research could be carried out towards the more complex NiAl-Cr-W-Re system. An approach into this system was done with the production of a NiAl-2Cr-3W/Re alloy as an attempt to: reduce the content of the expensive and strategic element Re; enhance the ease of production of NiAl-Cr-W alloys as observed in NiAl-Cr-Re alloys; and increase the amount and regularity of eutectic cells in the arc-melted samples. The attempt yielded encouraging results.

Bibliography

[1] M.J. Benzakein. What does the future bring? A look at technologies for commercial aircraft in the years 2035–2050. *Propulsion and Power Research*, 3(4):165–174, 2014. ISSN 2212540X. doi: 10.1016/j.jppr.2014.11.004. URL http://www.sciencedirect.com/science/article/pii/S2212540X14000728. (Page 2.)

[2] Y.S.H. Najjar and I.A.I. Balawneh. Optimization of gas turbines for sustainable turbojet propulsion. *Propulsion and Power Research*, 4(2):114–121, 2015. ISSN 2212-540X. doi: 10.1016/j.jppr.2015.05.004. URL http://dx.doi.org/10.1016/j.jppr.2015.05.004. (Page 2.)

[3] T. Godin, S. Harvey, and P. Stouffs. Theoretical analysis of environmental and energetic performance of very high temperature turbo-jet engines. *International Journal of Thermal Sciences*, 38(5):442–451, 1999. ISSN 12900729. doi: 10.1016/S1290-0729(99)80015-5. URL http://www.sciencedirect.com/science/article/pii/S1290072999800155. (Page 2.)

[4] X. Zhao, H. Yin, and Y. Zhao. Impact of environmental regulations on the efficiency and CO2 emissions of power plants in China. *Applied Energy*, 149:238–247, 2015. ISSN 03062619. doi: 10.1016/j.apenergy.2015.03.112. URL http://www.sciencedirect.com/science/article/pii/S0306261915004146. (Page 2.)

[5] J. Kotowicz, M. Job, and M. Brzęczek. The characteristics of ultramodern combined cycle power plants. *Energy*, 92:197–211, 2015. ISSN 03605442. doi: 10.1016/j.energy.2015.04.006. URL http://www.sciencedirect.com/science/article/pii/S0360544215004247. (Page 2.)

[6] T.M. Pollock and S. Tin. Nickel-Based Superalloys for Advanced Turbine Engines: Chemistry, Microstructure and Properties. *Journal of Propulsion and Power*, 22(2):361–374, 2006. ISSN 0748-4658. doi: 10.2514/1.18239. URL http://arc.aiaa.org/doi/abs/10.2514/1.18239. (Page 2.)

[7] R.C. Reed. *The Superalloys: Fundamentals and Applications*. Cambridge University Press, New York, 2006. ISBN 9780511541285. doi: 10.1017/CBO9780511541285. URL `http://dx.doi.org/10.1017/CBO9780511541285`. (Pages 2 and 12.)

[8] M.R. Jackson, B.P. Bewlay, R.G. Rowe, D.W. Skelly, and H.A. Lipsitt. High-temperature refractory metal-intermetallic composites. *JOM*, 48(1):39–44, 1996. ISSN 1543-1851. doi: 10.1007/BF03221361. URL `http://dx.doi.org/10.1007/BF03221361`. (Page 2.)

[9] B.P. Bewlay, J.J. Lewandowksi, and M.R. Jackson. Refractory metal-intermetallic in-situ composites for aircraft engines. *JOM*, 49(8):44–45, 1997. ISSN 1047-4838. doi: 10.1007/BF02914402. URL `http://link.springer.com/article/10.1007/BF02914402`. (Page 2.)

[10] P.R. Subramanian, M.G. Mendiratta, and D.M. Dimiduk. The development of Nb-based advanced intermetallic alloys for structural applications. *JOM*, 48(1):33–38, 1996. ISSN 1047-4838. doi: 10.1007/BF03221360. URL `http://link.springer.com/article/10.1007/BF03221360`. (Page 2.)

[11] K. Bochenek and M. Basista. Advances in processing of NiAl intermetallic alloys and composites for high temperature aerospace applications. *Progress in Aerospace Sciences*, 79:136–146, 2015. ISSN 03760421. doi: 10.1016/j.paerosci.2015.09.003. URL `http://www.sciencedirect.com/science/article/pii/S0376042115300154`. (Page 2.)

[12] Z.B. Jiao, J.H. Luan, and C.T. Liu. Strategies for improving ductility of ordered intermetallics. *Progress in Natural Science: Materials International*, 26(1):1–12, 2016. ISSN 10020071. doi: 10.1016/j.pnsc.2016.01.014. URL `http://www.sciencedirect.com/science/article/pii/S1002007116000277`. (Page 2.)

[13] D.M. Dimiduk, D.B. Miracle, and C.H. Ward. Development of intermetallic materials for aerospace systems. *Materials Science and Technology*, 8(4):367–375, 1992. doi: 10.1179/mst.1992.8.4.367. URL `http://dx.doi.org/10.1179/mst.1992.8.4.367`. (Page 2.)

[14] E.P. George, M. Yamaguchi, K.S. Kumar, and C.T. Liu. Ordered Intermetallics. *Annual Review of Materials Science*, 24:409–451, 1994. ISSN 0084-6600. doi: 10.1146/annurev.ms.24.080194.002205. URL `http://www.annualreviews.org/doi/abs/10.1146/annurev.ms.24.080194.002205`. (Page 2.)

[15] M. Zamanzade, A. Barnoush, and C. Motz. A Review on the Properties of Iron Aluminide Intermetallics. *Crystals*, 6(1):10, 2016. ISSN 2073-4352. doi: 10.3390/cryst6010010. URL `http://www.mdpi.com/2073-4352/6/1/10/htm`. (Page 2.)

[16] N.S. Stoloff, C.T. Liu, and S.C. Deevi. Emerging applications of intermetallics. *Intermetallics*, 8(9-11):1313–1320, 2000. ISSN 09669795. doi: 10.1016/S0966-9795(00)00077-7. URL `http://www.sciencedirect.com/science/article/pii/S0966979500000777`. (Pages 2 and 4.)

[17] M. Yamaguchi, H. Inui, and K. Ito. High-temperature structural intermetallics. *Acta Materialia*, 48(1):307–322, 2000. ISSN 13596454. doi: 10.1016/S1359-6454(99)00301-8. URL `http://www.sciencedirect.com/science/article/pii/S1359645499003018`. (Page 2.)

[18] A. Lasalmonie. Intermetallics: Why is it so difficult to introduce them in gas turbine engines? *Intermetallics*, 14(10-11):1123–1129, 2006. ISSN 09669795. doi: 10.1016/j.intermet.2006.01.064. URL `http://www.sciencedirect.com/science/article/pii/S0966979506000835`. (Page 2.)

[19] N. Cinca, C.R.C. Lima, and J.M. Guilemany. An overview of intermetallics research and application: Status of thermal spray coatings. *Journal of Materials Research and Technology*, 2(1):75–86, 2013. ISSN 22387854. doi: 10.1016/j.jmrt.2013.03.013. URL `http://www.sciencedirect.com/science/article/pii/S2238785413000148`. (Pages 2 and 3.)

[20] C.T. Liu. Environmental embrittlement and grain-boundary fracture in Ni3Al. *Scripta Metallurgica et Materialia*, 27(1):25–28, 1992. ISSN 0956716X. doi: 10.1016/0956-716X(92)90313-4. URL `http://www.sciencedirect.com/science/article/pii/0956716X92903134`. (Pages 2 and 3.)

[21] D.B. Miracle. Overview No. 104 The physical and mechanical properties of NiAl. *Acta Metallurgica et Materialia*, 41(3):649–684, 1993. ISSN 09567151. doi: 10.1016/0956-7151(93)90001-9. URL `http://www.sciencedirect.com/science/article/pii/0956715193900019`. (Pages 2, 3, 5, and 117.)

[22] D. Risanti, J. Deges, L. Falat, S. Kobayashi, J. Konrad, M. Palm, B. Pöter, A. Schneider, C. Stallybrass, and F. Stein. Dependence of the brittle-to-ductile transition temperature (BDTT) on the Al content of FeAl alloys. *Intermetallics*, 13(12):1337–1342, 2005. ISSN 09669795. doi: 10.1016/j.intermet.2005.02.007. URL `http://www.sciencedirect.com/science/article/pii/S0966979505000798`. (Pages 2 and 3.)

[23] K. Yoshimi, S. Hanada, and H. Tokuno. Effect of Frozen-in Vacancies on Hardness and Tensile Properties of Polycrystalline B2 FeAl. *Materials transactions, JIM*, 35(1): 51–57, 1994. doi: 10.2320/matertrans1989.35.51. URL `https://www.jstage.jst.go.jp/article/matertrans1989/35/1/35_1_51/_article`. (Pages 2 and 3.)

[24] V.M. Imayev, R.M. Imayev, and G.A. Salishchev. On two stages of brittle-to-ductile transition in TiAl intermetallic. *Intermetallics*, 8(1):1–6, 2000. ISSN 09669795. doi: 10.1016/S0966-9795(99)00065-5. URL `http://www.sciencedirect.com/science/article/pii/S0966979599000655`. (Pages 2 and 3.)

[25] R. Mitra. Mechanical behaviour and oxidation resistance of structural silicides. *International Materials Reviews*, 51(1):13–64, 2006. ISSN 09506608. doi: 10.1179/174328006X79454. URL `http://www.tandfonline.com/doi/abs/10.1179/174328006X79454`. (Pages 2, 3, and 4.)

[26] R.M. Aikin. On the ductile-to-brittle transition temperature in MoSi2. *Scripta Metallurgica et Materialia*, 26(7):1025–1030, 1992. ISSN 0956716X. doi: 10.1016/0956-716X(92)90224-3. URL `http://www.sciencedirect.com/science/article/pii/0956716X92902243`. (Pages 2 and 3.)

[27] R. Rablbauer, G. Frommeyer, and F. Stein. Determination of the constitution of the quasi–binary eutectic NiAl–Re system by DTA and microstructural investigations. *Materials Science and Engineering: A*, 343(1-2):301–307, 2003. ISSN 09215093. doi: 10.1016/S0921-5093(02)00388-X. URL `http://www.sciencedirect.com/science/article/pii/S092150930200388X`. (Pages 2, 3, 5, 12, and 13.)

[28] R. Mitra. *Structural Intermetallics and Intermetallic Matrix Composites*, volume 6. CRC Press, 2015. ISBN 9781466511866. URL `http://www.crcnetbase.com/isbn/9781466511880`. (Pages 2, 3, 4, and 5.)

[29] C.T. Liu and J.O. Stiegler. Ordered Intermetallics. In *Properties and Selection: Nonferrous Alloys and Special-Purpose Materials*, volume 2, chapter 2, pages 2555–2615. ASM Metals Handbook, 10 th edition, 1992. (Pages 3 and 5.)

[30] N.S. Stoloff and R.G. Davies. The mechanical properties of ordered alloys. *Progress in Materials Science*, 13:1–84, 1968. ISSN 00796425. doi: 10.1016/0079-6425(68)90018-2. URL `http://www.sciencedirect.com/science/article/pii/0079642568900182`. (Page 3.)

[31] C.C. Koch, C.T. Liu, and N.S. Stoloff. High-Temperature Ordered Intermetallic Alloys. In *Materials Research Society Symposia Proceedings*, page Vol 39, 1985. (Page 4.)

[32] N.S. Stoloff, C.C. Koch, C.T. Liu, and O. Izumi. High-Temperature Ordered Intermetallic Alloys II. In *Materials Research Society Symposia Proceedings*, page Vol 81, 1987. (Page 4.)

[33] C.T. Liu, A.I. Taub, N.S. Stoloff, and C.C. Koch. High-Temperature Ordered Intermetallic Alloys III. In *Materials Research Society Symposia Proceedings*, page Vol 133, 1989. (Page 4.)

[34] C.T. Liu, C.L. White, and J.A. Horton. Effect of boron on grain-boundaries in Ni3Al. *Acta Metallurgica*, 33(2):213–229, 1985. ISSN 00016160. doi: 10.1016/0001-6160(85)90139-7. URL `http://www.sciencedirect.com/science/article/pii/0001616085901397`. (Page 4.)

[35] S.C. Deevi and V.K. Sikka. Nickel and iron aluminides: an overview on properties, processing, and applications. *Intermetallics*, 4(5):357–375, 1996. ISSN 09669795. doi: 10.1016/0966-9795(95)00056-9. URL `http://www.sciencedirect.com/science/article/pii/0966979595000569`. (Page 4.)

[36] K. Kothari, R. Radhakrishnan, and N.M. Wereley. Advances in gamma titanium aluminides and their manufacturing techniques. *Progress in Aerospace Sciences*, 55:1–16, 2012. ISSN 03760421. doi: 10.1016/j.paerosci.2012.04.001. URL `http://www.sciencedirect.com/science/article/pii/S0376042112000516`. (Page 4.)

[37] R.D. Noebe, R.R. Bowman, and M.V. Nathal. Physical and mechanical properties of the B2 compound NiAl. *International Materials Reviews*, 38(4):193 – 232, 1993. ISSN 09506608. doi: 10.1179/095066093790326276. URL `http://www.tandfonline.com/doi/abs/10.1179/imr.1993.38.4.193`. (Pages 5 and 117.)

[38] D.B. Miracle and R. Darolia. *Intermetallic Compounds. Structural Applications of Intermetallic Compounds*, volume 3, chapter NiAl and its Alloys, page 20. Wiley, 2000. URL `http://eu.wiley.com/WileyCDA/WileyTitle/productCd-0471612421.html`. (Page 5.)

[39] Y. Terada, K. Ohkubo, K. Nakagawa, T. Mohri, and T. Suzuki. Thermal conductivity of B2-type aluminides and titanides. *Intermetallics*, 3(5):347–355, 1995. ISSN 09669795. doi: 10.1016/0966-9795(95)94253-B. URL `http://www.sciencedirect.com/science/article/pii/096697959594253B`. (Page 5.)

[40] E.A. Aiken. *Intermetallic Copounds*, chapter Corrosion Behavior, pages 491–516. Wiley, 1967. (Page 5.)

[41] J.L. Smialek. Oxide morphology and spalling model for NiAl. *Metallurgical Transactions A*, 9(3):309–320, 1978. ISSN 1543-1940. doi: 10.1007/BF02646380. URL `http://dx.doi.org/10.1007/BF02646380`. (Page 5.)

[42] J. Jedliński and S. Mrowec. The influence of implanted yttrium on the oxidation behaviour of β-NiAl. *Materials Science and Engineering*, 87:281–287, 1987. ISSN 00255416. doi: 10.1016/0025-5416(87)90390-9. URL `http://www.sciencedirect.com/science/article/pii/0025541687903909`. (Page 5.)

[43] C.A. Barrett. Effect of 0.1 at.% zirconium on the cyclic oxidation resistance of β-NiAl. *Oxidation of Metals*, 30(5):361–390, 1988. ISSN 1573-4889. doi: 10.1007/BF00659006. URL `http://dx.doi.org/10.1007/BF00659006`. (Page 5.)

[44] Q.X. Fan, S.M. Jiang, D.L. Wu, J. Gong, and C. Sun. Preparation and hot corrosion behaviour of two Co modified NiAl coatings on a Ni-based superalloy. *Corrosion Science*, 76:373–381, 2013. ISSN 0010938X. doi: 10.1016/j.corsci.2013.07.008. URL `http://www.sciencedirect.com/science/article/pii/S0010938X13003041`. (Page 5.)

[45] I. Ansara, N. Dupin, H.L. Lukas, and B. Sundman. Thermodynamic assessment of the Al–Ni system. *Journal of Alloys and Compounds*, 247(1-2):20–30, 1997. ISSN 09258388. doi: 10.1016/S0925-8388(96)02652-7. URL `http://www.sciencedirect.com/science/article/pii/S0925838896026527`. (Page 5.)

[46] N. Dupin, I. Ansara, and B. Sundman. Thermodynamic re-assessment of the ternary system Al-Cr-Ni. *Calphad*, 25(2):279–298, 2001. ISSN 03645916. doi: 10.1016/S0364-5916(01)00049-9. URL `http://www.sciencedirect.com/science/article/pii/S0364591601000499`. (Page 5.)

[47] G. Frommeyer and R. Rablbauer. High temperature materials based on the intermetallic compound NiAl reinforced by refractory metals for advanced energy conversion technologies. *Steel Research International*, 79(7):507–5013, 2008. ISSN 09215093. doi: 10.2374/SRI08SP101-79-2008-507. URL `https://www.stahleisen.de/LinkClick.aspx?fileticket=FczUH16%2B56U%3D&tabid=198&language=en-US`. (Pages 5, 9, 11, 12, 112, and 113.)

[48] R. Vaßen, M.O. Jarligo, T. Steinke, D.E. Mack, and D. Stöver. Overview on advanced thermal barrier coatings. *Surface and Coatings Technology*, 205(4): 938–942, 2010. ISSN 02578972. doi: 10.1016/j.surfcoat.2010.08.151. URL `http://www.sciencedirect.com/science/article/pii/S0257897210008091`. (Page 5.)

[49] Z. Bai, D. Li, H. Peng, J. Wang, H. Guo, and S. Gong. Suppressing the formation of SRZ in a Ni-based single crystal superalloy by RuNiAl diffusion barrier. *Progress in Natural Science: Materials International*, 22(2):146–152, 2012. ISSN 10020071. doi: 10.1016/j.pnsc.2012.03.007. URL `http://www.sciencedirect.com/science/article/pii/S1002007112000305`. (Pages 5, 6, and 7.)

[50] Y. Zhang, J.A. Haynes, B.A. Pint, I.G. Wright, and W.Y. Lee. Martensitic transformation in CVD NiAl and (Ni,Pt)Al bond coatings. *Surface and Coatings Technology*, 163-164:19–24, 2003. ISSN 02578972. doi: 10.1016/S0257-8972(02)00585-6. URL `http://www.sciencedirect.com/science/article/pii/S0257897202005856`. (Pages 5, 6, and 7.)

[51] M.W. Chen, R.T. Ott, T.C. Hufnagel, P.K. Wright, and K.J. Hemker. Microstructural evolution of platinum modified nickel aluminide bond coat during thermal cycling. *Surface and Coatings Technology*, 163-164:25–30, 2003. ISSN 02578972. doi: 10.1016/S0257-8972(02)00591-1. URL `http://www.sciencedirect.com/science/article/pii/S0257897202005911`. (Pages 5 and 6.)

[52] D.M. Zhu and R.A. Miller. Thermal-barrier coatings for advanced gas-turbine engines. *MRS Bulletin*, 25(7):43–47, 2000. ISSN 08837694. doi: 10.1557/mrs2000.123. URL `http://dx.doi.org/10.1557/mrs2000.123`. (Page 5.)

[53] D.D. Hass. *Thermal Barrier Coatings via Directed Vapor Deposition*. phdthesis, Department of Materials Science and Engineering, Charlottesville, VA, 2001. (Page 6.)

[54] A. Menduiña. Microstructure and Phase Equilibria in the NiAl-Cr-W and NiAl-Cr-Re Pseudo-Ternary Systems: Characterization of the Eutectic Trough. mathesis, School of Aeronautical and Space Engineering, Madrid, 2015. (Pages 6 and 16.)

[55] A.C. Karaoglanli, K. Ogawa, A. Türk, and I. Ozdemir. *Thermal Shock and Cycling Behavior of Thermal Barrier Coatings (TBCs) Used in Gas Turbines*, chapter 10, pages 237–260. InTech, 2013. ISBN 978-953-51-1166-5. doi: 10.5772/54412. URL `http://dx.doi.org/10.5772/54412`. (Page 6.)

[56] D.J. Sordelet, M.F. Besser, R.T. Ott, B.J. Zimmerman, W.D. Porter, and B. Gleeson. Isothermal nature of martensite formation in Pt-modified β–NiAl alloys. *Acta Materialia*, 55(7):2433–2441, 2007. ISSN 13596454. doi: 10.1016/j.actamat.2006.11.038. URL `http://www.sciencedirect.com/science/article/pii/S1359645406008482`. (Page 6.)

[57] R.R. Adharapurapu, J. Zhu, V.S. Dheeradhada, D.M. Lipkin, and T.M. Pollock. A combinatorial investigation of palladium and platinum additions to β–NiAl overlay coatings. *Acta Materialia*, 77:379–393, 2014. ISSN 13596454. doi: 10.1016/j.actamat.2014.02.030. URL `http://www.sciencedirect.com/science/article/pii/S1359645414001232`. (Pages 6 and 7.)

[58] R.W. Jackson, D.M. Lipkin, and T.M. Pollock. The oxidation and rumpling behavior of overlay B2 bond coats containing Pt, Pd, Cr and Hf. *Surface and Coatings Technology*, 221:13–21, 2013. ISSN 02578972. doi: 10.1016/j.surfcoat.2013.01.021. URL `http://www.sciencedirect.com/science/article/pii/S0257897213000893`. (Pages 6 and 7.)

[59] R. Darolia. Ductility and fracture toughness issues related to implementation of NiAl for gas turbine applications. *Intermetallics*, 8(9-11):1321–1327, 2000. ISSN 09669795. doi: 10.1016/S0966-9795(00)00081-9. URL `http://www.sciencedirect.com/science/article/pii/S0966979500000819`. (Pages 7 and 12.)

[60] E.P. George, C.T. Liu, J.A. Horton, C.J. Sparks, M. Kao, H. Kunsmann, and T. King. Characterization, processing, and alloy design of NiAl-based shape memory alloys. *Materials Characterization*, 32(3):139–160, 1994. ISSN 10445803. doi: 10.1016/1044-5803(94)90084-1. URL `http://www.sciencedirect.com/science/article/pii/1044580394900841`. (Page 7.)

[61] E.M. Schulson and D.R. Barker. A brittle to ductile transition in NiAl of a critical grain size. *Scripta Metallurgica*, 17(4):519–522, 1983. ISSN 00369748. doi: 10.1016/0036-9748(83)90344-7. URL `http://www.sciencedirect.com/science/article/pii/0036974883903447`. (Pages 7 and 8.)

[62] M.S. Choudry, J.A. Eastman, R.J. DiMelfi, and M. Dollar. Evidence of room temperature ductility in nanocrystalline NiAl from biaxial disk bend tests. *Scripta Materialia*, 37(6):843–849, 1997. ISSN 13596462. doi: 10.1016/S1359-6462(97)00159-0. URL `http://www.sciencedirect.com/science/article/pii/S1359646297001590`. (Page 7.)

[63] R. Bohn, T. Haubold, R. Birringer, and H. Gleiter. Nanocrystalline intermetallic compounds – An approach to ductility? *Scripta Metallurgica et Materialia*, 25(4):811–816, 1991. ISSN 0956716X. doi: 10.1016/0956-716X(91)90230-X. URL `http://www.sciencedirect.com/science/article/pii/0956716X9190230X`. (Page 7.)

[64] T. Haubold, R. Bohn, R. Birringer, and H. Gleiter. Nanocrystalline intermetallic compounds–structure and mechanical properties. *Materials Science and*

Engineering: A, 153(1-2):679–683, 1992. ISSN 09215093. doi: 10.1016/0921-5093(92)90270-B. URL `http://www.sciencedirect.com/science/article/pii/092150939290270B`. (Page 7.)

[65] J.H. Moll and B.J. McTiernan. *Powder Metal Technologies and Applications*, volume 7, chapter Powder Metallurgy Superalloys, pages 2230–2272. ASM International, 9th edition, 1998. (Page 7.)

[66] C. Suryanarayana. Mechanical alloying and milling. *Progress in Materials Science*, 46 (1-2):1–184, 2001. ISSN 00796425. doi: 10.1016/S0079-6425(99)00010-9. URL `http://www.sciencedirect.com/science/article/pii/S0079642599000109`. (Page 8.)

[67] C.C. Koch and J.D. Whittenberger. Mechanical milling/alloying of intermetallics. *Intermetallics*, 4(5):339–355, 1996. ISSN 09669795. doi: 10.1016/0966-9795(96)00001-5. URL `http://www.sciencedirect.com/science/article/pii/0966979596000015`. (Page 8.)

[68] S.K. Pabi, J. Joardar, I. Manna, and B.S. Murty. Nanocrystralline phases in Cu-Ni, Cu-Zn and Ni-Al systems by mechanical alloying. *Nanostructured Materials*, 9(1-8): 149–152, 1997. ISSN 09659773. doi: 10.1016/S0965-9773(97)00040-8. URL `http://www.sciencedirect.com/science/article/pii/S0965977397000408`. (Page 8.)

[69] C.C. Koch. Intermetallic matrix composites prepared by mechanical alloying–a review. *Materials Science and Engineering: A*, 244(1):39–48, 1998. ISSN 09215093. doi: 10.1016/S0921-5093(97)00824-1. URL `http://www.sciencedirect.com/science/article/pii/S0921509397008241`. (Page 8.)

[70] M.H. Enayati, F. Karimzadeh, and S.Z. Anvari. Synthesis of nanocrystalline NiAl by mechanical alloying. *Journal of Materials Processing Technology*, 200(1-3):312–315, 2008. ISSN 09240136. doi: 10.1016/j.jmatprotec.2007.09.023. URL `http://www.sciencedirect.com/science/article/pii/S0924013607008229`. (Page 8.)

[71] G.H. Xu, K.F. Zhang, and Z.Q. Huang. The synthesis and characterization of ultrafine grain NiAl intermetallic. *Advanced Powder Technology*, 23(3):366–371, 2012. ISSN 09218831. doi: 10.1016/j.apt.2011.04.016. URL `http://www.sciencedirect.com/science/article/pii/S0921883111000720`. (Page 8.)

[72] E.T. Kubaski, O.M. Cintho, J.L. Antoniassi, H. Kahn, and J.D.T. Capocchi. Obtaining NiAl intermetallic compound using different milling devices. *Advanced Powder Technology*, 23(5):667–672, 2012. ISSN 09218831. doi: 10.1016/j.apt.2011.08.005. URL `http://www.sciencedirect.com/science/article/pii/S0921883111001336`. (Page 8.)

[73] E. Liu, J. Jia, Y. Bai, W. Wang, and Y. Gao. Study on preparation and mechanical property of nanocrystalline NiAl intermetallic. *Materials & Design*, 53:596–601, 2014. ISSN 02613069. doi: 10.1016/j.matdes.2013.07.052. URL `http://www.sciencedirect.com/science/article/pii/S0261306913006808`. (Page 8.)

[74] J.L. González-Carrasco, P. Pérez, P. Adeva, and J. Chao. Oxidation behaviour of an ODS NiAl–based intermetallic alloy. *Intermetallics*, 7(1):69–78, 1999. ISSN 09669795. doi: 10.1016/S0966-9795(98)00012-0. URL `http://www.sciencedirect.com/science/article/pii/S0966979598000120`. (Page 8.)

[75] S.C. Ur and P. Nash. Secondary recrystallization and high temperature compressive properties of ODS MA NiAl. *Scripta Materialia*, 47(6):405–409, 2002. ISSN 13596462. doi: 10.1016/S1359-6462(02)00161-6. URL `http://www.sciencedirect.com/science/article/pii/S1359646202001616`. (Page 8.)

[76] S.Z. Anvari, F. Karimzadeh, and M.H. Enayati. Synthesis and characterization of NiAl–Al2O3 nanocomposite powder by mechanical alloying. *Journal of Alloys and Compounds*, 477(1-2):178–181, 2009. ISSN 09258388. doi: 10.1016/j.jallcom.2008.10.043. URL `http://www.sciencedirect.com/science/article/pii/S0925838808017167`. (Page 8.)

[77] L.Z. Zhou, J.T. Guo, and G.J. Fan. Synthesis of NiAl–TiC nanocomposite by mechanical alloying elemental powders. *Materials Science and Engineering: A*, 249(1-2):103–108, 1998. ISSN 09215093. doi: 10.1016/S0921-5093(98)00576-0. URL `http://www.sciencedirect.com/science/article/pii/S0921509398005760`. (Page 8.)

[78] S.X. Mao, N.A. McMinn, and N.Q. Wu. Processing and mechanical behaviour of TiAl/NiAl intermetallic composites produced by cryogenic mechanical alloying. *Materials Science and Engineering: A*, 363(1-2):275–289, 2003. ISSN 09215093. doi: 10.1016/S0921-5093(03)00652-X. URL `http://www.sciencedirect.com/science/article/pii/S092150930300652X`. (Page 8.)

[79] D.L. Bourell and J.R. Groza. *Powder Metal Technologies and Applications*, volume 7, chapter Consolidation of Ultrafine and Nanocrystalline Powder, pages 1176–1209. ASM International, 9th edition, 1998. (Pages 8 and 9.)

[80] M. Palm, J. Preuhs, and G. Sauthoff. Production scale processing of a new intermetallic NiAl–Ta–Cr alloy for high-temperature application. *Journal of Materials Processing Technology*, 136(1-3):114–119, 2003. ISSN 09240136. doi: 10.1016/

S0924-0136(02)01104-4. URL http://www.sciencedirect.com/science/article/pii/S0924013602011044. (Pages 9 and 11.)

[81] G.P. Cammarota and A. Casagrande. Effect of ternary additions of iron on microstructure and microhardness of the intermetallic NiAl in reactive sintering. *Journal of Alloys and Compounds*, 381(1-2):208–214, 2004. ISSN 09258388. doi: 10.1016/j.jallcom.2004.04.077. URL http://www.sciencedirect.com/science/article/pii/S0925838804005043. (Page 9.)

[82] P. Novák, D. Šotka, M. Novák, A. Michalcová, J. Šerák, and D. Vojtěch. Production of NiAl-matrix composites by reactive sintering. *Powder Metallurgy*, 54(3):308–313, 2011. ISSN 00325899 17432901. doi: 10.1179/003258909X12518163. URL http://www.tandfonline.com/doi/full/10.1179/003258909X12518163. (Page 9.)

[83] V. Udhayabanu, K.R. Ravi, and B.S. Murty. Development of in situ NiAl–Al2O3 nanocomposite by reactive milling and spark plasma sintering. *Journal of Alloys and Compounds*, 509(1):S223–S228, 2011. ISSN 09258388. doi: 10.1016/j.jallcom.2010.12.091. URL http://www.sciencedirect.com/science/article/pii/S0925838810030835. Suplement. (Page 9.)

[84] M. Yao, Z. Zhangjian, T. Jun, and L. Ming. Fabrication of Ultra-fine Grain Tungsten by Combining Spark Plasma Sintering with Resistance Sintering under Ultra High Pressure. *Rare Metal Materials and Engineering*, 40(1):4–8, 2011. ISSN 18755372. doi: 10.1016/S1875-5372(11)60008-8. URL http://www.sciencedirect.com/science/article/pii/S1875537211600088. (Page 9.)

[85] R. Orrù, R. Licheri, A.M. Locci, A. Cincotti, and G. Cao. Consolidation/synthesis of materials by electric current activated/assisted sintering. *Materials Science and Engineering: R: Reports*, 63(4-6):127–287, 2009. ISSN 0927796X. doi: 10.1016/j.mser.2008.09.003. URL http://www.sciencedirect.com/science/article/pii/S0927796X08000995. (Page 9.)

[86] G. Molénat, M. Thomas, J. Galy, and A. Couret. Application of Spark Plasma Sintering to Titanium Aluminide Alloys. *Advanced Engineering Materials*, 9(8):667–669, 2007. ISSN 1527-2648. doi: 10.1002/adem.200700094. URL http://dx.doi.org/10.1002/adem.200700094. (Page 9.)

[87] R. Muñoz-Moreno, E.M. Ruiz-Navas, B. Srinivasarao, and J.M. Torralba. Microstructural Development and Mechanical Properties of PM Ti–45Al–2Nb–2Mn–0.8 vol.%TiB2 Processed by Field Assisted Hot Pressing. *Journal of Materials Science & Technology*, 30(11):1145–1154, 2014. ISSN

10050302. doi: 10.1016/j.jmst.2014.08.008. URL http://www.sciencedirect.com/science/article/pii/S1005030214001601. (Page 9.)

[88] A. Varona-Caballero, S. Milenkovic, M.A. Jabbari-Taleghani, and M.A. Monge. Mechanical alloying and field assisted hot pressing of nanocrystalline B2-NiAl intermetallic compound. *Powder Metallurgy*, 57(3):212–219, 2014. ISSN 0032-5899. doi: 10.1179/1743290114Y.0000000099. URL http://www.tandfonline.com/doi/abs/10.1179/1743290114Y.0000000099. (Pages 9, 112, and 113.)

[89] A.R.C. Westwood. Materials for advanced studies and devices. *Metallurgical Transactions A*, 19(4):749–758, 1988. ISSN 1543-1940. doi: 10.1007/BF02628353. URL http://dx.doi.org/10.1007/BF02628353. (Page 9.)

[90] J.F. Zhang, J. Shen, Z. Shang, Z.R. Feng, L.S. Wang, and H.Z. Fu. Microstructure and room temperature fracture toughness of directionally solidified NiAl–Mo eutectic in situ composites. *Intermetallics*, 21(1):18–25, 2012. ISSN 09669795. doi: 10.1016/j.intermet.2011.10.002. URL http://www.sciencedirect.com/science/article/pii/S0966979511003153. (Pages 9, 10, 11, 13, 14, and 115.)

[91] K. Hagihara, Y. Sugino, and Y. Umakoshi. The effect of Ti-addition on plastic deformation and fracture behavior of directionally solidified NiAl/Cr(Mo) eutectic alloys. *Intermetallics*, 14(10-11):1326–1331, 2006. ISSN 09669795. doi: 10.1016/j.intermet.2005.11.029. URL http://www.sciencedirect.com/science/article/pii/S096697950600118X. (Pages 9, 16, 112, and 113.)

[92] D. Yu, H. Bei, Y. Chen, E.P. George, and K. An. Phase-specific deformation behavior of a relatively tough NiAl–Cr(Mo) lamellar composite. *Scripta Materialia*, 84-85:59–62, 2014. ISSN 13596462. doi: 10.1016/j.scriptamat.2014.04.025. URL http://www.sciencedirect.com/science/article/pii/S1359646214001791. (Pages 9 and 16.)

[93] W. Kurz and D.J. Fisher. Solidification Microstructure: Eutectic and Peritectic. In *Fundamentals of Solidification*, chapter 5, pages 97–120. Trans Tech Publications, 3 edition, 1986. ISBN 0878495223, 9780878495221. (Pages 10, 12, 13, 15, and 46.)

[94] A. Misra and R. Gibala. Plasticity in multiphase intermetallics. *Intermetallics*, 8(9-11):1025–1034, 2000. ISSN 09669795. doi: 10.1016/S0966-9795(00)00079-0. URL http://www.sciencedirect.com/science/article/pii/S0966979500000790. (Pages 10 and 11.)

[95] A. Misra, R. Gibala, and R.D. Noebe. Optimization of toughness and strength in multiphase intermetallics. *Intermetallics*, 9(10-11):971–978, 2001. ISSN

09669795. doi: 10.1016/S0966-9795(01)00098-X. URL `http://www.sciencedirect.com/science/article/pii/S096697950100098X`. (Pages 10, 11, and 46.)

[96] D.R. Johnson, X.F. Chen, B.F. Oliver, R.D. Noebe, and J.D. Whittenberger. Processing and mechanical properties of in-situ composites from the NiAl–Cr and the NiAl–(Cr,Mo) eutectic systems. *Intermetallics*, 3(2):99–113, 1995. ISSN 09669795. doi: 10.1016/0966-9795(95)92674-O. URL `http://www.sciencedirect.com/science/article/pii/096697959592674O`. (Pages 11, 12, 14, 15, 48, 112, 113, 120, and 121.)

[97] A. Misra, Z.L. Wu, M.T. Kush, and R. Gibala. Microstructures and mechanical properties of directionally solidified NiAl–Mo and NiAl–Mo(Re) eutectic alloys. *Materials Science and Engineering: A*, 239-240:75–87, 1997. ISSN 09215093. doi: 10.1016/S0921-5093(97)00563-7. URL `http://www.sciencedirect.com/science/article/pii/S0921509397005637`. (Pages 11, 16, and 46.)

[98] Z. Shang, J. Shen, L. Wang, Y. Du, Y. Xiong, and H. Fu. Investigations on the microstructure and room temperature fracture toughness of directionally solidified NiAl-Cr(Mo) eutectic alloy. *Intermetallics*, 57:25–33, 2015. ISSN 09669795. doi: 10.1016/j.intermet.2014.09.012. URL `http://dx.doi.org/10.1016/j.intermet.2014.09.012`. (Pages 11, 14, and 16.)

[99] G. Frommeyer, R. Rablbauer, and H.J. Schäfer. Elastic properties of B2-ordered NiAl and NiAl–X (Cr, Mo, W) alloys. *Intermetallics*, 18(3):299–305, 2010. ISSN 09669795. doi: 10.1016/j.intermet.2009.07.026. URL `http://www.sciencedirect.com/science/article/pii/S0966979509002131`. (Pages 11, 12, and 16.)

[100] R.S. Sundar, K. Kitazono, E. Sato, and K. Kuribayashi. Thermal cycling creep behavior of NiAl-Cr alloy. *Intermetallics*, 9(4):279–286, 2001. ISSN 09669795. doi: 10.1016/S0966-9795(01)00003-6. URL `http://www.sciencedirect.com/science/article/pii/S0966979501000036`. (Page 11.)

[101] R. Asthana, R. Tiwari, and S.N. Tewari. Compressive properties of zone-directionally solidified β-NiAl and its off-eutectic alloys with chromium and tungsten. *Materials Science and Engineering A*, 336(1-2):99–109, 2002. ISSN 09215093. doi: 10.1016/S0921-5093(01)01919-0. URL `http://www.sciencedirect.com/science/article/pii/S0921509301019190`. (Page 11.)

[102] L. Hu, W. Hu, G. Gottstein, S. Bogner, S. Hollad, and A. Bührig-Polaczek. Investigation into microstructure and mechanical properties of NiAl-Mo composites produced by directional solidification. *Materials Science and Engineering A*, 539:

211–222, 2012. ISSN 09215093. doi: 10.1016/j.msea.2012.01.083. URL http://www.sciencedirect.com/science/article/pii/S0921509312001190. (Page 11.)

[103] S. Bogner, L. Hu, S. Hollad, W. Hu, G. Gottstein, and A. Bührig-Polaczek. Microstructure of a eutectic NiAl-Mo alloy directionally solidified using an industrial scale and a laboratory scale Bridgman furnace. *International Journal of Materials Research*, 103(1):17–23, 2012. ISSN 18625282. doi: 10.3139/146.110632. URL http://www.hanser-elibrary.com/doi/abs/10.3139/146.110632?journalCode=ijmr. (Pages 11 and 14.)

[104] H. Bei and E.P. George. Microstructures and mechanical properties of a directionally solidified NiAl–Mo eutectic alloy. *Acta Materialia*, 53(1):69–77, 2005. ISSN 13596454. doi: 10.1016/j.actamat.2004.09.003. URL http://www.sciencedirect.com/science/article/pii/S1359645404005440. (Page 11.)

[105] S. Milenkovic and R. Caram. Microstructure of the microalloyed NiAl–V eutectics. *Materials Letters*, 55(1-2):126–131, 2002. ISSN 0167577X. doi: 10.1016/S0167-577X(01)00634-6. URL http://www.sciencedirect.com/science/article/pii/S0167577X01006346. (Page 11.)

[106] S. Milenkovic and R. Caram. Mechanical Properties and Fracture Behavior of Directionally Solidified NiAl–V Eutectic Composites. *Metallurgical and Materials Transactions A*, 46(2):557–565, 2015. ISSN 1543-1940. doi: 10.1007/s11661-014-2427-6. URL http://dx.doi.org/10.1007/s11661-014-2427-6. (Page 11.)

[107] S. Milenkovic and R. Caram. Oxidation behavior and thermal stability of a NiAl-V eutectic alloy. *Physica Status Solidi (A) Applications and Materials Science*, 210(5):1019–1024, 2013. doi: 10.1002/pssa.201200836. URL http://onlinelibrary.wiley.com/doi/10.1002/pssa.201200836/abstract. (Page 11.)

[108] S. Milenkovic and R. Caram. Growth morphology of the NiAl–V in situ composites. *Journal of Materials Processing Technology*, 143-144:629–635, 2003. ISSN 09240136. doi: 10.1016/S0924-0136(03)00449-7. URL http://www.sciencedirect.com/science/article/pii/S0924013603004497. (Pages 11 and 12.)

[109] S. Milenkovic, A.A. Coelho, and R. Caram. Directional solidification processing of eutectic alloys in the Ni-Al-V system. *Journal of Crystal Growth*, 211(1):485–490, 2000. ISSN 00220248. doi: 10.1016/S0022-0248(99)00783-6. URL http://www.sciencedirect.com/science/article/pii/S0022024899007836. (Page 11.)

[110] S. Milenkovic, A. Schneider, and G. Frommeyer. Constitutional and microstructural investigation of the pseudobinary NiAl-W system. *Intermetallics*, 19(3):342–349, 2011. ISSN 09669795. doi: 10.1016/j.intermet.2010.10.019. URL `http://dx.doi.org/10.1016/j.intermet.2010.10.019`. (Pages 11, 12, 13, 16, 26, 42, 44, 46, 48, 67, and 79.)

[111] J.T. Guo, K.W. Huai, Q. Gao, W.L. Ren, and G.S. Li. Effects of rare earth elements on the microstructure and mechanical properties of NiAl-based eutectic alloy. *Intermetallics*, 15(5-6):727–733, 2007. ISSN 09669795. doi: 10.1016/j.intermet.2006.10.020. URL `http://www.sciencedirect.com/science/article/pii/S0966979506002998`. (Page 11.)

[112] J.T. Guo, L.Y. Sheng, Y.X. Tian, L.Z. Zhou, and H.Q. Ye. Effect of Ho on the microstructure and compressive properties of NiAl-based eutectic alloy. *Materials Letters*, 62(23):3910–3912, 2008. ISSN 0167577X. doi: 10.1016/j.matlet.2008.05.038. URL `http://www.sciencedirect.com/science/article/pii/S0167577X08005041`. (Page 11.)

[113] L. Sheng, L. Wang, T. Xi, Y. Zheng, and H. Ye. Microstructure, precipitates and compressive properties of various holmium doped NiAl/Cr(Mo,Hf) eutectic alloys. *Materials & Design*, 32(10):4810–4817, 2011. ISSN 02613069. doi: 10.1016/j.matdes.2011.06.026. URL `http://www.sciencedirect.com/science/article/pii/S0261306911004328`. (Pages 11 and 16.)

[114] L. Sheng, F. Yang, T.F. Xi, Y.F. Zheng, and J.T. Guo. Microstructure and room temperature mechanical properties of NiAl–Cr(Mo)–(Hf, Dy) hypoeutectic alloy prepared by injection casting. *Transactions of Nonferrous Metals Society of China*, 23 (4):983–990, 2013. ISSN 10036326. doi: 10.1016/S1003-6326(13)62556-X. URL `http://www.sciencedirect.com/science/article/pii/S100363261362556X`. (Pages 11 and 16.)

[115] L.Y. Sheng, J.T. Guo, and H.Q. Ye. Microstructure and mechanical properties of NiA–Cr(Mo)/Nb eutectic alloy prepared by injection-casting. *Materials & Design*, 30 (4):964–969, 2009. ISSN 02613069. doi: 10.1016/j.matdes.2008.06.061. URL `http://www.sciencedirect.com/science/article/pii/S0261306908003361`. (Pages 11 and 16.)

[116] L.Y. Sheng, W. Zhang, J.T. Guo, Z.S. Wang, and H.Q. Ye. Microstructure evolution and elevated temperature compressive properties of a rapidly solidified NiAl–Cr(Nb)/Dy alloy. *Materials & Design*, 30(7):2752–2755, 2009. ISSN 02613069.

doi: 10.1016/j.matdes.2008.10.022. URL http://www.sciencedirect.com/science/article/pii/S0261306908005359. (Page 11.)

[117] D.R. Johnson, X.F. Chen, B.F. Oliver, R.D. Noebe, and J.D. Whittenberger. Directional solidification and mechanical properties of NiAl–NiAlTa alloys. *Intermetallics*, 3(2): 141–152, 1995. ISSN 09669795. doi: 10.1016/0966-9795(95)92679-T. URL http://www.sciencedirect.com/science/article/pii/096697959592679T. (Page 11.)

[118] P.L. Ferrandini, F.L.G.U. Araujo, W.W. Batista, and R. Caram. Growth and characterization of the NiAl–NiAlNb eutectic structure. *Journal of Crystal Growth*, 275 (1-2):147–152, 2005. ISSN 00220248. doi: 10.1016/j.jcrysgro.2004.10.101. URL http://www.sciencedirect.com/science/article/pii/S002202480401468X. (Page 11.)

[119] S.M. Merchant and M.R. Notis. A review: Constitution of the Al–C–rNi system. *Materials Science and Engineering*, 66(1):47–60, 1984. ISSN 00255416. doi: 10.1016/0025-5416(84)90140-X. URL http://www.sciencedirect.com/science/article/pii/002554168490140X. (Page 11.)

[120] K.A. Jackson and J.D. Hunt. Lamellar and rod eutectic growth. *Transactions of the Metallurgical Society of AIME*, 236(8):1129–1142, 1966. (Pages 13 and 42.)

[121] Y. Li. Bulk metallic glasses: Eutectic coupled zone and amorphous formation. *JOM*, 57(3):60–63, 2006. ISSN 1543-1851. doi: 10.1007/s11837-005-0236-5. URL http://link.springer.com/article/10.1007%2Fs11837-005-0236-5. (Page 13.)

[122] J.G. Webber and D.C. Van Aken. Studies of a quasi-binary β-NiAl and α-Re eutectic. *Scripta Metallurgica*, 23(2):193–196, 1989. ISSN 00369748. doi: 10.1016/0036-9748(89)90409-2. URL http://www.sciencedirect.com/science/article/pii/0036974889904092. (Page 13.)

[123] L.A. Cornish and M.J. Witcomb. A metallographic study of the Al–Ni–Re phase diagram. *Journal of Alloys and Compounds*, 291(1-2):145–166, 1999. ISSN 09258388. doi: 10.1016/S0925-8388(99)00245-5. URL http://www.sciencedirect.com/science/article/pii/S0925838899002455. (Page 13.)

[124] C. Seemüller, M. Heilmaier, T. Haenschke, H. Bei, A. Dlouhy, and E.P. George. Influence of fiber alignment on creep in directionally solidified NiAl–10Mo in-situ composites. *Intermetallics*, 35:110–115, 2013. ISSN 09669795. doi: 10.1016/j.intermet.2012.12.007. URL http://www.sciencedirect.com/science/article/pii/S0966979512004530. (Pages 14 and 119.)

[125] R. Gamboa. *Diagramas Ternarios: Teoría y Aplicaciones*. Sección de publicaciones de la Escuela Técnica Superior de Ingenieros Industriales. Universidad Politécnica de Madrid, Madrid, 2011. ISBN 9788474842425. URL `http://datos.bne.es/edicion/a5161251.html`. (Pages 15 and 16.)

[126] A. Misra, Z.L. Wu, M.T. Kush, and R. Gibala. Deformation and fracture behaviour of directionally solidified NiAl-Mo and NiAl-Mo(Re) eutectic composites. *Philosophical Magazine A*, 78(3):533–550, 1998. ISSN 0141-8610. doi: 10.1080/01418619808241921. URL `http://www.tandfonline.com/doi/abs/10.1080/01418619808241921`. (Page 16.)

[127] J. Peng, P. Franke, and H.J. Seifert. Experimental investigation and thermodynamic modelling of Al-Mo-Ni system and its extension into NiAl-Cr-Mo system. In *Intermetallics Congress*, Kloster Banz - Bad Staffelstein, 2015. URL `http://www.intermetallics-conference.de/programme/scientific-programme/`. (Page 16.)

[128] M.O. Lai and K.B. Lim. On the prediction of tensile properties from hardness tests. *Journal of Materials Science*, 26(8):2031–2036, 1991. ISSN 1573-4803. doi: 10.1007/BF00549163. URL `http://link.springer.com/article/10.1007%2FBF00549163`. (Page 30.)

[129] S.C. Krishna, N.K. Gangwar, A.K. Jha, and B. Pant. On the Prediction of Strength from Hardness for Copper Alloys. *Journal of Materials*, 2013:1–6, 2013. ISSN 2314-4866. doi: 10.1155/2013/352578. URL `http://www.hindawi.com/journals/jma/2013/352578/`. (Page 30.)

[130] H.A. Kuhn and G.F. Vandervoort. *Mechanical Testing and Evaluation*. ASM Metals Handbook, volume 8 edition, 2000. (Pages 31 and 33.)

[131] R.K.F. Lam, C.E. Melin, and G. Colella. Melting and casting of high purity chromium with controlled oxygen content, 2000. URL `http://www.google.com/patents/US6039788`. (Page 39.)

[132] S.T. Bluni, M.R. Notis, and A.R. Marder. Nucleation characteristics and microstructure in off-eutectic Al-Zn alloys. *Acta Metallurgica et Materialia*, 43(5):1775–1782, 1995. ISSN 09567151. doi: 10.1016/0956-7151(94)00397-Z. URL `http://www.sciencedirect.com/science/article/pii/095671519400397Z`. (Page 46.)

[133] M.D. Nave, A.K. Dahle, and D.H. StJohn. Halo formation in directional solidification. *Acta Materialia*, 50(11):2837–2849, 2002. ISSN 13596454. doi: 10.1016/S1359-6454(02)00104-0. URL `http://www.sciencedirect.com/science/article/pii/S1359645402001040`. (Page 46.)

[134] S.M. Li, B.L. Jiang, B.L. Ma, and H.Z. Fu. Halo formation in directional solidification of Ni–Ni3Nb hypereutectic alloy. *Journal of Crystal Growth*, 299(1):178–183, 2007. ISSN 00220248. doi: 10.1016/j.jcrysgro.2006.10.255. URL `http://www.sciencedirect.com/science/article/pii/S0022024806011626`. (Page 46.)

[135] K.W. Li, S.M. Li, Y.L. Xue, and H.Z. Fu. Halo formation in arc-melted Cr–Nb alloys. *Journal of Crystal Growth*, 357:30–34, 2012. ISSN 00220248. doi: 10.1016/j.jcrysgro.2012.07.042. URL `http://www.sciencedirect.com/science/article/pii/S0022024812005386`. (Page 46.)

[136] K.P. Gupta. *Phase diagrams of ternary nickel alloys*. Indian Institute of Metals, Calcutta, 1990. ISBN 8185307075. URL `http://trove.nla.gov.au/work/21674450?q&versionId=26028386`. (Page 49.)

[137] B. Predel. *Ni-Np – Pt-Zr*, chapter Ni-W (Nickel-Tungsten), pages 1–3. Springer Berlin Heidelberg, Berlin, Heidelberg, 1998. ISBN 978-3-540-70692-2. doi: 10.1007/10542753_2277. URL `http://materials.springer.com/lb/docs/sm_lbs_978-3-540-70692-2_2277`. (Page 52.)

[138] Y.C. Liang, J.T. Guo, Y. Xie, L.Y. Sheng, L.Z. Zhou, and Z.Q. Hu. Effect of growth rate on the tensile properties of DS NiAl/Cr(Mo) eutectic alloy produced by liquid metal cooling technique. *Intermetallics*, 18(3):319–323, 2010. ISSN 09669795. doi: 10.1016/j.intermet.2009.08.002. URL `http://www.sciencedirect.com/science/article/pii/S0966979509002155`. (Page 60.)

[139] S.V.N. Naidu, A.M. Sriramamurthy, and P.R. Rao. The Cr–W (Chromium–Tungsten) system. *Bulletin of Alloy Phase Diagrams*, 5(3):289–292, 1984. ISSN 0197-0216. doi: 10.1007/BF02868555. URL `http://link.springer.com/article/10.1007%2FBF02868555`. (Page 81.)

[140] H. Bei and E.P. George. Microstructures and mechanical properties of a directionally solidified NiAl–Mo eutectic alloy. *Acta Materialia*, 53(1):69–77, 2005. ISSN 13596454. doi: 10.1016/j.actamat.2004.09.003. URL `http://www.sciencedirect.com/science/article/pii/S1359645404005440`. (Pages 113, 114, and 117.)

[141] J.D. Whittenberger, S.V. Raj, I.E. Locci, and J.A. Salem. Effect of growth rate on elevated temperature plastic flow androom temperature fracture toughness of directionally solidified NiAl-31Cr-3Mo. *Intermetallics*, 7(10):1159–1168, 1999. ISSN 09669795. doi: 10.1016/S0966-9795(99)00023-0. URL `http://www.sciencedirect.com/science/article/pii/S0966979599000230`. (Page 117.)

[142] C.Y. Cui, J.T. Guo, and H.Q. Ye. Microstructure, brittle–ductile transition temperature and elevated temperature compressive behavior of the directionally solidified NiAl–Cr(Mo)–Hf alloy. *Materials Science and Engineering: A*, 385(1):359–366, 2004. ISSN 09215093. doi: 10.1016/j.msea.2004.06.065. URL `http://www.sciencedirect.com/science/article/pii/S0921509304009025`. (Page 117.)

[143] H.J. Frost and M.F. Ashby. *Deformation – Mechanism Maps: The Plasticity and Creep of Metals and Ceramics*. Pergamon Press, New York, 1st edition, 1982. ISBN 0-08-029338-7. doi: 10.1016/0378-3804(84)90015-9. URL `http://engineering.dartmouth.edu/defmech/`. (Pages 119 and 120.)

[144] E. Kassner. *Fundamentals of Creep in Metals and Alloys*. Elsevier Ltd, 3rd edition, 2015. ISBN 978-0-08-099427-7. URL `http://www.sciencedirect.com/science/book/9780080994277`. (Pages 119 and 120.)

[145] E. Kassner and M.T. Pérez-Prado. *Fundamentals of Creep in Metals and Alloys*. Elsevier Ltd, 1st edition, 2004. ISBN 978-0-08-043637-1. URL `http://www.sciencedirect.com/science/book/9780080436371`. (Page 120.)